CARBOTHERMIC REDUCTION OF PYROCHLORE AND NIOBIUM PENTOXIDE IN A TRANSFERRED ARC PLASMA

A

THESIS

BY

EARLE J. CHIN

Department of Chemical Engineering

McGill University, Montreal

Under the supervision of Prof. R.J. Munz

Submitted to the Faculity of Graduate Studies and Research of McGill University in partial fulfillment of the requirements for the degree of Doctor of Philosophy

McGill University
Montreal, CANADA

July 1989

Carbothermic Reduction of Pyrochlore and NB205 in a Transferred Arc Plasma

ABSTRACT

The carbothermic reductions of pyrochlore and niobium pentoxide were studied, with and without the addition of iron as a solvent, in an argon transferred-arc plasma with a single stationary pellet reactor system. A conversion-time model, based on experimental and theoretical studies, was proposed to describe the carbothermic reduction reaction systems. The experimental results confirmed the applicability of the model.

The carbothermic reductions of pyrochlore and niobium pentoxide were studied in the temperature ranges 1530 - 2440 and 1625 - 2855 K, respectively. The rate was independent of particle size but was influenced by the separation between the oxide and carbon particles. The rate was lower than the model predictions above a certain conversion, the level of which increased with temperature and carbon concentration.

The carbothermic reductions of pyrochlore and niobium pentoxide with iron addition were studied in the temperature ranges 1430 - 2125 and 1575 - 2440 K, respectively. The rates were independent of particle size but were enhanced by the presence of iron. Deviation from the model was observed to be less at high conversion levels.

Preliminary investigation of the conversion rate for the carbothermic reduction of a pyrochlore and ferric oxide mixture was done to simulate the type of reactants that would be used in a commercial process. The rate was improved by the addition of iron oxide.

RESUME

La réduction carbothermique du pyrochlore et du pentoxyde de niobium est étudiée dans un plasma d'arc transféré dans l'argon. L'étude est effectuée avec et sans addition de fer comme solvant dans un réacteur ne comprenant qu'une seule boulette stationnaire. Un modèle de conversion/temps s'appuyant sur les études expérimentales et théoriques est proposé pour décrire la réaction de réduction carbothermique. Les résultats expérimentaux confirment la validité du modèle.

Les réductions carbothermiques du pyrochlore et du pentoxyde de niobium sont étudiées dans les gammes de températures 1530 - 2440 et 1625 - 2855 K respectivement. Le taux de réaction est indépendant de la grosseur des particules mais est influencé par la séparation entre les particules d'oxyde et de carbone. Le taux est plus bas que les prédictions du modèle au dessus d'une conversion donnée, laquelle augmente avec la température et la concentration de carbone.

Les réductions carbothermiques du pyrochlore et du pentoxyde de niobium avec addition de fer sont étudiées dans les gammes de températures 1430 - 2125 et 1575 - 2440 K respectivement. Les taux sont indépendants de la dimension de la particule mais sont augmentés par la présence de fer. La déviation du modèle est plus faible à des taux de conversion élevés.

Des études préliminaires du taux de conversion pour la réduction carbothermique d'un mélange de pyrochlore et d'oxyde ferreux sont effectuées afin de simuler le type de réactants qui serait utilisé dans un procédé commercial. On observe une amélioration du taux par l'addition d'oxyde de fer.

ACKNOWLEDGEMENT

The author wishes to express his gratitude to all those who contributed to the work presented in this thesis.

To members of the Plasma Technology Group, McGill University, past and present, in particular Dr. W.H. Gauvin, Dr. D. Berk, Dr. P. Patterson, Mr. G.Q. Chen, Mr. P. Stuart, Dr. P. Parisi, Mr. M. Bronet, Dr. P. Tsantrizos, Dr. J.L. Meunier and colleagues Dr. B. Huang, Mr. I. Journeau, Mr. C. Ercan, and Mr. J. Li for the help in conducting the experiments and the many useful discussions.

To Mr. A. Gagnon and Mr. H. Alexander of the machine shop at McGill University, for constructing and maintaining the experimental apparatus. Mr. J. Dumont for making sure every thing under the sun is in stock.

To Mrs. H. Campbell and Mrs. M. Rideau of the Mining and Metallurgical Department, McGill University, for their help with the SEM and XRD analyses.

To Dr. J. Boivin of the Centre de Recherches Minerales of the Government of Quebec, for his help with the product chemical and XRD analyses.

To Niobec Inc. for providing the pyrochlore used in this work, and Noranda Inc. and the Quebec Government for financial support in forms of a research fellowship and an FCAR team grant, respectively.

To Mrs. J. Parker and N. Cavalluzzi for their help with preparing the manuscript and some of the drawings.

To Prof. R.J. Munz, his thesis supervisor, without whom this thesis would not be possible.

And finally, to the author's family, in particular to his wife Elizabeth and son William, Mr. Roberto Szente, Mr. Imtiaz Ahmed, Miss. M. Habelrih and Mrs. B. Ercan for their love, understanding, patience and encouragement.

TABLE OF CONTENTS

Page

LIST OF FIGURES

LIST OF TABLES

NOMENCLATURE

a = total surface area (m^2)

a_1 = initial amount of carbon (kg)

a_2 = initial amount of potassium perchlorate (kg)

A = pre-exponential constant or frequency factor in Arrhenius equation (-)

A_B = surface area of a solid grain (m^2)

b = stoichiometric coefficient of solid reactant

C_0 = initial concentration of second solid reactant (mole m^{-3})

C_1 = carbon monoxide concentration (volume %)

C_2 = carbon dioxide concentration (volume %)

C_T = total pressure of gases (kPa)

d_B = molar density of solid reactant (mole m^{-3})

d_p = particle size diameter (μm)

D = diffusion coefficient ($m^2\ s^{-1}$)

D_{CO2} = diffusion coefficient of CO_2 ($m^2\ s^{-1}$)

E = activation energy (J/mole)

F = grain shape factor for solid reactant (-)

F_B = grain shape factor for second solid reactant (-)

h = index of reaction, constant used in Eqn. (2.35) (-)

i = constant used in Eqn. (2.35) (-)

k = overall rate constant (s^{-1})

k_1 = rate constant, used in Eqn. (2.1) ($kg^{-2/3}\ s^{-1}$)

k_2 = intrinsic rate constant for diffusion controlled kinetics ($m^2\ s^{-1}$)

k_3 = rate constant, used in Eqn. (2.20) (mol $s^{-1}\ m^{-1}$))

k_4 = rate constant, used in Eqn. (2.21) ($m^2\ s^{-1}$)

k_5 = rate constant, used in Eqn. (2.22) (s^{-1})

k_6 = intrinsic rate constant for reaction controlled kinetics ($m\ s^{-1}$)

k_7 = rate constant, used in Eqn. (2.11) ($m\ s^{-1}$)

k_8 = rate constant, used in Eqn. (2.11) ($m^3\ mole^{-1}$)

k_9 = intrinsic rate constant, used in Eqn. (2.32) (kPa^{-1})

k_{10} = intrinsic rate constant, used in Eqn. (2.33) (kPa^{-1})

k_{11} = intrinsic rate constant, used in Eqn. (2.34) (kPa^{-1})

k_{12} = rate constant, used in Eqn. (2.36) (s^{-1})

k_{13} = rate constant, used in Eqn. (2.37) (s^{-1})

k_{14} = intrinsic rate constant, used in Eqn. (4.14) (kg^{-1})

k_D = overall rate constant for diffusion controlled kinetics (s^{-1})

k_R = overall rate constant for reaction controlled kinetics (s^{-1})

K = overall rate constant, used in Eqn. (4.16) (s^{-1})

K' = equilibrium constant (-)

L = thickness of the sample (m)

m = constant in Eqn.(2.27) (-)

$Nb(\%)$ = niobium content in product at any time t (wt. %)

n = order of reaction (-)

n_e = number of unit cells per m^3 of bed (-)

p = number of reaction cells (-)

p_{CO2} = partial pressure CO_2 (kPa)

q = constant in Eqn. (2.22) (-)

r = radius of pellet, grain or particle (m)

R = universal gas constant (8.314 joules/g.mole K)

t = time (s)

T = reaction temperature (K)

T_C = pellet temperature (°C)

u = utilization factor (-)

v_T = pyrometer output voltage (v)

V_1 = carbon monoxide output voltage (v)

V_2 = carbon dioxide output voltage (v)

V_B = volume of a solid grain (m^3)

V_{tot} = total volume occupied by powder compact (m^3)

W = weight of unreacted oxygen in metal oxide(s) (kg)

$W°_c$ = initial weight of carbon in the pellet (kg)

$W°_n$ = initial weight of niobium pentoxide in the pellet (kg)

W_o = initial weight of oxygen in metal oxides (kg)

x = fractional conversion (-)

x_C = initial weight of carbon in pellet (kg)

x_p = fraction conversion when reaction cells begin to interpenetrate (-)

z = ratio (volume of product)/(initial volume of product) (-)

Z = volumetric reaction parameter, ($= 1-3V_{tot}/4\pi n_e r^2$)

GREEK NOTATIONS

α = relative molar quantity of solids (-)

β = ratio of solid reactants reactivities used in Eqn. (2.26) (-)

$\sigma_c°$ = initial mass concentration of carbon in the pellet (kg m^{-3})

μ = dimensionless modulus as defined by Eqn. (2.33) (-)

τ = dimensionless time (-)

θ = dimensionless factor used in Eqn. (2.35) (-)

ϕ = dimensionless modulus as defined by Eqn. (2.32) (-)

CHAPTER I

GENERAL INTRODUCTION

The Province of Quebec has a large reserve of pyrochlore ore which can be processed to give a pyrochlore concentrate containing 61 % niobium pentoxide. This pyrochlore concentrate is an important raw material for the production of ferroniobium which is used as a microalloying addition to steels. The niobium is viewed as the key ingredient in many HSLA steels. Ferroniobium is currently produced by the labour intensive alumino-thermic reduction of pyrochlore in massive reactors. A techno-economic study has shown that the carbothermic reduction of pyrochlore in a proposed plasma process may be competitive (Liang and Munz, 1981). The proposed plasma process would use Quebec's plentiful and inexpensive electricity in a transferred arc furnace. The ability to produce a commercial grade ferroniobium carbide alloy in a laboratory-scale Plasmacan furnace has been demonstrated by Hilborn (1988).

Plasma technology offers simple production techniques. The plant would be small but highly productive. It would require little labour, but would be highly energy intensive. It would be continuous in operation and would exhibit the unique ability of instantaneous start-up and shut-down, typical of plasma operations. The industrial application of such a process will require operational and kinetic data which are crucial to proper plant design. The literature on the carbothermic reduction of niobium pentoxide and/or pyrochlore in plasma systems is scarce and is

limited to qualitative studies.

The primary objective of this thesis is to study the kinetics of the carbothermic reduction of niobium pentoxide, available as the pure oxide or in pyrochlore concentrate, with and without the addition of iron in a transferred arc plasma reactor. The iron is used as a solvent for the dissolution of the niobium product. Since the use of pure iron is economically unacceptable in a commercial process, a preliminary investigation of the carbothermic reduction of pyrochlore and ferric oxide mixtures is also included in the scope of this work. To the author's knowledge, this is the first time that a kinetic study of this kind has been mentioned in the literature. As part of the project, a reactor system, complete with all auxiliary units, was constructed and commissioned. Measurement techniques were developed to provide the required kinetic data.

The thesis can be divided into four main parts which are contained in nine Chapters.

The first part comprises Chapters I to IV and consists of a statement of the objective and the organization of the thesis, a literature review of niobium and its production methods, plasma technology and its application to metallurgical processing, published studies on the reduction of metal oxides and ferroalloy production in plasmas, the theoretical treatments of solid-solid reactions, and finally the experimental apparatus and procedures.

The second part comprises Chapters V and VI and concerns the carbothermic reduction of niobium pentoxide and pyrochlore in the absence of iron.

The third part comprises Chapters VII and VIII and concerns the carbothermic reduction of niobium pentoxide and pyrochlore in the presence of iron.

The fourth part Chapter IX concerns the carbothermic reduction of mixtures of pyrochlore and ferric oxide. The mixture of pyrochlore and ferric oxide represents a more realistic feed for a commercial process.

It must be emphasized at this time that each of the five Chapters detailing the experimental results and discussion is completely self-standing. This organization of the thesis into five separate Chapters may lead to some overlap and repetition of ideas, but it is felt that it contributes markedly to the clarity of the presentation.

CHAPTER II

LITERATURE REVIEW

2.1 INTRODUCTION

The review of the literature is presented under the following four main headings:

1. Niobium and Related Important Compounds
2. Plasma Technology and Its Application to Metallurgical Processing
3. Metallurgical Reactions In Plasmas
4. Modelling of the Carbothermic Reduction Of Metal Oxides

Since ferroniobium is the most industrially utilized form for niobium, the first section provides a brief introduction to niobium and its derivatives which are of commercial importance. Some studies of niobium pentoxide reduction in plasma and other high temperature systems are also included here. The second section will look at plasmas as a high temperature heat source for metallurgical processing and gives an introduction to plasma generating devices and the types of plasma reactors which are of industrial significance. The third section will summarize the results of previous works which used plasmas for metallurgical reactions.

Finally, since the understanding and interpretation of a reaction is best obtained from its mathematical representation, the fourth section gives an overview of the theoretical models

representing non-catalytic heterogeneous reactions. Particular emphasis will be placed on those that are used to describe the carbothermic reduction of metal oxides.

2.2 Niobium and Important Related Materials

Charles Hatchet, an English chemist, identified niobium as an element distinct from tantalum in 1801 while examining a mineral sample from New England. However, he described it as columbium in honour of the New World in a paper subsequently presented to the Royal Society. A German chemist, Heinrich Rose separated the element in oxide form from tantalite in 1844 and renamed it niobium after Niobe, mythical daughter of Tantalus in Grecian mythology. `Niobium' was adopted as the official name by the International Union of Chemists in 1948, although the original name is still used in the United States of America, Canada and Mexico.

Niobium can be produced from four different compounds: niobium oxide, K_2NbF_7 and the chlorides $NbCl_5$ and $NbCl_3$. Detailed descriptions have been documented of the niobium metallurgy especially of extraction and reduction processes as well as powder metallurgical fabrication and consolidation by electron beam melting (EBM) (Miller 1959), (Kieffer and Braun, 1963), and (Winkler and Bakish, 1971).

One of the very important recent uses of niobium, which takes advantage of its high melting point (2740 K) and resistance to heat, is the production of heat resistant alloys for rocketry equipment, jet planes and gas turbines. Niobium is also used in

superconducting alloys, is of major interest as a construction material in nuclear technology and is used in the manufacture of corrosion-resistant apparatus for the chemical industry. Other areas of applications are in the vacuum tube industry as gas absorbers (getters) used to maintain the high vacuum and in the manufacture of cryotrons which are better switches in electronic computers than vacuum or semi-conductors.

Niobium carbide forms part of certain ultra-hard and refractory alloys and cast carbides. But, the major area of application for niobium is the manufacture of stainless, heat, corrosion resistant, and tool steels. It is also used in high-coercivity magnetic alloys and for alloying aluminium, copper, molybdenum, and zirconium. Presently, the use of niobium as a microalloy by far dominates the consumption picture (Stuart, 1981). The major areas of application for niobium-microalloyed high strength low alloy (HSLA) steels are found from high-pressure pipelines through ship-plate, truck frames and automobiles. To demonstrate the present usage pattern, reported end uses as metal and alloys in fabricated form for the United State in 1985 were: construction 40 %, transportation 27 %, and oil and gas industries, machinery, and others, each 11 %. This was equivalent to a consumption of 3500 tonnes of niobium and 2500 tonnes of ferroniobium. Growth in worldwide consumption is estimated at 5 % per year through 1990 (Engineering and Mining Journal, 1986). Much of the niobium destined for steel consumption is produced in the form of ferroniobium which is used in carbon, stainless and HSLA steels to improve corrosion resistance and increase high tempera-

ture strength. The niobium content in these materials is usually in the range 0.025 to 0.1 %.

The use of niobium in stainless steel is nearly always to produce niobium carbide to either remove carbon, which would otherwise form the detrimental chromium carbide, or to create a precipitation hardening dispersion of carbides (Keown and Pickering, 1981). The former is important in corrosion resisting stainless steel and the latter in heat resisting stainless steel.

2.2.1 Source of Niobium

The major niobium ores used for ferroniobium production are columbite, $(Fe,Mn)(Nb,Ta)_2O_6$ and pyrochlore $(Na_2,Ca)(Nb,Ta)_2O_6F$, the latter of which was used in this work. The three principal producers of pyrochlore in the world are Companhia Brasileira de Metalurgia e Mineracao (CBMM), Mineracao Catalao Goias and Niobec Inc.. CBMM is the largest producer and supplier of niobium materials to the world market. Niobec Inc produces its pyrochlore concentrate from its deposit in Ste. Honore, Quebec, Canada. The concentrate contains typically about 62 % Nb_2O_5.

2.2.2 Production Of Ferroniobium

Practically all the commercial alloy requirements are met by the alumino-thermic process, which reduces the niobium oxide completely. Occasionally the alloy is produced in an electric furnace by reduction with carbon or ferro-silicon.

2.2.2.1 The Alumino-thermic Reduction Process

The alumino-thermic reduction of pyrochlore results in a pure product without the addition of external heat (Belitskus, 1972), (Filho and de Fuccio, 1981), (Pinkus and Guimaraes, 1981).

Since the ultimate use of the product metal is alloying of steel, the metal is produced as an alloy with iron. The lower melting point of the ferroniobium aids in metal-slag separation.

Alumino-thermic reduction is a batch process. The charge includes the pyrochlore concentrate, aluminium powder, iron scrap or powder and/or iron oxides such as natural hematite (Fe_2O_3) or mill scale (Fe_3O_4), usually a flux, and often a thermal booster (Filho and de Fuccio, 1981), (Belitskus, 1972). The reaction is initiated by applying a flame or pouring a small quantity of water onto a "fuse" mixture of sodium peroxide and aluminium. The reaction vessels are usually steel cylinders up to 1.5 m in diameter and depth, and lined with magnesite refractory bricks. The reaction time averages about ten minutes. After the reaction is complete, part of the molten slag is tapped, the remainder is used to protect the metal from oxidation during cooling and solidification. The metal is then cooled, the slag is broken away and the ferroniobium is crushed. The final product contains 50 - 70 % niobium by weight, 4 % silicon and 0.5 % carbon.

The ferroniobium product from the alumino-thermic reduction of pyrochlore is dependent on the charge preparation, the cooling period and the mechanical treatment of the final product rather than the reduction time. The process is extremely labour intensive. In addition, the cost of aluminium for the reduction reaction is close to $1.00(Can)/kg Nb higher than that of carbon.

2.2.2.2 Specifications of Commercial Ferroniobium

The ASTM specification for low alloy ferroniobium is shown in Table 2.1. Typical compositions of ferroniobium and slag pro-

Table 2.1 ASTM Specification of Low Alloy FeNb (60-70% Nb)

Elements	Max wt.%
Ta	5
C	0.5
Mg	3
Si	4
Al	3
Sn	0.25
P	0.1
S	0.1
Cr	1
W	1
Ti	1
Pb	0.25
Co	0.25

Source: ASTM Designation: A 550-73, "Standard Specification for Ferro Columbium," 1978, pp348-349

duced by CBMM are shown in Table 2.2. Traditionally the carbon content of the ferroniobium is low (<0.5 weight %). But, the feasibility of using a high carbon ferroniobium alloy could be considered since the alloy represents a minor alloying agent (<0.15 %) in most steels. It is quite possible that the current specifications on ferroniobium are an artifact of the existing alumino-thermic reduction process.

2.2.3 Alternate Routes for Niobium / Niobium Carbide / Ferroniobium Production

The high temperature of plasmas makes them ideal for melting and smelting refractory metals or processing hard-to-reduce metal oxides. It was this characteristic that initially attracted the interest into the carbothermic reduction of these types of compounds in a plasma system. A search of the open literature revealed that little or no experimental work or kinetic study on the plasma reduction of pyrochlore has been reported. Only the articles that are of particular interest to this work will be presented in this section.

2.2.3.1 Niobium

Goldsmith et al. (1971) investigated the carbothermic reduction of chemical grade niobium pentoxide in a high intensity arc. The process, pioneered by Sheer et al. (1963), involves the use of a high intensity arc in which the niobium pentoxide and carbon, in stoichiometric proportion, are incorporated into the anode. The anode is then consumed or eroded by the reaction occurring at the face of the electrode upon which the discharge

Table 2.2 Typical Chemical Analysis of CBMM Ferroniobium and Slag

Element	Ferroniobium wt.%	Compounds	Slag wt.%
Nb	66.0	Al_2O_3	48
Fe	30.5	CaO	25
Si	1.5	TiO_2	4
Al	0.5	BaO	2
Ti	0.1	Re_2O_3	4
P	0.1	(Rare Earth	
S	0.04	Oxides)	
C	0.08	Nb_2O_5	Traces
Pb	0.02	U_3O_8	0.05
		ThO_2	2

Source: Filho and de Fuccio (1981).

terminates. Vacuum conditions were employed to remove the excess carbon and oxygen in the metal product. The anode carbon content was varied between 17.70 - 18.02 wt. %; stoichiometric carbon requirement for the reduction of niobium pentoxide is 18.4 %. Vacuum conditions were not required for the reduction reaction but were necessary to meet target product purity specifications.

Akashi et al. (1973) obtained high purity niobium metal (Nb=99.4 %, C=0.31 %) from the carbothermic reduction of pure niobium pentoxide (molar ratio Nb_2O_5/C = 1:5) at temperatures higher than 2870 K under argon or argon-hydrogen (5-20 %) plasma arcs. They found that most of the carbon and oxygen in the sample were removed rapidly through the reaction at the interface between molten niobium pentoxide and solid carbon. Electron beam remelting under high vacuum was needed to improve the purity of the plasma arc product. The reduction rate of the sample was estimated through continuous semi-quantitative chromatographic determination of carbon monoxide content in the exhaust gas. The carbon monoxide content in the exhaust gas reached a maximum within the reaction period of 1 minute. Reactions were studied for periods of up to 20 minutes. A simplified reaction kinetic model was used to describe the reaction between spherical carbon particles and molten niobium oxide. The niobium content of the sample at any time, t, during the reaction was expressed by the equation:

$$Nb(\%) = 69.3\ W^{\circ}_n/(0.699\ W^{\circ}_n+2.332\ W^{\circ}_c(1+k_1W^{\circ}_c{}^{2/3}t)^{-3/2}) \qquad (2.1)$$

where Nb(%) is the niobium content (wt. %) in the product at any

time t, t is the reaction period since the beginning of the reaction, W°_n and W°_C are the weights of niobium pentoxide and carbon in the sample at t=0, respectively, and k_1 is a constant related closely to the rate constant of the interfacial reaction, surface area of the carbon particle and its grain size. The niobium recovery reached 85 %.

Moiseyev et al. (1981) also studied the carbothermic reduction of 'technically pure' niobium pentoxide in argon and argon-hydrogen (0.3 - 0.38 wt. %) plasma arc. The reduction of niobium pentoxide with carbon (18.4 - 24.0 wt. %) was examined in the temperature range 1500 - 4000 K. The highest niobium recovery (98 - 99 %) in the metallic product was reported to take place at 3400-3600 K. The reacting mixtures were contained in a graphite crucible. It was found that for the case of an argon plasma, any oxygen or nitrogen that might be present in the argon contaminated the product. The argon-hydrogen plasma removed oxygen and nitrogen from the sample and facilitated carbide formation. This was attributed to the fact that the hydrogen, which dissolves in niobium, deoxidizes it and eliminates the film of nitrides, the presence of which would normally prevent carbide formation. The carbon content in the product for the argon/hydrogen plasma varied between 3.5 to 4.8 wt. %.

Mimura et al. (1985) investigated the carbothermic reduction of niobium pentoxide in an argon plasma at about 2900 K. The carbon to niobium pentoxide mole ratio was varied between 4.8 and 5.1. Reduction proceeded rapidly with melting of each pellet, but the elimination of carbon and oxygen as carbon monoxide degassing

proceeded slowly in the Nb-C-O molten state. A niobium product of above 99 % purity was obtained after a reaction time of 12 minutes. The carbon and oxygen content in the reduced niobium product was dependent on the carbon to niobium pentoxide mole ratio. It was suggested that it would be able to adjust the carbon/oxygen ratio in the final product by changing the carbon to niobium pentoxide mole ratio in the initial reacting mixture. The product obtained from the reduction step was then refined with electron beam melting. Deoxidation was found to be possible through the evaporation of NbO and /or NbO_2, but decarburization as carbon monoxide degassing was possible only when excess oxygen was present in the reduced niobium product. Electron beam refining of the reduced product from a pellet mixture containing a carbon to niobium pentoxide mole ratio of 4.9, gave ductile high-purity niobium with carbon and oxygen content of 20 and 70 ppm, respectively.

The carbothermic reduction of niobium oxide in high temperature vacuum furnaces has also been studied by several workers (Ono and Mariyana, 1973), (Suri and Gupta, 1978), (Ono et al., 1980).

Ono and Mariyana (1973) investigated the carbon and oxygen contents in crude niobium metal obtained by different reduction conditions in a high temperature vacuum furnace. The carbon to niobium pentoxide (99.9 %) mole ratio was varied between 4.9:1 and 5.1:1, reaction temperatures were between 2075 - 2175 K, operating vacuum conditions were in the range 0.0016 - 0.021 kPa, and annealing times were between 120 - 200 minutes. The results

showed that carbon (0.20 - 0.44 wt. %) content was always larger than that of oxygen (0.05 - 0.23 wt. %). They also showed that the C/Nb_2O_5 mole ratio had no effect on decarburization of niobium metal. Ono and Mariyana (1973) reasoned that the carbon potential in their graphite-heated vacuum furnace could not be controlled.

Suri and Gupta (1978) investigated the production of a pure niobium metal via a two-step process involving first the preparation of niobium carbide followed by the interaction of carbide and oxide. The niobium oxide was mixed with varying amounts of carbon (31.6 to 32.6 wt. %), pelletized and placed into the furnace in a graphite crucible. The reaction temperature was varied between 1925 to 2025 K, the annealing time was in the range 15 to 45 minutes and the vacuum varied between 1.07×10^{-5} to 2.00×10^{-5} kPa. The niobium carbide product analysis showed total carbon in the range 9.47 to 11.45 wt. %, free carbon was between 0.1 to 0.4 wt. % and oxygen was from 0.30 to 0.86 wt. %. Total metal recovery as carbide was between 98.6 to 99.8 wt. %. For preparing the niobium metal in the second step, the mixture of niobium pentoxide and carbide was such as to give an oxygen-to-carbon ratio of between 1.010 to 1.185. Reaction temperature was varied between 2275 to 2325 K, with heating for 90 minutes under a vacuum of 2.6×10^{-6} kPa. A niobium metal purity of over 99.5 % was obtained for a oxygen to carbon ratio of 1.03. Reaction charges with ratios other than 1.03 yielded a less pure metal product.

Ono et al. (1980) investigated the carbothermic reduction of niobium pentoxide in a vacuum furnace with a graphite heating

element. The carbon to niobium pentoxide mole ratio was 5:1. They showed that the reduction process is divided into two steps. The main reduction occurs with the evolution of carbon monoxide. The refining period occurs later, once the reduction is almost complete, and then only the decomposition of residual sub-oxides and carbides takes place. The resulting oxides and carbides are then refined to a homogeneous Nb-C-O solid solution in a porous, sintered form. Further refining of the niobium metal obtained by carbothermic reduction was performed in an electron beam furnace. Previous tests in the vacuum furnace confirmed that final purification of the niobium metal obtained by carbothermic reduction in the electron beam furnace occurred through carbon and oxygen removal as carbon monoxide as well as volatilization of niobium suboxides such as NbO and NbO_2. Therefore, in practice, it is preferable to produce the niobium containing an excess oxygen by the carbothermic reduction and subsequently eliminate the residual oxygen by volatilization of suboxides in the electron beam furnace.

2.2.3.2 Niobium Carbide

Matsumoto and Saito (1974) studied the preparation of niobium carbide by the carburization of niobium pentoxide with graphite in an argon plasma. The niobium pentoxide (99.9 % + pure) and graphite were mixed in the desired molar ratios ($5 < C/Nb_2O_5 < 8$) and baked at 1374 K in a reducing atmosphere provided by graphite powder packing. X-ray diffraction patterns and chemical analysis showed that the product was mostly stoichiometric NbC, although NbC and Nb were also identified when the C/Nb_2O_5 ratio

was equal to 5 and 6. Carbon monoxide was the only gaseous product detected with a gas chromatogram. The reaction was affected by C/Nb_2O_5 molar ratio, current and reaction time. Total conversion was obtained for reaction times greater than 3 minutes. The optimum C/Nb_2O_5 molar ratio was 7 and the overall reaction was given by:

$$Nb_2O_5 + 7C = 2NbC + 5CO \qquad (2.2)$$

Shimada et al. (1983) studied the formation of niobium carbide by solid state reaction of niobium pentoxide (99.9 %) with carbon at temperatures of 1275 to 1560 K. The carbon sources were active carbon and graphite. The mixture of the oxide and carbon powders with C/Nb_2O_5 molar ratios of 7 to 12 was contained in an alumina or graphite boat and reacted for 120 minutes at a specific temperature. A flowing atmosphere of argon or argon and hydrogen was maintained in the furnace. X-ray diffraction analysis showed NbC as the main product. The results showed that pure hydrogen did not give a higher conversion than pure argon. Increasing the molar ratio of C/Nb_2O_5 and covering the graphite crucible greatly improved the rate of conversion to niobium carbide. X-ray diffraction analysis of the product obtained for different reaction times pointed to the following reaction mechanism:

$$Nb_2O_5(S) + C(S) = 2NbO_2(S) + CO(g) \qquad (2.3)$$

$$NbO_2(S) + 3C(S) = NbC(S) + 2CO(g) \quad (2.4)$$

The unexpected beneficial effect observed when the crucible was covered, was attributed to the following reaction mechanism:

$$Nb_2O_5 + CO(g) = 2NbO_2 + CO_2(g) \quad (2.5)$$

$$NbO_2(S) + 4CO(g) = NbC(S) + 3CO_2(g) \quad (2.6)$$

The CO_2 formed in equations (2.5) and (2.6) would be immediately converted to CO by reaction with the excess carbon present in the graphite crucible:

$$CO_2(g) + C = 2CO(g) \quad (2.7)$$

They found that the rates were best fitted by first order kinetics in which "nucleation" is the rate-determining step and was expressed by the equation:

$$\ln(1-x) = -kt \quad (2.8)$$

where x is the fractional conversion, k is the rate constant and t is time. The activation energy for NbC formation was determined to be 376.4 kJ/mol from Arrhenius plots.

2.2.3.3 Ferroniobium

Following their successful attempt at producing ferrovanadium by the carbothermic reduction of vanadium oxide in an

argon/hydrogen plasma (MacRae et al. 1976), the Bethlehem Steel Corporation (Gold et al. 1977) also included the reduction of niobium, manganese and chromium oxides in their experimental program. However, no information has been published in these areas.

Nagamori and Plumpton (1985) studied the reduction of a low grade concentrate, containing 1.8 wt. % TaO and 13.7 wt. Nb_2O_5, by carbon at 1875 K in a resistance furnace. The niobium and tantalum were selectively absorbed in liquid iron. The amount of carbon was varied from 10 to 40 wt. %. The optimum level of excess carbon for good metal recovery was found to be 10 wt. %. Metallic iron addition was such that the combined contents of the carbides did not exceed 20 wt. % in the ferroalloy. To slag off the gangue rich in zirconia (13.4 % in the concentrate), silica and lime were added as flux. A dilution ratio ($\%SiO_2$ + %CaO)/ $\%ZrO_2$ greater than 6 was required to achieve phase separation. To ensure good metal recovery, a high silica slag is desired to tie down Na_2O in the slag, thus freeing Nb_2O_5 (and Ta_2O_5) from Na_2O and so facilitating the reduction of the Nb_2O_5 by carbon. It was found that a high temperature (1975 K) not only provides a faster reaction rate but also produces less viscous melts which in turn ensure a more rapid settling and a better phase separation. Up to 95 % of the niobium was recovered in the metal.

Liang and Munz (1981) carried out a techno-economic assessment on the carbothermic reduction of pyrochlore in a thermal plasma reactor to produce a 70 % ferroniobium. The overall process flow sheet is shown in Figure 2.1. The results of the analysis showed that the process was marginally profitable under the

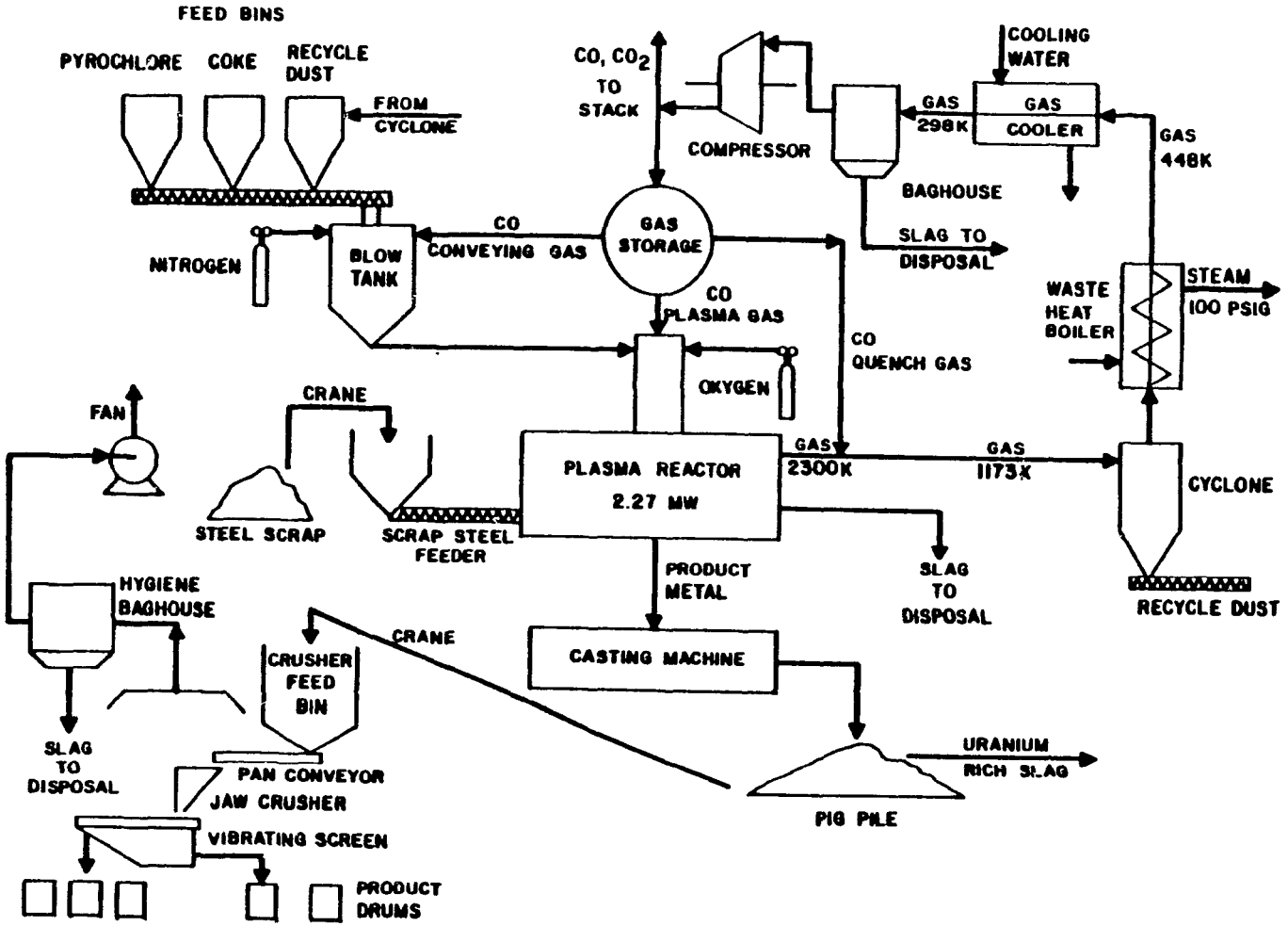

Figure 2.1 Flow Sheet of the Ferroniobium Production Plant as Proposed by Liang and Munz (1981)

assumptions made having a discounted cash flow rate of return of 26.4 %. The process was sensitive to capital cost and product added value but insensitive to other variables. Since little or no experimental work was available on the plasma reduction of pyrochlore, several major technical assumptions were made. Some of these include the degree of conversion from pyrochlore to ferroniobium which can be obtained in the plasma reactor and the ability to refine the molten product by controlling the partial pressure of oxygen in the reactor. The niobium/niobium carbide produced would then be dissolved in iron to obtain a ferroniobium product. Liang (1982) had expressed some concern about the use of carbon monoxide as a plasma gas. Although carbon monoxide has been successfully tested with hydrogen in the Westinghouse arc heater (Fey 1976), and used as a plasma gas (Schnell et al 1978), (Rains and Kadlec 1970), (Eriksson et al. 1983), (Camacho 1977), its operational characteristics are not available in the open literature.

Hilborn (1988) investigated the carbothermic reduction of a pyrochlore concentrate (62 % Nb_2O_5) in iron in a 50 kW Plasmacan furnace. Optimum conversion (34 %) was obtained with a specific energy of 8 kWh/kg, C/Nb_2O_5 mole ratio of 7 and Nb/Fe weight ratio of 0.18. Increasing C/Nb_2O_5 ratio did not improve conversion but caused it to decrease. The explanation for this observation was that any carbon in excess of the saturation limit of the iron present in the reaction mixture, remained as a solid and was unavailable for reaction at the liquid iron-liquid oxide interface. This also interfered with the formation of a molten film

which is the primary reaction site in the Plasmacan furnace. X-ray diffraction analysis showed that the metal product in the crucible consisted of iron, NbC, iron carbides, trace graphite, and was devoid of oxides. The slag was distinct from the metal and consisted of melted pyrochlore with iron, NbC, and graphite. The results suggested that ferroniobium of commercial grades could be made in this type of furnace if sufficient time and energy is available for the completion of the reaction. Batch experiments showed that complete conversion to NbC is possible in a furnace.

2.2.4 CONCLUSION

Niobium has emerged from its position as a scarce exotic metal to a position of great importance in the world's steel industry. Most of the niobium used in steel is produced as ferro-niobium, nearly all of which is produced by the labour intensive alumino-thermic process. The development of a plasma process for the carbothermic reduction of pyrochlore would offer the advantage of a smaller more efficient plant. Its labour costs would be low, as would the costs of reductants, but the plant would be highly energy intensive. Continuous feeding operation would allow the rapid start-up or shut-down, typical of plasma operations. Environmental problems would be minimal since the process would be totally enclosed and almost noiseless.

Little or no experimental work on the carbothermic reduction of pyrochlore with and without iron additions in a plasma medium has been reported in the literature. Such work is required for the rational design of a plant based on the proposed process.

The conversion-time relationships for the carbothermic reduction of niobium pentoxide under non-plasma conditions have been successfully correlated by a nucleation or homogenous model.

2.3 Plasma Technology and its Application to Metallurgical Processing.

2.3.1 Introduction

Interest in the application of plasma technology to chemical and metallurgical processing has been increasing rapidly since the availability of commercial plasma-generating devices capable of reliable performance at powers as high as 30 MW. The specific application usually dictates the type of plasma generating device used. Many plasma reactors for metallurgical processes utilize transferred arcs in order to take advantage of the enhanced thermal efficiency offered as a result of the heat transferred at the arc root to their anodic molten bath.

A short review on the application of thermal plasma and plasma reactors and furnaces to extractive metallurgy, with particular attention to its use for the reduction of oxide ores and for producing ferroalloys will be presented.

2.3.2 Description of Plasmas

A gas at room temperature usually has two or more atoms combined. When the gas is heated, the molecules dissociate into individual atoms at about 2300 K. At still higher temperatures, at about 3300 K, some of the electrons are displaced from the atoms forming ions and the plasma state is reached (Upadhya et al. 1984).

Plasmas are divided into cold plasma (pressure < 100 torr) and thermal plasma (100 torr < pressure < 10 atm) (Fauchais et al., 1983). Thermal plasmas, i.e. plasmas which approach a state of local thermodynamic equilibrium (LTE), formed by electrical discharges typically have temperatures between 2,000 and 15,000 K, and are at atmospheric pressure. These are the most applicable to high-temperature chemical and metallurgical processing, and for the purpose of this review, further discussion of plasmas will be limited to this type.

A dc arc can be divided into three regions. The anode region, adjacent to the anode surface, the cathode region, adjacent to the cathode, and the arc column generated between the two. The voltage gradients near both the anode and cathode surfaces are very steep (particularly near the anode) while that of the arc column is in general less steep and constant with arc length. This is shown in Figure 2.2. The nature of the arc voltage characteristics in all three regions is a function of the anode and cathode materials, plasma gas, gas velocity, arc current and arc stabilization. Choi (1981), Pfender et al (1987) and Parisi (1988) give an extensive review of the pertinent theory and relevant literature dealing with these regions of the arc.

The choice of plasma gas is important. The gases used in most plasma generators are: argon, helium, nitrogen, hydrogen, oxygen, air, carbon dioxide, and methane (Fauchais et al., 1983), (Bhat ,1972). The characteristics of an argon transferred-arc plasma have been studied in detail by Choi and Gauvin (1982) and Mehmetoglu and Gauvin (1983). Similar work was also done for

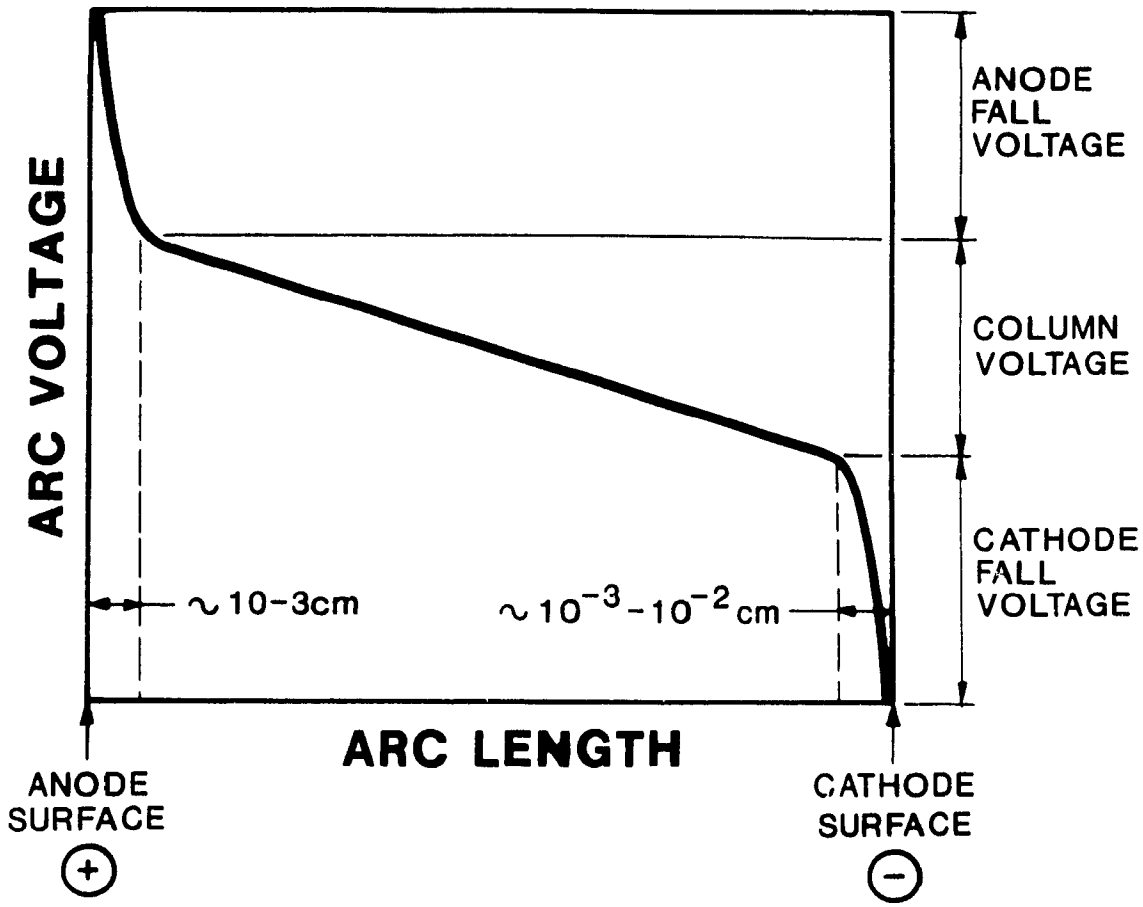

Figure 2.2 The Three Regions of a Transferred-Arc

nitrogen as the plasma by Tsantrizos and Gauvin (1982). Some properties of interest in selecting a gas are listed in Table 2.3 (Bhat, 1972). If long anode and cathode service life is desired, inert gas must be used to prevent reaction with the electrodes. If a low-voltage power supply is desired, a mono-atomic gas must be used. Diatomic gases, like hydrogen, raise the voltage of the arc and permit the use of higher power without an appreciable increase in the current levels. Cathode erosion is proportional to arc current raised to the power n, where n could reach 1.6 (Guile, 1984). In industrial installations where both operating cost and long service life of electrodes are necessary, the choice is an inexpensive inert gas.

2.3.3 Plasma Devices

The discharge which is used to create thermal plasmas may be due to inductive or capacitive coupling or as is most common by striking an arc between two electrodes in the presence of a plasma forming gas. The three principal methods for generating thermal plasmas are shown in Figure 2.3. Induction plasma generators have the advantage of achieving high purity plasma flames but are generally low in efficiency and expensive to operate (Boulos et al., 1980), (Pfender, 1987).

Arc plasma generators are most commonly used, especially in metallurgical processing and at higher power levels. They may be roughly classified as transferred arc or non-transferred arc devices depending on whether the second electrode is external to the plasma torch or not (see Figure 2.3). In transferred arc devices, the external electrode often forms the workpiece or

Table 2.3 Properties of Gases Used in Plasma Applications

Gas	Dissociation Energy (Kcal/gmole)	Particle After Dissociation	Ionization Voltage (volts)	Open Arc Voltage[1]	Arc Temp. (K)	Heat Content of Gas[2] (Watts/ft.^{3}[NTP])
Ar	0	Ar	15.68	18	10300	75
He	0	He	24.46	26	15300	110
H_2	104	H	13.53	70	8600	260
O_2	110	O	13.55	40	9200	425
N_2	225	N	14.48	40	9200	425
Air	---	--	--	60	9200	425

1. Constant arc length and power
2. 10% thermal ionization
Source: Bhat, 1972

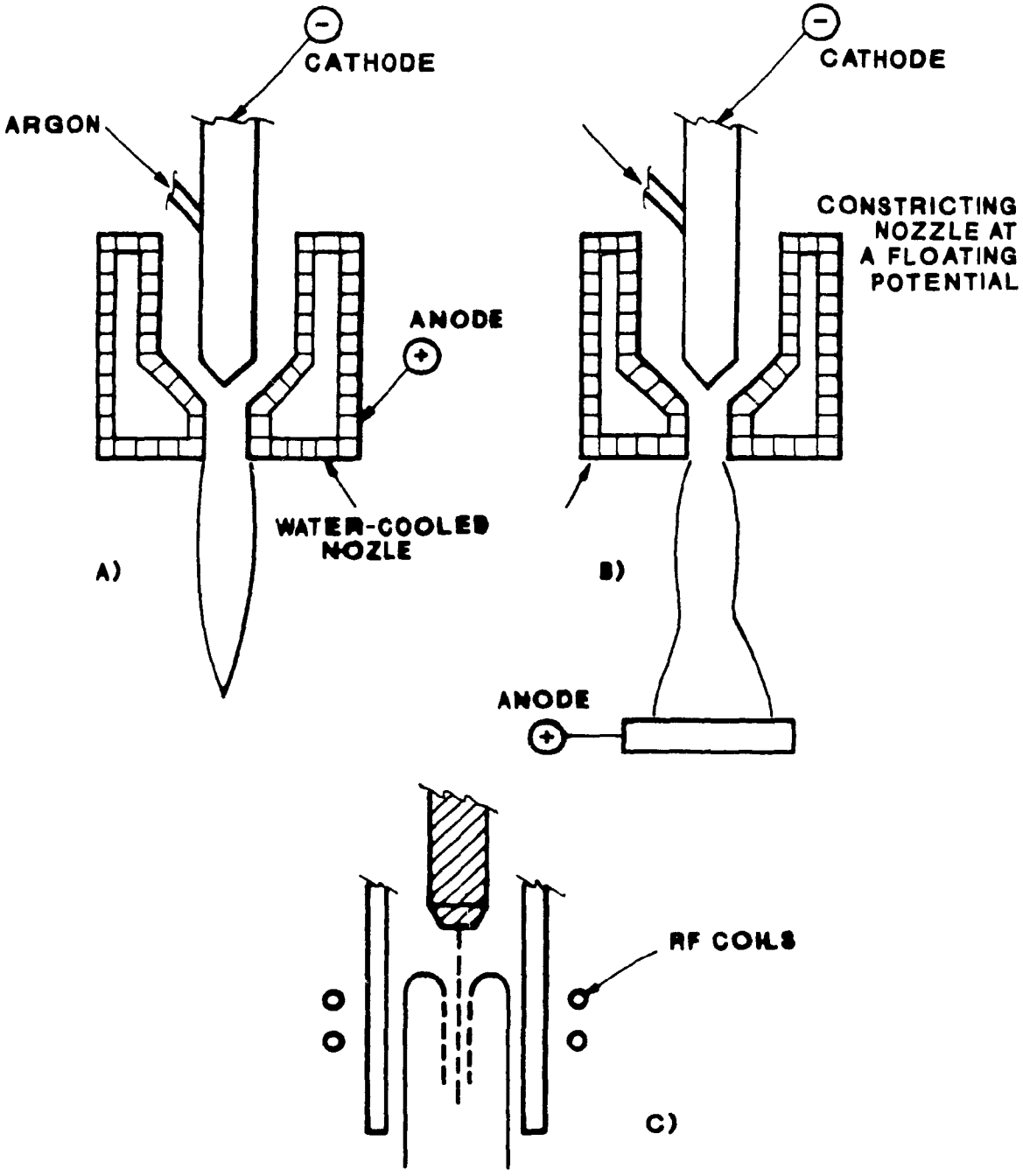

Figure 2.3 Three Principal Methods For Generating Thermal Plasmas
(a) Non-Transferred Arc
(b) Transferred Arc
(c) Induction-Coupled

material to be treated. The efficiency of this device is generally higher than the non-transferred plasma torch because the heat transferred to the anode contributes to the process and is not lost as in non-transferred devices. Also, transferred arc generators allow the energy in the plasma gas to be continuously renewed while in the presence of the reactants and thus minimizes the effects of localized quenching of the plasma gas.

Gauvin et al. (1981) and Fauchais (1983) have reviewed the use of plasmas for high temperature heterogeneous systems for both laboratory and industrial applications. The consensus was that transferred arcs do have higher thermal efficiency than other plasma generating devices, and thus offer the most promising approach to the design of commercial reactors.

2.3.4 Electrode Materials

Three materials commonly used as electrodes in plasma torches are graphite, tungsten and copper.

Graphite requires no cooling. However, the graphite electrode is consumed in the plasma generation process and, therefore, some type of electrode feeding mechanism is required. The consumed graphite electrodes may be a source of contamination of the plasma stream. Graphite electrodes cannot be used with an oxidizing gas.

Copper is used both as an anode and cathode in plasma devices. But, requires a very efficient cooling system.

Tungsten is more commonly used as a cathode, but rarely used as an anode in plasma devices. Tungsten is compatible with all inert gases and hydrogen, but suffers severe erosion in an oxi-

dizing atmosphere. The excellent thermionic emission and high melting point of tungsten makes it an ideal cathode material. Copper is the anode material commonly used with a tungsten cathode. Experiments with air have shown that it is possible to use zirconium or hafnium cathodes, whose thermo-emissive oxides are slightly volatile, with an oxidizing plasma gas (Fauchais et al., 1983).

Laboratory scale plasma torches usually use tungsten cathodes since under inert conditions their erosion rates are least and their control is the easiest. Large industrial devices usually use copper electrodes.

2.3.5 Plasma Reactors and Furnaces

The reduction/smelting processes represent some of the most promising applications for plasmas from the stand point of both tonnage and electric power consumption. Plasma based processes for iron-making have been demonstrated in the laboratory and in pilot plants with both transferred arc and non-transferred arc concepts. The use of plasma energy in ferroalloy production has received the most attention, because the process generally requires a high energy per unit of product (endothermic reaction) with the bulk of this energy at a relatively high temperature (ie high enthalpy).

The latest designs of plasma furnaces which are currently being utilized on either a laboratory or industrial scale and which could be applicable for ferroniobium production, as proposed by Liang and Munz (1981), will now be reviewed. A partial list of the large capacity installations currently in operation

or in construction around the world is presented in Table 2.4 (Gauvin et al., 1987). General reviews on the latest developments in design and operation of plasma devices and reactors have been done by Barcza and Stewart (1983), Gauvin and Choi (1983), Drouet (1984), Barcza et al. (1985), Fauchais (1985), Flemings (1985), Feinman (1987), Gauvin et al. (1987) and Parisi (1988) to name but the most recent.

One system that has given reliable performance but which does not utilize a transferred arc was developed by SKF in Sweden and is shown schematically in Figure 2.4. In this system, the plasma flame from a tubular torch, is fed together with a stream of pre-reduced fine mineral particles mixed with pulverized coal through a tuyere at the base of a low-shaft blast furnace filled with coke. The reaction chamber consists of a cavity, about half a metre in diameter, dug by the plasma flame into the bed of coke. Although the temperature levels are quite low (the torch basically operates as a gas heater), the overall energy utilization of the plasma flame is quite high, and coke consumption is reduced through the use of coal as a reductant.

The Freital plasma system is shown in Figure 2.5 and consists of four plasma torches (Plasmatrons) mounted around the side of a furnace at an angle of about 30 degree from the horizontal (Barcza, 1987). The Plasmatrons are of the water-cooled, non-consumable electrode, transferred-arc type with tungsten cathodes. Control of the arc length is achieved by axial movement of the torches which can be completely retracted from the furnace for maintenance. This technology is marketed by Voerst-Alpine.

Table 2.4 High Capacity Iron and Steel Plasma Installation

Product	Company	Process	Capacity
Iron Direct Reduc.	SKF Sweden	SKF Torches Gas Reforming	6 MW 72 000 tpa
Iron Direct Reduc	USCO South Africa	Huels Torches Gas Reforming	3X8 MW 320 000 tpa
Pig Iron	Cockerill Belgium	Westinghouse Arc Super-Heated Blast	3.5 MW 1 TUYERE
Pig Iron	SKF Sweden	Coke-Filled Shaft SKF Torches	7X6 MW 250 000 tpa
Pig Iron	ASEA South Africa	Transferred Arc Graphite Cathode	40 MW 600 000 tpa
Steel	Mannesmann GHH West Germany	Transferred Arc Graphite Cathode	6 MW 15-ton
Steel	ASEA/Krupp West Germany	Transferred Arc Graphite Cathode	18 MW 55-ton
Steel	Veb Edelstahlwerke Freital, GDR	Transferred Arc Multiple Torches	3X3 MW 10-ton
Steel	Veb Edelstahlwerke Freital, GDR	Transferred Arc Multiple Torches	4X3 MW 30-ton
Steel	Voest Alpine Linz Austria	Transferred Arc Multiple Torches	4X7 MW 45-ton
Ferro-chromium	Middleburgh St. & Al., South Africa	Transferred Arc Hollow Graphite Cat.	20 MVA 50 000 tpa
Ferro-chromium	SKF Sweden	Coke-Filled Shaft SKF Torches	4X6 MW 60 000 tpa
Ferro-manganese	Samancor South Africa	Transferred Arc	10.8 MVA 30 000 tpa
TiO_2 Slag	Richard's Bay Mining, South Africa	Graphite Electrodes A C Transferred Arc	6X10 MW 500 000 tpa

SOURCE: Gauvin et al., 1987

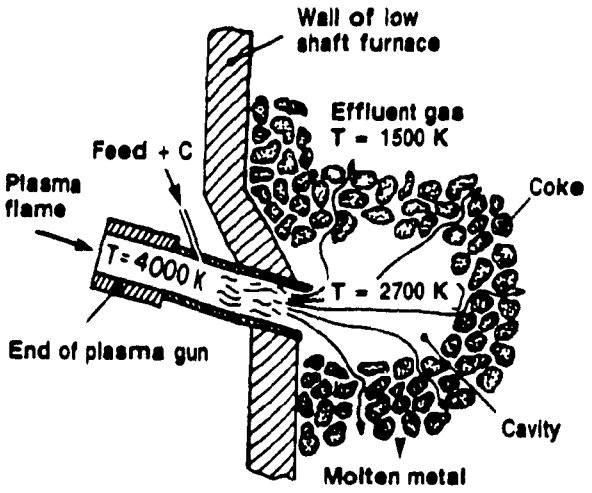

Figure 2.4 SKF's System

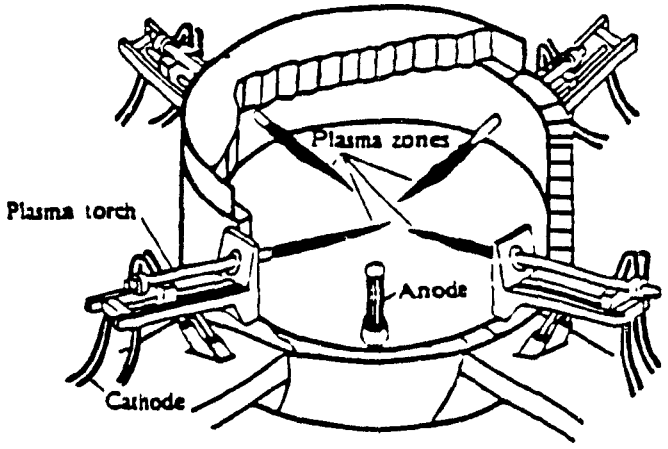

Figure 2.5 The Freital/Vorst Alpine Steel Scrap Melting Furnace

The use of a laboratory closed-hearth, extended carbon arc furnace, commonly referred to as the Extended Arc Flash Reactor (EAFR), for the reduction of many types of oxide ore fines, has been developed at the University of Toronto (Pickles et al., 1977). The EAFR plasma system was patented by Segsworth and Alcock (1977) and is shown in Figure 2.6. This design has many advantages provided that the feed material is not too fine and carbon contamination from the electrodes can be tolerated. It is now being tested for the treatment of waste dust and fines at the Ontario Research Foundation, Mississauga, Ontario, in a reactor rated at 1 MW (Sommerville et al., 1986).

Curr et al. (1983) of Mintek in South Africa recently described an experimental 100-KVA furnace shown in Figure 2.7, with a hollow graphite cathode, through which a mixture of argon and nitrogen was passed as the plasma gas. Based on this work, Middleburg Steel and Alloys has built and has been operating a 20-MW plasma furnace since October 1984. It was described in detail by Barcza (1984)

A combined induction-plasma furnace, shown in Figure 2.8, has been developed in Japan by Daido Steel Co. (Asada and Adachi, 1971). The plasma torch supplements the energy of the induction coil. Bhat (1981) has described a 1-tonne furnace of this design and its use by Daido Steel Co. for producing a range of alloys which includes ultra-low carbon steels, high delta-ferrite stainless steels and alloys, electric magnetic materials and non-ferrous alloys. Tezuka et al. (1974) described its use for the melting of nickel base alloys.

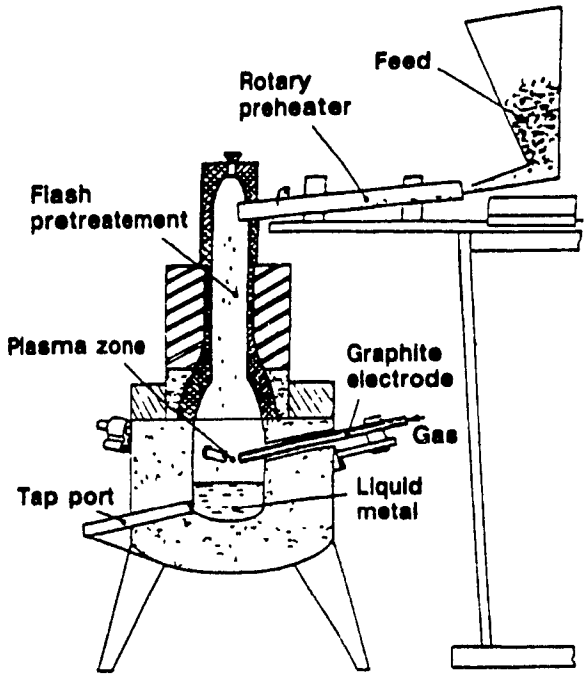

Figure 2.6 University of Toronto Furnace

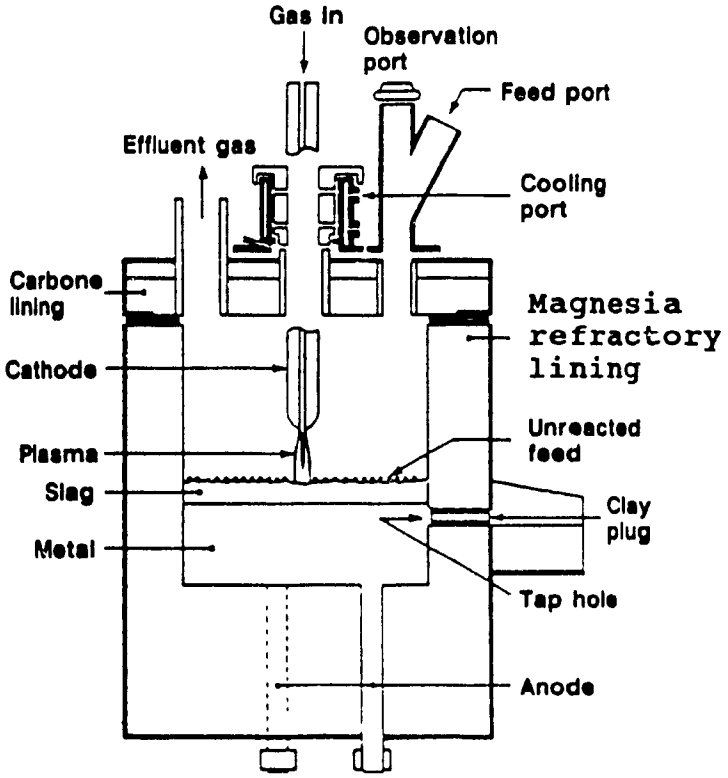

Figure 2.7 Mintek's Furnace

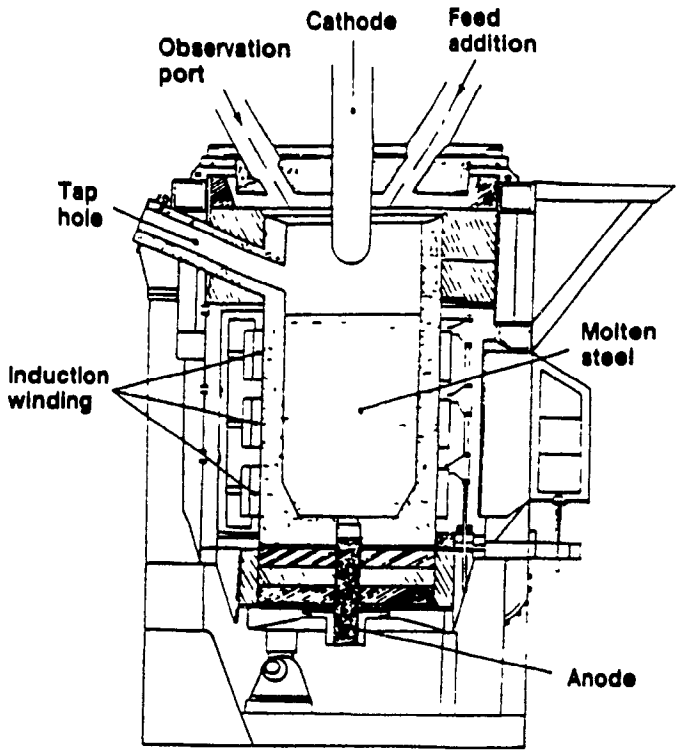

Figure 2.8 Daido Steel Co. Combined Induction and Plasma Furnace

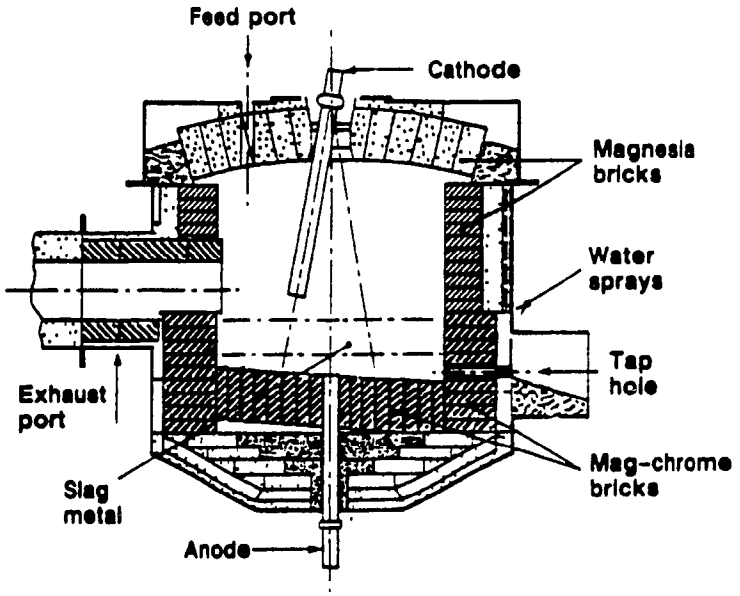

Figure 2.9 Tetronics Furnace

The Tectronics Plasma System, shown in Figure 2.9, is characterized by a rotating cathode assembly making a small angle (9°) with the vertical which aids both stirring and anode energy distribution. Two of its most recent applications were for the production of ferrochromium at a power of 0.55 MW, conducted at Faringdon in collaboration with Mintek of Randburg, South Africa (Barcza et al., 1981) and for platinum group metals (PGM) recovery from automobile exhaust catalytic units in a Texasgulf plant (Met. Bull.,1984). Originally designed by Tylko as the forerunner to the later sustained shockwave plasma (SSP) reactor, the rotating cathode furnace (commonly known as the expanded precessive plasma (EAP) furnace), is now promoted through Foster Wheeler (Maske and Moore, 1982).

The SSP reactor is currently under investigation at the Mineral Resource Research Center of the University of Minnesota (Reid 1980), (Tylko 1979). The main idea of the SSP reactor is to use the plasma medium itself as the reaction medium and effect "in-flight" reduction of the mineral concentrate (Tylko et al. 1981), (Udupa et al. 1984).

Krupp Research Institute developed an AC 3-phase plasma torch and furnace (Neuschutz et al., 1985). In this furnace, shown in Figure 2.10, three AC-plasma torches are mounted in the roof of the furnace. The torches are inclined towards the centre to keep the plasma arc at a reasonable distance from the furnace walls in order to minimize refractory wear. The plasma torch consists of a water-cooled outer steel shroud with a replaceable nozzle and a central current bearing rod with the tungsten elec-

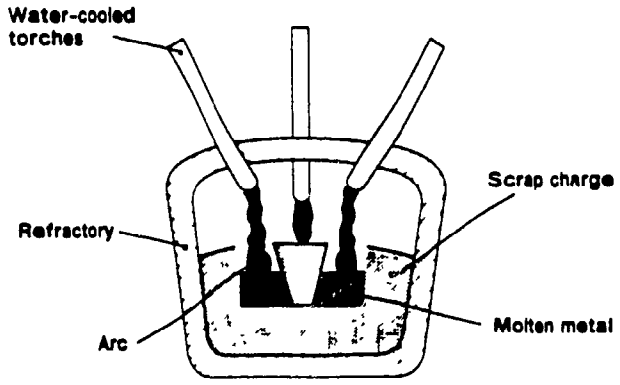

Figure 2.10 Krupp Three-Phase AC Plasma Arc Furnace

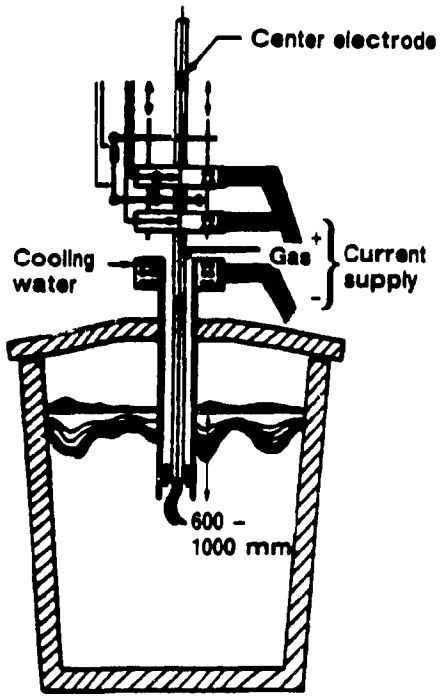

Figure 2.11 SINTEF Immersed Arc

trode at the tip.

A novel immersed transferred-arc plasma heater was developed by Jon Arne Bakken and colleagues at SINTEF (Norwegian Institute of Technology, Trondheim, Norway) in collaboration with National Industri A/S, is shown in Figure 2.11 (Barcza, 1987). The arc is formed between two coaxial electrodes which can be supplied from either a DC or an AC power supply. Inert gas is introduced via the annulus between the electrodes. A cavity is formed at the end of the arc heater in which the arc can be sustained a metre or so below the surface of the metal.

Bethlehem Steel Co. (MacRae, 1979) developed a falling film reactor, shown in Figure 2.12, in which they reduced hematite with mixture of hydrogen and methane and vanadium trioxide with coke fines, at powers up to 1 MW. Its distinguishing feature is the location of the anode, which takes the form of a vertical cylinder embedded in the wall on which the feed impinges to form a molten film.

Finally, the Plasmacan transferred-arc type reactor designed by Gauvin and Kubanek (1981) is shown in Figure 2.13. In this type of reactor, the powdered feed, ranging in size from a few microns to upward of a millimetre in diameter, is introduced tangentially in a high-velocity cold carrier gas (generally the same as the plasma gas) and forcefully projected against the inner wall of a cylindrical "sleeve" where it is exposed to the intense radiation of the plasma column generated between the cathode and the molten bath of product, which acts as the anode. Since both the sleeve and crucible (anode) can serve as reaction sites, res-

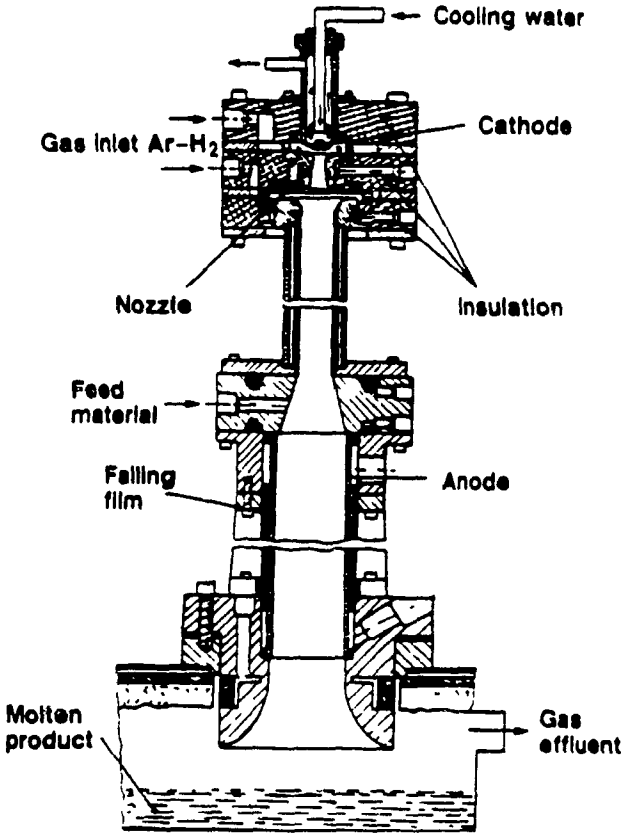

Figure 2.12 Bethlehem Steel Co. Furnace

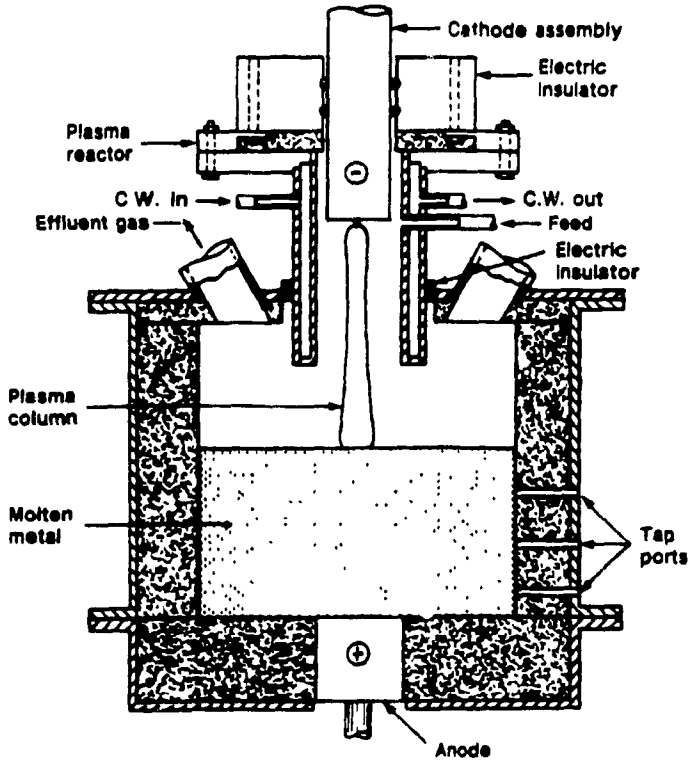

Figure 2.13 PLASMACAN Furnace

idence times for reactions can be adjusted to ensure completion. Several small-scale (up to 125 kW) versions of this design have been demonstrated by Noranda and by McGill (Gauvin and Choi 1983), (Parisi 1984, 1988). A 1-MW reactor of this design is currently being tested by Davy McKee in their R and D division in Stockton-on-Tees, England (Gauvin and Choi, 1983).

2.3.6 Conclusion

The literature review indicates that although there are a variety of plasma furnaces and reactors available, and their metallurgical applications have been proven at the developmental stage, their commercial utilization is limited. As far as metallurgical applications are concerned, it is in the iron and steel industry that the major developments have taken place.

2.4 Metallurgical Reactions in Plasmas

The use of plasma technology has been successfully demonstrated for the beneficiation of ores (Kreibaum, 1986), producing fumed silica (Gans and Gauvin, 1988), chlorination of oxides (Biceroglu, 1978), thermal decomposition of sulphides (Munz and Gauvin, 1975) and halides (Tsantrizos, 1988) to produce their respective metals, and producing refractory nitrides (Matsumoto and Kanzaki, 1983) and carbides (Matsumoto and Shirato, 1970).

Plasma reactors provide a source of high-intensity heat flux at high temperatures. This will continue to have potential for commercial development of new extractive metallurgical processes if fossil fuels are more expensive than electricity. Besides, the reluctance of operators to switch from conventional fuels to

electricity is slowly disappearing. Thus, the near-term potential for plasma systems would be in countries such as Canada and Brazil. These countries have abundant, inexpensive hydro-electric power and the desire to develop highly efficient metals and chemical industries. The advantages of plasma furnaces compared to conventional electric furnaces have been well documented and are based on actual operating data (Bhat 1981), (Gauvin and Choi 1983), (Barcza 1987). They include:

1. Higher melting efficiency compared to similar sizes of conventional electric arc furnaces.
2. Ability to produce alloys with low carbon content.
3. Superior recovery of the alloy metals contained in the scrap and of those added to the melt.
4. Ability to inject and alloy the melt with nitrogen through the gas phase instead of through the use of expensive nitrogen containing alloys.
5. Higher quality product compared to that from conventional electric arc or induction melting furnaces.
6. Achieving low oxygen and hydrogen residuals in the melt.
7. Reduction of iron losses to below two percent.
8. Suppression of noise to a level below 60 dB.
9. Elimination of discontinuous shock loading of the electric power transmission mains (flicker).
10. Thirty percent lower capital investment compared to a modern Ultra High Power (UHP) electric arc furnace system.

Compared to conventional pyrometallurgical reduction and smelting techniques based on fossil fuels, plasma processes would

have the following additional advantages:

1. Flexibility in reductant selection.
2. Ability to concentrate energy with resultant smaller reactor size and pollution abatement systems.
3. Ability to operate independently of oxygen potential.
4. Ability to transfer heat energy to the gas phase with high efficiency and without the contamination of combustion products.
5. Much lower capital investment requirements resulting from smaller reactor size and the ability to handle finely-divided feed material, without expensive feed preparation.
6. Reduced manpower needs resulting from continuous operation and ease of automation for plasma processes.
7. Less restrictions in choice of plant location; ability to locate near ore supply as electricity can be transported to the site cheaply and efficiently.

The principal advantage of using plasmas in the reduction of mineral concentrates is due to the improved reaction kinetics and thermodynamics available at the elevated temperatures achieved by the plasma medium. This advantage is not merely due to increased reaction rates achieved at increased operating temperatures but, also, due to the presence of more reactive species at these high temperatures. This makes plasma ideal for melting and smelting refractory metals or processing hard-to-reduce metal oxides. An example being niobium pentoxide, the main component of pyrochlore, the principal reactant being studied in this work. This section will cover the reaction and processing of metals from

their ores and the production of ferroalloys.

2.4.1 Reduction of Metal Oxides

Plasma reduction of metal oxides have been attempted by several investigators (Gilles and Clump 1970), (Stokes 1969), (Everest et al. 1971), (Brown 1967), (Maske, 1985), (Brent, 1987). However, in all of these works, as in most other investigations, the intention was to determine important process parameters and assess their quantitative effects, rather than to make a detailed kinetic study.

Everest et al. (1971) investigated the carbothermic reduction of alumina in a 30 kW rotating plasma furnace and were able to identify aluminium metal, gamma alumina and trace amounts of the oxycarbides, Al_2OC and Al_4O_4C, when the exit gases were quenched with argon. Quenching with air resulted in the formation of a mixture of gamma and delta Al_2O_3. Comparing these results to a previous work carried out on the thermal decomposition of alumina in a plasma system, it would appear that the major evaporating aluminium suboxide species in a non-reducing atmosphere is AlO (Rains and Kadlec, 1970), but that the specie Al_2O is predominant under reducing conditions (Everest et al., 1971). Akashi et al. (1973) studied the carbothermic reduction of alumina in a non-transferred argon-hydrogen (5 %) plasma jet. In addition to the products obtained by Everest et al. (1971), he identified the existence of aluminium carbide (AlC) in the condensate material taken from the inner wall of the reaction chamber. Recently, Matsuomoto et al. (1983) effected the carbothermic reduction of alumina in an argon plasma arc under reduced pressure. His results

were consistent with those of Akaski et al. (1973) and Everest et al. (1971). Borgianni et al. (1969) obtained low conversions (< 60 %) to metals when Al_2O_3, CuO, NiO and TiO_2 powders were injected into an argon induction plasma.

Although Brown's (1967) attempt to reduce zirconium dioxide to the metal by passing powdered (10-micron particles) zirconia through a dc plasma flame in a carbon reaction chamber resulted in an increase in the zirconium content of the product, his work was not conclusive in that the presence of metallic zirconium was not clearly identified and the small differences in zirconium content between the reactants and the products might have been due to experimental error.

Stokes (1969) demonstrated the feasibility of preparing pure iron powder by injection of iron oxide conveyed with hydrogen into a helium plasma. No conversions were obtained in the attempted reduction of titanium dioxide and zirconium dioxide with hydrogen in the same work. Using a direct current arc plasma jet, Gilles and Clump (1970) attempted to reduce iron ore with hydrogen. The results indicated that heat transfer to the oxide particles was a prime factor influencing the reaction rate. Their conversions were up to 69 % with a 100 % hydrogen plasma.

Greenwald and Groteke (1971) developed a reduced-pressure plasma furnace for the bath reduction of metal oxides, in which the oxide batch is heated by a single-phase alternating current plasma struck between graphite electrodes. They claim to have achieved successful catalytic reductions of hematite when the furnace was operated at a pressure of 70 kPa and a melt tempera-

ture of approximately 1100 K. They produced 50 kg batches of steel having a carbon content of 0.35 %. They have also claimed similar reduction of other metal oxides such as chromium oxide and zinc oxide.

Gold et al. (1977) reported the development of a single-step plasma reactor system to convert iron oxide directly to molten iron in a hydrogen-natural gas mixture. The iron ore was pneumatically conveyed to the plasma reactor and injected into the hot reducing gases produced by a dc arc. Molten iron and slag were collected in a holding cubicle, which was poured intermittently. The electrical energy consumed was given as 2.6 kWh/kg iron (not including energy losses from the reactor) at a hydrogen-to-natural gas ratio of two. This value compared favourably with a minimum thermodynamic process energy requirement of about 2.2 kWh/kg iron. It was suggested that the specific energy requirement would be decreased by a reactor scale-up from 100 kW to 1 MW, by the use of finer powder and by an increase in the natural gas-to-hydrogen ratio.

Pickles et al. (1977) reported the successful treatment of steel plant wastes in the patented extended arc flash reactor (EAFR) (Segsworth and Alcock, 1977). The ratio of the total energy consumed to that predicted from theoretical considerations were reported to vary from about 1.3 to 6. The high ratios were typical for the reduction of those dusts which contained large concentration of chromic oxide and required lengthy holding periods for slag reduction, thus contributing to the high power consumption. The quality of the product, it is claimed, is compara-

ble to that obtained by conventional processes such as the BF/BOF route or the submerged arc furnace.

Tylko et al. (1981) studied the in-flight reduction of Fe_3O_4 in taconite and selective reduction of $FeOCr_2O_3$ in lean chromite (Cr/Fe = 1.51) concentrates with graphite and charcoal in an open argon plasma. The reaction takes place in the Sustained Shock Wave Plasma (SSP) reactor. Mechanisms were proposed for the reduction of both taconite ore and chromite. The reduction of taconite takes place in two stages, Fe_3O_4 -> FeO -> Fe with the final metallization stages (FeO -> Fe) requiring an excess of stoichiometric carbon. The selective reduction of $FeOCr_2O_3$ in the chromite concentrate is generally associated with low melting point silicate phases. It was postulated that the action of the SSP produces microfissures along the microcrystalline boundaries in the chromite particles creating channels of plasma which provide activated passages along which reduction can proceed rapidly. A similar mechanism was put forward for the reduction of chalcopyrite by carbon in the presence of desulphurizers (calcium oxide and sodium carbonate) in the same SSP reactor system (Udupa et al., 1987). A similar experimental program was used for the carbothermic reduction of a copper nickel concentrate (Reid et al. 1983)

Kamiya et al. (1984) studied the reduction of molten iron oxide and FeO bearing slags by hydrogen(7 %)-argon plasma. They found that the reduction of molten iron oxides proceeded linearly with time and the reaction rate was proportional to the partial pressure of atomic hydrogen. It was thus concluded that the rate

determining step is the chemical reaction between FeO and the hydrogen atom formed by thermal dissociation in the plasma. The results also showed that the rate of reduction of FeO bearing slag was lower than that of molten iron oxide and was proportional to the FeO concentration in the slag. It was postulated that the reduction rate was also controlled by the mass transport rate of FeO across the boundary layer between the interface and the molten slag bulk. It was also observed that the reduction of both materials took place only on the cavity formed at the surface of the melt by the momentum of the plasma jet.

Taniuchi and Mimura (1978) investigated the carbothermic reduction of vanadium pentoxide in an argon dc plasma jet. Briquettes made of vanadium pentoxide (99.5 %) and graphite were contained in a water-cooled copper crucible and placed in the plasma jet. The results showed that the optimum mixing ratio (molar) of carbon and vanadium pentoxide was about 4.5 and is smaller than the stoichoimetric ratio of 5. When the mixing ratio was less than 4.5, the oxygen remaining in the product increased, while the vanadium carbide increased when the ratio was greater. Most of the reduction reaction took place during the time it took for briquette to be fused, which for a 3.5 g briquette was within 45 seconds, and accounted for 90 % of the product vanadium content. Maximum vanadium content (96 %) in the product was reached within 10 minutes and showed no appreciable reduction with time. Pure vanadium metal was not obtained because of the strong affinity of vanadium for carbon and oxygen.

Maske (1985) studied the reduction of a low grade chromite

ore "in bath" in a transferred-arc molten-anode plasma furnace and "in-flight" in a transferred-arc ancillary-anode plasma furnace. Coal and char were the reductants used in the former furnace, while graphite and coal were used in the latter. Complete in bath reduction of the chromite was easily accomplished, but when reduction was attempted "in-flight" only 50 % of the total chromium and 60 % of all the iron oxide were reduced within the arc. The low conversion obtained for the " in-flight" reduction was contributed to the inefficient dissolution of the chromite in the slag, but was not apparent in the "in bath" reduction. Up to 200 % stoichiometric carbon for the reduction of the chromium and iron oxide was added for the "in-flight" tests. The plasma gases used were argon and nitrogen.

Brent (1987) investigated the reduction of ilmenite in a dc transferred-arc plasma furnace to give a high-grade titania slag and a pig iron by-product. Calcined anthracite was used as the reducing agent and argon was used as the plasma gas. The best grade of titanium dioxide slags and iron recovery were obtained with 10 % excess carbon.

SKF of Sweden (1983) have developed a number of processes using plasma heaters for the recovery of metals from waste oxides and metal concentrates. The Plasmared Process utilizes plasma heaters to preheat and upgrade reducing gases for the direct reduction of iron ore. A full scale plant with a capacity of 30,000 tonnes per year is in operation at Hofors since January 1981. The Plasmamelt, Plasmadust and Plasmazinc processes utilize plasma heaters to preheat reducing gas at the tuyere of the blast

furnace. A preliminary economic analysis indicates that the Plasmamelt process might be competitive with conventional blast furnace iron furnace. A 35,000 tonnes per year Plasmadust plant for the reduction of steel mill waste oxide in order to recover their metal content (mainly zinc) is scheduled to start up in 1984 in Sweden (Eriksson et al. 1983).

2.4.2 Ferroalloys

MacRae et al. (1976) describe the production of ferrovanadium in a 500 kW Bethlehem Steel falling film plasma furnace (described earlier). Vanadium pentoxide is pre-reduced to vanadium oxide by H_2 and is tangentially injected into an argon/hydrogen plasma with ground coke particles. A falling film is formed due to the swirling centrifugal force of the plasma gas. Reduction takes place and a stable carbide is formed; the molten product is collected in the reactor crucible and dissolved in the initial charge of iron. The molten ferrovanadium produced contained 40-90 % vanadium, and the energy consumption was reported to be 7.7 kWh/kg vanadium. The ferrovanadium was technically accepted to the steel industry.

Barcza et al. (1981) investigated the production of ferrochromium from chromite and coal fines in an EPP furnace. They claimed energy consumption levels in their system were lower than those of a conventional furnace. Also, the increase in the value of chromium/iron ratio with the EPP plasma systems was more than that obtained by the conventional submerged arc furnaces. The approach favouring "in-bath" instead of "in-flight" reactions was found to be a suitable method for the production of ferrochromium

in a transferred-arc plasma system. The suggested mechanism for the reduction reaction was the rapid dissolution of chrome spinel at low oxygen partial pressures into the liquid slag phase, followed by the reduction, by carbon, of the dissolved oxides of chromium and iron.

Pickles et al. (1976) have successfully produced high carbon ferrochromium by reduction of low grade chromite ores with a variety of reducing agents in a 30 kW, Extended Arc Flash Reactor (EAFR) (described earlier). The premixed chromite fines and reductant was introduced into the plasma via a rotary preheater. The plasma was stabilized in mixtures of argon, nitrogen and hydrogen. Anthracite, graphite or coke fines were used as reductants. Metal recoveries of between 84 and 94 % were obtained at energy requirements of about 12 kWh/kg alloy. When hydrogen or carbon monoxide was injected into the furnace, reduction of iron oxide occurred. In the absence of hydrogen, no reduction of chromium oxide by carbon monoxide was found, but in the presence of hydrogen, they found that the chromite was reduced to chromium, iron and silicon. This showed that chromium oxide and silica can be reduced by hydrogen when iron is present to decrease the activity of the metal products.

Mehmetoglu et al (1985) studied the production of ferrochromium in a rf plasma tailflame. Pellets pressed from chromite ore and carbon were reduced in an argon rf plasma tail flame. They found that the maximum metallization levels were obtained with 300 % and 350 % stoichiometric graphite at 1925 and 2475 K. It was also found that the degree of metallization was a function of

pellet porosity.

Pickles and Alcock (1983) investigated the production of ferronickel and ferrovanadium from fly ash in the EAFR plasma system. The mixture of ash and required amount of carbonaceous reductant (petroleum coke, anthracite or coke) was batch-charged into the furnace. Ferronickel was produced after the first heat and ferrovanadium from the slag material of the preceding heat after it was mixed with the additional required amount of reductant. It was found that the gas capacity for reduction for a stable oxide like MnO, Cr_2O_3 or V_2O_3 is too small for a significant amount of any of these metals to be produced by gas-solid or gas-liquid reactions under conventional or plasma steelmaking conditions. The need for liquid-liquid (metal-slag) contact to bring about the reduction of the stable oxide to form ferroalloys was also found for manganese alloy production in the same plasma system (Donyina et al. 1982). Ferronickel with 30-40 % nickel and ferrovanadium with 50-60 % vanadium were produced in the two-stage process. The iron and nickel recoveries were reported to be about 90 %, while vanadium recovery was about 85 %.

Parisi (1988) did a preliminary investigation into the production of ferrovanadium in a Plasmacan transferred-arc plasma reactor. An intimate mixture of vanadium pentoxide (3-10 microns) and graphite particles was fed into the reactor and the product dissolved in the molten iron bath. The plasma gas was argon. The results showed that it was possible to produce a commercial grade ferrovanadium (30-70 % vanadium).

Schoukens and Curr (1984) investigated the plasma production of ferromanganese by smelting manganese ores and slags. The reactions were done in dc transferred-arc furnaces with melt anode; hollow graphite cathodes were used for the 30 kW furnace and water-cooled tungsten cathodes (Tetronics design) were used at 550 kW. The studies demonstrated that at higher slag basicities there are higher yields of manganese from the slag phase.

Brent et al (1986) produced alloys of titanium and iron by the reduction of a titania-rich slag in a dc transferred-arc plasma furnace of the molten-anode configuration. Tests were conducted at 50 and 200 kW. The ferrotitanium alloy typically contained 56.5 % titanium and had a titanium to aluminium ratio of 4.2. The study showed it was probably not practical or theoretically feasible to meet the titanium to aluminium specification by the alumino-thermic reduction in a single stage operation.

The techno-economic analysis of the application of plasma technology for the production of ferromolybdenum by the plasma decomposition of molybdenite (Gauvin et al. 1981) and the production of ferroniobium by the carbothermic reduction of pyrochlore (Liang and Munz 1981) has been done so as to evaluate the competitiveness of plasma processes with conventional processes. In the case of ferromolybdenum production, the results of analysis stressed the importance of preparing comprehensive flowsheets and economic assessments in the early stages of the industrial development of a plasma process.

The ferroniobium plasma process appeared to be marginally profitable under the assumptions made, and was quite sensitive to

capital cost and product added value.

2.4.3 Conclusion

The literature indicates that few fundamental kinetic studies have been done in plasma systems. There are numerous reasons for this deficiency but the primary one lies in the nature of plasma systems. The most outstanding deterrents are the difficulties of obtaining reliable measurements under a very difficult experimental situation. The important kinetic parameters such as residence time, reaction temperature, gas velocity, gas concentration and gas temperature may not be varied independently. Furthermore, conventional measurement techniques may not be used in most cases; simple measurements, such as gas and reaction temperatures and velocities, usually require the development of sophisticated and often indirect techniques.

In the case of the carbothermic reduction of pyrochlore, the presence of several other metal species makes the kinetics of the reduction reaction unpredictable. The concentration of carbon monoxide which can be used in a transferred-arc is not known a priori; both arc stability and electrode erosion problems may be encountered (Tsantrizos, 1988). The direct measurement of a molten bath temperature in a plasma environment may not be possible.

The choice of a plasma generating device depends on its application, the nature of the feed material, and, more particularly on the nature of the desired product (for example, whether it must be obtained as a fine powder or as a molten material). The degree of purity of the material to be produced often imposes severe limitations on the choice of the plasma generating system.

In the recent past, workers in the field have displayed a great deal of ingenuity and creativity in the design of the plasma systems capable of meeting the criteria of the potential industrial applications they were pursuing. It is now quite clear that different reactions will require different unique design characteristics. Before the design of a plasma system can be undertaken, it is imperative to obtain the necessary kinetic data and operating parameters, which in turn will govern the design of virtually every component in the plasma system. The major aims of this work are to provide the kinetic data for the carbothermic reduction of pyrochlore and the pure niobium oxide with and without the addition of iron.

2.5 Modelling of The Carbothermic Reduction of Metal Oxides

2.5.1 General Considerations

Reactions between solids are important in materials processing. They are usually carried out in powdered compact or in beds of granular solids. One major example of this type of reaction is the reduction of metal oxides by carbon to give the metal or metal carbide. While these reactions and their mechanisms are of industrial interest and some laboratory scale kinetic measurements have been made, unlike the case of simple gas-solid reactions, no general modelling equations are available for the interpretation of the experimental data. The absence of comprehensive theoretical treatment is due to the complexity of these systems.

The reduction of metal oxides with carbon can be divided

into two main groups, namely: (a) direct reduction or true solid-solid reactions, and (b) reactions between solid reactants that take place via liquid or gaseous intermediates.

Direct reduction or true solid-solid reaction takes place in the solid state between two species in contact with each other, or through the diffusion of species in the solid state. This may be written as follows:

$$3MO(s) + 3C(s) = 2M(s) + MC(s) + CO(g) + CO_2(g) \qquad (2.9)$$

Models derived specifically to describe the progress of solid-solid type of reaction have been documented and reviewed by Hulbert (1969), Tamhankar and Doraiswamy (1979), Bramford and Tipper (1980), and Doraiswamy and Sharma (1984).

It is generally accepted and supported by experimental proof that the reduction of metal oxides by carbon occurs through the gaseous intermediates of carbon monoxide and carbon dioxide (Bodenstein, 1927), (Baldwin, 1955), (Rao, 1971), (Fruehan, 1977), and (Abraham and Ghosh, 1979). The exception is under very high vacuum conditions where the true solid-solid reaction is the predominant mechanism (Yun, 1961), (Habashi, 1969), and (Roa, 1971). The reaction mechanism including the gaseous intermediates is:

initiation:

$$2MO(s) + 3C(s) = M(s) + MC(s) + 2CO(g) \qquad (2.10)$$

propagation:

$$MO(s) + CO(g) = M(s) + CO_2(g) \quad (2.11)$$

$$CO_2(g) + C(s) = 2CO(g) \quad (2.12)$$

The cessation or termination of either Reaction (2.11) or (2.12) would result in the termination of the reaction. The excess gas generated diffuses out of the system through the interparticle pores where the CO_2/CO ratio can vary over a large range, depending on the type of metal oxide and carbon in the mixture. For example, in the carbothermic reduction of higher oxides of iron (Fruehan, 1977), manganese (Kor, 1978) and lead oxide (Lin and Rao, 1975), the reaction product is essentially pure carbon dioxide. For the wustite-carbon mixture (Fruehan, 1977), (Yun, 1961), the CO_2/CO ratio in the gas evolved is initially close to the value for the iron-wustite equilibrium, but decreases with the progress of the reduction.

In addition to those models, derived for solid-solid reactions, mathematical models were developed specifically to represent the progress of reactions occuring through gaseous intermediates by Rao (1974), Rao and Chuang (1974), Sohn and Szekely (1973) and Wynnyckyj and Rankin (1988). Some carbothermic reduction reactions, as well as other solid-solid reactions, which involve gaseous intermediates and also produce a gas product (Baura and Wynnyyckyj, 1981), occur such that a shrinking core is

evident. The rate-controlling step would be either the outward diffusion of the product gas or its Poiseuille flow through the outer portion of the pellet or bed.

2.5.2 Reaction Models

Several reaction models have been developed to describe the processes of chemical reaction and mass transfer occuring during the reaction. In any mixed powder reaction, the solid particles of reactants should contact each other and react. For the reaction to continue, one of the reactants must diffuse through a product shell. This situation gives rise to several possibilities:

1. Product formation controlled by diffusion of reactants through a continuous product shell.
2. Product formation controlled by phase boundary reaction.
3. Product formation controlled by kinetic equations based on the concept of an order of reactions
4. Product formation controlled by nuclei growth.

2.5.2.1 Diffusion Control

For these types of models, it is assumed that:

1. the particles are spherical,
2. the diffusion of the mobile reactant species through the product layer is the rate controlling step,
3. the temperature of the sample remains constant during the reaction process.

Jander (1927) was probably the first to derive a mathematical expression for a solid-solid reaction. In addition to the assumptions mentioned before, he also made the assumption of a

constant cross-sectional area and an unchanging volume or density during the progress of the reaction. His rate expression is:

$$[\ 1-(1-x)^{1/3}\ ]^2 = k_D t \qquad (2.13)$$

where $k_D = 2k_2Da/r^2$, and is equal to the overall reaction rate constant, k_2 is the local value of the rate constant, a is the area of contact, x is conversion, D is diffusion coefficient and r the particle radius.

Serin and Ellickson (1941) attempted to modify Jander's rate expression by eliminating the assumption of constant reaction cross-section. This gave the following expression:

$$(1-x) = 6/\pi^2\ \Sigma_{n=odd}\ (1/p^2)\ \exp\ (-p^2\pi^2Dt/r^2) \qquad (2.14)$$

where p is the number of reaction cells or particles of radius r. This model was used by Tomas et al. (1969) to describe the solid state reaction between phathalic anhydride and sulfathiazole.

Zhuravlev et al (1948) introduced the assumptions that the rate of interface advance under diffusion control was also proportional to the amount of unreacted species present and, the particle was contracting during reaction, he obtained the following equation:

$$[\ (1-x)^{-1/3} - 1\ ]^2 = k_D t \qquad (2.15)$$

Kroger and Ziegler (1954) postulated that defect in the

structure of the solid reactant could be of consequence to the reaction rate. Assuming that the rate of defect removal is inversely proportional to time (the Tammann treatment), Equation (2.13) derived by Jander could be modified by replacing t by ln(t) to give:

$$[\ 1-(\ 1\ -x)^{1/3}\ ]^2 = k_D \ln(t) \qquad (2.16)$$

Dunwald and Wagner (1934) assumed that diffusion into and out of the spherical reacting particles was governed by Fick's second law of diffusion and can be written as :

$$6\ /\ \ln\ \{\ \pi^2\ (\ 1-x)\ \}\ = k_D t \qquad (2.17)$$

Carter (1961) and Valensi (1936) accounted for the change in volume due to reaction by introducing a parameter z, which is the ratio between the volume of the final product and that of an equivalent amount of the initial reactant. The expression is:

$$\{\ z\ -\ [1+(z-1)x]^{2/3}\ -\ (z-1)(1-x)^{2/3}\ \}\ /\ 2(z-1)\ =\ k_D t \qquad (2.18)$$

If this derivation is repeated for no volume change, an equation is obtained which is identical with that of Ginstling and Brounstein (1950), Equation (2.19).

Ginstling and Brounstein (1950) begin their derivation from Fick's second law for a constant diffusion coefficient and fixed the concentration gradient to give a constant flux through each

annular section of the reaction layer. They describe the rate of reaction of spheres by the equation:

$$1 - 2/3x - (1-x)^{2/3} = k_D t \qquad (2.19)$$

El-Guindy and Davenport (1970) used Equation (2.19) to describe the carbothermic reduction of ilmenite. Carbon monoxide and carbon dioxide were suggested to be the diffusing gaseous intermediates.

Wynnyckyj and Rankin (1988) developed equations for the solid-solid reaction via a gaseous intermediate, where diffusion of the gaseous intermediate through a product layer is the rate controlling step. The rate controlling diffusional step was referred to as " intrinsic transport ". The more general case is one where the partial pressure of the diffusing intermediate is sufficiently low for gas transport to be slow from the beginning. The other assumptions were: a) the powder mixture is an infinite, lattice-like array of particles and spaces, b) the reactant which produces the gaseous intermediate is of uniform radius r, and is the centre of the lattice sites. The reacting system consists of n_e expanding reacting cells, each centered on the reactant producing the gaseous intermediate. The model identifies two stages in the reaction, the first stage when the reaction cells first begin to interpenetrate which account for a maximum conversion (x_p) of only 72 % of the other reactant or $x < x_p$, and the second stage when total interpenetration has occurred or $x > x_p$.

The equation used to describe the first stage model ($x < x_p$)

is:

$$3/2 + Zx - 3/2(Zx+1)^{2/3} = Zk_3t/C_0(Z+1)r^2 \qquad (2.20)$$

where $Z = 1 - 3V_{tot}/4\pi n_e r^2$

Z is defined as the volumetric reaction parameter, V_{tot} is the total compact volume of the reactants and k_3 is the reaction rate constant. A simpler and less accurate solution similar to Jander's approach is given by:

$$[\ (Zx+1)^{1/3} - 1\ ]^2 = Zk_4t/r^2 \qquad (2.21)$$

where k_4 is another form of the "intrinsic transport" rate constant.

The equation used to describe the second stage model ($x>x_p$) is:

$$[\ (Z+1)^5/18.33q^{4.667} - q^{1/3}/18.33 - 1\ ]^2 = k_5t \qquad (2.22)$$

where $q = 0.741(Z+1)$ and $k_5 \propto 1/r^2$.

Equations (2.20) and (2.22) are not applicable once the pressure of the product gas is substantially greater than the ambient pressure.

2.5.2.2 Phase Boundary Reaction Control

When the diffusion of the reactant species through the product layer is fast compared to reaction, the overall rate is con-

trolled by the reactions at the boundary phase. Models have been developed for different geometries and their corresponding conditions.

Jach (1963) derived the following expression for a sphere reacting from the surface inwards:

$$1 - (1-x)^{1/3} = k_R t \qquad (2.23)$$

where, $k_R = k_6/r$ and equal to the overall rate constant, k_6 is the local rate constant, x is the fractional conversion and t is the time. This expression is identical to the one derived for the gas-solid reactions (Levenspiel, 1972).

Maru et al. (1973) described the kinetic data obtained for the reaction between $Cr_{23}C_6$ and Cr_2O_3 particles with Equation (2.23). They suggested that the gaseous intermediates for the reaction were carbon monoxide and carbon dioxide. Rao (1971) also used a similar equation for the conversion-time relationship obtained for the carbothermic reduction of hematite catalyzed by the addition of lithium oxide (5 %). It was suggested that the reaction proceeded via the same gaseous intermediates, with the oxidation of carbon by carbon dioxide, Reaction (2.12), constituted the rate-limiting step for the overall reaction.

For the case of a cylinder, reacting from the edge inwards, or for a circular disk, the conversion-time relationship is represented by the following expression (Jach, 1963):

$$1 - (1-x)^{1/2} = k_R t \qquad (2.24)$$

Sharp et al. (1966) derived the following expression for the case of a cube reacting and contracting:

$$8k_R^3t^3 - 12k_R^2t^2 + 6k_Rt = x \qquad (2.25)$$

Sohn and Szekely (1973) developed a model for the representation of reactions between solids, proceeding through gaseous intermediates controlled by chemical kinetics in the absence of diffusional effects, and where there is a net generation of gaseous products. The governing equations were non-dimensionalized and solved numerically to obtain the desired relationship between the advancement of the reaction front and time. It was further assumed that the system was isothermal, first order and irreversible. The conversion and the rate of reaction are related to the dimensionless time through two parameters α and β. The parameter α represents the relative molar quantities of the two solids in the pellet and β corresponds to the ratio of the reactivities of the two reactant solids. The quantities α and β allow the definition of asymptotic regimes and to identify rate controlling steps. For the case of the carbothermic reduction of metal oxides, when the value $\alpha\beta$ approaches zero, Reaction (2.12) is rate limiting and when it is very large Reaction (2.11) is rate limiting. This situation corresponds to the well-known ones for the "topochemical model" (Sohn and Szekely, 1972), and the expressions are the same; as if each particle was under kinetic control, for fixed gas concentrations. For the case when Reaction

(2.12) is rate limiting, the expression may be written as:

$$1 - (1-x)^{1/F} = \beta b k_7 C_T A_B t / d_B F_B V_B (1+k_8 C_T) \qquad (2.26)$$

where F_B and F are the grain shape factors for the solid reactants for Reactions (2.11) and (2.12), respectively, which has a value of 1,2 or 3 for flat plates, long cylinders, or spheres, respectively; k_7 and k_8 are reaction constants for the gas-solid reactions of the gaseous intermediates as in Reactions (2.11) and (2.12), b is stoichiometric coefficient for the solid reactant of the type as in Reaction (2.11), C_T is the total gas concentration, A_B, V_B, and d_B are the grain surface area, grain volume and grain density, respectively, for the solid reactant of the type as in Reaction (2.11).

Ajersch (1987) used Equation (2.26) to describe the data for the carbothermic reduction of hematite in the form of compressed pellets. The reaction was assumed to be via gaseous intermediates carbon monoxide and carbon dioxide. It was also suggested that increasing nucleation sites for the C-CO_2 reaction leads to increased rates of CO generation, thus increasing the rate of reaction.

2.5.2.3 Nuclei Growth Control

The theory of nucleation and growth of the product phase was originally formulated to describe the kinetics of phase change processes (Avrami, 1939,1940,1941). The general form of the expression for conversion against time was:

$$\ln (1-x) = -(kt)^m \qquad (2.27)$$

The parameter m accounts for the reaction mechanism, number of nuclei present, composition of original and product phases and the geometry of the nuclei.

The application of the nuclei growth model is more often used to describe decomposition reactions and is sometimes used to describe solid-solid reactions. Typical conversion-time behavior at low temperature for this system shows three periods: (a) induction period, (b) acceleratory period, and (c) decaying period. These three stages arise from the following succession of events: (1) formation of nuclei of the metallic phase at localized sites on the oxide surface, (2) growth of these nuclei, and (3) overlap of the growing nuclei and a decrease in the metal/oxide interface. The length of the induction period is related to the rate of nuclei formation. If the nuclei are formed fast (as is the case at high reaction temperature or when the surface to volume ratio is small) the entire surface gets covered rapidly with the metallic phase and a metal/oxide interface develops. The reaction then proceeds in a topochemical manner and the previously described rate expressions for product layer diffusion and chemical reaction controlled systems can be applied. On the other hand, if the nucleation rate is not very fast, the metal/oxide interface will be irregular.

Klinger et al. (1966) used the nuclei growth model to explain qualitatively the reaction between silica and carbon for temperatures greater than 1885 K and for instances when the reac-

tion was allowed to continue for long periods of time. The rate-controlling step was attributed to the phase transformation of the silica.

Hulbert and Klawitter (1967) have applied it to the reaction between zinc oxide and barium carbonate and obtained the average value of m as 1.52. This might have been due to the fact that the rate controlling-step was the decomposition of barium carbonate.

Padilla and Sohn (1985) used Equation (2.27) to describe the reaction between the alumino-silicate found in coal wastes and limestone and soda ash (lime-soda sinter process) to produce sodium aluminate and dicalcium silicate. The model fitted the data reasonably well and the value of m was determined to be 1 from the plot of ln[ln(1-x)] versus ln(t).

2.5.2.4 Kinetic Equation Based on The Concept of an Order of Reaction

The integrated form of the general kinetic equation for an n^{th} order reaction is represented by:

$$[\ 1/(1-x)^{n-1} - 1]\ /\ (n-1) = kt \qquad (2.28)$$

For certain values of n, Equation (2.28) leads to some of the equations based on physical models. When n = 2/3 and 1/2, Equation (2.28) is identical to Equations (2.23) and (2.24).

When the rate determining step is the nucleation at each active site, a first order kinetic equation which is analogous with radioactive decay is obtained and is expressed as:

$$\ln(1-x) = -kt \qquad (2.29)$$

Shimada et al. (1983) used this type of equation to describe the solid state carbothermic reduction of niobium pentoxide and tantalum pentoxide at 1275 to 1560 K. The experimental results also seem to indicate that the reduction reactions were achieved through the gaseous intermediates, carbon monoxide and carbon dioxide, since covering the reaction vessel promoted niobium and tantalum carbide formation.

Whenever the rate of reaction is proportional to the volume or concentration of unreacted material present, this is equivalent to a first order reaction and the conversion-time relationship is the same as Equation (2.29).

The first order reaction equation, with the same expression as Equation (2.29) has been used to describe the conversion-time relationship for the carbothermic reduction of calcium phosphate (Hussein et al., 1974), Mn_3O_4 (Kor, 1978), stannic oxide (Padilla and Sohn, 1979), hematite and ferrous oxide (Fruehan, 1977) and hematite (Rao, 1971). Except for the case of calcium phosphate, where carbon monoxide was not acting as a reducing agent, the reduction reactions were assumed to be accomplished via the gaseous intermediates carbon monoxide and carbon dioxide as suggested by Reactions (2.11) and (2.12). The overall rate was determined by Reaction (2.12) - the oxidation of carbon by carbon dioxide. The model was shown to represent all the data fairly well. A similar rate expression was previously found to describe the kinetics of the oxidation of graphite, charcoal and

char in carbon dioxide (Turkdogan and Vinters, 1969), (Rao and Jalan, 1972), (Matsui et.al., 1987) and the reduction of iron oxides in hydrogen and carbon monoxide (Turkdogan and Vinters, 1972).

There is a type of gas-solid reaction involving two solid components which is analogous to the reactions involving gaseous intermediates. This is the chlorination of metal oxide-carbon compacted porous pellets. Serayakov et al (1970) analyzed this problem using a volumetric-reaction model and assuming homogeneous reaction where the contact area between the solid constituents was the rate-determining factor. The reaction was assumed to be limited by the step involving the transfer of an unidentified intermediate product from the surface of one solid phase to another. In terms of fractional conversion based on the maximum amount of oxide that can be reacted, the conversion-time relationship is given by the expression:

$$-\ln (1-x) = kt \qquad (2.30)$$

This model fitted their experimental data reasonably well and Equation (2.30) is identical to Equation (2.29) for first order reaction systems.

Biceroglu (1978) proposed a simplified model to describe the reaction of the chlorination of compacted zirconium dioxide-carbon porous pellets in an induction chlorine plasma. The model assumes that mass transfer resistance (ash diffusion) is absent or negligibly small, and that the rate is proportional to a con-

tact area or to a distance of separation between the zirconium dioxide and the carbon particles. The latter in turn is assumed to be proportional to a functional form of initial carbon concentration in the pellet and also to the amount of unreacted zirconium dioxide left in the pellet. The resulting conversion-time relationship may be written in terms of the fractional conversion of zirconium dioxide and is given by the expression:

$$-\ln(1-x) = kt \qquad (2.31)$$

The overall rate constant, k, by definition is not a function of particle diameter, hence the conversion-time relationship given by Equation (2.31) is not affected by variations in the particle diameter. This model fitted the experimental data very well. Equation (2.31) is also identical to Equations (2.29) and (2.30).

An equation identical to the one derived by Biceroglu (1978), Equation (2.31), was used by Fruehan and Martonik (1976) to fit the conversion-time data for the carbothermic reduction of magnesium oxide. Indications were that the oxidation of carbon by carbon dioxide was the rate limiting step, however, the exact mechanism was not known. The model fitted the data fairly well.

2.5.2.5 General Model

Rao and Chuang (1974) developed a generalized physico-chemical model for reaction between particulate solids and occuring through gaseous intermediates. This is an extension of the model which was originally derived to describe the carbothermic reduction of hematite. The governing equations were non-

dimensionalized and solved numerically for a wide range of reaction processes the diffusion-controlled and the reaction-controlled cases as the extremes. The following assumptions were made:

1) the reaction was isothermal,
2) the structural properties of the reactants remain constant during the reaction,
3) the rate of movement of the interface is slower than the rate of diffusion (pseudo-steady state approximation (Birchoff, 1963)),
4) Reaction (2.12) is the rate-controlling step,
5) the gas phase is in equilibrium with the metal oxide

The solution resulted in a plot of dimensionless time against fractional conversion for combinations of generalized dimensionless moduli "ϕ^2" and "μ". For the carbothermic reduction of metal oxides, the generalized dimensionless moduli were defined as:

$$\phi^2 = (2u-1)RTL^2k_9\sigma_C^\circ \; / \; D_{CO2} \qquad (2.32)$$

$$\mu = [\; k_{10} + (k_{11}/K') \;]\; p_{CO2} \qquad (2.33)$$

where u is the utilization factor for the desired intermediate reaction, R is the universal gas constant, L is the sample thickness, T is the temperature, k_9, k_{10}, k_{11} are the intrinsic rate constants for Reaction (2.12) fitting a Langmuir-Hinshelwood type rate equation, σ_C° is the initial mass concentration of

carbon in the sample, D_{CO2} is the effective diffusivity of carbon dioxide gas, K' is the equilibrium constant of the system and p_{CO2} is the partial pressure of carbon dioxide at the exterior of the sample.

As "ϕ^2" approaches zero, the overall rate is controlled by chemical kinetics especially for small and moderate values of μ. As "ϕ^2" approaches infinity, the overall rate is controlled solely by the diffusion of the gaseous intermediate within the particle. A distinction between the two regimes is not possible for large values of μ.

The approximate analytical solution developed for the carbothermic reduction of hematite (Rao, 1974) predicts the fractional conversion of carbon (x_C) against dimensionless time (τ) as:

$$x_C = 1 - \exp(-\tau/\mu) \qquad (2.34)$$

There was reasonable agreement between the predicted and the experimental data.

Taplin (1974) suggested a generalized expression to describe the kinetics of solid-solid reactions. He suggested the following empirical or index-of-reaction equation:

$$dx/d(t^i) = k(1-\theta x)^h \qquad (2.35)$$

The exponent of time, i, depends on the kinetic regime. The index of reaction, h, which has frequently been misinterpreted as the

reaction order, depends on the kinetic regime and the particle size distribution. The expression has been shown to adequately represent different types of kinetic regimes with different values of i,θ and h. For example, in the case of linear kinetics where the reaction rate varies as the area of the interface, the equation is shown to be valid for different particle shapes, with i and θ values of 1, and h having values of 2/3, 1/2, and 0 for sphere, elongated cylinder, and thin disk, respectively. Mixed regime kinetics have also been represented by Equation (2.35). For example, in the case of reactions which are controlled by mixed linear and parabolic kinetics, this has been approximated by the index-of-reaction equation with i having a value of 2/3 (Taplin 1973).

2.5.2.6 Empirical Equations

Apart from the different models previously presented, a number of authors have proposed different empirical models to describe the kinetics of solid-solid reaction.

Patai and Hoffman (1950), in their study of the carbon black and solid potassium perchlorate, have used the empirical rate expressions:

$$dx/dt = k_{12}(a_1-x)(a_2-0.5x) \qquad (2.36)$$

and

$$dx/dt = k_{13}\,[(a_1-x)(a_2-0.5x)]\,/\,0.5x \qquad (2.37)$$

where a_1 and a_2 are the initial amounts of carbon and potassium perchlorate.

Akashi et al. (1973) obtained high purity niobium metal by the carbothermic reduction of pure niobium pentoxide under argon or argon-hydrogen (5-20 %) plasma arcs. A simplified reaction kinetic model was used to describe the reaction between the spherical carbon pellets and molten niobium pentoxide. The niobium content of the product at any time, t, during the reaction was expressed by the equation:

$$Nb(\%) = 69.9W^\circ_n / \{0.699W^\circ_n + 2.332W^\circ_c\ (1+k_1W^\circ_c{}^{2/3}t)^{-3/2}\} \quad (2.38)$$

where Nb(%) is the niobium content (wt. %) in the product at any time t, t is the reaction period since the beginning of the reaction, W°_n and W°_c are the weights of niobium pentoxide and carbon in the sample at t=0, and k_9 is a constant closely related to the rate constant of the interfacial reaction, surface area of the carbon particle and its grain size.

2.5.3 Conclusion

In the preceding section, several examples of solid-solid reactions and their possible mechanisms have been reviewed. Also presented were the different mathematical models that were developed to describe the conversion-time relationships for the different kinetic regimes. Special emphasis was placed on the carbothermic reduction of metal oxides.

It would appear that it is generally believed that the carbothermic reduction of metal oxides occurs via the reaction prod-

ucts carbon monoxide and carbon dioxide. In all the cited work, the authors assumed the overall reaction rate was controlled by the reaction of carbon dioxide with carbon. The proof for the appropriateness of this assumption was indirect. The conversion-time relationship for this rate-controlling step was commonly described by an irreversible first order reaction rate expression where the reaction was assumed to be taking place throughout the pellet or particle (homogeneous reaction). Nucleation was sometimes cited as the process of initiation for the reaction.

Finally, due to the chemical complexity of ores and concentrates, like pyrochlore, and the influence of added components, like iron, on the chemical activity of each of the species already present, the modelling of the reaction rate of such a system will be complicated. Thus, the choice of an appropriate model will be justified, if it agrees with the conceptual representation of the progress of the reaction and if the reliability and accuracy of the experimental data are good enough to take into account the complexities of the more sophisticated models. But, at the same time it must be relatively simple to be applicable for its intended use - the evaluation and design of an industrial process.

CHAPTER III

EXPERIMENTAL EQUIPMENT AND PROCEDURE

3.1 Introduction

This section describes the experimental apparatus used in this work. The reactant materials, measurement techniques and the experimental procedure are also presented in this section.

3.2 APPARATUS

The apparatus used in this work is shown schematically in Figure 3.1. It consisted of the following separate units:

1. Power supply
2. Gas and water flowrate instrumentation
3. Control console
4. Cathode assembly
5. Anode assembly
6. Stainless steel reactor/graphite crucible
7. Auto-ignition system
8. Current reducing system
9. Test-stand

The various parts are discussed below.

3.2.1 Power Supply

The power was supplied by a Thermal Dynamics 40-kW selenium rectifier, model TDC IA-40, having a drooping characteristic. The input voltage is 3-phase, 60-Hertz, 575-volts, while the output circuit can provide 80, 160, or 320 volts (dc). The 320 open circuit voltage was used for all the experiments. The rectifier was

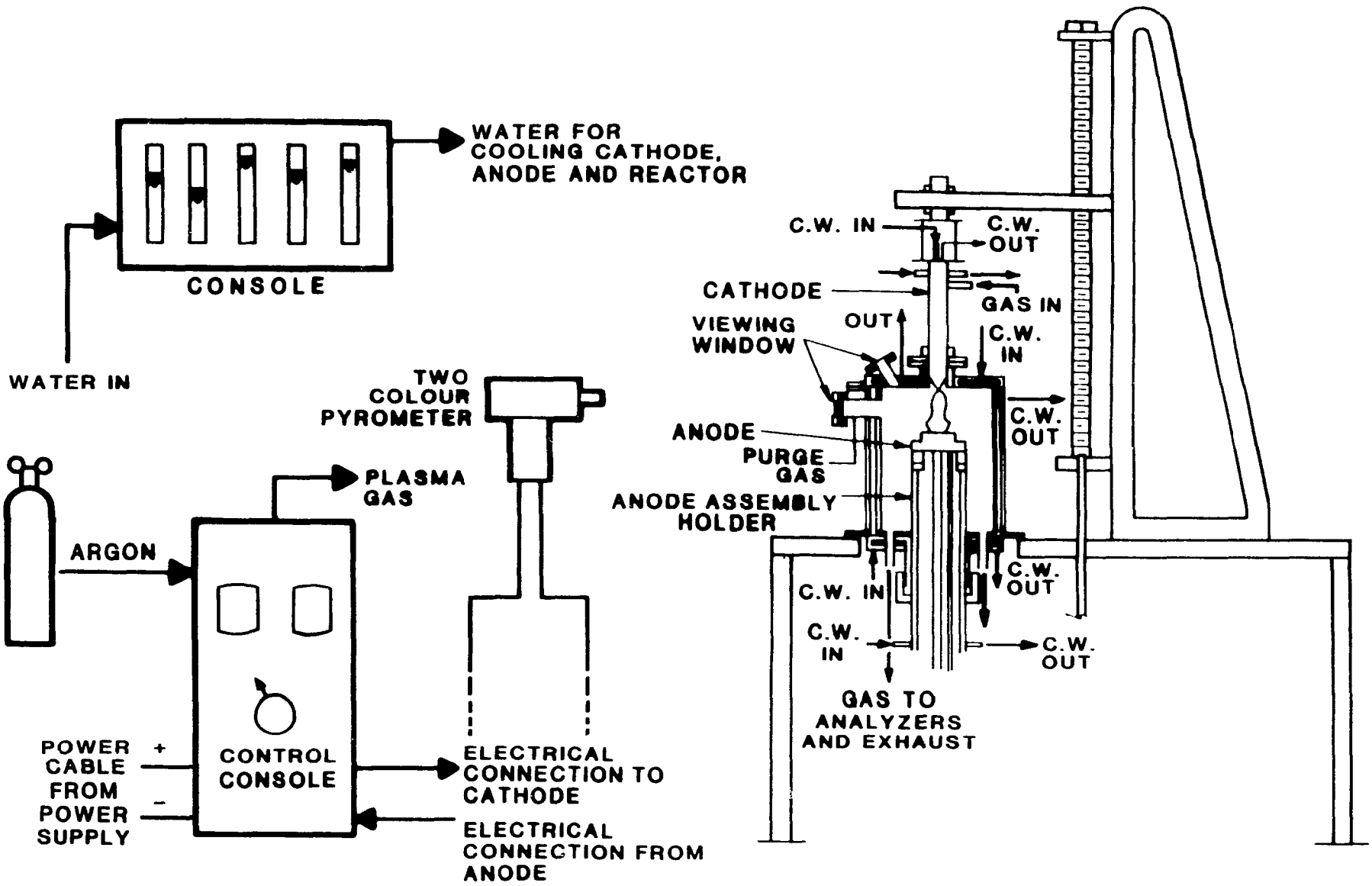

Figure 3.1 Schematic Drawing of Equipment

connected to a control console.

3.2.2 Gas and Water Flowrate Instrumentation

Argon gas was supplied from a gas cylinder and its pressure was regulated by a two-stage pressure regulator. The pressure of the rotameter was maintained at a constant value of 379 kPa. The flow of 29.2 ± 0.152 (95 % confidence limit) litres per minute was measured by a rotameter which was calibrated at 379 kPa and 295 K. Another rotameter was placed at the exit of the exhaust from the reactor to detect any gross leaks in the system.

Water for cooling the reactor and the cathode and anode assemblies was supplied at 690 kPa and its flowrate was measured by six rotameters.

3.2.3 Control Console

The control console is equipped with all the controls for the starting system (a high frequency starter) as well as for the gas flow rate and the current flow to the torch and an ammeter and voltmeter. The console contains a safety interlock device which requires a preset pressure of argon gas. The required pressure is 379 kPa.

3.2.4 Cathode Assembly

The cathode assembly design is based on the Sheer et al. (1973) " Fluid Convection Cathode " design. It is similar to that used by Parisi (1988) and Tsantrizos (1988).

The cathode assembly, shown in Figure 3.2, comprised a water-cooled 2 % thoriated-tungsten cathode tip surrounded by a water-cooled concentric sheath nozzle. The plasma gas was introduced through the annulus between the two. A nozzle orifice

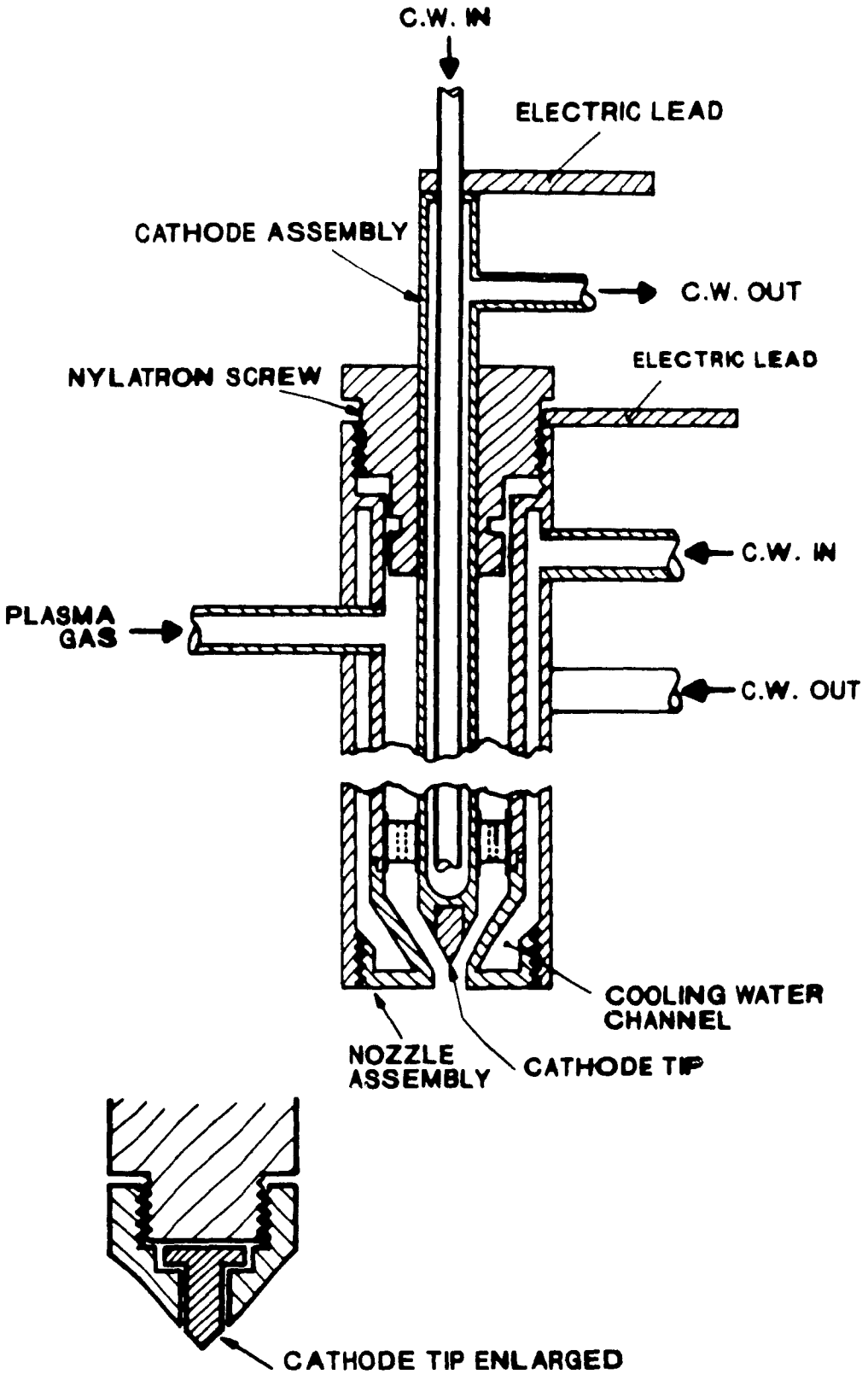

Figure 3.2 The Cathode Assembly (Not to Scale)

diameter of 0.79 cm was used. To increase the working life of the cathode assembly, the nozzle tip contained a cylindrical section 3.2 mm long rather than being sharp-edged (Parisi, 1988). The end of the water-cooled concentric sheath consisted of a screwed-on insert which could be easily removed and replaced if it was damaged or worn. The 2 % thoriated-tungsten cathode tip insert was also removable and was encased in a threaded brass holder (see Figure 3.2). The holder with the tip insert was then screwed onto the water-cooled cathode. This design was incorporated to allow easy changing of the cathode tips for those of different materials or to replace worn or damaged ones. The vertical position of the cathode tip is adjustable via a nylotron screw arrangement so that the protrusion of the cathode tip into the nozzle could be adjusted as desired. Normally, the cathode tip was positioned (withdrawn) about 1.5 mm from the exit of the nozzle.

This construction proved to be very durable and lasted for the duration of the experimental program.

3.2.5 Anode Assembly

The anode assembly was made of copper and brass and is shown in Figure 3.3. It consisted of four parts; the anode disc, the disc holder, the anode holder and the anode assembly holder. The anode disc diameter is 6.35 cm and the thickness is 3.175 mm. The disc was soft-soldered to the disc holder and was heavily cooled by water impinging on the back, directly beneath the arc. The anode holder contains an 'O'-ring, coolant inlet and outlet tubes and a thin copper block to which the positive electric (or anode

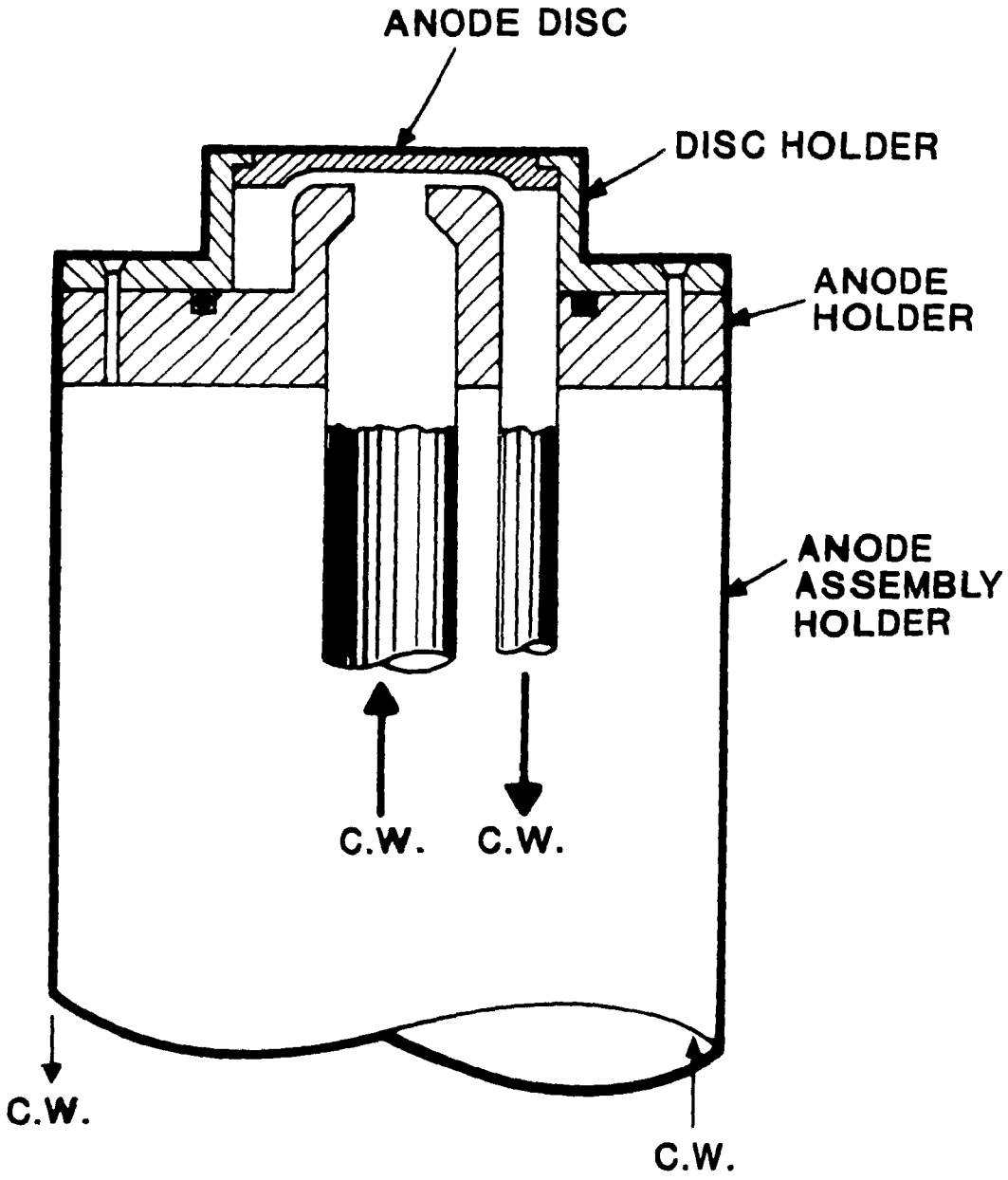

Figure 3.3 The Anode Assembly (Not to Scale)

terminal) is attached. The disc and the anode holder are attached to the brass anode assembly, which is water-cooled. The holder is movable in a vertical direction, passing through a gas-tight 'O'-ring seal in the bottom flange section of the reactor. For this work, the holder was kept at a fixed height.

3.2.6 Stainless Steel Reactor/Graphite Crucible

The reactor was previously used by Choi (1980) and consisted of a top flange, a main cylindrical body and a bottom flange as shown in Figure 3.1. The top flange comprised an opening to accommodate the cathode assembly and a viewing port for observing the crucible and the plasma arc. The main cylindrical body (12.7 cm id.) contained double water-cooled walls and a rectangular viewing port (1.27 cm x 10.16 cm) for pellet temperature measurement. The windows for both viewing ports were made of quartz. The bottom flange contained an opening for the anode assembly holder and four equally-spaced exhaust gas exits. Only two diametrically opposed exits were used in this work.

The graphite crucible containing the reactants was placed in the centre of the plasma arc on top of the anode. A schematic drawing of the crucible and its position relative to the anode and cathode is shown in Figure 3.4. The distance between the tip of the cathode and the top of the pellet was kept constant at about 3 cm. The crucible was cylindrical in shape (19.5 mm id., 20mm -height), with a wall thickness of 3 mm. There was 6 mm high raised cylindrical platform (12.8mm id.) in the bottom of the crucible. This feature was for centering the pellet in the crucible and to help minimize the temperature gradient in the pel-

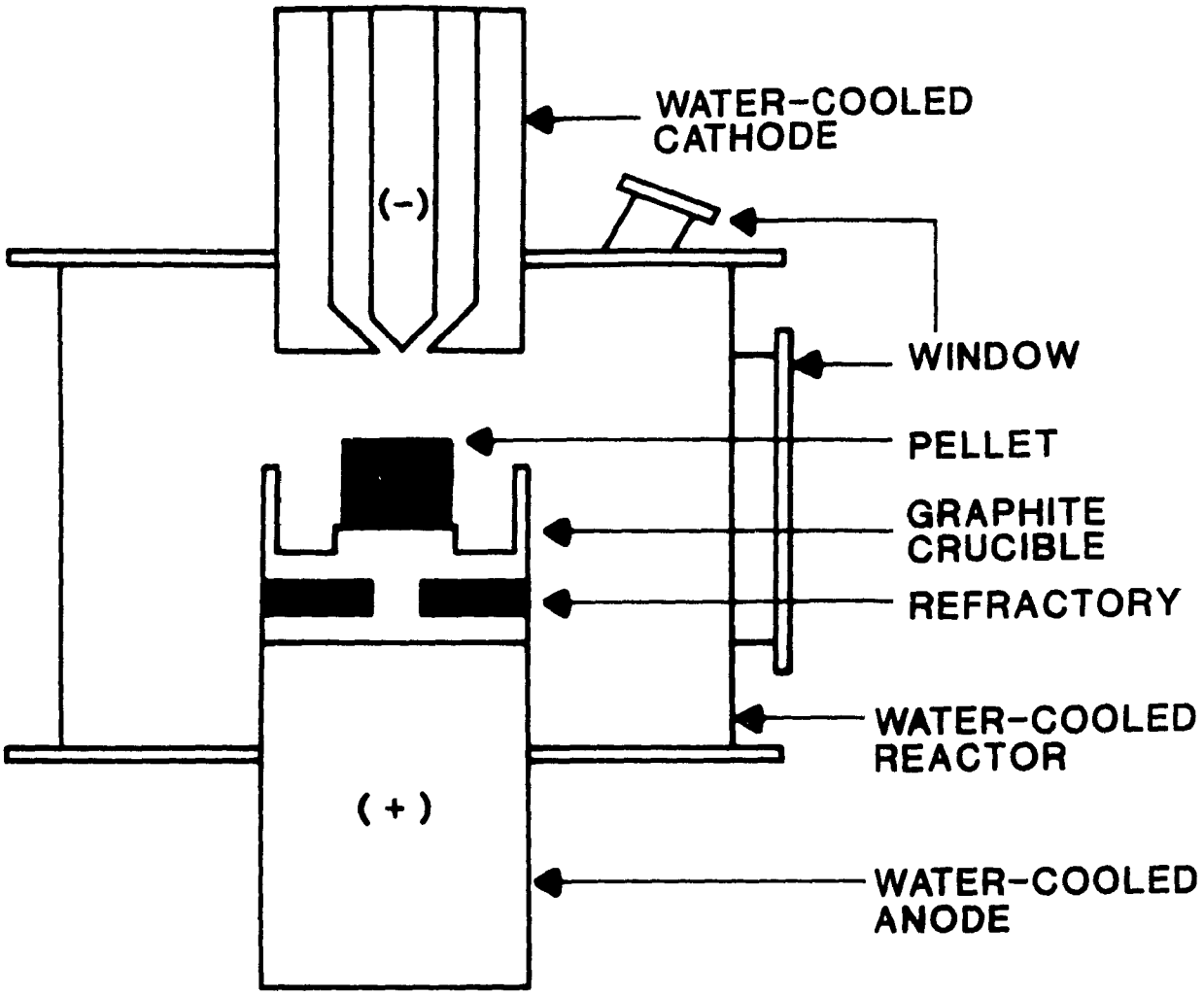

Figure 3.4 Schematic Drawing Showing the Position of Crucible and Pellet Relative to the Anode and Cathode

let. A donut-shaped piece of boron nitride was sandwiched between the crucible and a circular graphite disc. The boron nitride was included to insulate the crucible from the water cooled anode and thus further help to minimize the temperature gradient in the pellet. A threaded graphite rod (6.3 mm od.) joined the crucible to the circular graphite disc and also provided the electrical contact between the crucible and the anode.

3.2.7 Auto-ignition System

The most common method currently used for initiating or igniting the plasma arc in a transferred-arc plasma system involves lowering the cathode to within a few millimetres of the stationary anode surface and then striking a high frequency spark. Another version (Huels, Aerospatiale commercial torches) is to introduce an auxiliary anode between the cathode and the fixed anode. The method described here permitted transferred arcs to be initiated with electrode separations of as much as 10 cm and has been treated in detail by Parisi (1988). A bank of thin-walled stainless steel tubes (1.3 ohm/m) having an equivalent resistance of 2.4 ohms was used to connect the nozzle to the anode. The stainless steel tubes had an outside diameter of 31.8 mm and a wall thickness of 0.165 mm. A circuit diagram is given in Figure 3.5.

To initiate the transferred arc, a high frequency generator was used to strike an arc between the cathode tip and the nozzle, creating a d.c. jet extending to the anode. This zone of ionized electrically-conducting gas would then allow the formation of the transferred-arc between the cathode tip and the anode, which has

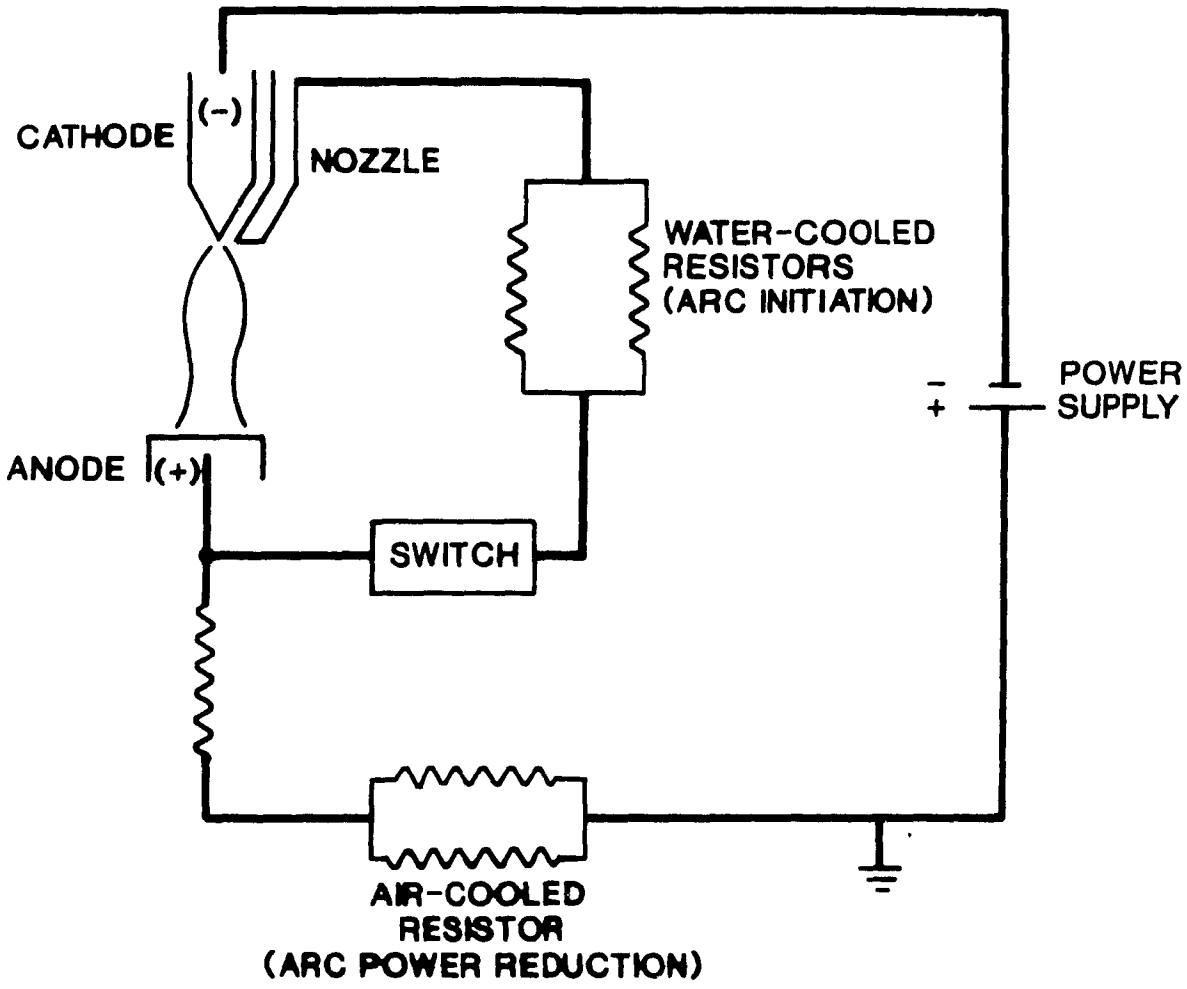

Figure 3.5 Schematic Drawing of the Auto-ignition and the Power Reducing Systems for The Plasma Reactor

no resistance in its circuit. The switch in the auto-ignition circuit would then open, thus preventing any current from flowing through that circuit. The switch was a mechanical circuit breaker capable of withstanding the rectifier's open circuit voltage of 320 volts.

3.2.8 Power Reducing System

During preliminary experiments, it was found that the rectifier was capable of producing more than enough power to obtain high pellet reaction temperatures. Low temperature could however not be achieved because the lower power settings still allowed currents in excess of 100 amperes. This severely limited the operating range for the pellet reaction temperatures. To overcome this, a bank of resistors was connected in series between the anode and the rectifier. The bank of resistors consisted of three resistors, manufactured by Ohmite Mfg. Co., Skokie, Illinois, which were connected in series and had values of 0.1, 0.1, and 0.3 ohm. They were air-cooled and are shown in Figure 3.5. The use of these resistors in various combinations allowed the use of currents as low as 65 amperes. For currents greater than 100 amperes, the resistors were removed from the circuit.

3.2.9 Test-Stand

The test-stand, shown in Figure 3.1, consisted of a four-legged metal table and a supporting beam to which the movable cathode assembly was attached. The stainless steel reactor was supported at the centre of the table. To facilitate easy removal, the bottom of the reactor was affixed with four toggle clamps. The vertical up and down movement of the anode assembly and

holder for loading and unloading the reactor was achieved with a scissors jack.

3.3 Materials

The different materials used in this work are described in the following sections.

3.3.1 Source of Niobium Pentoxide

The niobium pentoxide used in this work was available in two different forms: a) as the pure niobium pentoxide and b) as present in a pyrochlore concentrate.

The niobium pentoxide used was from BDH Chemicals Ltd., Poole, England. The minimum assay for niobium pentoxide was 99.5 % and the typical trace analysis of the material by induction coupled plasma emission spectroscopy is given in Table 3.1. Particle size was analyzed using an X-ray sedimentometer (SediGraph 5000D Particle Size Analyzer, Micromeritics Instrument Corp., Norcross, Georgia) which measured the sedimentation rates of the niobium pentoxide particles suspended in ethyl alcohol, and presented the data as a cumulative mass percent distribution in terms of equivalent spherical diameter. The result given in Figure 3.6, showed that about 97 mass percent of the particles had an equivalent diameter less than 40 microns and the mass median diameter corresponded to 8.8 microns. The melting point of niobium pentoxide is 1758 K ± 5 K and the density is 4470 kg/m^3 (Weast and Astle, 1979.)

The pyrochlore used in this work was donated by Niobec Inc.,Ste. Honore, Quebec. Analysis of the pyrochlore was per-

TABLE 3.1 Analysis of Niobium Pentoxide Used In Kinetic Study

Impurity	CONCENTRATION, PPM
W	60
Ti	50
Na	30
Si	10
Mg	3

Loss on Ignition : 0.4% (at 1000^{o}C)

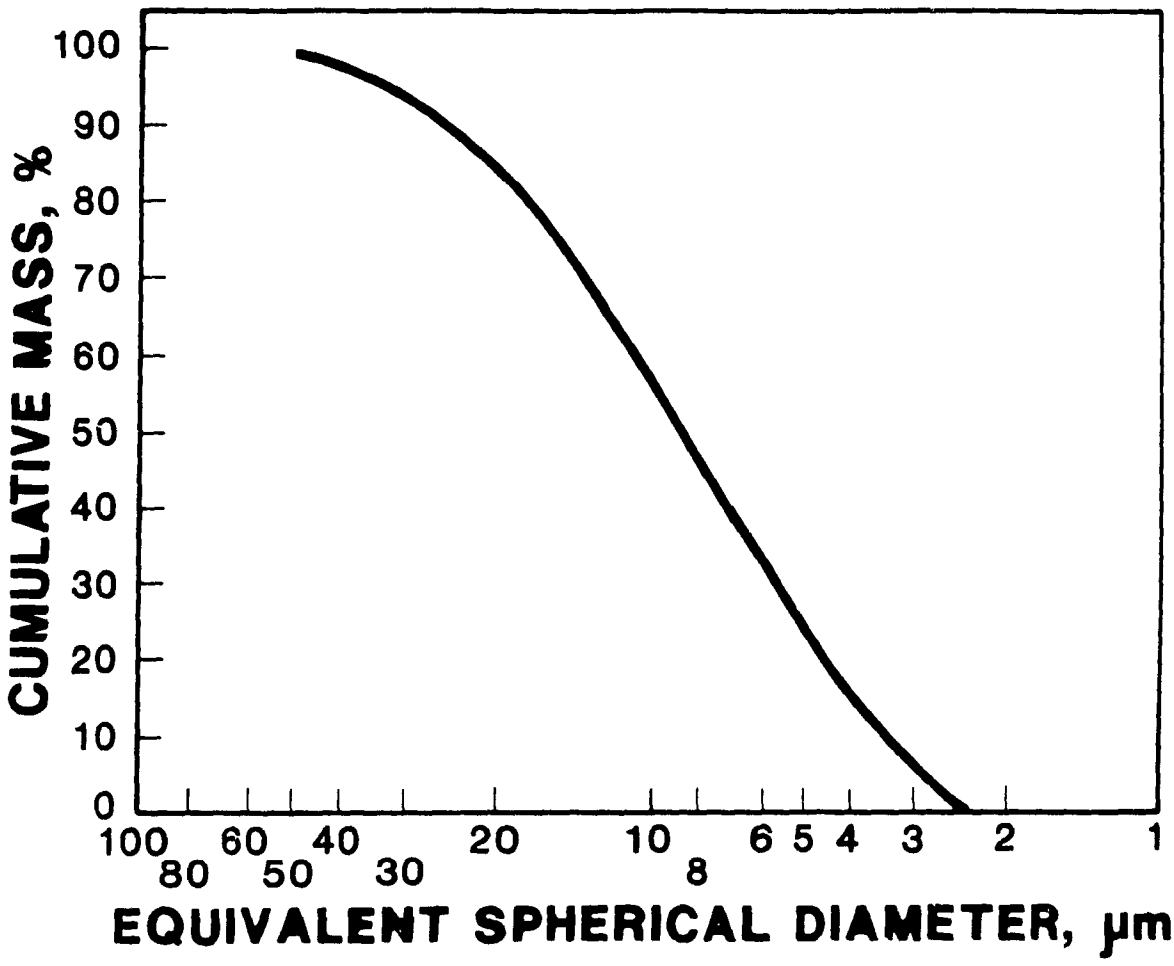

Figure 3.6 Niobium Pentoxide Particle Size Distribution

formed by the same company and the results are given in Table 3.2. Particle size was determined using standard Tyler screens. The particle size distribution is shown in Figure 3.7. and the median mass diameter was 60 microns. The melting point of pyrochlore was estimated to be 1535 K by the cooling curve method described below. The density of pyrochlore was measured with a water pycnometer. The density was 4305.6 kg/m^3, with a standard deviation of 103.98 kg/m^3.

Different pyrochlore particle sizes were required for the experimental work. These were obtained by sieving the pyrochlore and taking those fractions between the two sieve sizes. The average of the two sieve sizes would be considered as the average particle size for that fraction. The corresponding sieve sizes used to obtain average particle sizes of 31, 98, and 230 microns, were 38 and 35 microns, 106 and 90 microns and 250 and 210 microns respectively. Separate x-ray diffraction patterns of the three fractions were identical to that of the original sample. This proved the homogeneity of all the pyrochlore source used in the experimental work.

3.3.2 Graphite

The graphite particles used throughout the work were from Great Lakes Carbon Corporation. Using the ASTM procedure for ash determination (C 561-85), the ash content for the graphite particles was found to be 0.44 %. The density of graphite is 2250 kg/m^3 (Weast and Astle, 1979).

Different graphite particle sizes were obtained by sieving as for pyrochlore. The corresponding sieve sizes used to obtain

Table 3.2 Analysis of Niobec Pyrochlore Used In Kinetic Study

Component	Weight %
Nb_2O_5	62.2
Ta_2O_5	0.28
TiO_2	3.12
SiO_2	2.91
P_2O_5	0.09
S	0.07
SnO_2	0.03
Fe,total	1.36
ThO_2	0.48
U_3O_8	0.06
CaO	13.4
MgO	0.14
Al_2O_3	0.44
Na_2O	5.98
K_2O	0.29
SrO	0.93
C	0.09
PbO	0.03
BaO	0.10
ZrO_2	0.86
F	3.66
total RDO	0.85
Cu	trace

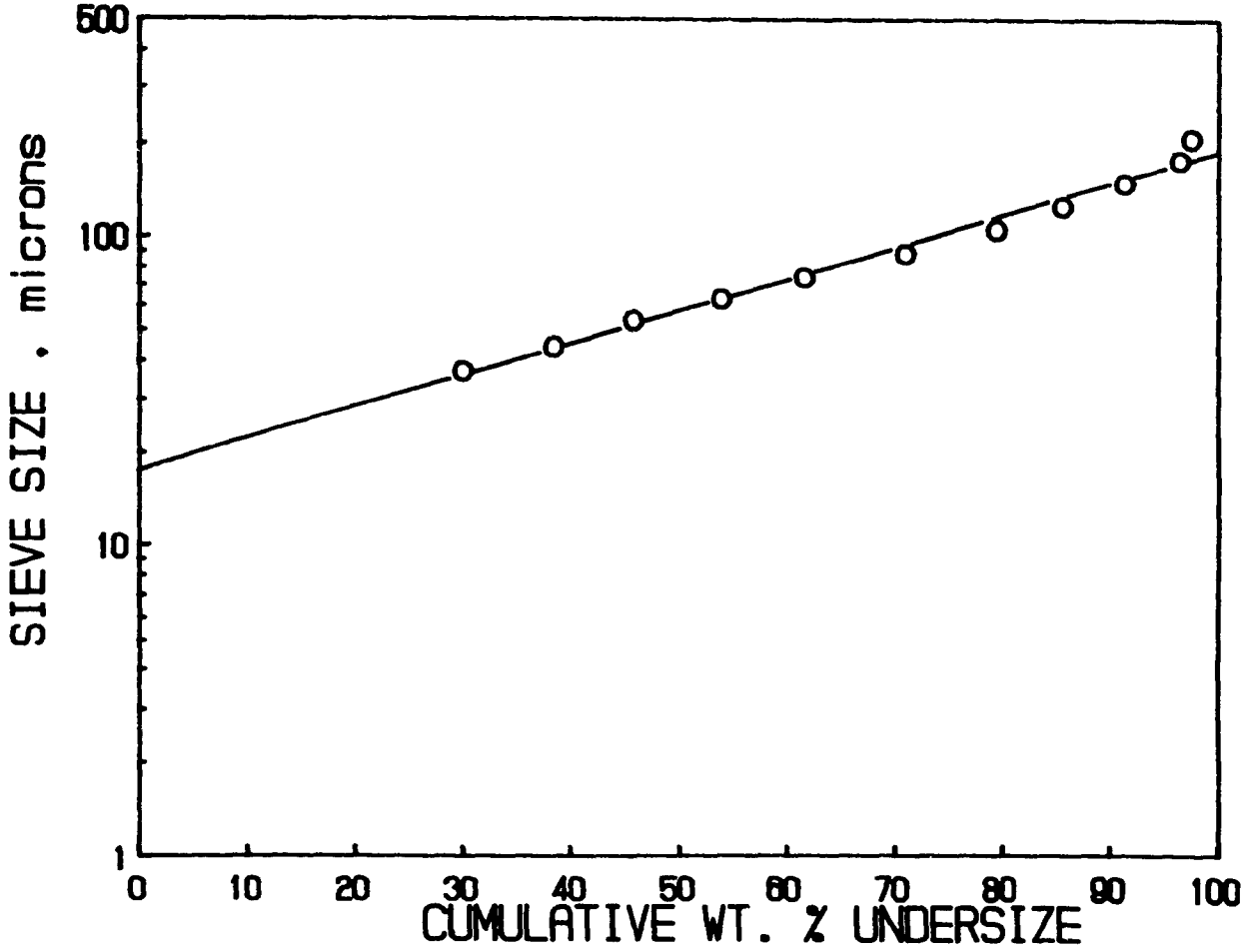

Figure 3.7 Pyrochlore Particle Size Distribution

average particle sizes of 165 and 460 microns were 180 and 149 microns and 500 and 420 microns respectively.

The graphite rods (2.54 cm diameter) used to make the graphite crucibles were supplied by Speer Carbon, St. Laurent, Quebec. Typical chemical analysis for the rods are given in Table 3.3.

3.3.3 Iron

The iron powder was supplied by Aldrich Chemical Company Inc., Milwaukee, Wisconsin. The minimum assay for iron was 97 %. The particle size was 100 % less than 45 microns. The melting point of iron is 1808 K and the density is 7860 kg/m^3 (Weast and Astle, 1979)

3.3.4 Iron Oxide

The iron oxide used in this work was certified red anhydrous ferric oxide, having a minimum purity of 99.8 % and was supplied by Fisher Scientific, Fairlawn, New Jersey. Analysis of the material supplied by the company is given in Table 3.4. The particle size was 100 % less than 45 microns. The melting point of ferric oxide is 1838 K and the density is 5240 kg/m^3 (Weast and Astle, 1979).

3.3.5. Plasma Gas

The plasma gas throughout the work was argon, with a purity of 99.99 %. This was supplied in cylinders by Cryo Gaz, Montreal, Quebec.

Table 3.3 Analysis of Graphite Rod Used For Crucible

MATERIAL	CONCENTRATION %	PPM
Carbon	97	-
Sulphur	1.3	-
Ash	0.5	-
Ca	-	300
Fe	-	200
Si	-	400
V	-	100

Table 3.4 Analysis of Ferric Oxide Used In Kinetic Study

COMPONENT	CONCENTRATION, %
Arsenic (As)	about 0.002; P.T.
Nitrate (NO_3)	0.01
Phosphate (PO_4)	0.005
Sulphate (SO_4)	0.04
Manganese (Mn)	0.013
Copper (Cu)	0.004
Substance not ppt'd by NH_4OH	0.04
Zinc (Zn)	0.005

3.4 Measurement Techniques

3.4.1 Preparation of Pellets

Each set of experimental measurements was carried out with cylindrical pellets of slightly different heights and porosities compacted from a chosen combination of the previously described materials. A die compaction method with pressure applied to both ends of the powder mass was used to prepare the pellets. The die consisted of a cylindrical holder and two cylindrical punches. The presence of graphite, which is a good lubricant, made the preparation of the pellets easy but the pellets would crumble when placed in the plasma. A 50-50 mixture of molasses and water was added to the pellets as a binder, and the pellets dried in an oven at 353 K for twenty-four hours. This process greatly improved the mechanical strength of the pellets.

In order to keep the amount of molasses constant throughout the experimental work the available niobium pentoxide and the amount of binder was kept constant at 2.9 and 0.5 gram respectively. The weight of 0.5 gram of molasses represented between 1.2 to 7.6 % of the pellet's weight, depending upon the types of reactants that made up the pellet. The weight of the amount of available niobium pentoxide was chosen after several trials so as to: a) provide enough material for product analysis, b) minimize the temperature gradient along the axis of the pellet during the reaction and c) ensure the total volume concentration of carbon monoxide and carbon dioxide in the exhaust gas did not exceed 10 percent. The amount of the other reactants were added accordingly.

The dimensions and densities of the pellets made with different amounts of graphite only, or graphite with either iron or ferric oxide, mixed with niobium pentoxide and pyrochlore respectively are given in Appendix I. Photographs of two pellets made from graphite mixed with niobium pentoxide and pyrochlore, respectively, are shown in Figure 3.8. Pellets containing iron additions were of similar shape and appearance.

3.4.2 Measurement of Arc Voltage and Current

The total arc voltage and current were measured for all the test for general reference.

Voltage measurements were made via the voltmeter attached to the control console and a strip chart recorder (Hewlett Packard model 7155B). A voltage divider was used to reduce the voltage to the strip recorder. In this case, the voltage was divided by 16.

The arc current was measured via a voltmeter (Micronta 22-185 Digital Multimeter) and a strip chart recorder (Esterline Angus Model T171B) connected to a shunt which was connected in series with the arc. The reading accuracy of the arc current and voltage were ± 1 amperes and ± 0.8 volt respectively.

3.4.3 Measurement of Reaction Time

The reaction time was measured from the strip chart recorder (Graphtec Corp.,SR6211) which was used to record the carbon monoxide and carbon dioxide concentrations in the exhaust gas from the reaction. The chart speed was calibrated at 500 mm per minute.

(a)

(b)

Figure 3.8 Photographs of Unreacted Oven-dried Pellets, (12.4 mm dia., 24.0 wt. % C) :
(a) Nb_2O_5 + C, d_pC = 165 μm,
(b) Pyrochlore + C, d_pC = <45 um

3.4.4 Measurement of Pellet Temperature

Generally, thermocouples or optical pyrometry can be used to measure solid temperature in the range 1400 and 2500 K. In this work the latter was selected, since thermocouple temperature measurements were found to be impossible (Munz, 1974), (Sayegh, 1977), (Biceroglu,1978) in the case of induction plasma systems. The temperature of the reacting pellet was measured using a Milletron's THERM-O-SCOPE manufactured by Capintec Instruments Inc.,Ramsey, New Jersey. The THERMO-O-SCOPE is an automatic radiation ratio (two colour) pyrometer. The temperature reading is dependent on the ratio of the intensity of the radiation at two wavelengths. This method practically eliminates the effect of changing emissivity and reflectivity on temperature reading, provided the emissivity is independent of wavelength. For non-metals, the wavelength dependency of emissivity is quite weak, while for metals, the peak emissivity is exhibited near the visible wavelength region, with a decrease at values of wavelength higher and lower than this (Welty, 1974). As far as the correction for the quartz window transmittance was concerned, this is eliminated by the two wavelength pyrometer. The two wavelengths used for this pyrometer were 0.65 and 0.55 microns. The working range of the pyrometer was between 1220 to 3770 K. The pyrometer had an automatic calibration feature. The minimum target image required for good measurements was 1 mm. Two close up lens, giving a magnification of x 4, were used to obtain more than sufficient object sizes for good temperature measurements and visual observations of the reaction. The pyrometer's recorder output was

0 - 1 volt dc full scale.

It was found that the intensity of the plasma arc interfered with the measurement of the pellet temperature during the reaction. Matsumoto and Saito (1974) reported a similar problem. To overcome this problem, the temperature decay curve was recorded in volts on a strip chart recorder (Graphtec Corp., SR6211) immediately after the plasma is extinguished. This curve was then plotted on semi log paper and extrapolated back to the time of plasma shut down. The pyrometer output was calibrated using a tungsten lamp as recommended by the manufacturer . The temperature recorded by the pyrometer was checked using a high resolution pyrometer (Pyro Micro Optical Pyrometer, The Pyrometer Instrument Co.,Inc., Northvale, New Jersey). The temperature was found to be a linear function of output voltage and could be expressed as:

$$T_C = 926.54 + 2139.99\ v_T \qquad (3.1)$$

where T_C is the temperature in Celsius and v_T is the pyrometer output in volts. The regression line is shown in Figure 3.9 and had a correlation coefficient of 0.9999.

The precision of the two colour pyrometer was examined by measuring the melting point of several pure materials using the cooling curve method. The materials used were gamma alumina, niobium pentoxide, iron and stainless steel (ss316L). The results are summarized in Table 3.5. Since the melting point of Niobec's pyrochlore was unavailable either in the open literature or from

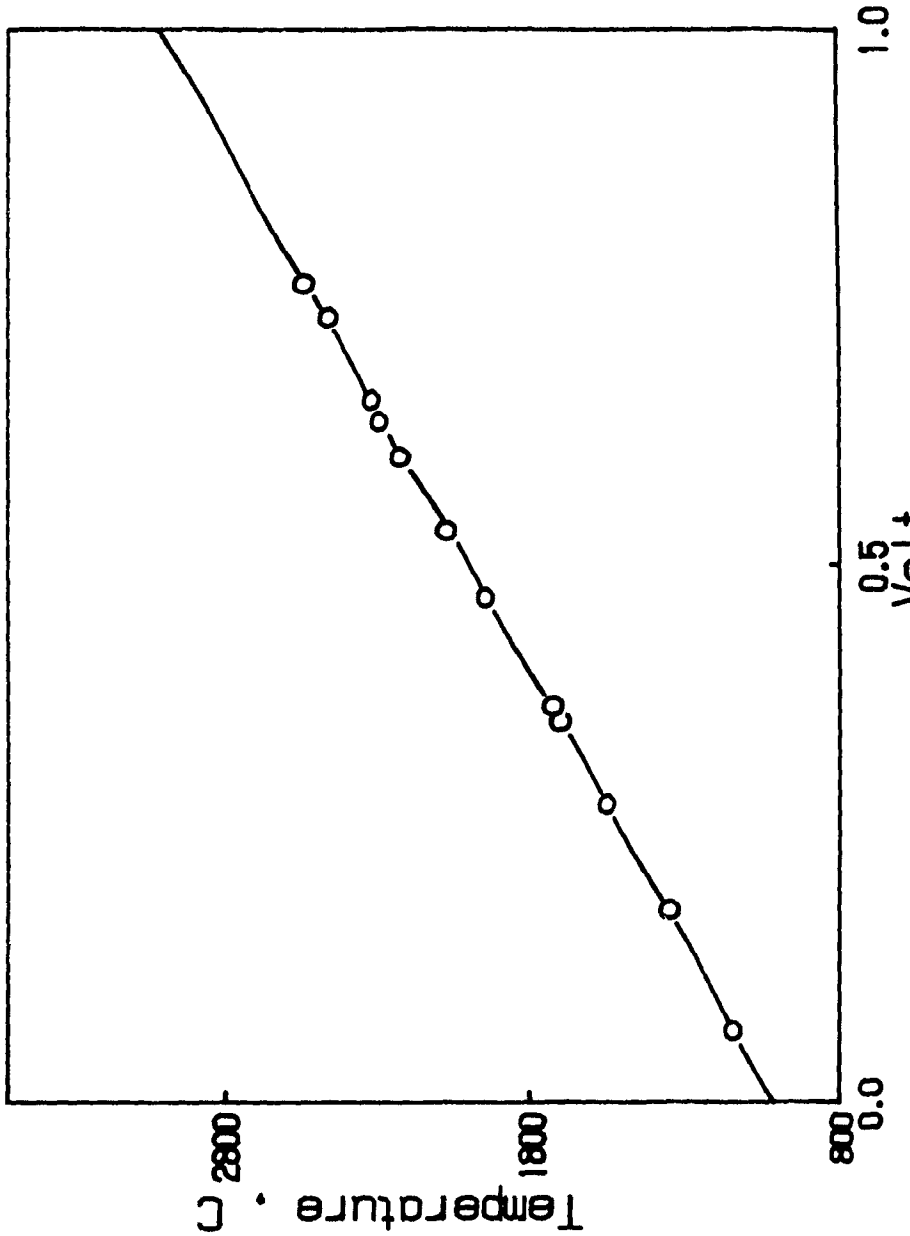

Figure 3.9 Calibration for Two Colour Pyrometer

Table 3.5 Melting Point Determination Using Two Colour Pyrometer

MATERIAL	MELTING POINT , K		
	MEASURED	STANDARD DEVIATION	THEORECTICAL
Gamma Alumina	2345	16	2288±15[1]
Nb_2O_5	1744	16	1758±5[1]
Iron	1782	41	1808[1]
Stainless Steel (ss316L)	1646-1685	18	1644-1672[2]
Niobec Pyrochlore	1535	21	unavailable

1. Weast and Astle (1979)
2. Perry and Chilton (1973)

the company, it was estimated by this method to be 1535 K with a standard deviation of 21 K.

3.4.5 Measurement of Carbon Monoxide

The carbon monoxide in the exhaust gas from the reactor was measured using a Horiba Mexa-201GE Infra red CO analyzer. The repeatability of the analyzer is ± 0.04 volume % or ± 2 % of the reading whichever is greater. The measuring range of the analyzer was 0 - 10.0 volume percent. The output of the recorder is 0 - 1 volt dc full scale and was recorded on a strip chart recorder (Graphtec Corp., SR6211).

The meter was calibrated using different certified concentrations of carbon monoxide, carbon dioxide and argon gas mixtures. The gas mixtures were supplied by Liquid Carbonic, St. Laurent, Quebec. The carbon monoxide concentration was found to be a linear function of output voltage and could be expressed as:

$$C_1 = 10.04\ V_1 - 0.004 \qquad (3.2)$$

where C_1 is the volume percent carbon monoxide and V_1 is the analyzer output in volt. The regression line is shown in Figure 3.10 and had a correlation coefficient of 0.9999.

Random samples of the exhaust gas were taken from some of the experiments to identify the types of gases that were present in the off-gas. These are discussed under those specific experiments.

3.4.6 Measurement of Carbon Dioxide

The carbon dioxide in the exhaust gas from the reactor was

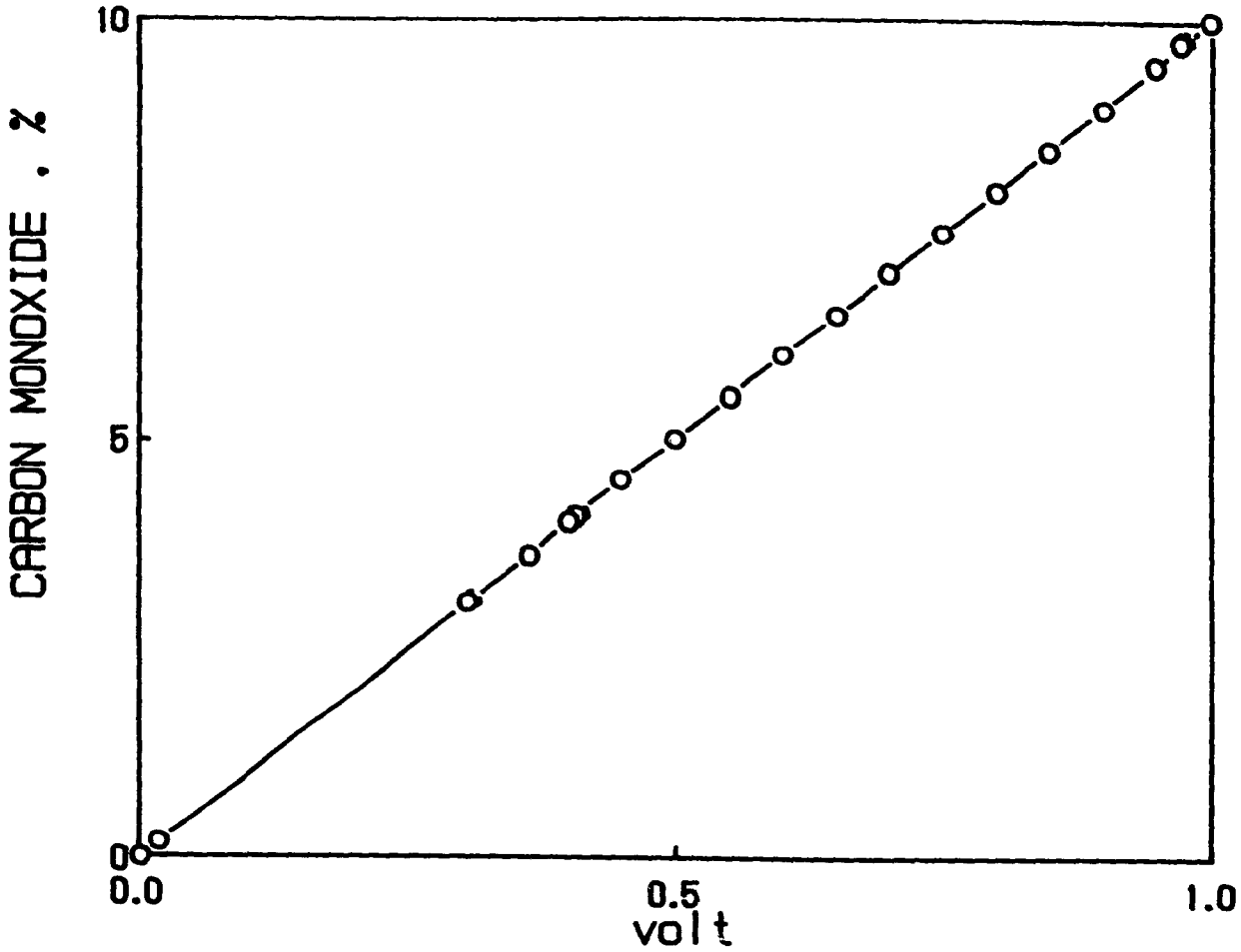

Figure 3.10 Calibration for Carbon Monoxide Analyzer

measured using an Horiba Mexa 211GE Infra red CO_2 analyzer. The repeatability of the analyzer was ± 0.3 volume percent or ± 2 % of reading, whichever is greater. The measuring range of the analyzer was 0 - 20 volume percent. The output of the recorder was 0 - 1 volt dc full scale and was recorded on a strip chart recorder (Graphtec Corp., SR6211).

The meter was calibrated with different certified concentrations of carbon monoxide, carbon dioxide and argon gas mixtures. The gas mixtures were supplied by Liquid Carbonic, St. Laurent, Quebec. The carbon dioxide concentration was found to be a linear function of output voltage and could be expressed as:

$$C_2 = 20.22\ V_2 \qquad (3.3)$$

where C_2 is the volume percent carbon dioxide and V_2 is the analyzer output in volt. The regression line is shown in Figure 3.11 and had a correlation coefficient of 0.9999.

3.4.7 Measurement of Exhaust Gas Temperature

The exhaust gas temperature was measured by a grounded K-type thermocouple (1.587 mm o.d.). The thermocouple was connected to a digital temperature meter (EireLec, Model Gamma-K). The precision of the temperature meter was ± 0.55°C.

3.4.8 Reaction Conversion

The reaction conversion (x) is defined as:

$$x = (\text{total } O_2 \text{ in CO and } CO_2 \text{ in exhaust gas})/(\text{total } O_2 \text{ in oxides}) \quad \ldots\ (3.4)$$

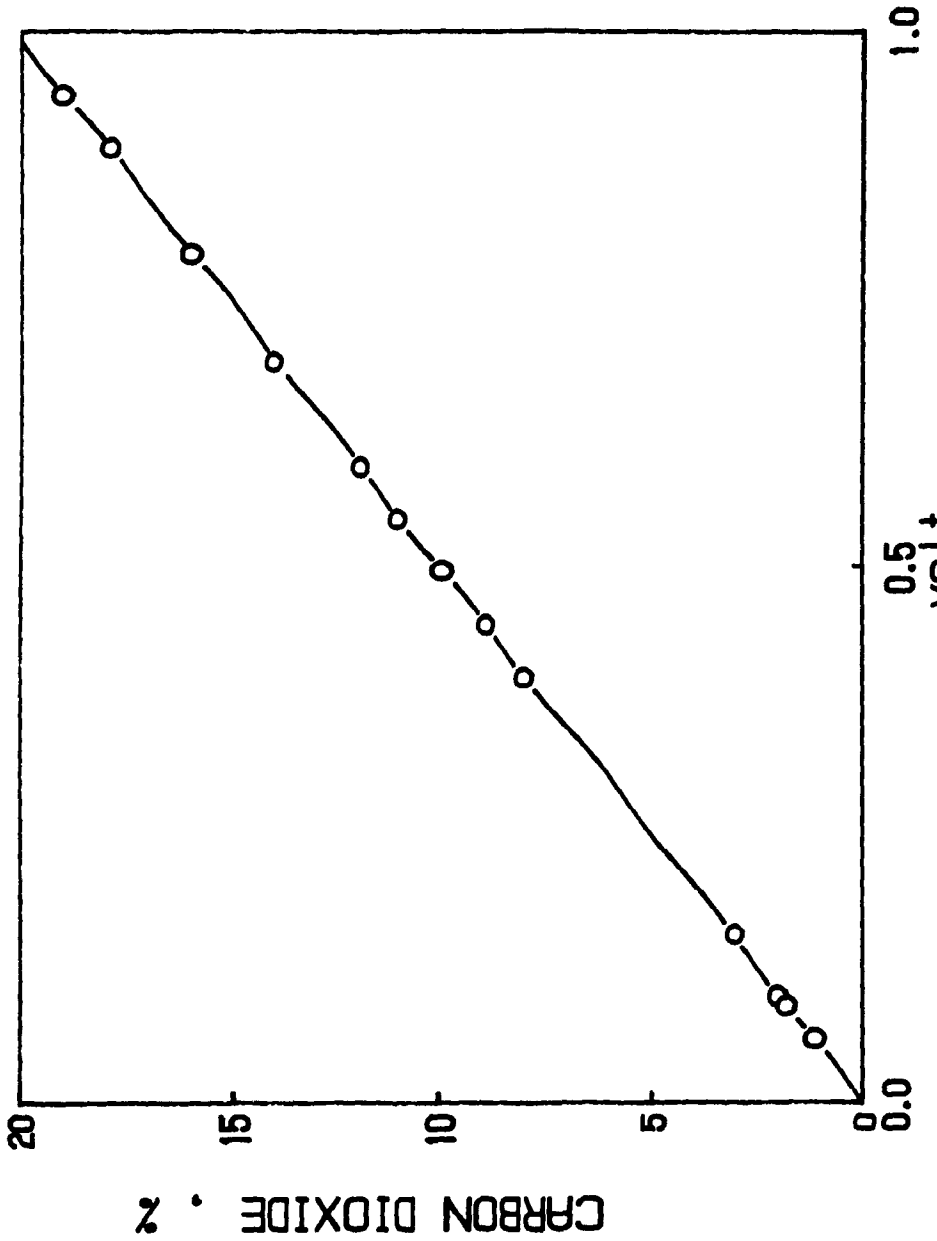

Figure 3.11 Calibration for Carbon Dioxide Analyzer

Since the gas samples are not taken in situ for the definition of x to be valid, it was assumed that a) the reactor was operating as a constant stirred tank reactor (CSTR), and b) the accumulation rate of carbon monoxide and carbon dioxide in the reactor was negligible since their concentrations compared to that of the carrier/plasma gas, argon, were relatively small.

The assumption of a CSTR to describe the mixing characteristics of the reactor was verified by comparing the response curve of the reactor and the predicted residence time distribution (RTD) curve for a CSTR to a step input. Carbon monoxide was used as the inert tracer in an argon environment at 300 K. A termination point of about five times the mean residence time is considered an adequate length of time to give a proper response curve in the case where an inert tracer is used and there is no chemical reaction (Nauman and Buffhan, 1983). The value of the Peclet number varies from 0 to ∞, which is indicative of a range of systems with mixing characteristics from a perfectly mixed system (CSTR), to a plug flow system. From Figure 3.12, it can be seen that the reactor has a Peclet number whose value is less than 5 and its response curve shape is quite close to that for a CSTR, but shifted to the right. The time shift is equivalent to the dead-time for the sampling lines to the reactor. This suggests that the CSTR assumption is valid.

The reaction conversion measured by the gas analysis was calculated by taking CO and CO_2 concentration measurements from the strip chart recorder for every 1.2 second. The measurement of the carbon monoxide and carbon dioxide concentrations in the

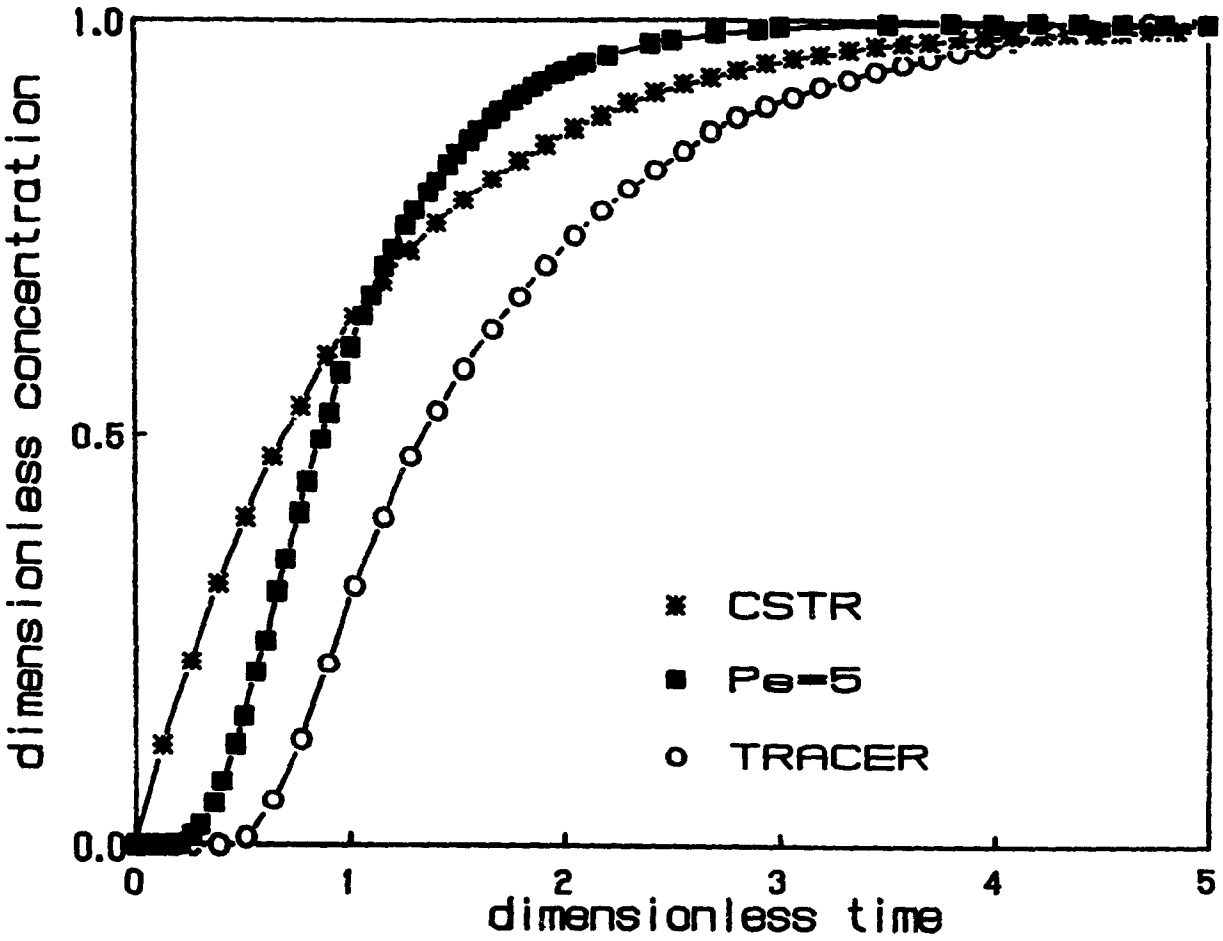

Figure 3.12 Comparison of Residence Time Distribution Curves for Plasma Reactor With That for a CSTR and a Reactor With a Peclet Number of 5

exhaust gas are possible sources of error. However, this was minimized by recalibrating both meters before each experiment. The total conversion obtained by this method was also compared to that obtained by weight loss. Pellets were weighed before and after the reaction on a Mettler PE300 digital balance which could give readings to within ± 0.0001 gm. The accuracy of the balance was ± 0.2 mg.

Several blank runs were carried out in an argon plasma to check the conversion due to niobium pentoxide and pyrochlore, respectively, and (a) the graphite crucible and (b) the binder (molasses and water solution) and the graphite crucible. The weight of the reactants used to make the pellets and the plasma power levels were the same as those used in the experiments.

For case (a), the CO and CO_2 concentrations measured in the exhaust gas were found to be negligible, thus indicating no reaction. Similar results were obtained when iron and ferric oxide was added to the oxides.

For case (b), when binder was added to each respective pellet mixture a small amount of CO and CO_2 was measured in the exhaust gas. Blank runs were done for each pellet mixture consisting of graphite and niobium pentoxide and pyrochlore, respectively, and graphite with and without iron or ferric oxide additions. The CO and CO_2 concentrations in the exhaust gas due to the reaction between the graphite and oxygen in the molasses and the oxygen in the oxides were measured as a function of time. The conversion measured was then adjusted accordingly by subtracting these values from the total measured during the actual exper-

iments.

3.5 PROCEDURE

Before an experimental run, the inside of the reactor was thoroughly cleaned. The cathode tip was also cleaned with fine abrasive paper. The pellet was measured and weighed. The weight of the pellet and the crucible were also recorded. The pellet was then placed on the raised platform in the centre of the crucible. The crucible and the pellet were then placed in the centre of the anode. The anode assembly was then raised into place by a scissors jack. The reactor bottom was closed and secured by four toggle clamps. The argon flow was set at the desired flowrate (29.2 l/min) and confirmed by the rotameter in the reactor exhaust line. The reactor was purged for several minutes to remove any residual oxygen. This proved to be very effective since analysis by gas chromotography of gas samples taken from the exhaust line near the end of the purging time showed no trace of oxygen. The pyrometer was placed in its predetermined position for pellet temperature measurement. The calibration of the CO and CO_2 analyzers were then checked with a calibration gas mixture and then connected to their respective sampling line. The strip chart recorders were then turned on, the arc initiated and the plasma current set at the desired level. The knife switch isolating the measuring instruments for the arc's current and voltage were then connected. The pyrometer was then properly focussed on the pellet. Visual observations of the reaction were also made. When the CO and CO_2 concentrations in the exhaust gas were relatively

small, indicating the end of the reaction, the torch was turned off. Argon flow was also turned off immediately while the pellet's cooling curve was being measured and recorded. After the cooling curve was recorded, the argon flowrate was turned back on and the rest of the CO and CO_2 for any reaction during the pellet's cooling curve measurement recorded. The argon gas flow was maintained while the reacted pellet cooled. This was followed by the crucible's and pellet's final weight measurements and microscopic examination.

The temperature of the reacting pellet was controlled by the current to the plasma and where the arc struck the pellet. The fluctuations in arc voltage for all the experiments were negligible. For a desired temperature, an attempt was made to keep these conditions constant. Several runs were carried out at each current level but the actual temperature of each experiment was used in correlating the data rather than grouping all results at a single current as repetitions. If a considerable temperature fluctuation was recorded for a kinetic run (which happened in an appreciable nu. ber of experiments) the results of that run were ignored. When the graphite concentration was high, some pellets continued to crack and fell apart once the arc was extinguished. This only contributed to the loss of solid. The experiments were designed to obtain conversion-time relationship as a function of particle size, reaction temperature, graphite, iron and ferric oxide concentrations.

CHAPTER IV

THE CARBOTHERMIC REDUCTION OF NIOBIUM PENTOXIDE AND PYROCHLORE WITH AND WITHOUT IRON ADDITIONS : THEORETICAL OVERVIEW - CHEMISTRY AND KINETIC MODEL

4.1 REDUCING AGENTS

Aluminothermit is currently used to produce niobium or its ferroalloy. But, there are other possible reductants which can be considered such as calcium, magnesium, silicon and carbon. Figure 4.1 shows the free energies of oxide formation for these reducing agents. The standard free energies of formation for the reactions shown in Figure 4.1 were taken from Kubaschewski and Alcock (1979) and Turkdogan (1980). A large negative free energy change for the reduction reaction is desired in order to minimize oxide and reductant contamination in the metal product. Calcium and magnesium are autothermic, and as indicated in Figure 4.1 have high reducing potentials at low temperatures. However, these two have low boiling points and reduction with these agents must be performed in pressure tight vessels. Reaction with silicon and carbon are highly endothermic which must be conducted in furnaces where additional energy may be added. Silicon is not favoured because it forms stable silicides and its reducing potential is inferior to that of aluminium, magnesium and calcium. Carbon is a relatively poor reducing agent at low temperatures but improves with increasing temperature.

4.2 CARBOTHERMIC REDUCTION

Carbon is the least expensive raw material and the other

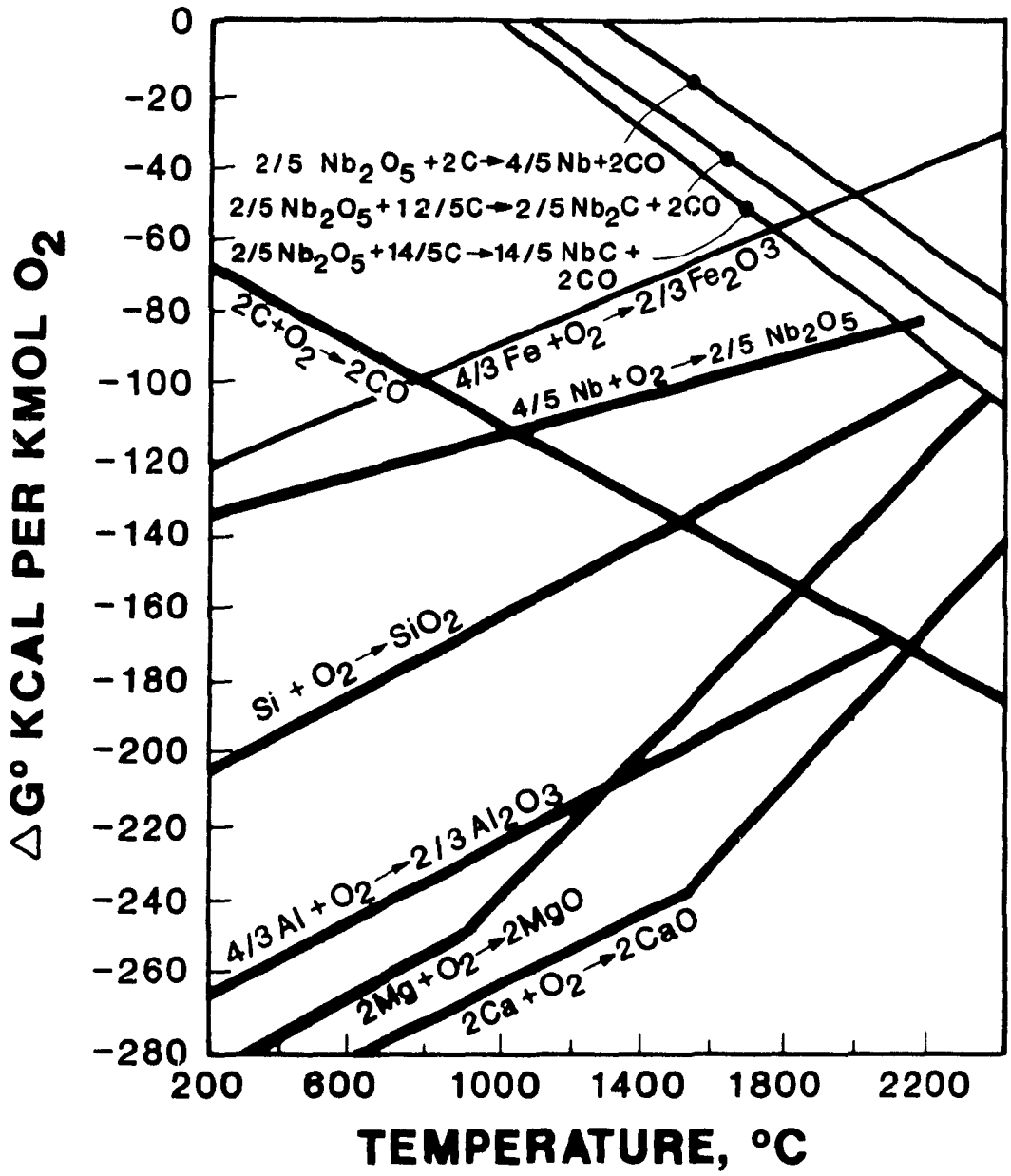

Figure 4.1 Free Energies of Formation
Basis: 1 mole O_2

reductants are applicable only to a batch process. Although the use of carbon requires a high temperature, because it is a highly endothermic reaction, semi-continuous or continuous operation is feasible (Liang and Munz, 1981). At the experimental reaction temperatures (1400 - 2850 K) used in this work, the following reactions may take place for the carbothermic reduction of the niobium pentoxide (Kolchin, 1970):

$$Nb_2O_5 + C = 2NbO_2 + CO \quad (4.1)$$

$$Nb_2O_5 + CO = 2NbO_2 + CO_2 \quad (4.2)$$

$$CO_2 + C = 2CO \quad (4.3)$$

$$NbO_2 + C = NbO + CO \quad (4.4)$$

$$2NbO + 3C = Nb_2C + CO \quad (4.5)$$

$$Nb_2C + C = 2NbC \quad (4.6)$$

$$NbO + Nb_2C = 3Nb + CO \quad (4.7)$$

These reactions are all possible and probably occur simultaneously. Thermodynamically, the overall carbothermic reduction of niobium pentoxide only and that contained in pyrochlore may be represented by:

$$Nb_2O_5 + 7C = 2NbC + 5CO \quad (4.8)$$

$$Nb_2O_5 + 6C = Nb_2C + 5CO \quad (4.9)$$

showing that, at atmospheric pressure, Nb_2C and NbC, instead of the metal are the products. This can be seen in the more negative free energy changes for the carbides than the metal as shown in Figure 4.1.

If it is assumed that the carbothermic reduction reaction takes place via the gaseous intermediates carbon monoxide and carbon dioxide, the following reactions applies:

$$Nb_2O_5 + 5CO = 2Nb + 5CO_2 \quad (4.10)$$

$$CO_2 + C = 2CO \quad (4.11)$$

$$2Nb + C = Nb_2C \quad (4.12)$$

$$Nb_2C + C = 2NbC \quad (4.6)$$

It can be shown thermodynamically that at equilibrium, the ratio of carbon monoxide to carbon dioxide decreases with increasing temperature (Upadhya et al., 1986). The CO/CO_2 ratios were estimated to be about 4680 and 460 at temperatures of 1475 and 2275 K, respectively from the Ellingham Diagram. Hence, the end product of the carbothermic reduction of niobium pentoxide is

essentially carbon monoxide, rather than carbon dioxide.

In practice, in order to obtain a high yield of the product, an excess of carbon must be added to the reactant system. The presence of excess carbon at the end of the reduction favours the formation of NbC rather than Nb_2C (see Figure 4.2) (Elliott, 1965). This product may or may not be acceptable to the steel industry because of its high carbon content. An additional process step to remove the excess carbon may be required. The suboxides (NbO and NbO_2) will be formed if the niobium pentoxide is in excess of carbon or if the reaction temperature is too low (<2085 K) (Kolchin, 1970), (Nagamori, 1984).

4.3 IRON ADDITION

The use of liquid metal solvents to carry out carbothermic reduction reactions, especially for the more reactive metals, have received attention recently (Howell et al., 1988). For this work, iron was added as the solvent for the product from the carbothermic reduction of niobium pentoxide. Such an application has been demonstrated in a plasma system by Hilborn (1988) and in non-plasma systems by Zimmerley and Back (1961), Hunter and Fursman (1966) and Nagamori and Plumpton (1985).

When solid niobium pentoxide is added to a system containing a liquid CaO-SiO slag phase in equilibrium with a liquid Fe-C phase, a portion of the niobium pentoxide enters the slag, while the remainder is reduced by carbon and enters the alloy. Such a situation would be typical for the carbothermic reduction of pyrochlore in the presence of iron. Nagamori and Plumpton (1985)

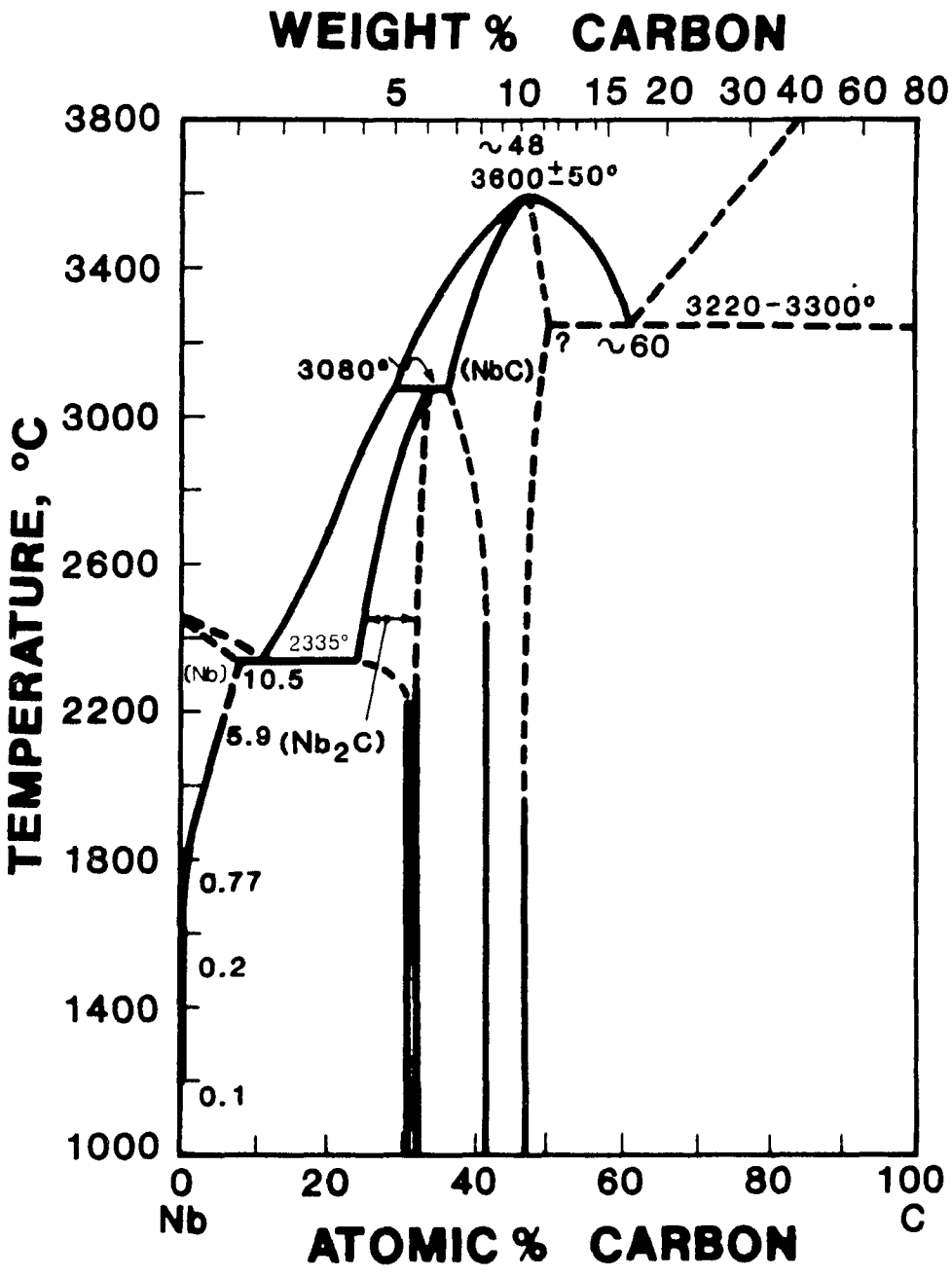

Figure 4.2 The Phase Diagram of Nb-C System

made thermodynamic estimations of the distribution of niobium as metallic niobium and niobium carbide between the slag and the ferroalloy for a low grade pyrochlore concentrate. This defined the distribution ratio, L_m, of any particular element, m, between metal and slag by :

$$L_m = (\%\ m \text{ in Fe}) \ / \ (\%\ m \text{ in slag}) \qquad (4.13)$$

The results gave the following series of distribution ratios:

$$L_{Nb} > L_{Ta} > L_{Si} > L_{Ti} > L_V > L_{Al} > L_{Zr}$$

On the basis of the above distribution ratio series, and their relative values, Nagamori and Plumpton (1985) concluded that one could reduce niobium and tantalum pentoxides preferentially without reducing SiO_2, TiO_2, etc. by means of controlling the amount of carbon in the charge.

The ferroniobium product from the carbothermic reduction of niobium pentoxide and pyrochlore cannot take up more than 30 wt. % NbC or 26 wt. % Nb at 2273 K due to the NbC solubility limit in iron, see Figure 4.3 (Guha and Kolan, 1972). Therefore, unless the Nb content of the ferroniobium product produced by the carbothermic reduction is less than 26 wt. %, the product will not run and could not be tapped. The current industrial standard for ferroniobium demands that the Nb content be greater than 60 wt. % Nb. In the case where iron was added in the form of Fe_2O_3, this oxide is reduced first since the standard free energy of forma-

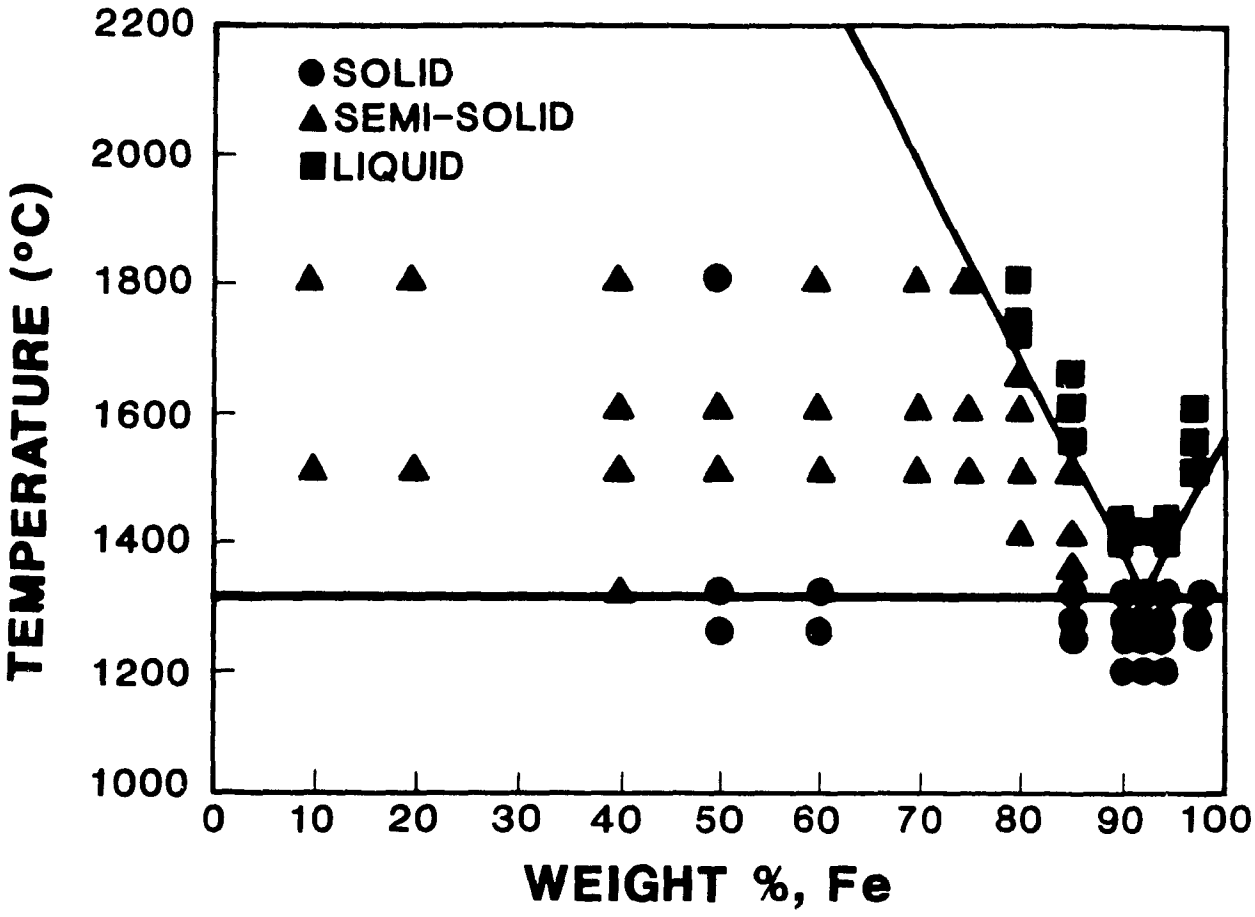

Figure 4.3 The Phase Diagram of NbC-Fe System

tion for Fe_2O_3 is larger than that for Nb_2O_5 (see Figure 4.1).

4.4 MATHEMATICAL MODELLING OF THE REACTION

The mathematical treatment of a heterogeneous reaction involving pellets composed of two solid components, such as graphite and niobium pentoxide or pyrochlore exhibits a higher degree of complexity than that of a single solid component reaction. The degree of contact between the solid constituents may influence the progress of the reaction due to the mechanistic behavior of the solid reducing agent and the nature of the intermediate product (if it forms and exists during the reaction).

As seen in the Literature Review, the mechanism for the carbothermic reduction of metal oxide is generally accepted as taking place via the gaseous intermediates carbon monoxide and carbon dioxide (Wynnyckyj and Rankin, 1988), (Ajersch, 1987), (Sohn and Szekely, 1973), (Rao, 1974), (Rao and Chang, 1974), (Rao, 1971), (Padilla and Sohn, 1979), (Fruehan, 1977). The exception is at the initiation of the reaction and for reduction under high vacuum conditions, where true solid-solid (direct) reaction is the predominant mechanism (Rao, 1974), (Yun, 1961), (Habashi, 1969), (Rao, 1971). The proof for the appropriateness of the gaseous intermediates assumption in most cases was indirect. Other reaction mechanisms also include nucleation growth (Shimada et al., 1983), (Klinger et al., 1966). However, some investigators have indicated the importance of the degree of contact between metal oxide and carbon particles (El-Guindy and Davenport, 1970), (Ajersch, 1987). A related reaction system in

which interparticle contact between metal oxide and carbon is of significance to the reaction rate is the chlorination of oxides in the presence of carbon (Biceroglu, 1978), (Serayakov et al., 1970).

A relatively simple approach is followed here in developing a time-conversion relationship for the carbothermic reduction of niobium pentoxide and pyrochlore with and without the addition of iron. The model assumes that mass transfer resistance (ash diffusion) is negligible or absent, and that the rate is proportional to a contact area or to a distance of separation between the niobium pentoxide and the graphite particles. The latter in turn is assumed to be proportional to a functional form of initial carbon concentration in the pellet and also to the amount of oxygen in the unreacted niobium pentoxide left in the pellet. Mathematically the rate may be written as :

$$-dW/dt = k_{14}\ W\ f(x_C) \qquad (4.14)$$

where k_{14} is the intrinsic rate constant, W is the weight of oxygen in the unreacted niobium pentoxide or pyrochlore in the pellet at time t, and x_C is the initial concentration of carbon in the pellet and f is the functional relationship for the concentration of carbon.

Equation (4.14) may be rearranged and integrated to give:

$$-(\ln W - \ln W_o) = k_{14}\ f(x_C)\ t \qquad (4.15)$$

or

$$-\ln(W/W_o) = Kt \qquad (4.16)$$

where W_o is the initial weight of oxygen in the niobium pentoxide or pyrochlore in the pellet, and K is the overall rate constant defined as :

$$K = k_{14}\ f(x_c) \qquad (4.17)$$

Equation (4.16) may be written in terms of fractional conversion of the niobium pentoxide or pyrochlore, which is by definition:

$$x = (W_o - W)/W_o \qquad (4.18)$$

and thus:

$$(W/W_o) = 1-x \qquad (4.19)$$

Insertion of Equation (4.19) into Equation (4.16) yields:

$$-\ln(1-x) = K\ t \qquad (4.20)$$

If Equation (4.20) represents the conversion-time relationships for the carbothermic reduction of niobium pentoxide and pyrochlore, with and without the addition of iron, the plot of -ln(1-x) versus time should give a straight line. It should be

noted that the overall rate constant K as defined by Equation (4.17) is not a function of the particle diameter, hence the conversion-time relationship given by Equation (4.20) will not be affected by variations in the particle diameter.

A relationship similar to Equation (4.20) was derived by Biceroglu (1978) for the chlorination of zirconium dioxide compacted with carbon as discussed in the Literature Review.

CHAPTER V

CARBOTHERMIC REDUCTION OF NIOBIUM PENTOXIDE : EXPERIMENTAL RESULTS AND DISCUSSION

5.1 Introduction

Experiments were performed to study the time-conversion relationship, and the effect of temperature, graphite particle size and graphite concentration on the rate of the carbothermic reduction of niobium pentoxide. The amount of graphite added per pellet was varied between 15.9 to 38.7 wt. % which was equivalent to C/Nb_2O_5 mole ratios of 5 to 14. This corresponded to a pellet diameter of 12.9 mm and heights of between 15.5 and 20.6 mm, respectively (see Appendix I). The C/Nb_2O_5 mole ratio for the reaction stoichiometry to produce NbC is 7 (24.0 wt. % C). The graphite particle diameter was varied between 100 % less than 45 and 463 microns and the niobium pentoxide particle diameter was kept constant at 10 microns.

5.2 Microscopic Examinations

Measurements of the pellet diameter before and after reaction indicated some shrinkage during the reaction. The surface of an unreacted pellet was smooth and relatively non-porous whereas a partially reacted pellet exhibited a very porous surface as seen in Figure 5.1, where the initial carbon concentrations were 24.0 and 38.7 wt. % for Figure 5.1(a) and 5.1(b), respectively. The surface is less porous in the latter due to the higher carbon content. The arc struck the top of the pellet and thus the temperature (and hence the rate of reaction) was the highest here.

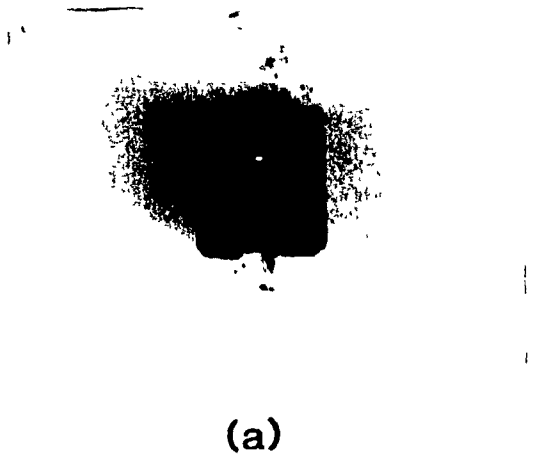

(a)

(b)

Figure 5.1 Photographs of Partially Reacted Pellets
(12.9 mm dia., $d_p C$ = <45 μm, $d_p Nb_2O_5$ = 10 μm) :
(a) 1675 K, x = 0.77, 24.0 wt. % C, pellet ht. = 14.0 mm
(b) 1925 K, x = 1.00, 38.7 wt. % C, pellet ht. = 20.0 mm

This also contributed to some melting and coalescing of the product. Close examination of other partially reacted pellets showed the presence of unreacted niobium pentoxide in larger concentration in the bottom half than in the top.

The reduction reaction left the pellet very friable, which made it difficult to mount and polish for microscopic examination. The NbC produced was also very hard and this also contributed to the difficulty in sample preparation. Thus, the specimens examined by scanning electron microscopy were obtained by fracturing the sample. Scanning electron micrographs of the typical reaction products are shown in Figure 5.2. EDX (energy dispersed X-ray spectrometer) analysis identified the white areas as niobium-rich, i.e. either niobium oxide or NbC, and the black areas as carbon. It can also be seen that there is some liquefaction of the niobium pentoxide. The melting point of niobium pentoxide is about 1760 K. The main product of the reaction, NbC, is expected to solidify immediately upon formation due to its very high melting point of 3875 K. The solid NbC would form either as an ash layer around the microscopic graphite and/or oxide particles or be dispersed randomly at the reaction (contact) points between the microscopic graphite and oxide particles. If the gaseous intermediates (CO and CO_2) were major contributors to the progress of the reduction reaction, it would be expected that liquefaction would hinder the reduction process because of the reduced porosity of the particle. Diffusion resistance through the product ash layer would also become apparent at relatively high temperatures, this does not seem to be the rate-controlling factor

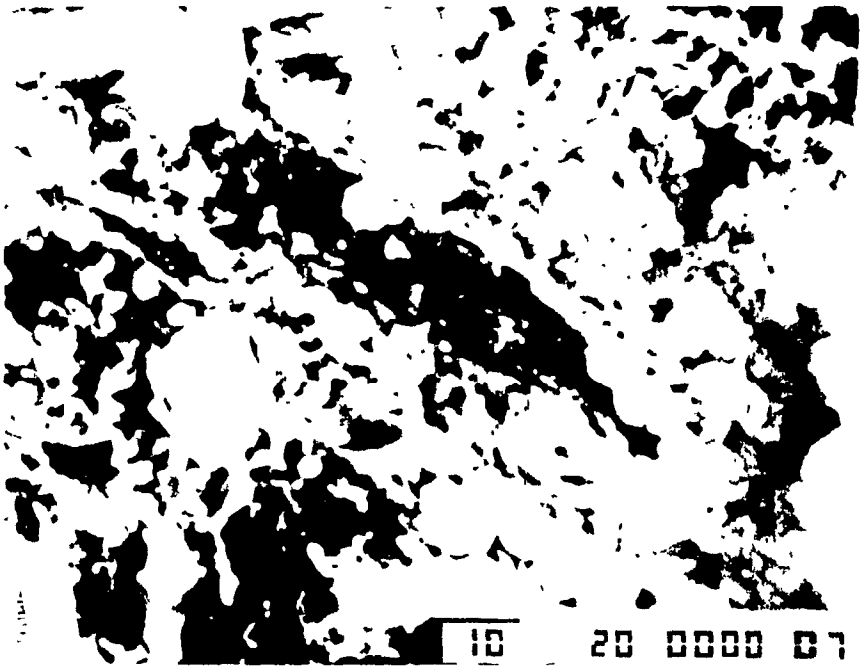

(a)

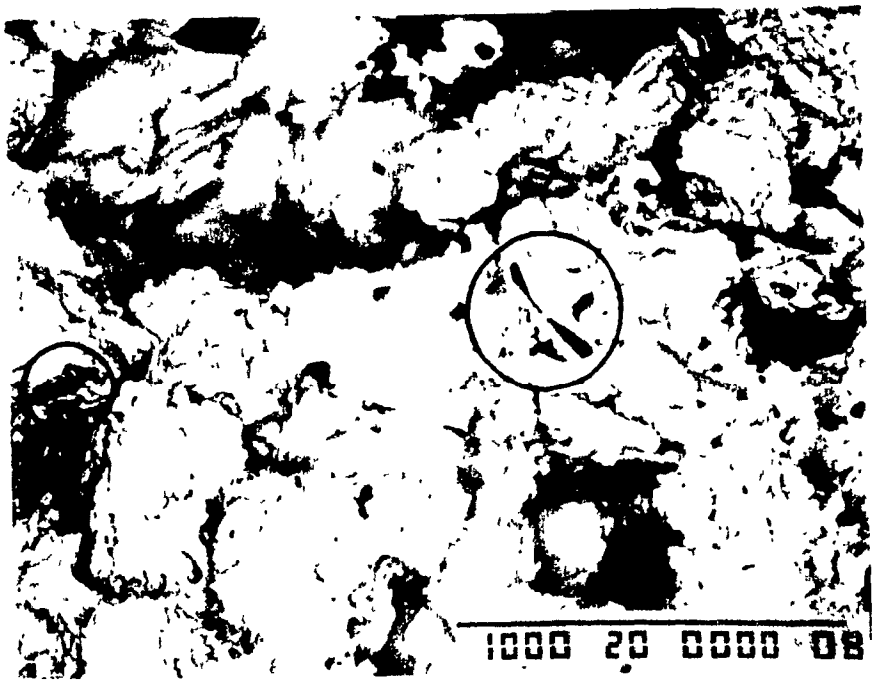

(b)

Figure 5.2 Scanning Electron Micrographs (With Back Scatter) of Partially Reacted Pellets (12.9 mm dia., d_p Nb_2O_5 = 10 μm) :
(a) 1830 K, 24.0 wt. % C, d_pC = <45 μm, x = 0.64, pellet ht. = 15.0 mm, X 1000,
(b) 2780 K, 38.7 wt. % C, d_pC = 463 μm, x = 0.85, pellet ht. = 11.9 mm, X 50.

for the given temperature range due to the highly porous nature of the reacted layer. The progress of the reaction is expected to be strongly influenced by the degree of contact between the carbon and the solid and/or liquid oxide particles. This is shown in Figure 5.3, which shows individual niobium pentoxide particles in contact with the carbon particles. The product of the reaction is shown scattered randomly over the surface of the carbon particle rather than in any sort of continuous shell around either the carbon or oxide particle. The foregoing discussion was supported by the experimental data for the influence of graphite particle size on the reaction rate which are presented in a later section.

Examination of the encircled areas in Figure 5.2(b) shows that a shrinking-core type morphology (Levenspiel, 1972),(Szekely et al., 1976), probably exists in certain sections of the pellet. It shows a sectioned graphite particle surrounded by an ash layer of niobium rich material.

5.3 X-ray Analysis

A number of reacted pellets were selected for x-ray powder diffraction (XRD) analysis. The samples were analyzed by the XRD facility at Centre Recherches Minerales (CRM) in Ste. Foy, Quebec. The XRD analysis results showed that for the case of a C/Nb_2O_5 mole ratio of 7, the major phases identified in the product were NbC, Nb_2C, Nb and NbO_2. For a mole ratio of 10, the phases identified were NbC and C. The results are summarized in Table 5.1. These results were in agreement with those obtained by

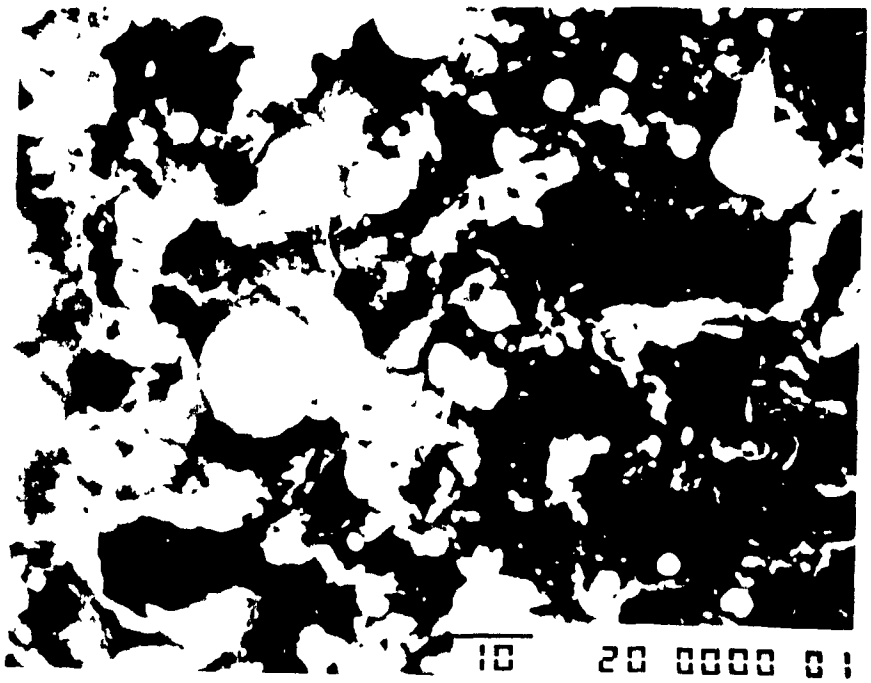

(a)

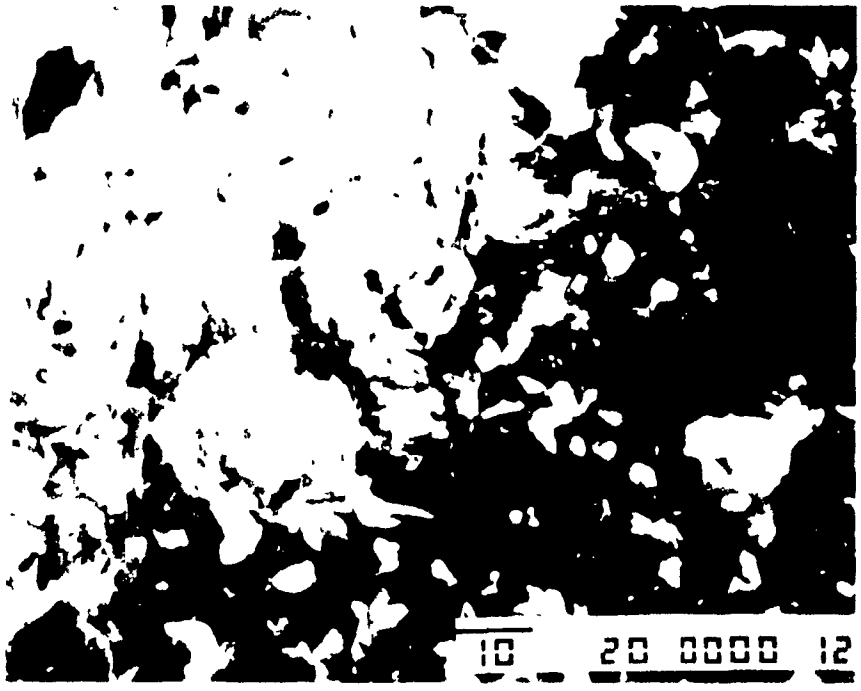

(b)

Figure 5.3 Scanning Electron Micrographs (With Back Scatter) of Partially Reacted Pellets (12.9 mm dia., d_p Nb_2O_5 = 10 μm) :
(a) 1830 K, 24.0 wt. % C, d_pC = <45 μm, x = 0.64, pellet ht. = 15.0 mm, X 1000,
(b) 2780 K, 38.7 wt. % C, d_pC = 463 μm, x = 0.85, pellet ht. = 11.9 mm, X 1000.

Table 5.1 XRD Analysis of Compounds for the Carbothermic Reduction of Niobium Pentoxide

MOLE RATIO	MAJOR PHASES C/Nb_2O_5
7	NbC, Nb_2C, Nb, NbO_2
10	NbC, C

Shimada et al. (1983) and thermodynamic predictions of Kolchin (1970).

5.4 Mass Balance

Conversion was previously defined in Equation (3.4), as the ratio of total oxygen in the carbon monoxide and carbon dioxide in the exhaust gas to the total initial oxygen in the oxide reactant(s). This method of measurement for conversion was checked for consistency by comparing the result to that calculated from the pellet's weight loss. Because the latter measurement was subject to higher experimental error, it was used primarily as an indicator for possible anomalies during an experimental run. As the results, which are presented in Appendix II, indicate, there was good agreement between the two methods. The fractional conversion by weight loss was consistently higher, but the difference was generally less than 0.10. The exceptions were caused by the excessive break-up of the pellets during the reaction. The main source of error for the method involving the pellet's weight loss can be attributed to weight loss due to reactant and product entrainment in the exhaust gas. The need for a binder was demonstrated by the reaction with the pellet where only water was employed as the binder. This showed a difference of 0.30 in the calculated fractional conversion between the two methods. Graphite seems to demonstrate some binding ability since the difference for those reactions with the smallest carbon concentration (15.9 wt. %) was notable higher than the rest.

5.5 CO/CO_2 Ratio

Measurements for CO and CO_2 were made in the exhaust gas to measure the progress of the reaction and to obtain some understanding of the reaction mechanism. Figure 5.4 shows the variation of CO and CO_2 concentrations with time that were typically obtained during the carbothermic reduction of niobium pentoxide. The presence of CO_2 in the exhaust gas does not necessarily confirm the reduction mechanism as occurring via the gaseous intermediates CO and CO_2, since its presence could have resulted from the carbon deposition reaction. This will be discussed later.

A comparison of the CO/CO_2 ratio at two different temperatures, 2450 and 1625 K, using graphite and niobium pentoxide particle sizes of 165 and 10 microns, respectively, is shown in Figure 5.5. The average ratios for the rest of the experiments are summarized in Appendix II. The ratios for early experiments are not reported since a CO_2 meter was not available then. This was of little consequence to the results, since for those reactions in which CO_2 measurements were made, the fractional conversion that was contributed by CO_2 generation was typically less than 0.03.

Assuming complete gas equilibrium and that the reduction reaction had taken place via gaseous intermediates, the CO/CO_2 ratios at 2450 and 1625 K should be about 850 and 1700, respectively. Thus, the exhaust gas should essentially be all CO. From Figure 5.5, the highest values of CO/CO_2 were about 18 and 12, respectively, which are much less than expected. Also, the CO/CO_2

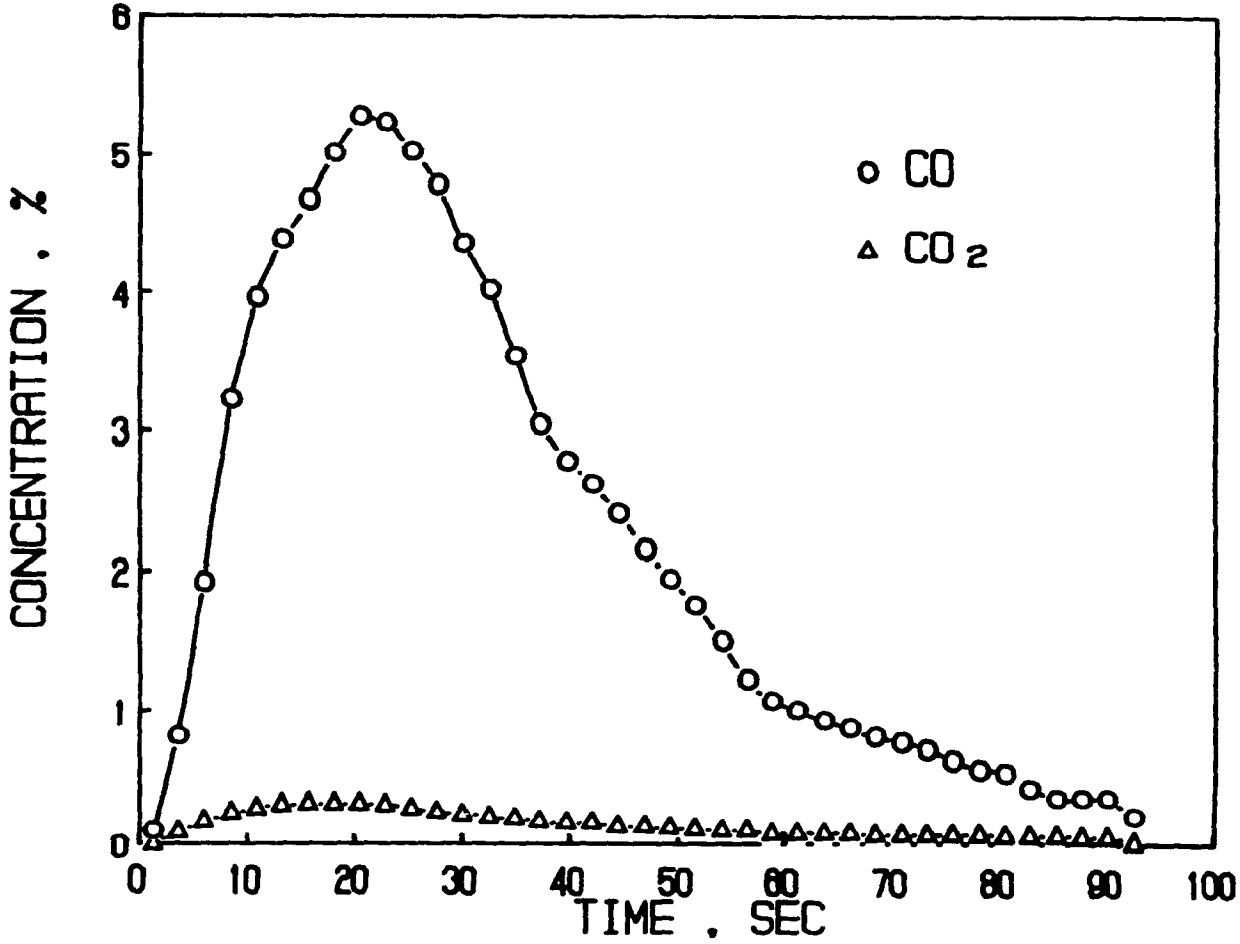

Figure 5.4 CO and CO_2 Concentration Versus Reaction Time for the Carbothermic Reduction of Nb_2O_5 (d_p Nb_2O_5 = 10 μm) : 2450 K, d_pC = 165 μm, 24.0 wt. % C, pellet dia. = 12.9 mm, pellet ht. = 16.7 mm

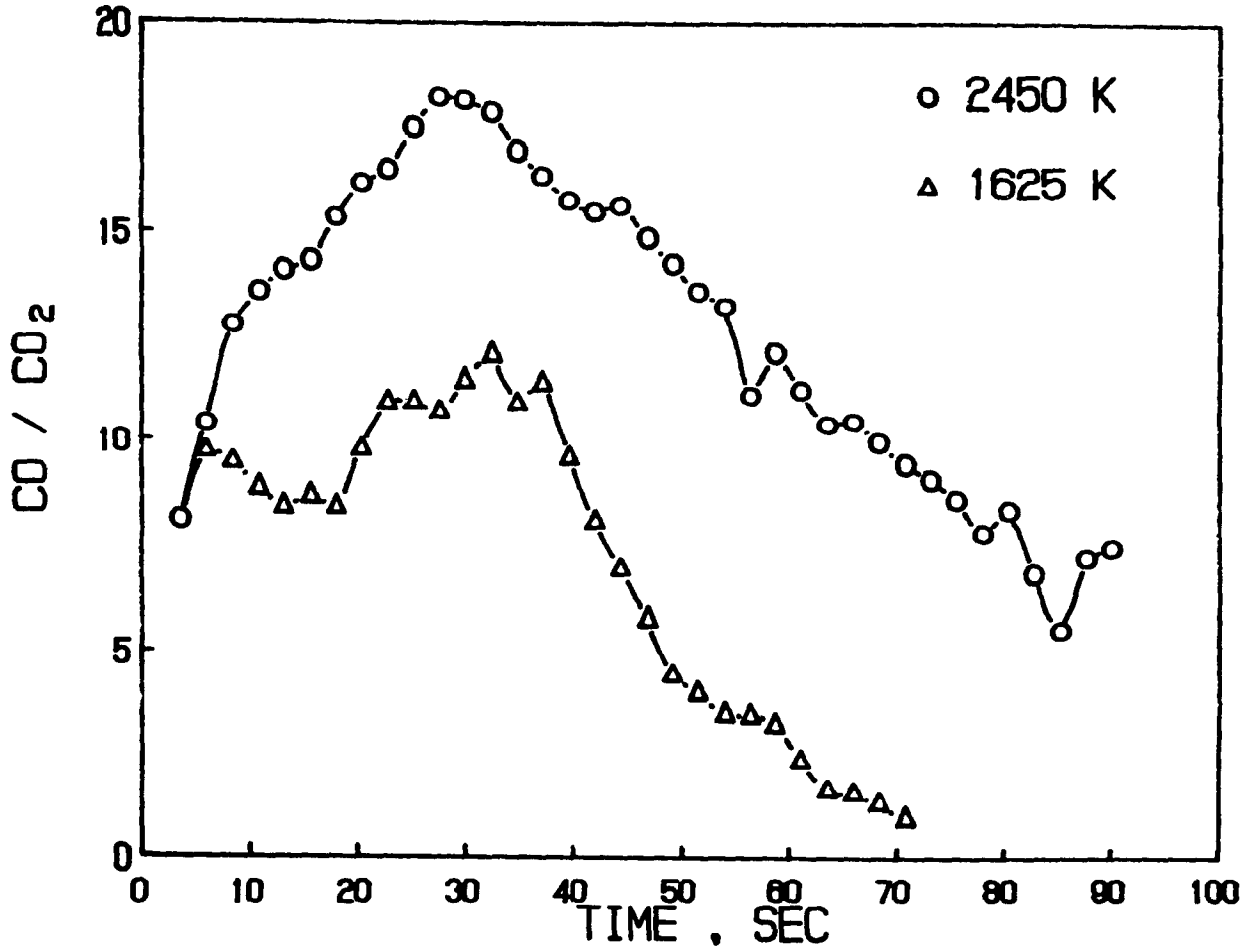

Figure 5.5 The Effect of Temperature on CO/CO_2 Ratio Versus Reaction Time for the Carbothermic Reduction of Nb_2O_5 (d_p Nb_2O_5 = 10 μm) : 24.0 wt. % C, d_pC = 165 μm, pellet dia. = 12.9 mm, pellet ht. = 16.7 mm

ratios did not follow the expected trend and might have been due to the fact that the temperature history of the exhaust gas was unknown. The presence of CO_2 could be due to carbon deposition from the exhaust gas as it cools from the high temperatures in the plasma to slightly above room temperature (Turkdogan, 1980). This is represented by the following equation:

$$2CO = CO_2 + C \qquad (5.1)$$

The temperature at which carbon deposition may start is below 1000 K, and this reaction is catalyzed by iron, cobalt and nickel (Turkdogan, 1980).

The presence of CO_2 in the exhaust suggests the possibility that the reduction reaction might have occurred via the gaseous intermediates CO and CO_2, but it is inconclusive. Verification of the true reaction mechanism and composition of the exhaust gas would require in situ sampling of the exhaust gas which the present system was not designed to do.

5.6 Conversion-Time Relationship

The experimental rate data for different graphite particle sizes were plotted according to several rate expressions which were previously discussed and presented in the Chapter II. These equations were (a) diffusion controlling - Equations (2.13), (2.15), (2.19), and (2.20); (b) chemical reaction controlling - Equation (2.23), and (c) nucleation/logarithmic growth - Equations (2.29), and (2.31). Although the equations listed in (a)

and (b) statistically fitted the conversion-time data as well as the equations of (c), they were rejected as appropriate models because their predicted dependencies of reaction rate on particle size was not observed. The choice of the current model as the most appropriate one will be justified in the following sections.

The examination of reacted pellets led to the conclusion that the carbothermic reduction of niobium pentoxide particles does not progress according to the shrinking-core model, that is, on a sharp reaction front, but rather it takes place randomly throughout the pellet at contact points between the carbon and the solid and/or liquid oxide, at the interparticle level. The overall reduction rate of niobium pentoxide with time, under chemical-reaction control, has thus been represented by the logarithmic expression given by Equation (4.20) developed earlier. The applicability of Equation (4.20) was further tested by varying the graphite particle diameter (100 % less than 45, 165, 462 microns), while keeping the carbon concentration constant at 24.0 % and using a constant niobium pentoxide particle diameter of 10 microns.

Typical experimental conversion-time data at different temperatures are given in Figure 5.6 - 5.8. The plots show that a relatively small induction period is associated with each reaction; this decreases with increasing temperature. The delay is between 15 to 5 seconds. This induction period may include the time required for the sample to (i) attain reaction temperature, (ii) effect changes within the reaction sample, eg. melting (endothermic) and (iii) slow processes preceding establishment of

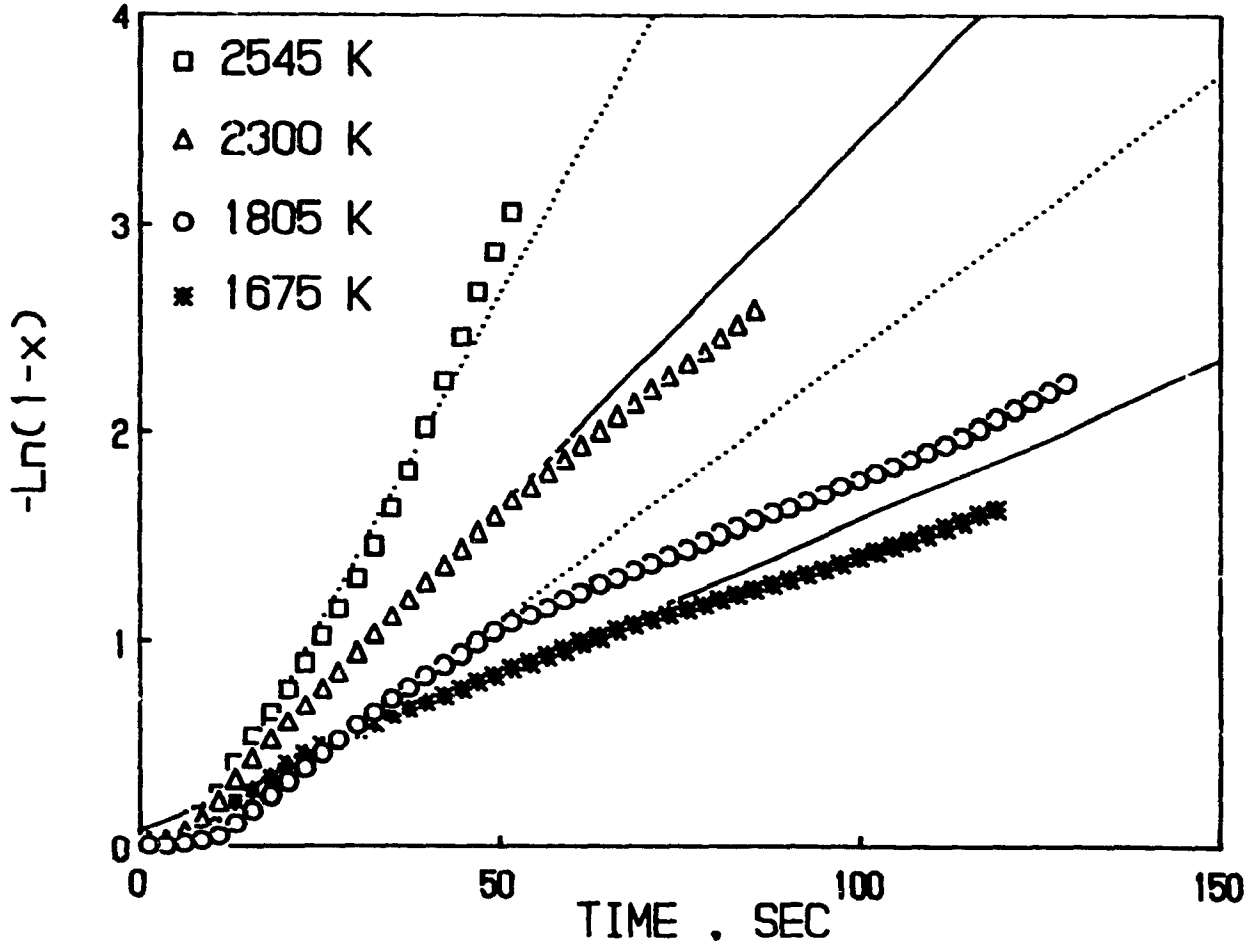

Figure 5.6 The Effect of Temperature on Conversion Using the Kinetic Model for the Carbothermic Reduction of Nb_2O_5 (d_p Nb_2O_5 = 10 μm) : 24.0 wt. % C, d_pC = <45 μm, pellet dia. = 12.9 mm, pellet ht. = 15.1 mm

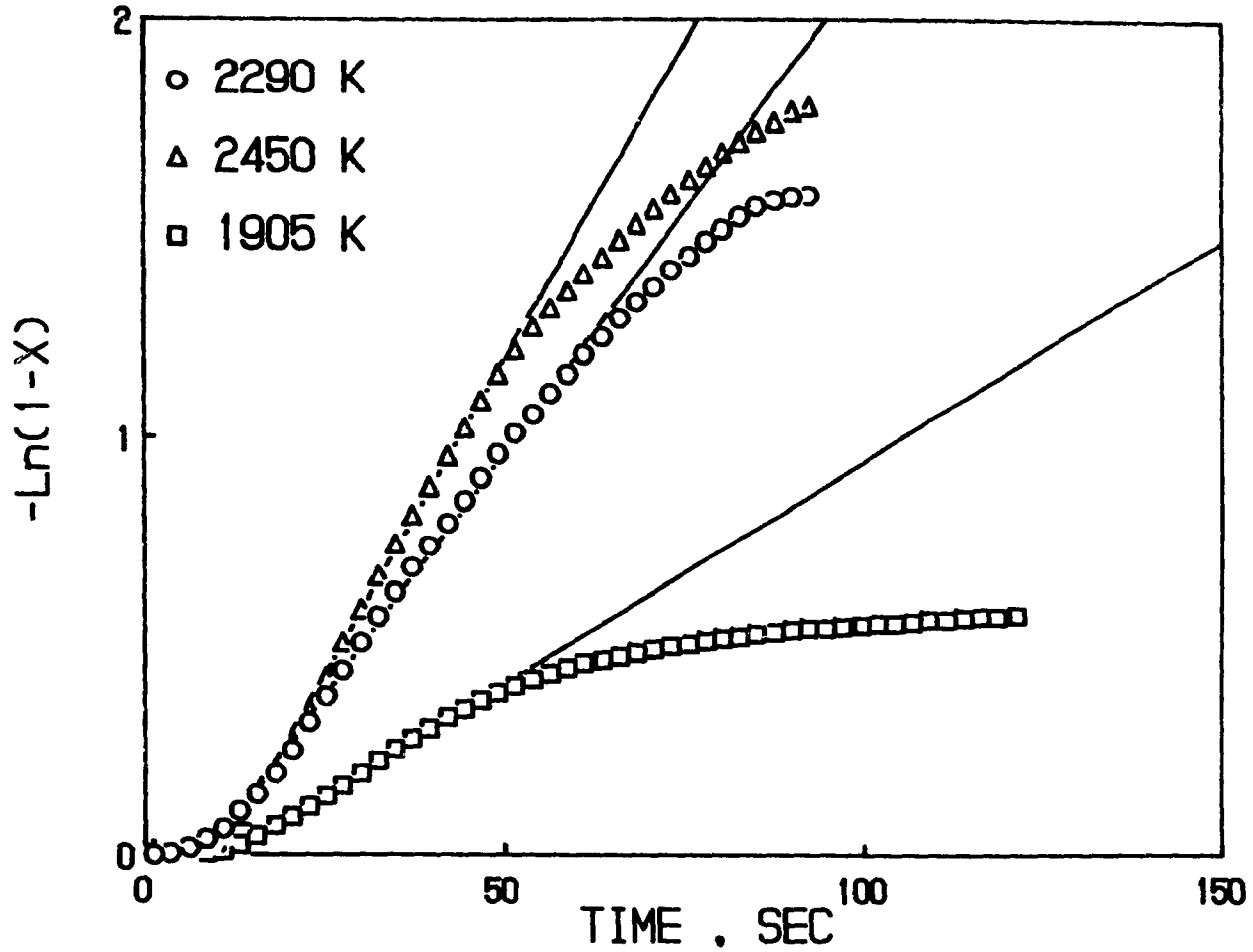

Figure 5.7 The Effect of Temperature on Conversion Using the Kinetic Model for the Carbothermic Reduction of Nb_2O_5 (d_p Nb_2O_5 = 10 μm) : 24.0 wt. % C, d_pC = 165 μm, pellet dia. = 12.9 mm, pellet ht. = 16.7 mm

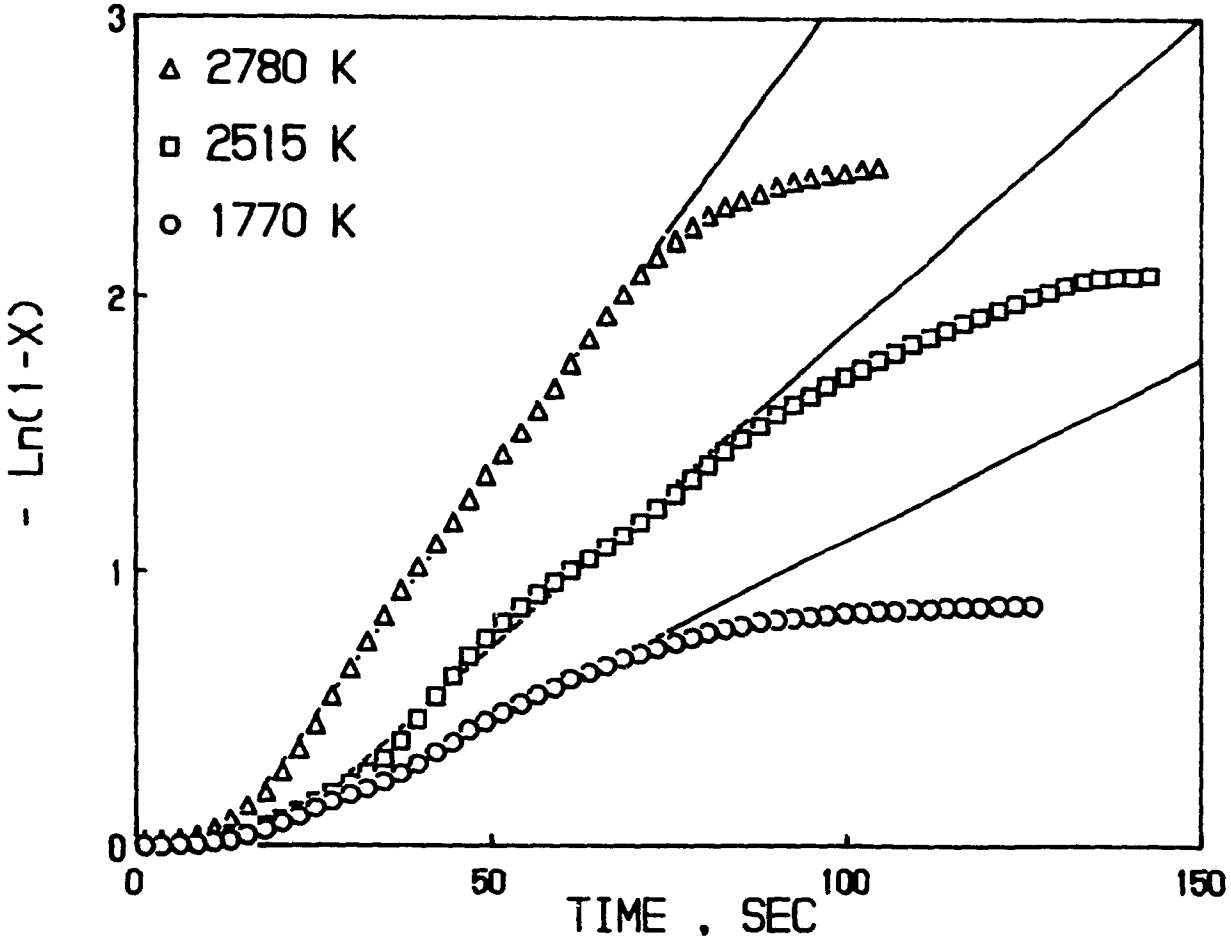

Figure 5.8 The Effect of Temperature on Conversion Using the Kinetic Model for the Carbothermic Reduction of Nb_2O_5 (d_p Nb_2O_5 = 10 μm) : 24.0 wt. % C, d_pC = 463 μm, pellet dia. = 12.9 mm, pellet ht. = 14.0 mm

the main reaction. First order estimates for the time required for heating and melting of the oxide at a reaction temperature of 1765 K, assuming a plasma energy efficiency of 30 %, was about 11 seconds. It is seen that, if the induction period is subtracted, the plots of $-\ln(1-x)$ versus time are linear as expected, but only to a certain conversion level; beyond this the rate of conversion is less than the model predictions. The fractional conversion at which the deviation from the logarithmic model occurs increases with increasing temperature. For pellets made with graphite particle diameters of <45, 165 and 463 microns, at pellet temperatures of 1675, 1770, and 1905 K, the deviation starts at about 60, 30 and 45 % conversion, respectively, and then the reaction almost stops. At higher pellet temperatures of 2545, 2450, and 2780 K it takes place at 90, 70 and 90 % conversion, respectively, and then the reaction continues at a slower rate. The difference in the conversion levels at which deviation from the model occurs can be attributed to the effects of a heat transfer limitation which leads to a non-isothermal pellet, rather than a change in rate controlling mechanism. At low temperatures, heat transfer to the rest of the pellet by the plasma arc root is limited to conduction which is restricted by the porosity of the already reacted top section of the pellet. The lower, cooler section of the pellet contributes little to CO/CO_2 production since the reaction rate is an exponential function of temperature. At higher temperatures, the whole pellet becomes more isothermal because radiation heat transfer becomes important and in this case the porosity of the pellet becomes an advantage.

This results in a higher conversion level before deviation from the model occurs.

If there was a change in the reaction mechanism, one would expect the deviation from kinetic to diffusion control to occur at lower conversion levels as the temperature increases.

In the present case, the opposite effect is observed. These observations support using only the linear portion of the $-\ln(1-x)$ versus time data to calculate the overall reaction rate constant, since it is the temperature of the upper section of the pellet which was measured and reported. Another contributing factor to the observed reduction in the rate of conversion after a certain conversion level could be due to macroscopic changes, such as the development of cracks, in the pellet.

Figure 5.9 shows the typical conversion-time data for pellets with much higher carbon concentrations of 31.1 and 38.7 wt. % at temperatures of 1945 and 1855 K, respectively. Although the conditions are not exactly alike, a useful comparison can be made. These results are quite different since deviation from the logarithmic model takes place at higher fractional conversion levels for comparable levels of temperature. This suggests that with higher initial carbon concentration, a higher degree of surface area contact between the oxide and the carbon particles is achieved at all times during the reaction. The high carbon concentration could also contribute to achieving isothermal conditions in the whole pellet. Thus, at an initial carbon concentration of 38.7 wt. %, there is no decrease in the rate of conversion as the reaction progresses.

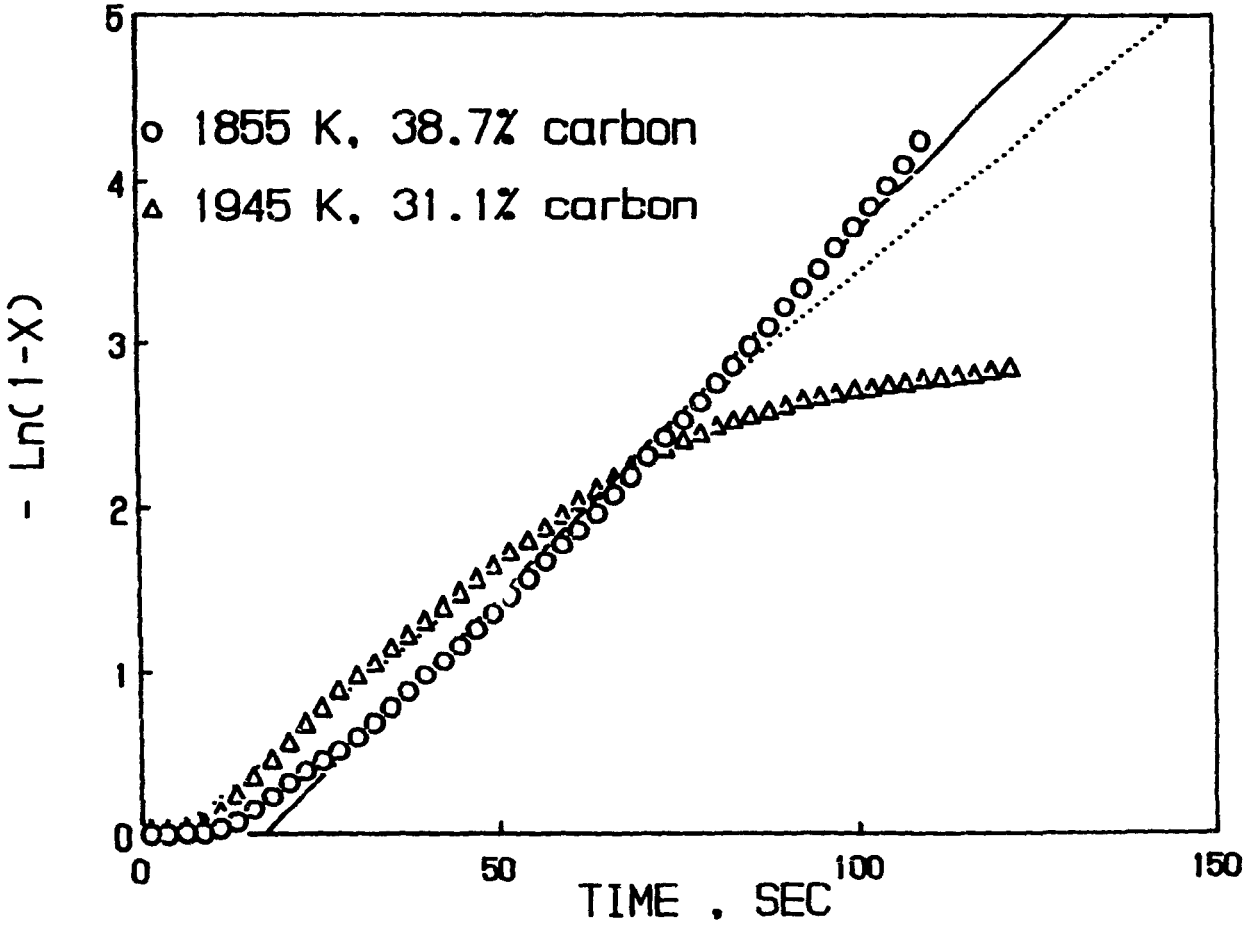

Figure 5.9 The Effect of Initial Pellet Carbon Concentration on Conversion Using the Kinetic Model for the Carbothermic Reduction of Nb_2O_5 (d_p Nb_2O_5 = 10 μm) : d_pC = <45 μm, pellet dia. = 12.9 mm, pellet ht. = 15.1 mm

5.7 Influence of Particle Diameter

The overall rate constant, K, as defined by Equation (4.17), was not expected to be influenced by the change in particle diameter under chemical reaction control. Accordingly, an Arhenius plot of the rate constants of different particle diameters is expected to yield a single straight line, if ash diffusion is not contributing. Otherwise, the overall rate constant would decrease with increasing particle diameter due to a corresponding increase in the diffusion resistance.

The overall rate constants corresponding to the linear portion of -ln(1-X)-versus-time data were plotted according to an Arrhenius-type relationship in Figure 5.10 for pellets having different graphite particle diameters of 100 % less than 45, 165 and 463 microns, respectively. The niobium pentoxide particle diameter was kept constant at 10 microns since it was the only one commercially available. The results of the treated experimental data for each of these cases are presented in Tables II-A, II-B, and II-C of Appendix II. The data of Figure 5.10 show that, to a first approximation, the overall rate constants for graphite particle diameters of 165 and 463 microns all seem to lie on the same line. In the case for the graphite particle diameter of 100 less than 45 microns, it would appear that there was a slight dependency of the overall rate constant on particle size. But the dependency is not large enough to justify the use of the other rate expressions previously discussed in Chapter II. For instance, at a temperature of 2515 K, the ratio of the overall

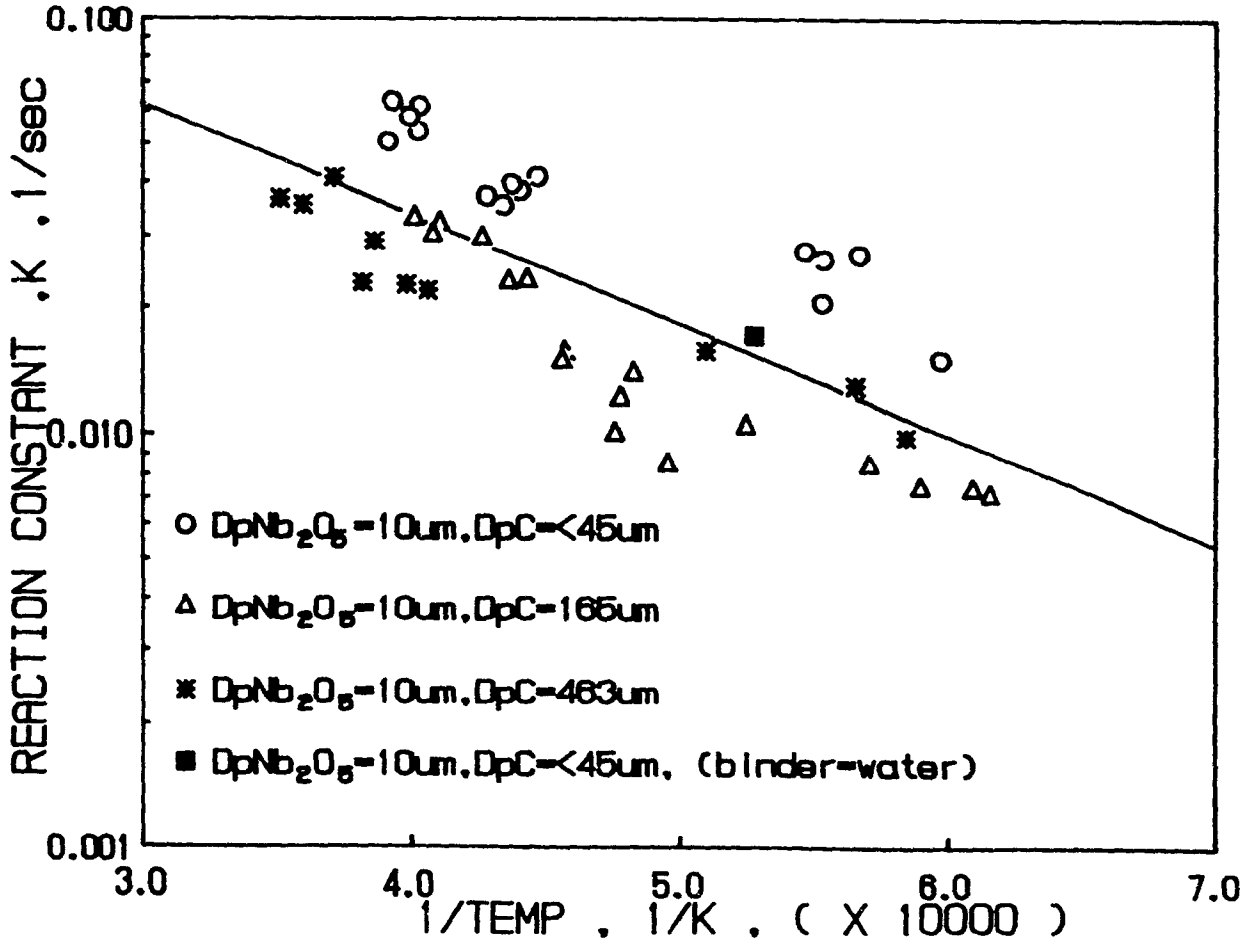

Figure 5.10 Arrhenius Plot for the Carbothermic Reduction of Nb_2O_5 for Different Graphite Particle Size (d_p Nb_2O_5 = 10 μm) : d_pC = <45, 165, and 463 μm, 24.0 wt. % C, pellet dia. = 12.9 mm, pellet ht. = 15.1 mm

reaction rate constants corresponding to a graphite particle diameter ratio of about 1:10 (<45 microns:463 microns) is only 3:1. If the reaction or diffusion controlled model was the appropriate one, the overall rate constants should be inversely proportional to the particle radius or the square of particle radius, respectively. That is, for a reaction or diffusion controlled model, the predicted ratios of the overall rate constants should be 10:1 or 100:1, respectively. The small dependency might have been due to the larger relative surface area which become available for better contact and reaction with the oxide as discussed earlier. Thus, it would appear that the overall rate constant is independent of carbon particle size and Equation (4.17) adequately represents the overall rate constant.

5.8 Influence of Temperature

The influence of reaction temperature on the reaction rate was measured from 1625 to 2855 K. The choice of the temperature levels was dictated solely by the currents under which the arc was stable.

The Arrhenius plots in Figure 5.10 show that the reaction rate is a function of temperature. Also shown in this figure, is the overall rate constant obtained from the reaction in which water only was used as the binder. This was to determine what effect, if any, the molasses-water binder that was used to improve the mechanical strength of the pellets had on the reaction. As it can be seen the presence of the binder had no influence on the reaction rate. The treated data are presented in

Table II-G of Appendix II.

The data in Figure 5.10 were used in a linear regression analysis program (LOTUS), to obtain the values of the activation energies. For the graphite particle diameters of 100 % less than 45, 165, and 463 microns, the least square fits yielded activation energies and 95 % confidence intervals of 43.911 ± 9.786, 61.015 ± 13.675, 41.820 ± 12.211 kJ/mole, with corresponding correlation coefficients of 0.878, 0.867 and 0.886, respectively. The fact that the slopes of the Arrhenius plots are roughly parallel, confirmed the consistency of the previously proposed rate controlling resistance as being chemically reaction. If the data for all three carbon particle sizes are used, i.e. it is agreed that the reaction rate was independent of particle size, the activation energy and the 95 % confidence interval for the carbothermic reduction of niobium pentoxide was found to be 50.268 ± 14.093 kJ/mole. The corresponding correlation coefficient was 0.572, which is significant beyond the 0.01 level. The straight line in Figure 5.10 is the resulting regression line.

5.9 Influence of Carbon Concentration

Analysis of the kinetic data with respect to the carbon concentration was based on the initial carbon content of the individual pellets. The experimental runs covered a carbon concentration range from 15.9 to 38.7 wt. % and the treated data are summarized in Tables II-A to II-G of Appendix II. The carbon concentration equivalent to the amount required by the reaction stoichiometry to produce NbC is 24.0 wt. %. As in the previous cases,

only those data corresponding to the linear portion of the time-conversion expression (Equation 4.20) were considered.

The previously obtained overall activation energy value, the overall rate constants, and their corresponding temperatures were used to calculate respective values for the pre-exponential constant, A, as defined by the Arrhenius equation:

$$A = K/\exp(-E/RT) \qquad (5.2)$$

where K is the overall rate constant, E is the overall activation energy, and T is the pellet temperature. The calculated values for A were then plotted against the pellet carbon concentration in Figure 5.11. Using the one-tailed student t-test, it was shown that the average values of A were statistically different for average initial carbon concentrations of 15.9, 24.0, 31.1 wt. %, respectively, at a 0.01 level of significance. Whereas, for the higher average carbon concentrations of 31.1 and 38.7 wt. %, the values of A were not statistically different at the same level of significance.

The rate of carbothermic reduction is seen to increase with increasing carbon concentration, but changes very little after a certain carbon concentration. This observation may be attributed to the existence of an optimum ratio of carbon-to-niobium pentoxide in the original mix, yielding an optimum contact area, and consequently a maximum reaction rate. Increasing the carbon concentration above this optimum amount will not give a significant increase in the reaction rate and would only serve to increase

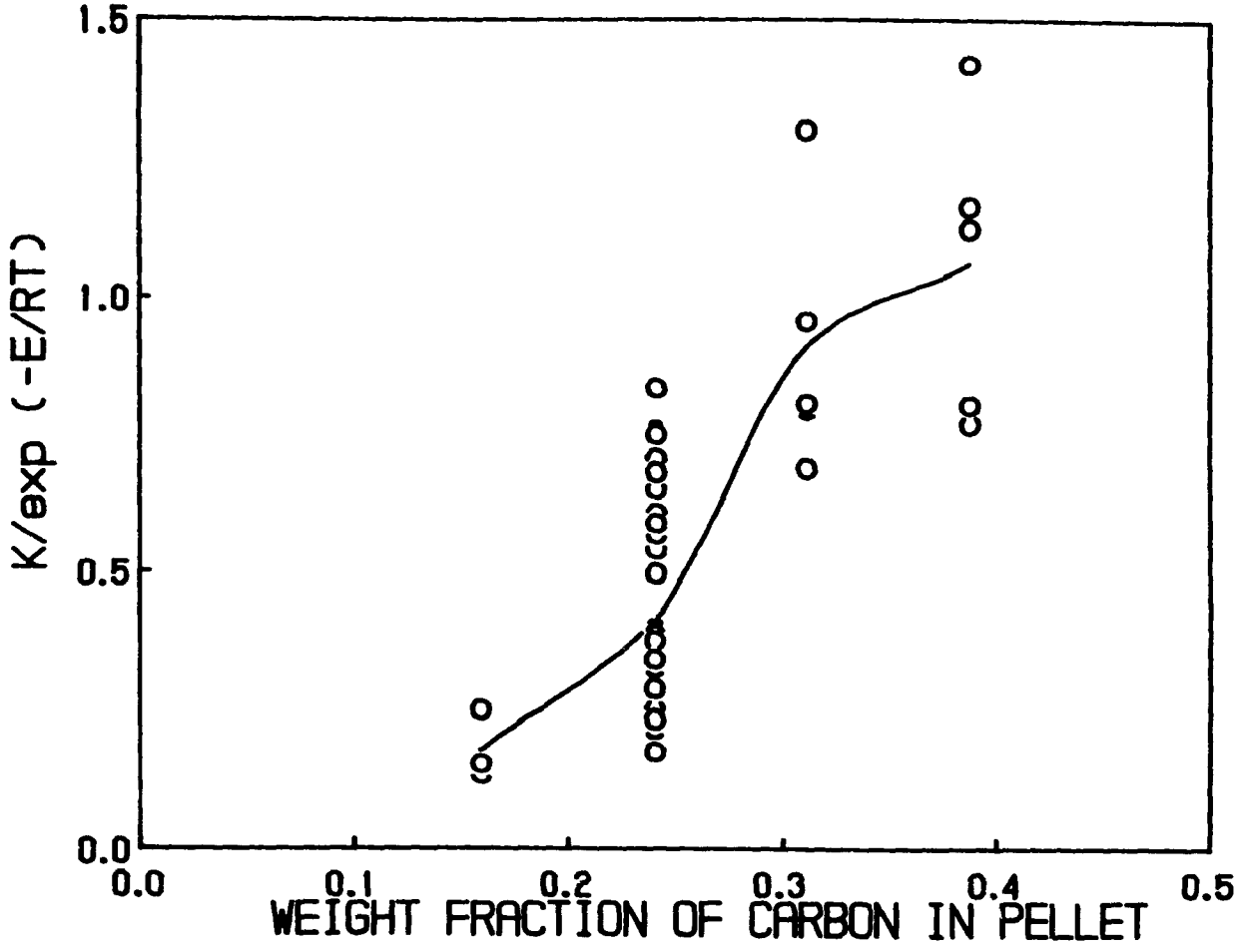

Figure 5.11 The Effect of Carbon Concentration on Reaction Rate

the carbon concentration in the final product.

5.10 CONCLUSION

1- The kinetics of the carbothermic reduction of niobium pentoxide were studied in the temperature range 1625 to 2855 K in an argon transferred-arc plasma. Influences of temperature, carbon concentration and graphite particle size in the pellet on the rate were determined experimentally, using single stationary pellets composed of niobium pentoxide and graphite particles.

2- The microscopic examination of sectioned partially reacted pellets shows that the reaction did not progress according to the shrinking-core model but rather that it took place randomly on the graphite particle surface where the oxide made contact with it. This suggested the importance of the degree of contact between the oxide and carbon particles for the progress of the reaction.

3- The overall reduction of niobium pentoxide with time under chemical reaction control was represented by a logarithmic expression (Equation 4.20) based on the volumetric reaction model. For pellets having an initial carbon concentration level less than 25.0 wt. %, the rate of conversion was less than the model predictions above a conversion level which increased with the reaction temperature. The pellets of higher carbon concentrations showed no such deviations. These behaviors were attributed to the limit imposed on the reaction

rate by heat transfer limitations in the pellet and the degree of contact between the constituent particles, respectively. The latter was indicated by the microscopic examinations of partially reacted pellets.

4- The Arrhenius plots of the experimental data indicated that the overall rate was independent of carbon particle size and was chemical reaction controlled. The activation energy was calculated to be 50.3 ± 14.1 kJ/mole.

5- Experimental data indicated the existence of an optimum ratio of the carbon and niobium pentoxide in the original mix yielding an optimum contact area, consequently, a maximum reduction rate.

CHAPTER VI

CARBOTHERMIC REDUCTION OF PYROCHLORE : EXPERIMENTAL RESULTS AND DISCUSSION

6.1 Introduction

Experiments were performed to study the time-conversion relationship, and the effect of temperature, graphite and pyrochlore particle sizes and carbon concentration on the rate for the carbothermic reduction of pyrochlore. More specifically, the reduction of the contained niobium pentoxide in pyrochlore. The amount of graphite added per pellet was varied between 10.4 to 27.8 wt. % which was equivalent to C/Nb_2O_5 mole ratios of 5 and 14. This corresponded to a pellet diameter of 12.9 mm and the pellet heights were between 11.3 and 21.9 mm (see Appendix III). The C/Nb_2O_5 mole ratio for reaction stoichiometry to produce NbC only, or to completely reduce all the oxide in the pyrochlore to their respective carbides are 7 (or 16.3 wt. % C) (Equation 4.8) and 11.8 (or 24.7 wt. % C), respectively. The fractional conversion equivalent to the complete reduction of the oxygen in the niobium pentoxide only in the pyrochlore to produce carbon monoxide and carbon dioxide is 0.67. The graphite particle diameter was varied between 100 % less than 45 and 463 microns and the pyrochlore particle diameter between 31 and 230 microns.

A few runs were carried out with pellets of larger diameter (18.5 mm) containing C/Nb_2O_5 mole ratio of 7, to determine any change in mechanism with pellet size.

6.2 Microscopic Examinations

Measurements of the pellet diameter before and after reaction indicated some shrinkage in the size during the reaction. The surface of an unreacted pellet was smooth and relatively non-porous whereas a partially reacted pellet exhibited a very porous surface as seen in Figure 6.1, where the initial carbon concentrations were 16.3 and 27.8 wt. % for Figure 6.1(a) and 6.1(b), respectively. As seen, the surface of the former appear to be more sintered and thus less porous due probably to the higher pellet temperature and lower carbon concentration. Close examination of the bottom of the same pellet revealed very tiny holes formed by the escaping gas during the reduction reaction. The arc struck the top of the pellet and thus the temperature (and hence the rate of reaction) was the highest here. This also contributed to more melting and coalescing of the product. The two layers are clearly visible.

The reduction reaction left the pellet very hard, which made it difficult to mount and polish for microscopic examination. As in the case of the reduction of niobium pentoxide, the NbC produced was also very hard and this also contributed to the difficulty in sample preparation. Thus, the specimens used for examination by scanning electron microscopy were obtained by fracturing the sample. Scanning electron micrographs of the typical reaction products from three parts of a partially reacted pellet are shown in Figure 6.2. The sample in Figure 6.2(a) is from the bottom of the pellet and shows the distribution of graphite and

(a)

(b)

Figure 6.1 Photographs of Partially Reacted Pellets
(D_p Pyrochlore = 60 μm, d_pC = <45 μm),
(a) 1765 K, x = 0.71, 16.3 wt. % C,
pellet dia. = 12.8 mm, pellet ht. = 14.6 mm,
(b) 1495 K, x = 0.45, 27.8 wt. % C,
pellet dia. = 12.9 mm, pellet ht. = 20.6 mm.

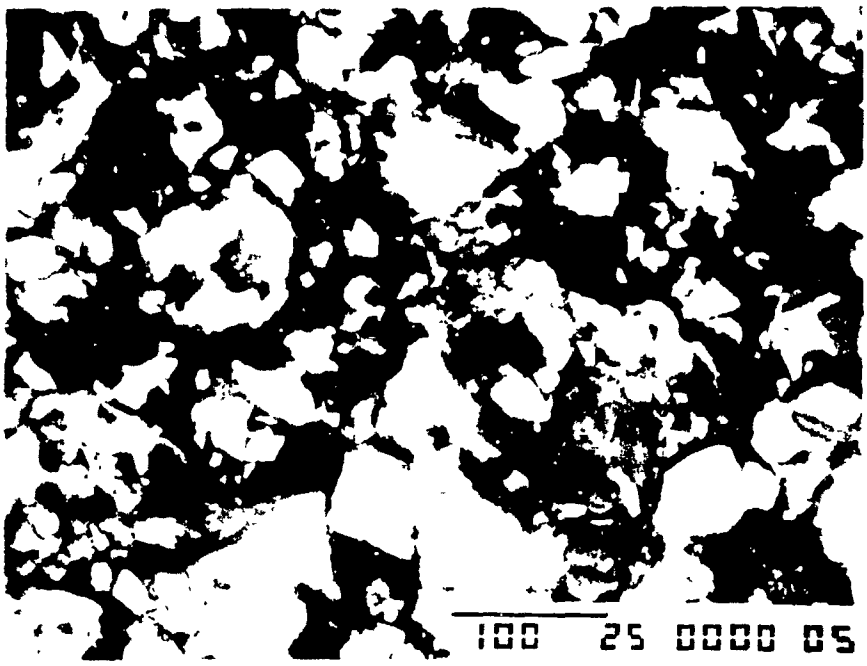

(a)

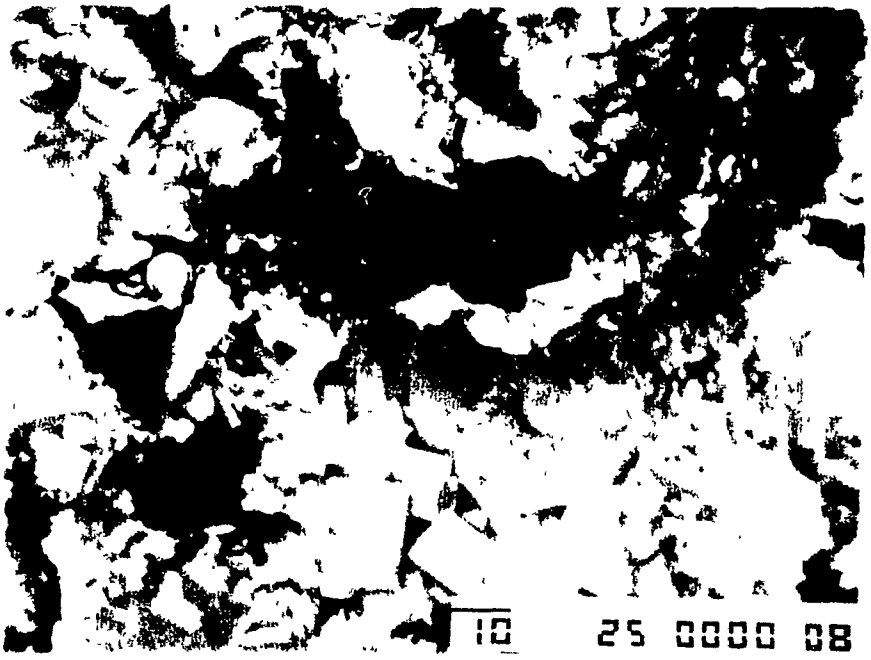

(b)

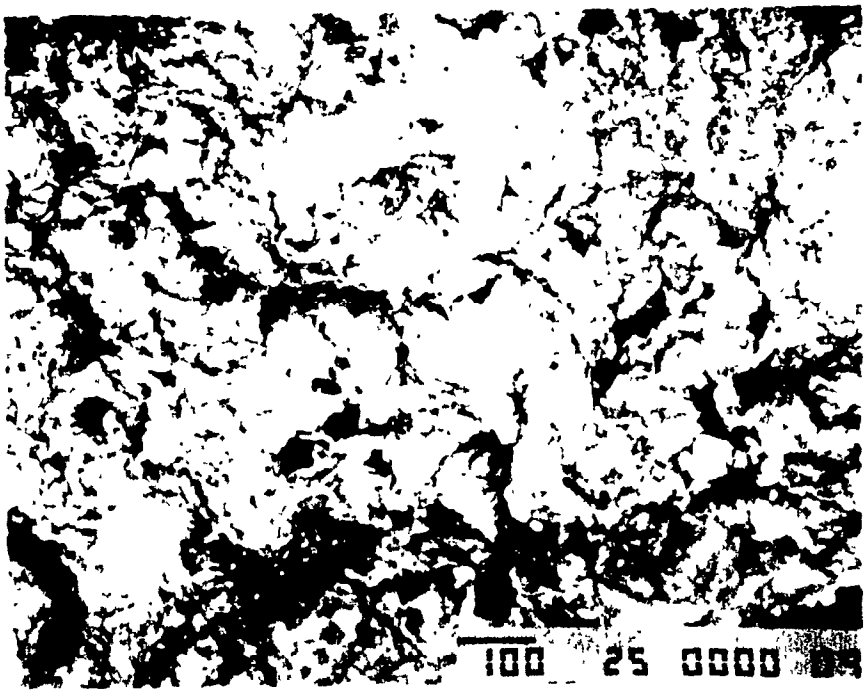

(c)

Figure 6.2 Scanning Electron Micrographs (with back scatter) of Three Sections of a Partially Reacted Pellets :
(a) bottom (X 200), (b) middle (X 750), (c) top (X 100)
16.3 wt. % C, D_p Pyrochlore = 60 μm, D_pC = <45 μm
pellet dia. = 12.8 mm, pellet ht. = 16.1 mm

pyrochlore particles with little or no reaction. Figure 6.2(b) is from the middle of the pellet where there was partial reaction. It shows the metallic looking NbC product at points around the graphite particles and a separate calcium, silicon and titanium rich slag material (cubic-shaped crystals), identified by EDX (energy dispersed x-ray spectrometer) analysis. Because of the pellet size and the nature of reactor design, separation of the reaction product from the slag was not possible. It can also be seen that there was some melting of the pyrochlore. The melting point of Niobec's pyrochlore is about 1535 K. The main product of the reaction NbC, is expected to solidify immediately upon formation due to its high melting point of 3875 K. The solid NbC would form either as an ash layer around the microscopic graphite and/or oxide particles or be dispersed randomly at the reaction (contact) points between the microscopic graphite and oxide particles. If the gaseous intermediates (CO and CO_2) were major contributors to the progress of the reduction reaction, it would be expected that melting would hinder the reduction process because of the reduced porosity of the particle. Diffusion resistance through the ash layer would also become important at relatively high temperatures. However, diffusion does not seem to be the rate-controlling factor for the given temperature range due to the highly porous nature of the reacted layer. The progress of the reaction is expected to be strongly influenced by the degree of contact between the carbon and the solid and/or liquid pyrochlore particles. This is shown in Figure 6.2(b), which shows individual pyrochlore particles (grey) in contact with the carbon

particles (black). The product of the reaction (white) is shown scattered randomly over the surface of the graphite particle rather than in any sort of continuous shell around either the graphite or oxide particle. The foregoing discussion was supported by the experimental data for the influence of graphite and pyrochlore particle sizes on the reaction rate which are presented in a later section.

Figure 6.2(c) is the top section of the pellet which was the root of the plasma. It is very metallic in appearance, although the material seems to be very porous. The completeness of the reduction reaction is apparent from the lack of carbon present.

6.3 X-ray Analysis

As in the case of niobium pentoxide, a number of reacted pellets were selected for x-ray powder diffraction (XRD) analysis. The XRD analysis results showed that for the case of C/Nb_2O_5 mole ratio of 7 (16.3 wt. % C), the major phases identified in the product were NbC, Nb_2C, the minor phases were latrappite ($(Ca,Na)(Nb,Ti,Fe)O_3$), pyrochlore and traces of Nb metal. For a mole ratio of 10, the only phase identified was NbC. In the case when the mole ratio was 14 (27.8 wt. % C), the phases identified were NbC and C. The results are in agreement with those obtained by Hilborn (1988). The other minor elements, e.g. Ti and Ca, were not detected because their concentrations were probably below the detection limit for XRD analysis.

Analysis was also done on samples taken from the reactor walls. The major phases identified were pirssonite (Na_2CO_3, $CaCO_3$

.H_2O) and a fluorine bearing compound.

The results are summarized in Table 6.1.

6.4 Mass Balance

Conversion was previously defined in Equation (3.4) as the ratio of total oxygen in the carbon monoxide and carbon dioxide in the exhaust gas to the total initial oxygen in the oxide reactants. This method of measurement for conversion was checked for consistency by comparing the result to that calculated from the pellet's weight loss. The latter method of measurement was subject to higher experimental error and it was used primarily as an indicator for possible anomalies during an experimental run. The fractional conversion by weight loss (Appendix III) was consistently higher, but the difference was generally less than 0.20. This difference was due mainly to the loss of fluorine, sodium and calcium which were volatilized during the reaction. These elements were identified from the results of the x-ray analysis of the samples taken from the reactor's wall. These elements were also identified as the most probable elements to be volatilized during the reaction from an approximate mass balance. The mass balance was based on the thirteen most abundant elements present in the reactants. The elemental analysis by emission spectroscopy, was done on the combined products from two experiments under similar experimental conditions and conversions. The difference between the summation of the percentage elemental composition and 100 % was all attributed to oxygen. The results are summarized in Table 6.2. Since the analysis did not include all

Table 6.1 XRD Analysis of Compounds for the Carbothermic Reduction of Pyrochlore

C/Nb_2O_5 (mole)	COMPOUNDS	
	Major Phases	Minor Phases
7	NbC, Nb_2C	Latrappite, Pyrochlore, Nb
10	NbC	
14	NbC, C	
Sample from reactor walls[1]	Pirssonite, compound with F	Nb compound

1 - C/Nb_2O_5 (mole) = 7

Table 6.2 Mass Balance for the Combined Products From Experiment Numbers 60 and 61

Weight of pellets, before reaction - 11.27 grams
Weight of pellets, after reaction - 6.24 grams
Average conversion (based on exhaust gas analysis) - 0.96
Average conversion (based on O loss in mass balance) - 0.67
Average pellet tempareture - 2145 K

	Before Rx.				After Rx.	
	pyrochlore		added	total		
Element	%	g	g	g	%	g
Fe	4.5	0.407	0.00	0.407	5.70	0.356
C	0.08	0.007	1.74	1.747	4.96	0.309
Al	0.005	0.00	-	0.00	0.005	0.000
Ca	8.06	0.729	-	0.729	5.34	0.333
K	0.36	0.033	-	0.033	0.05	0.003
Mg	0.44	0.040	-	0.040	0.17	0.011
Mn	0.30	0.027	-	0.027	0.10	0.006
Na	5.00	0.452	-	0.452	0.05	0.003
Nb	44.1	3.988	-	3.988	63.8	3.981
P	0.03	0.003	-	0.003	0.02	0.001
Sr	1.26	0.114	-	0.114	1.00	0.062
Ti	1.68	0.152	-	0.152	2.61	0.163
U	0.029	0.026	-	0.026	0.041	0.003
O + others (diff.)	33.89	3.065	-	3.065	16.15	1.008
TOTAL	100.0	9.043		10.78	100.0	6.239

the elements present in pyrochlore, the results are more qualitative than quantitative.

Experiments with fractional conversion differences greater than 0.20 were caused by weight loss due to reactant and product entrainment in the exhaust gas. The need for a binder was also demonstrated by the reaction with the pellet where water only was used as binder. This showed a difference of 0.27 in the calculated fractional conversion between the two methods.

Conversion is based on the total available oxygen in pyrochlore as defined in Equation (3.4). The complete reduction of the contained niobium pentoxide in pyrochlore is equivalent to a fractional conversion of 0.67. If it is also assumed that all the fluorine and sodium were volatilized during the reaction, this would result in an additional increase in the weight loss based fractional conversion of 0.31. Examination of the data of Appendix III, shows that most of the weight loss based conversions were greater than 0.67 and they increased with increasing temperature and graphite concentration. This would suggest that there was reduction of oxides other than niobium pentoxide. The graphite for reduction of the other oxides is made available from the graphite crucible and the carbon left over from the reduction of niobium pentoxide.

6.5 CO/CO_2 Ratio

Measurements for CO and CO_2 were made in the exhaust gas to measure the progress of the reaction and to obtain some understanding of the reaction mechanism. The measurement of CO_2 for

all the experiments was not done since a CO_2 meter was not available initially. This was of little consequence to the results, since for those reactions in which CO_2 measurements were made, the fractional conversion that was contributed by the generation of CO_2 was typically less than 0.03. This was also observed for the case of the carbothermic reduction of pure niobium pentoxide. Figure 6.3 shows the typical variation of exhaust gas CO and CO_2 concentrations with time during the carbothermic reduction of pyrochlore.

A comparison of the CO/CO_2 ratios at two different temperatures, 1615 and 1765 K, using graphite and pyrochlore particle diameters of 100 % less than 45 and 60 microns, respectively, are shown in Figure 6.4. The average ratios for the rest of the experiments are summarized in Appendix III.

Assuming complete gas equilibrium and that the reduction reaction had taken place via gaseous intermediates, the CO/CO_2 ratios at 1615 and 1765 K should be about 1610 and 1170, respectively. Thus, the exhaust gas should essentially be all CO. From Figure 6.4, the highest values were about 275 and 175, respectively, which are much less than expected. The scatter is due to taking the ratio of large and small numbers. The presence of CO_2 could be due to carbon deposition from the exhaust gas as it cools from the high temperatures in the plasma to slightly above room temperature (Turkdogan, 1980). This is represented by the following equation:

$$2CO = CO_2 + C \qquad (6.1)$$

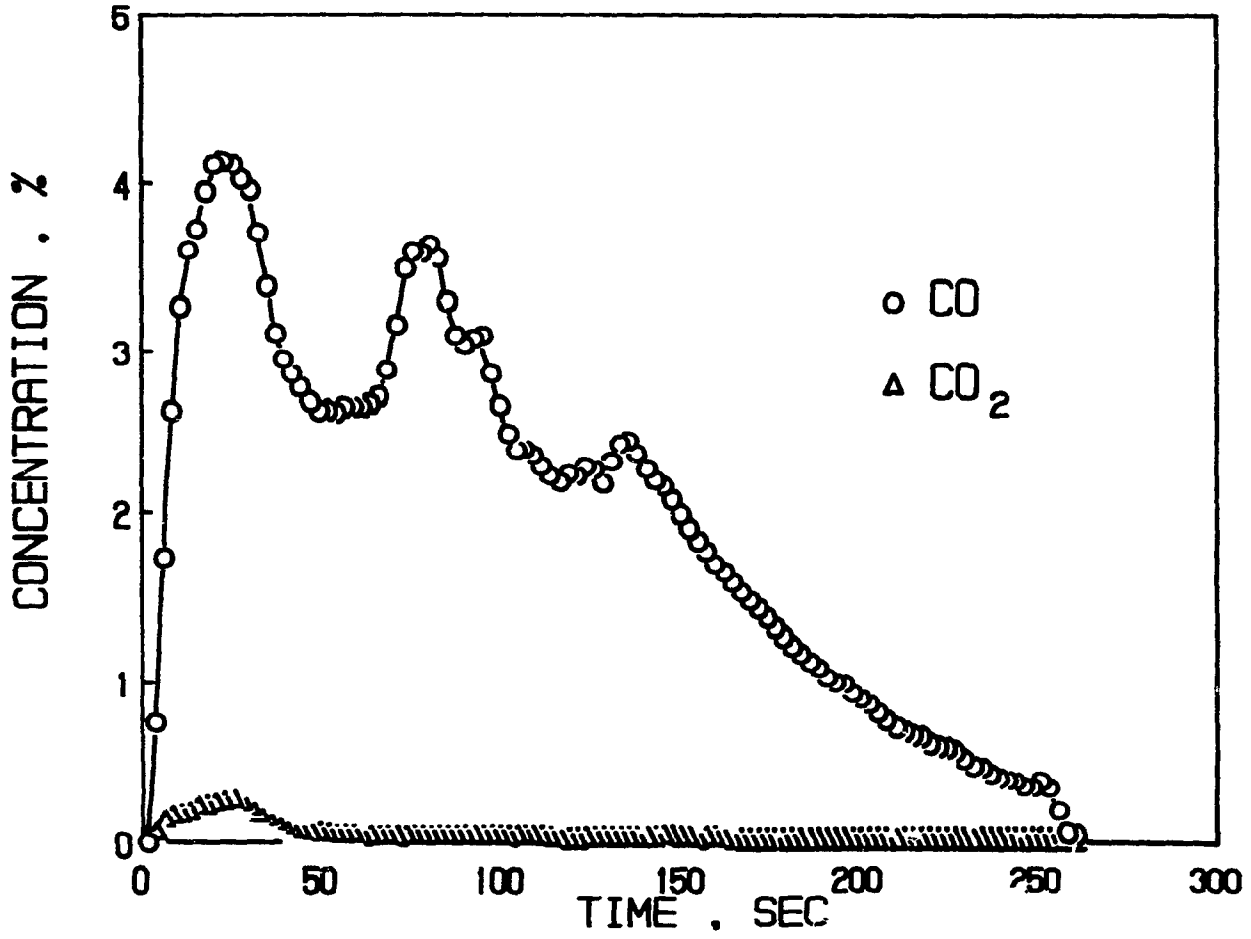

Figure 6.3 CO and CO_2 Concentration Versus Reaction Time for the Carbothermic Reduction of Pyrochlore : 1765 K, 16.3 wt. % C, d_p Pyrochlore = 60 μm, d_pC = <45 μm, pellet dia. = 18.5 mm, pellet ht. = 16.5 mm

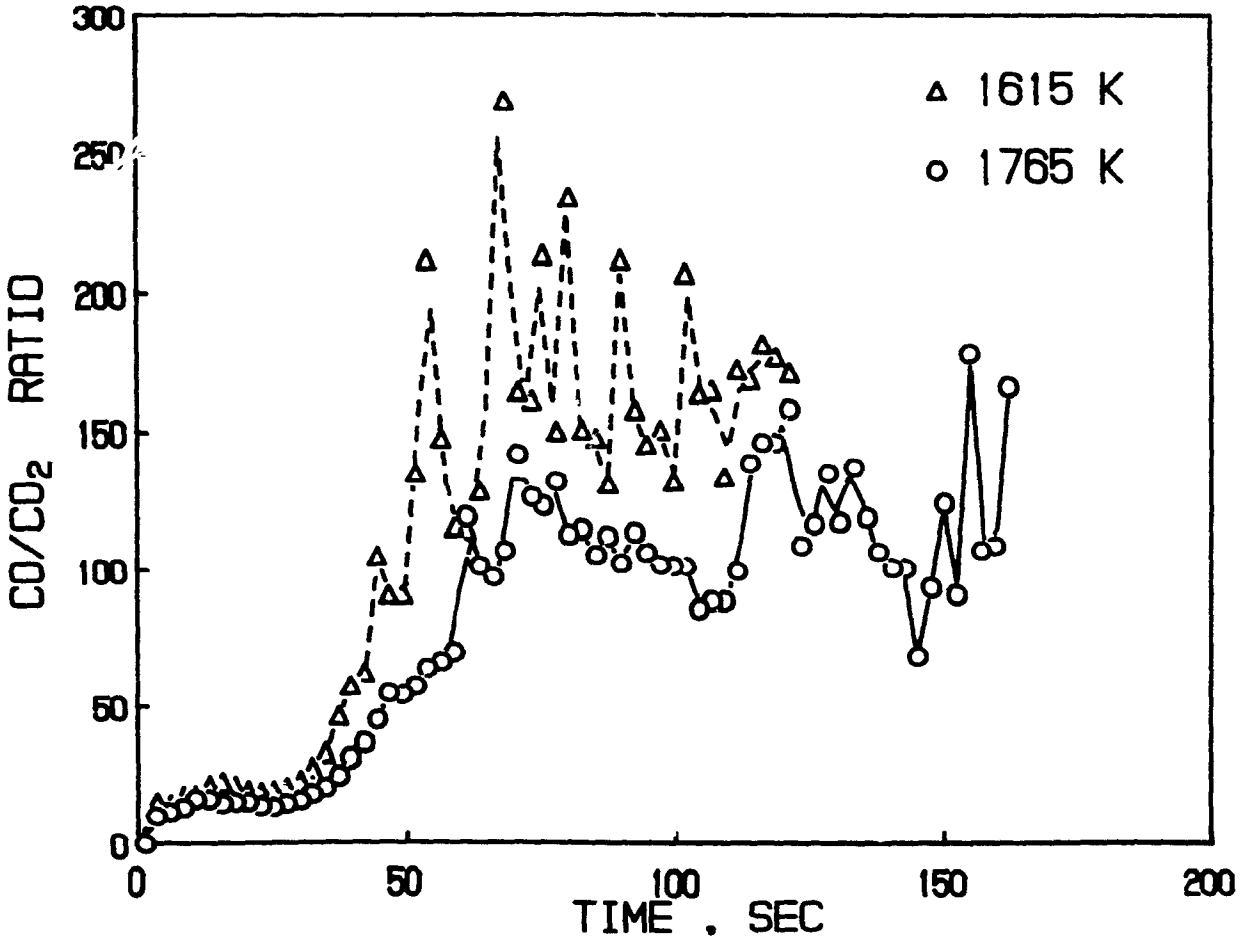

Figure 6.4 The Effect of Temperature on CO/CO_2 Ratio Versus Reaction Time for the Carbothermic Reduction of Pyrochlore : 16.2 wt. % C, $d_p C$ = <45 μm, d_p Pyrochlore = 60 μm, pellet dia. = 18.5 mm, pellet ht. = 11.3 mm

The temperature at which carbon deposition may start is below 1000 K, and the reaction is catalyzed by iron, cobalt and nickel (Turkdogan, 1980).

The presence of CO_2 in the exhaust suggests the possibility that the reduction reaction might have occurred via the gaseous intermediates CO and CO_2, but it is inconclusive. Verification of the true reaction mechanism and composition of the exhaust gas would require in situ sampling of the exhaust gas which the present system was not designed to do.

6.6 Conversion-Time Relationship

The experimental rate data for different graphite and pyrochlore particle sizes were plotted according to several rate expressions which were previously discussed and presented in Chapter II. These equations were (a) diffusion controlling - Equations (2.13), (2.15), (2.19), and (2.20); (b) chemical reaction controlling - Equation (2.23), and (c) nucleation/logarithmic growth - Equations (2.29) and (2.31). Although the equations listed in (a) and (b) statistically fitted the conversion-time data as well as the equations of (c), they were rejected as appropriate models because their predicted dependencies of reaction rate on particle size was not observed. The choice of the current model as the most appropriate one will be justified in the following sections.

The examination of reacted pellets led to the conclusion that the carbothermic reduction of pyrochlore particles does not

progress according to the shrinking-core model, that is, on a sharp reaction front, but rather it takes place randomly at contact points between the carbon and the solid and/or liquid pyrochlore, at the interparticle level. The overall reduction of pyrochlore with time, under chemical-reaction control, has been represented by the logarithmic expression given by Equation (4.20) developed earlier.

The applicability of Equation (4.20) was further tested by varying the graphite particle diameter (100 % less than 45, 165, 463 microns) and the pyrochlore particle diameter (31, 60, 98, 230 microns), while keeping the graphite concentration constant at 16.3 wt. %. The typical conversion-time data for pellets made with graphite particle diameters of 100 % less than 45 and 463 microns while the pyrochlore particle diameter was kept constant at 60 microns, at different temperatures are given in Figures 6.5 and 6.6. In another series of experiments, the pyrochlore particle diameter was increased to 230 microns and the graphite particle diameter was kept constant at 100 % less than 45 microns. The typical conversion-time data at different temperatures are shown in Figure 6.7. The plots show that there is a relatively small induction period associated with each reaction, which decreases with increasing temperature. The delay is between 5 to 15 seconds. This induction period may include the time required for the sample to (i) attain reaction temperature, (ii) effect changes within the reaction sample, e.g. melting (endothermic) and (iii) slow processes preceding establishment of the main reaction. The time required for heating and melting of the oxide

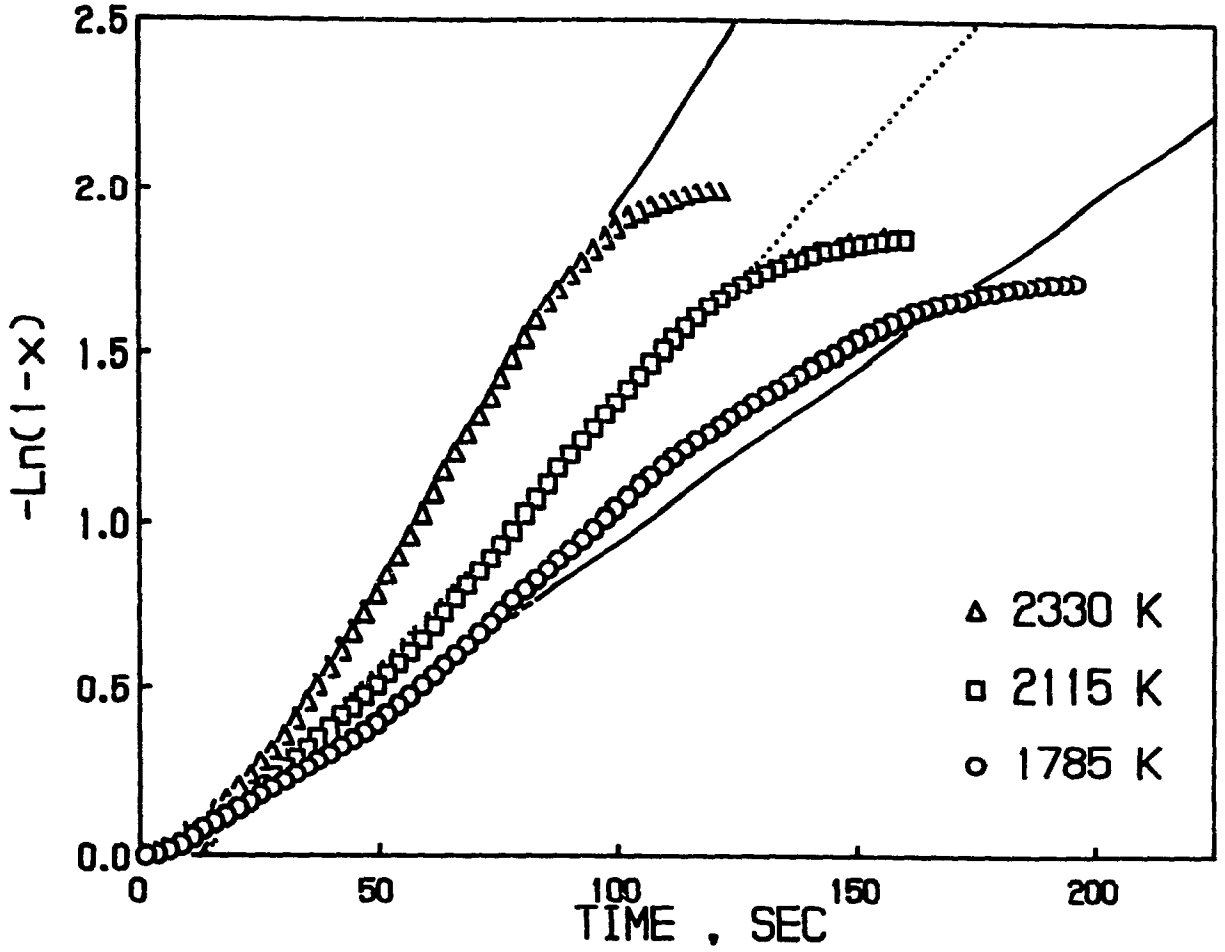

Figure 6.5 The Effect of Temperature on Conversion Using the Kinetic Model for the Carbothermic Reduction of Pyrochlore : 16.3 wt. % C, d_pC = <45 μm, d_p Pyrochlore = 60 μm, pellet dia. = 12.8 mm, pellet ht. = 16.1 mm

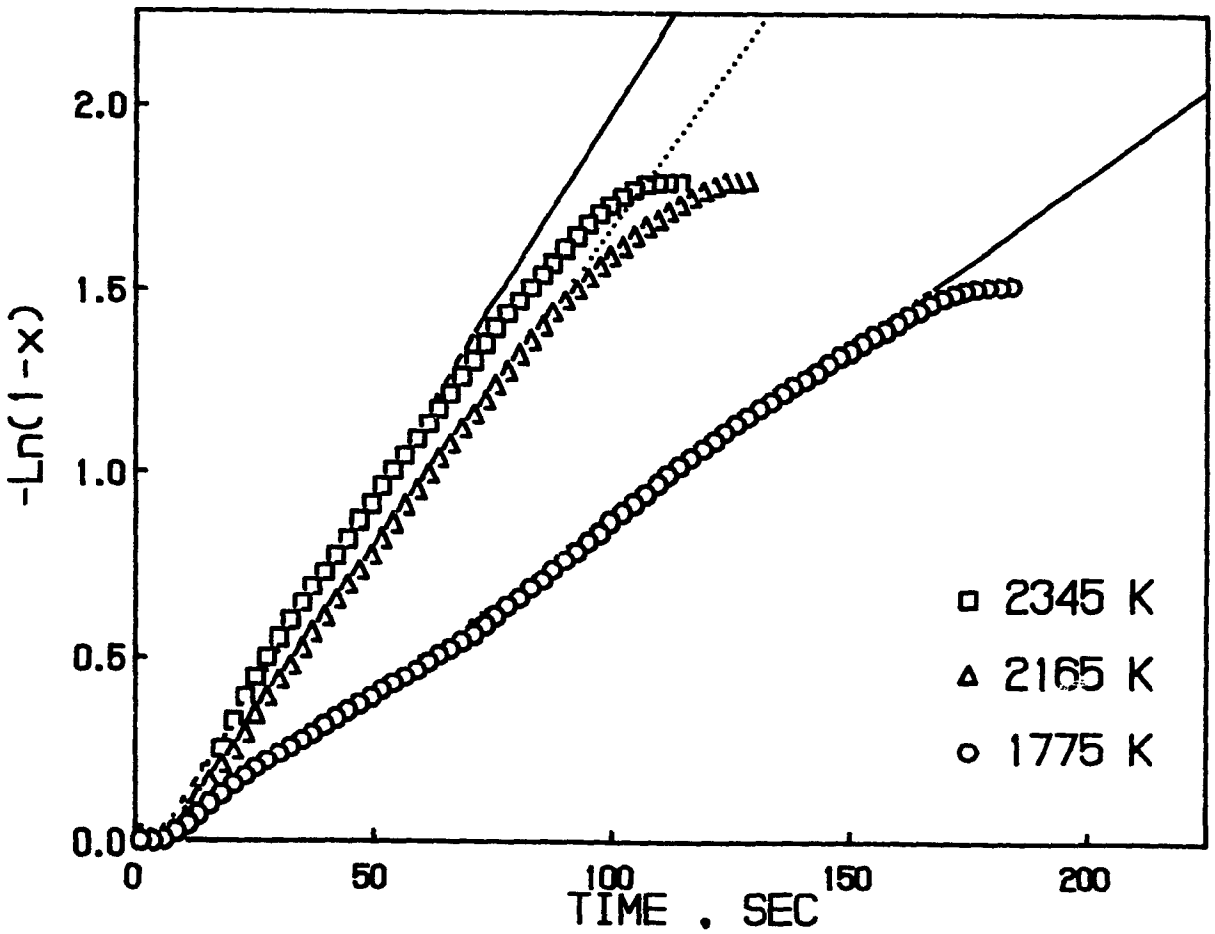

Figure 6.6 The Effect of Temperature on Conversion Using the Kinetic Model for the Carbothermic Reduction of Pyrochlore : 16.3 wt. % C, d_pC = 463 μm, d_p Pyrochlore = 60 μm, pellet dia. = 12.8 mm, pellet ht. = 16.6 mm

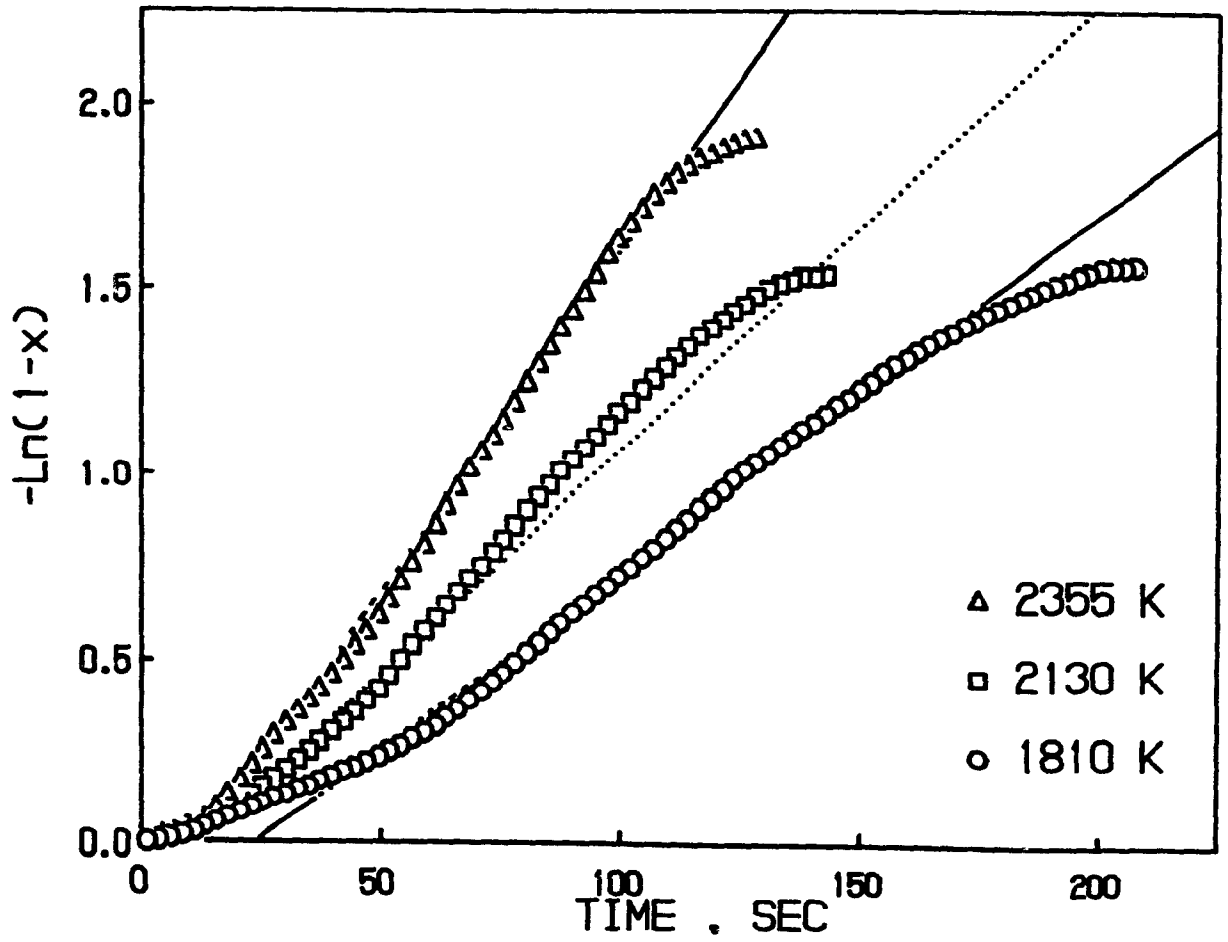

Figure 6.7 The Effect of Temperature on Conversion Using the Kinetic Model for the Carbothermic Reduction of Pyrochlore : 16.3 wt. % C, d_pC = <45 μm, d_p Pyrochlore = 230 μm, pellet dia. = 12.8 mm, pellet ht. = 15.0 mm

at a reaction temperature of 2140 K, assuming a plasma energy efficiency of 30 %, was estimated to be about 15 seconds. It is seen that, if the induction period is subtracted, the plot of time versus -ln(1-x) holds a linear relationship as expected, but only to a certain conversion level beyond which the rate of conversion is less than the model predictions. The fractional conversion at which the deviation from the logarithmic model occurs increases with increasing temperature. Figures 6.5 and 6.6 show that, for pellets made with graphite particle diameters of 100 % less than 45 and 463 microns and constant pyrochlore particle diameter of 60 microns, at pellet temperatures of 1785 and 1775 K, the deviation starts at about 80 and 75 % conversion, respectively. At higher pellet temperatures of 2330 and 2345 K it takes place at 86 and 80 % conversion, respectively. Figure 6.7 shows a similar trend for pellets made with increased pyrochlore particle diameter, while the graphite particle size was kept constant. It shows that at a pellet temperature of 1810 K, the deviation starts at about 75 % conversion, whereas at 2355 K, it starts at 85 % conversion.

As in the case for the carbothermic reduction of niobium pentoxide, the difference in the conversion levels at which deviation from the model occurs can be attributed to the effects of heat transfer limitations which lead to a non-isothermal pellet, rather than a change in the rate controlling mechanism.

The effect of using higher initial concentrations of carbon on the form of the conversion curve is shown in Figure 6.8. Although the temperatures are not exactly alike, a comparison can

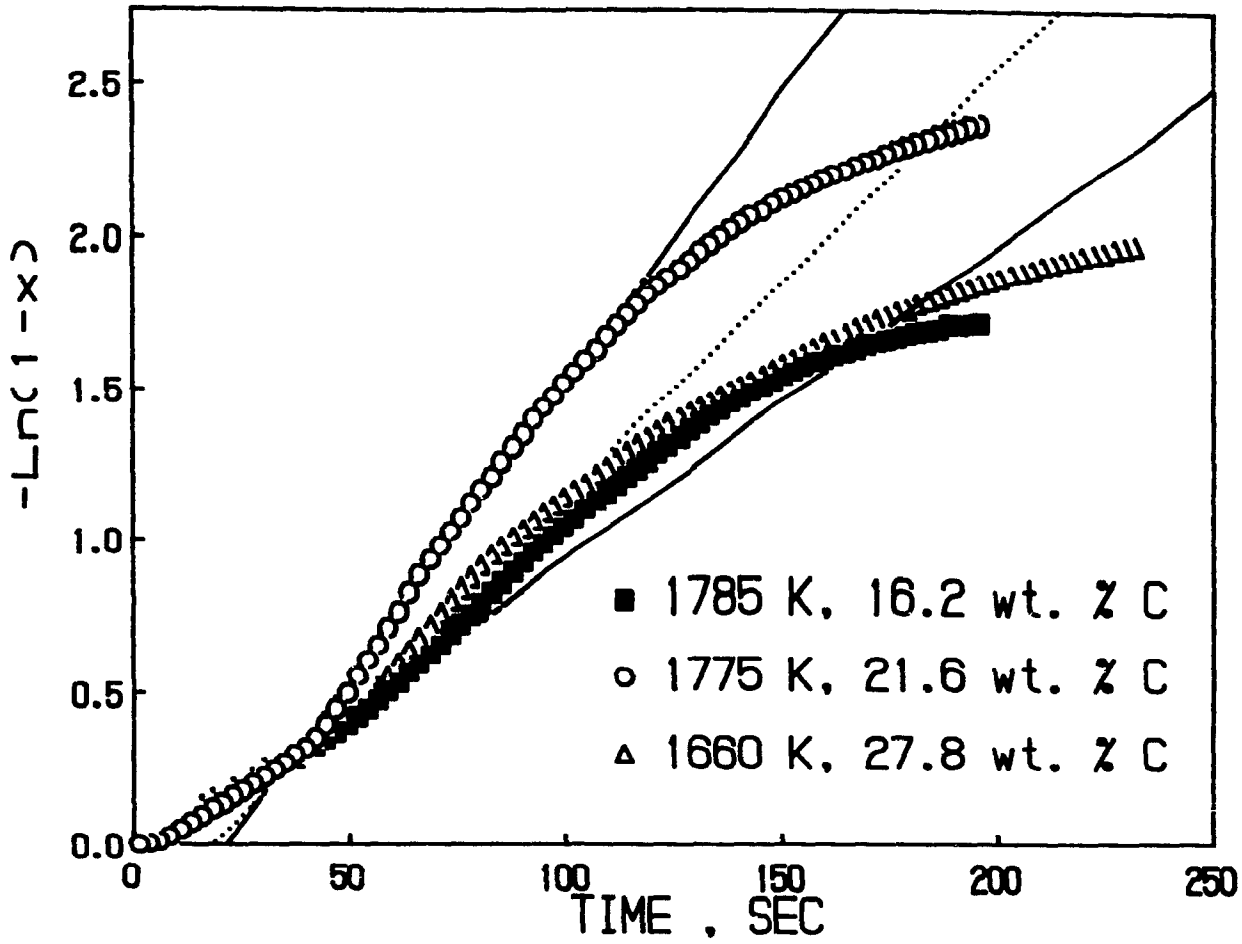

Figure 6.8 The Effect of Initial Pellet Carbon Concentration on Conversion Using the Kinetic Model for the Carbothermic Reduction of Pyrochlore : $d_p C$ = <45 μm, d_p Pyrochlore = 60 μm, pellet dia. = 12.9 mm, pellet ht. = 20.5 mm

still be made. The level of fractional conversion at which deviation from the logarithmic model takes place is higher for pellets with higher initial graphite concentrations for comparable levels of temperature. This may suggest that with higher initial graphite concentration, a higher degree of contact between the oxide and the carbon particles is achieved at all times during the reaction. The high carbon concentration would also improve intra-pellet heat transfer resulting in more isothermal conditions. Thus there is no decrease in the rate of conversion as the reaction progresses.

6.7 Influence of Particle Diameter

The overall rate constant, K, as defined by Equation (4.17), was not expected to be influenced by the change in particle diameter. Accordingly, an Arrhenius plot of the rate constants of different particle diameters is expected to yield a single straight line, if ash diffusion is not contributing. Otherwise, the overall rate constant would decrease with increasing particle diameter due to a corresponding increase in the diffusion resistance.

The overall rate constants corresponding to the linear portion of $-\ln(1-X)$-versus-time data were plotted according to an Arrhenius-type relationship in Figures 6.9 and 6.10. Figure 6.9 is for pellets having different graphite particle size diameters of 100 % less than 45, 165 and 463 microns, respectively. The pyrochlore particle diameter was kept constant at 60 microns. The results of the treated experimental data for each of these cases

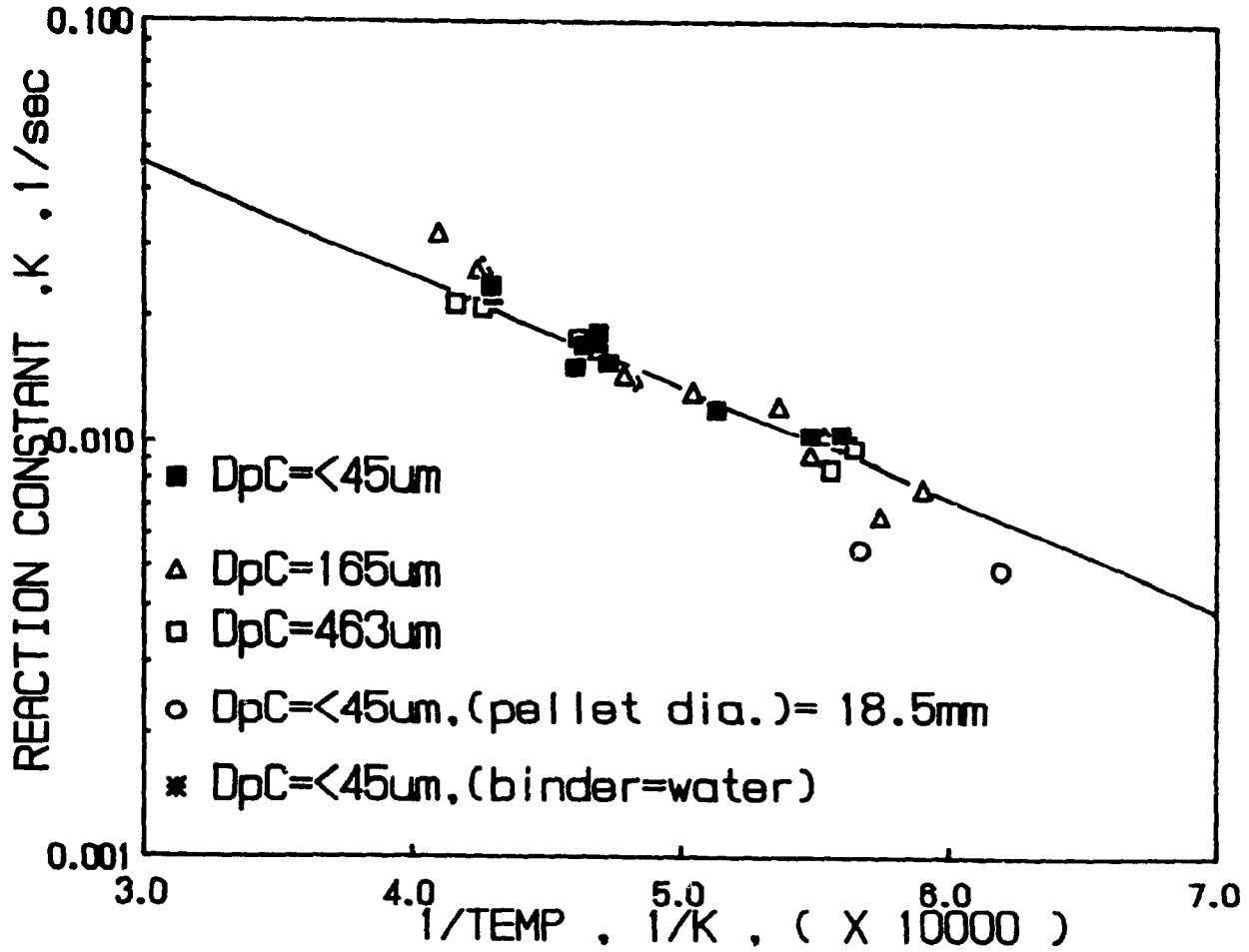

Figure 6.9 Arrhenius Plot for the Carbothermic Reduction of Pyrochlore for Varying Graphite Particle Size : d_p C = <45, 165, and 463 μm, d_p Pyrochlore = 60 μm, 16.3 wt. % C, pellet dia. = 12.8 mm, pellet ht. = 16.2 mm

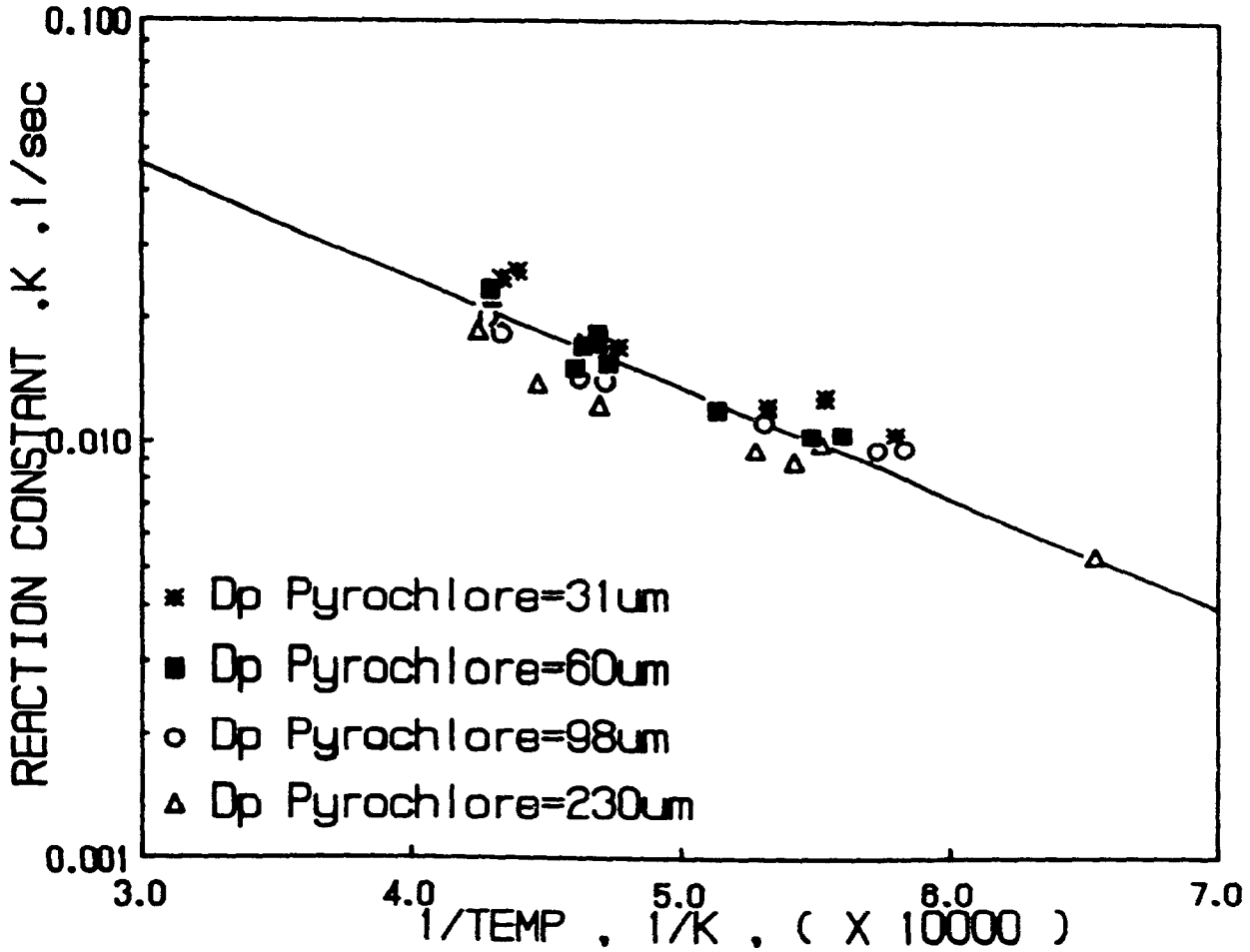

Figure 6.10 Arrhenius Plot for the Carbothermic Reduction of Pyrochlore for Varying Pyrochlore Particle Size : d_p Pyrochlore = 31, 60, 230 μm, d_pC = <45 μm, 16.3 wt. % C, pellet dia. = 12.8 mm, pellet ht. =16.2 mm

are presented in Tables III-A, III-B, and III-C of Appendix III. Figure 6.10 is for pellets having different pyrochlore particle diameters of 31, 60, 98 and 230 microns while the graphite particle diameter was kept constant at 100 % less than 45 microns. The results of the treated data for each of these cases are presented in Tables III-D, III-A, III-E, and III-F of Appendix III. The data for pyrochlore particle diameter of 60 microns are reproduced for comparison. The data in Figure 6.9 show that the overall rate constants for the three different carbon particle diameters of 100 % less than 45, 165 and 463 microns all lie on the same line. The data in Figure 6.10 also show that the overall rate constants for the four different pyrochlore particle diameters of 31, 60 98 and 230 microns all lie on the same line. In the case for the pyrochlore particle diameter of 230 microns, it would appear that there was a slight dependency of the overall rate constant on particle size. The dependency is not large enough to justify the use of the other rate expressions previously discussed in Chapter II. For instance, at a temperature of 1850 K, the ratio of the overall rate constants corresponding to a pyrochlore particle diameter ratio of 1:7.5 (31 microns:230 microns) is only 1.25. If the reaction or diffusion model was the appropriate one, the overall rate constants should be inversely proportional to the particle radius or the square of the particle radius, respectively. That is, for a reaction or diffusion controlled model, the predicted ratios of the overall rate constants should be 7.5:1 or 56:1, respectively. The small variation with size might have been due to the larger relative surface area

which become available for contact and reaction with the pyrochlore as discussed earlier. Thus, it would appear that the overall rate constant is independent of graphite and pyrochlore particle size and Equation (4.17) adequately represents the overall rate constant.

6.8 Influence of Temperature

The investigation of the influence of reaction temperature on the reaction rate was carried out using different temperatures ranging from 1530 to 2440 K. The choice of the temperature levels was dictated solely by the currents under which the arc was stable

The Arrhenius plots in Figure 6.9 and 6.10 show that the reaction rate is a function of temperature. Also shown in Figure 6.9, are the overall rate constants obtained from the reactions in which the pellet diameter was increased from 12.8 to 18.5 mm.

Experiments were also done with pellets made with water only as binder. The overall rate constants are also shown in Figure 6.9. The pellets for both sets of experiments were made with graphite and pyrochlore particle diameters of 100 % less than 45 and 60 microns, respectively. As it can be seen, the pellet diameter and the presence of the binder had no influence on the reaction rate. The treated data are presented in Table III-J and III-K of Appendix III.

The data in Figure 6.9 were used in a linear regression analysis program (LOTUS) to obtain the values of the activation

energies. For the carbon particle diameters of 100 % less than 45, 165, and 463 microns and constant pyrochlore particle diameter of 60 microns, the least square fits yielded activation energies and 95 % confidence intervals of 52.775 ± 10.968, 65.477 ± 11.387, and 52.206 ± 12.099 kJ/mole, with corresponding correlation coefficients of 0.939, 0.942 and 0.973, respectively. For pyrochlore particle diameters of 31, 98 and 230 microns and constant graphite particle diameter of 100 % less than 45 microns (Figure 10), the least square fits yielded activation energies and 95 % confidence intervals of 48.773 ± 16.118, 37.888 ± 10.675 and 43.330 ± 9.085 kJ/mole, with corresponding correlation coefficients of 0.924, 0.943 and 0.958, respectively. The fact that the lines of the Arrhenius plots are roughly parallel, confirmed the consistency of the previously proposed rate controlling resistance as being chemically reaction. If the data for all graphite and pyrochlore particle sizes are used, i.e. it is agreed that the reaction is independent of particle size, the activation energy and the 95 % confidence interval for the carbothermic reduction of pyrochlore was found to be 51.368 ± 5.903 kJ/mole. The corresponding correlation coefficient was 0.865, which is significant beyond the 0.01 level. The straight lines in Figures 6.9 and 6.10 are the resulting regression line.

A comparison of the results from the Arrehenius plots for the carbothermic reduction of niobium pentoxide and pyrochlore (Figures 5.10, 6.9 and 6.10) shows that the overall activation energies are the same, but the reaction rate for the reduction of niobium pentoxide is slightly higher. This might be due to the

diluting effect caused by presence of the other oxides that are in the pyrochlore concentrate. This would cause a reduction of the degree of contact between the carbon particles and the liquid and/or solid niobium pentoxide. Since the overall activation energies are the same, strongly suggests that the reaction mechanism is the same for both systems.

6.9 Influence of Carbon Concentration

Analysis of the kinetic data with respect to the carbon concentration was based on the carbon content of the individual pellets. The experimental runs covered a carbon concentration range from 10.3 to 27.8 wt. % and the treated data are summarized in Tables III-A to III-K of Appendix III. As in the previous cases, only those data corresponding to the straight line portion of the time-conversion expression (Equation (4.20)) were considered.

The previously obtained activation energy value, the overall rate constants, and their corresponding temperatures were used to calculate respective values for the pre-exponential constant, A, as defined by the Arrhenius equation:

$$A = K/\exp(-E/RT) \qquad (6.2)$$

where K is the overall rate constant. The calculated values for A were then plotted against the pellet carbon concentration in Figure 6.11. Using the one-tailed student t-test, it was shown that the average values of A were statistically different for average initial graphite concentrations of 10.3, 16.2 and 21.5, respec-

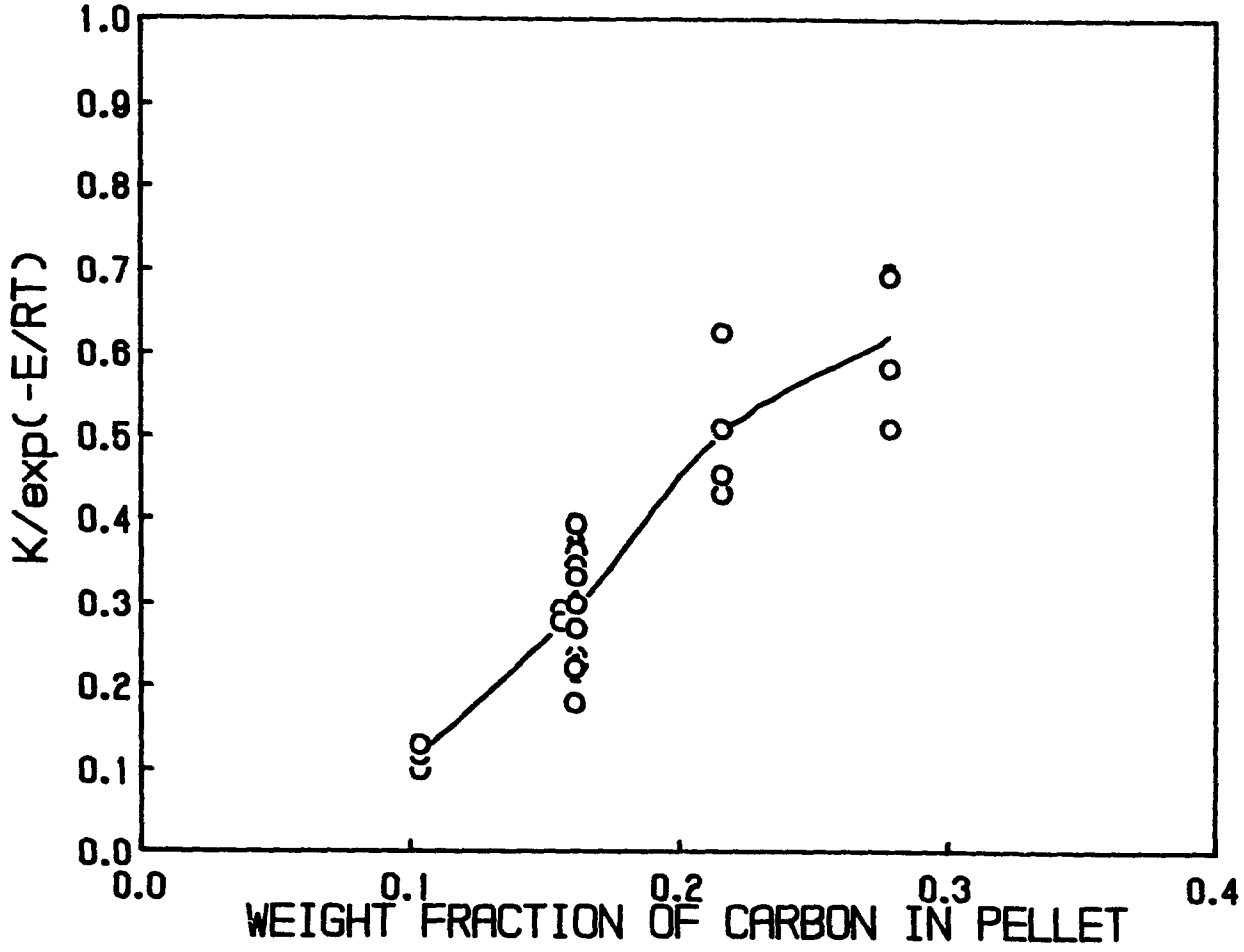

Figure 6.11 The Effect of Carbon Concentration on Reaction Rate

tively, at a 0.01 level of significance. Whereas, for higher average graphite concentrations of 21.5 and 27.8 wt. %, the values of A were not statistically different at the same level of significance.

The rate of carbothermic reduction is seen to increase with increasing graphite concentration, but changes very little after a threshold graphite concentration. This observation may be attributed to the existence of an optimum ratio of graphite-to-pyrochlore in the original mix, yielding an optimum contact area, and consequently a maximum reaction rate. Increasing the graphite concentration above this optimum amount will not give a significant increase in the reaction rate and would only serve to increase the carbon concentration in the final product.

A comparison of the effect of initial carbon concentration on the carbothermic reduction of niobium pentoxide and pyrochlore, showed that for the same C/Nb_2O_5 mole ratio, the reduction rate for niobium pentoxide was larger than pyrochlore.

6.10 CONCLUSION

1- The kinetics of the carbothermic reduction of pyrochlore were studied in the temperature range 1530 to 2440 K in an argon transferred-arc plasma. Influences of time, temperature, graphite concentration and graphite and pyrochlore particle sizes in the pellet on the rate were determined experimentally, using a single stationary pellet composed of pyrochlore and graphite particles.

2- The microscopic examination of sectioned partially reacted

pellets shows that the reaction did not progress according to the shrinking-core model but rather that it took place randomly on the graphite particle surface where the oxide made contact with it. This suggested the importance of the degree of contact between the oxide and carbon particles for the progress of the reaction.

3- The overall reduction of pyrochlore with time under chemical reaction control was represented by a logarithmic expression (Equation 4.20) based on the volumetric reaction model. In general, for pellets having a graphite concentration level less than 17.0 %, deviation from this model occurred at conversion levels which decreased with increasing reaction temperature. The pellets of higher graphite concentrations showed no such deviations. These behaviors were attributed to unavoidable non-isothermal effects and the degree of contact between the constituent particles, as was also indicated by the microscopic examinations of partially reacted pellets.

4- The Arrhenius plots of the experimental data indicated that the overall rate was independent of graphite and pyrochlore particle sizes and was chemical reaction controlled. The activation energy was calculated to be 51.4 kJ/mole.

5- Experimental data indicated the existence of an optimum ratio of the niobium pentoxide and the graphite in the original mix yielding a maximum contact area per unit volume, consequently, a maximum reduction rate.

6- The values of the activation energies for the carbothermic reduction of pyrochlore and niobium pentoxide were the same,

but the reaction rate of the former was lower.

CHAPTER VII

CARBOTHERMIC REDUCTION OF NIOBIUM PENTOXIDE IN THE PRESENCE OF IRON : EXPERIMENTAL RESULTS AND DISCUSSION

7.1 Introduction

Experiments were performed to study the time-conversion relationship, and the effect of graphite particle size, iron and graphite concentrations and temperature on the rate for the carbothermic reduction of niobium pentoxide in the presence of iron. The investigation was done in three series of experiments. In the first series of experiments, the Nb/Fe weight ratio in the pellet were 0.21 and 1.46 and the C/Nb_2O_5 mole ratio was kept constant at 7. The resulting initial iron and carbon concentrations in the pellet were 71.9 and 26.7 wt. % and 6.7 and 17.6 wt. %, respectively. In the second and third series of experiments, the C/Nb_2O_5 mole ratio was increased to 10 and 14 and the Nb/Fe weight ratio was kept constant at 0.21. The resulting initial iron and carbon concentrations in the pellet for the former mixture composition were 68.9 and 9.5 wt. %, respectively, and 66.6 and 12.9 wt. %, respectively, for the latter. The pellet diameter was 18.5 mm and heights were between 14.3 and 17.1 mm, except in the case of low initial iron concentration, when it was 12.9 mm (see Appendix I). The graphite particle diameters used in the experiments were 100 % less than 45 (or <45) and 463 microns. The niobium pentoxide and the iron particle diameters were kept constant at 10 and 100 % less than 45 (or <45) microns. The C/Nb_2O_5 mole ratio for the reaction stoichiometry to produce NbC is 7

(Equation (4.8)). The Nb/Fe weight ratio for commercial grade ferroniobium is about 1.5.

7.2 Microscopic Examinations

The reaction of the pellets was observed to have taken place in a mollified state. Within a short period (about 5 seconds) after the plasma is started, the entire top of the pellet is molten. Although the average shape of the reacting pellet was still cylindrical, the top surface was in constant motion as bubbles of carbon monoxide (and carbon dioxide) rose to the surface and burst. Occasionally, some tiny droplets of liquid were ejected from the surface. These observations were more exaggerated at high pellet temperature. When the pellet had reacted for the desired length of time the plasma was extinguished; at this point the pellet collapsed into a distorted cylinder and froze, usually in less than one second after shutdown.

The surface of an unreacted pellet was smooth and relatively non-porous. A partially reacted pellet exhibited a porous but hard surface as seen in Figure 7.1, where the initial iron concentrations were 26.7 and 71.8 wt. % and the C/Nb_2O_5 mole ratio was kept constant at 7, for Figure 7.1(a) and 7.1(b), respectively. The arc struck the top of the pellet and thus the temperature (and hence the rate of reaction) was the highest here. This also contributed to the melting and coalescing of the product. Close examination of the partially reacted pellets showed the presence of unreacted material in larger concentrations in the bottom half than in the top.

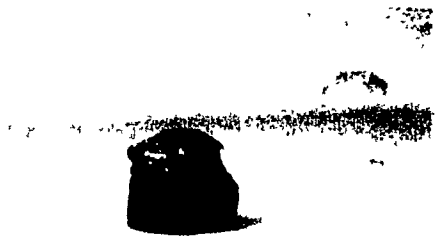

(a)

(b)

Figure 7.1 Photographs of Partially Reacted Pellets
(d_p Nb_2O_5 = 10 μm, d_p Fe = <45 μm) :
(a) 2285 K, x = 0.78, 17.6 wt. % C, 26.7 wt. % Fe,
d_pC = <45 μm, pellet dia. = 12.9 mm, pellet ht. = 17.1 mm,
(b) 1620 K, x = 0.92, 6.7 wt. % C, 71.8 wt. % Fe,
d_pC = 463 μm, pellet dia. = 18.5 mm, pellet ht. = 14.3 mm.

The reduction reaction left the pellet very hard. This made it difficult to mount and polish for microscopic examination. Thus, the specimens examined by scanning electron microscopy were obtained by fracturing the sample. A scanning electron micrograph of the top section of the typical reaction product with initial iron and carbon concentrations of 26.7 and 17.6 wt. %, respectively, is shown in Figure 7.2. EDX (energy dispersed x-ray spectrometer) analysis identified the white areas as iron-niobium rich, i.e. either a niobium oxide and/or NbC and iron matrix, which would be assumed to be the desired ferroniobium and/or ferro-niobium carbide product. Graphite particles (black) can also be seen dispersed in the ferroalloy matrix.

The melting points of niobium pentoxide, iron and niobium carbide are about 1760, 1785 and 3875 K, respectively. The solubility of the NbC product in iron will be a function of the temperature and the iron concentration in the pellet. If there is insufficient iron for complete dissolution of the niobium carbide produced, the rest will precipitate from solution. The solid NbC would form either as an ash layer around the graphite and/or oxide particles or be dispersed randomly at the reaction (contact) points between the graphite and oxide particles. If gaseous intermediates (CO and CO_2) were major contributors to the progress of the reduction reaction, it would be expected that melting would hinder the reduction process because of the reduced porosity of the particle. Diffusion resistance through the product ash layer would also become apparent at relatively high temperatures. The role of iron in the reaction is most probably to

Figure 7.2 Scanning Electron Micrographs (With Back Scatter) of Top Section of a Partially Reacted Pellets : X150, d_p Nb_2O_5 = 10 μm, d_p Fe = <45 μm, d_pC = <45, 17.6 wt. % C, 26.7 wt. % Fe, pellet dia. = 12.9 mm, pellet ht. = 15.0 mm,

improve contact between the carbon and the solid and/or liquid oxide particles. This is achieved by the reduction reaction taking place between the dissolved carbon in the iron and the oxide in the liquid state (Hilborn, 1988). Carbon dissolves readily in iron and it is probable that the iron will be saturated in carbon. Its concentration will be of the order of 4.5 to 12.8 wt. % for the temperature range 1575 to 2400 K (Chipman et. al.,1952). The amount of improvement in the reaction rate due to iron is dependent on the iron concentration. If there is insufficient dissolved carbon, further reduction will proceed by reaction with solid carbon and again the degree of contact between carbon and oxide becomes important. Diffusion limitation of the dissolved carbon across the iron-oxide interface would also become apparent at relatively high temperatures. The foregoing discussion was supported by the experimental data for the influence of iron concentration and niobium pentoxide and graphite particle sizes on the reaction rate which are presented in later sections.

7.3 X-ray Analysis

As in the previous cases, a number of reacted pellets were selected for x-ray powder diffraction (XRD) analysis. The results of all these analyses are summarized in Table 7.1. The XRD analysis results showed that in the case where the initial carbon and iron concentrations were 17.6 and 26.7 wt. %, respectively, with an average fractional conversion of 0.87, the major phase identified in the product was NbC. Iron and NbO_2 were identified as the minor phases. When the initial iron concentration was increased

Table 7.1 XRD Analysis of Products for the Carbothermic Reduction of Niobium Pentoxide in the Presence of Iron

Wt.% IRON	COMPOUNDS	
	Major Phases	Minor Phases
26.7 [1]	NbC	NbO_2, Fe
71.8 [1]	NbC, Fe, C	Nb_2C (trace)
68.9 [2]	NbC, NbO_2, Fe	

1 - C/Nb_2O_5 mole ratio = 7.
2 - C/Nb_2O_5 mole ratio = 10.

to 71.8 wt. %, giving an initial carbon concentration of 6.7 wt. %, the major phases were identified as iron, NbC and C, with trace amounts of NbC_2. The fractional conversion for this sample was 0.97. The C/Nb_2O_5 mole ratio for the two cases presented above was 7. When the ratio was increased to 10, giving initial carbon and iron concentrations of 9.5 and 68.9 wt. %, respectively, the major phases were identified as iron, NbC and NbO_2. The average fractional conversion for this sample was 0.94. The results indicate that Nb_2O_5 is reduced to NbO_2, followed by the formation of NbC. They are in agreement with those obtained by Shimada at al. (1983) and thermodynamic predictions by Kolchin (1970) for the carbothermic reduction of niobium pentoxide.

7.4 Mass Balance

Conversion was previously defined in Equation (3.4) as the ratio of total oxygen in the carbon monoxide and carbon dioxide in the exhaust gas to the total initial oxygen in niobium pentoxide. As in the previous cases, this method of measurement for conversion was checked for consistency by comparing the result to that calculated from the pellet's weight loss. The latter measurement was subject to higher experimental error and it was used as an indicator for possible anomalies. The results, which are presented in Appendix IV, indicate that there was fair agreement between the two methods for those experiments with the lowest initial iron concentration (26.7 wt. %). The fractional conversion by weight loss was consistently higher, but the difference was generally less than 0.30. In those experiments with high

initial iron (66.6 to 71.8 wt. %) concentration, the differences in conversion between the two methods were much higher. In these cases, the fractional conversion by weight loss was also consistently higher. The large differences (between 0.56 and 2.27) were caused by the evaporation and ejection of materials, primarily iron, during the reaction. Very fine particles were subsequently entrained in the exhaust gas. Another contributing factor was the decreasing ability of the binder to improve the pellet's mechanical strength with increasing iron and graphite concentrations, since the ratio of binder to niobium pentoxide was kept constant regardless of the pellet's composition. The difference in calculated conversion also increased with increasing temperature.

An approximate mass balance was done on the product from one of the preliminary experiments to verify the supposition that iron was the major material lost during the reaction. The initial iron concentration and C/Nb_2O_5 mole ratio of the pellet were 73.2 wt. % and 7, respectively. The elemental composition of the product was measured by emission spectroscopy. The results are summarized in Table 7.2. They confirm that iron is the main element lost during the reaction, but some niobium was also lost. The calculated conversion based on the oxygen loss from the mass balance result was in good agreement with that calculated by the analysis for CO and CO_2 in the exhaust gas.

7.5 CO/CO_2 Ratio

Measurements for CO and CO_2 were made in the exhaust gas to measure the progress of the reaction and to obtain some under-

TABLE 7.2 Mass Balance for the Product From Preliminary Experiment

Weight of pellet, before reaction - 11.17 grams
Weight of pellet, after reaction - 7.22 grams
Average conversion (based on exhaust gas analysis) - 1.0
Average conversion (based on O loss in mass balance) - 1.0
Average pellet temperature - 2025 K

Element	Before Reaction %	Before Reaction g	After Reaction %	After Reaction g
Nb	14.2	1.59	20.2	1.46
C	6.4	0.72	7.85	0.57
Fe	73.2	8.18	71.9	5.19
O	6.1	0.68	0.0	0.0
TOTAL	99.9	11.17	99.95	7.22

standing of the reaction mechanism. Figure 7.3 shows the variation of CO and CO_2 concentrations with time that were typically obtained during the carbothermic reduction of niobium pentoxide in the presence of iron. Random samples were also taken from the exhaust gas and analyzed by gas chromatography to determine the types of gas present and their concentrations. Carbon monoxide and carbon dioxide were the only gases detected.

A comparison of the CO/CO_2 ratio at two different temperatures, 2045 and 2215 K, using graphite and niobium pentoxide particle diameters of <45 and 10 microns, respectively, is shown in Figure 7.4. The average ratios for the rest of the experiments are summarized in Appendix IV. Assuming complete gas equilibrium and that the reduction reaction had taken place via gaseous intermediates, the CO/CO_2 ratios at 2045 and 2215 K should be about 695 and 530, respectively. Thus, the exhaust gas should essentially be all CO. From Figure 7.4., the highest values of CO/CO_2 were about 33 and 56, respectively, which are much less than expected. As discussed in the previous sections, the presence of CO_2 in the exhaust gas does not necessarily confirm the reduction mechanism as occurring via the gaseous intermediates CO and CO_2. The CO_2 could be due to carbon deposition from the exhaust gas as it cools from the high temperatures in the plasma to slightly above room temperature (Turkdogan, 1980). This is represented by the Equation (5.1). The temperature at which carbon deposition may start is below 1000 K, and this reaction is catalyzed by iron, cobalt and nickel (Turkdogan, 1980).

As before, the presence of CO_2 in the exhaust suggests the

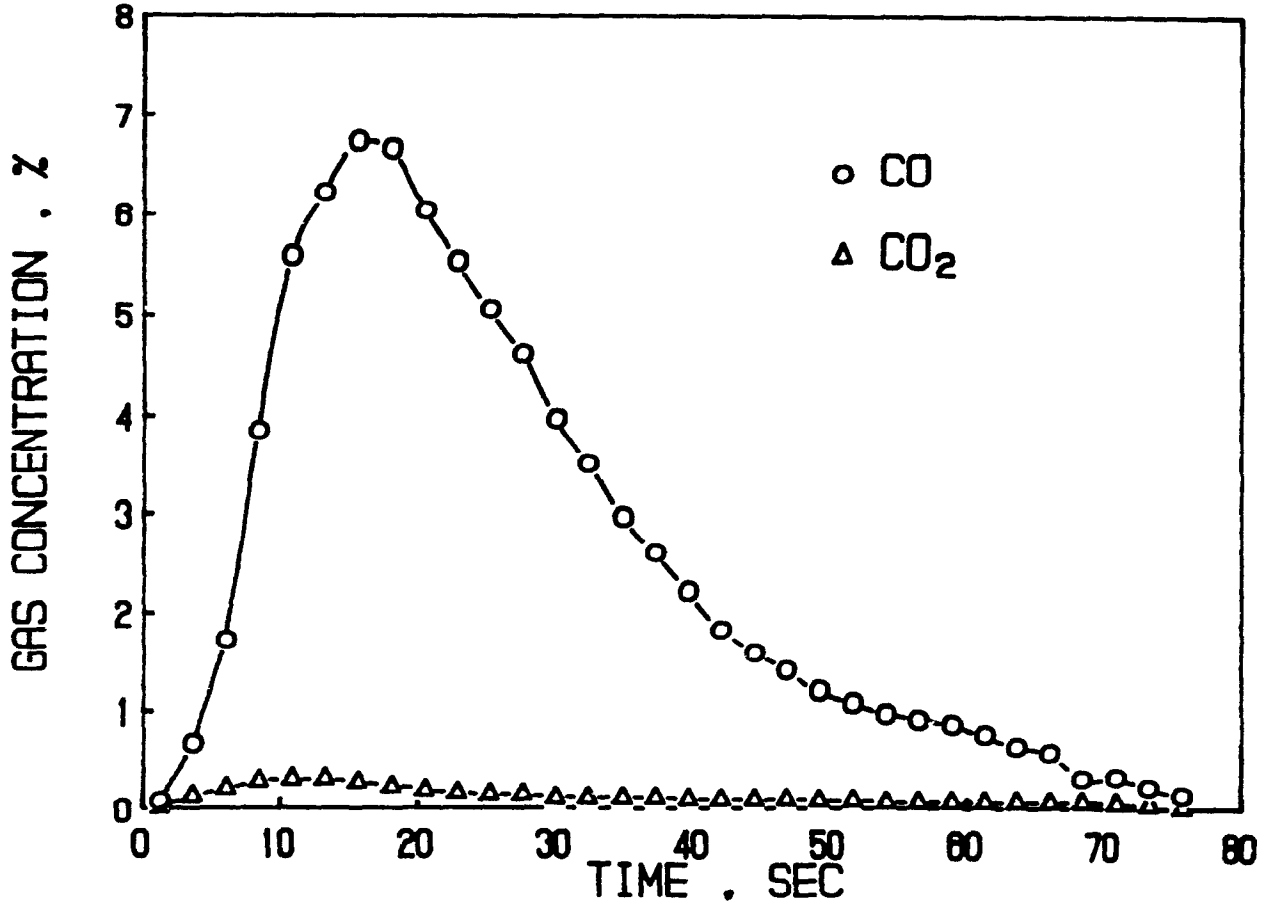

Figure 7.3 CO and CO_2 Concentration Versus Reaction Time for the Carbothermic Reduction of Nb_2O_5 (d_p Nb_2O_5 = 10 μm) in the Presence of Iron: d_pC = <45 μm, d_p Fe = <45 μm, 2045 K, 24.0 wt. % C, 26.7 wt. % Fe, pellet dia. = 12.9 mm, pellet ht. = 16.1 mm

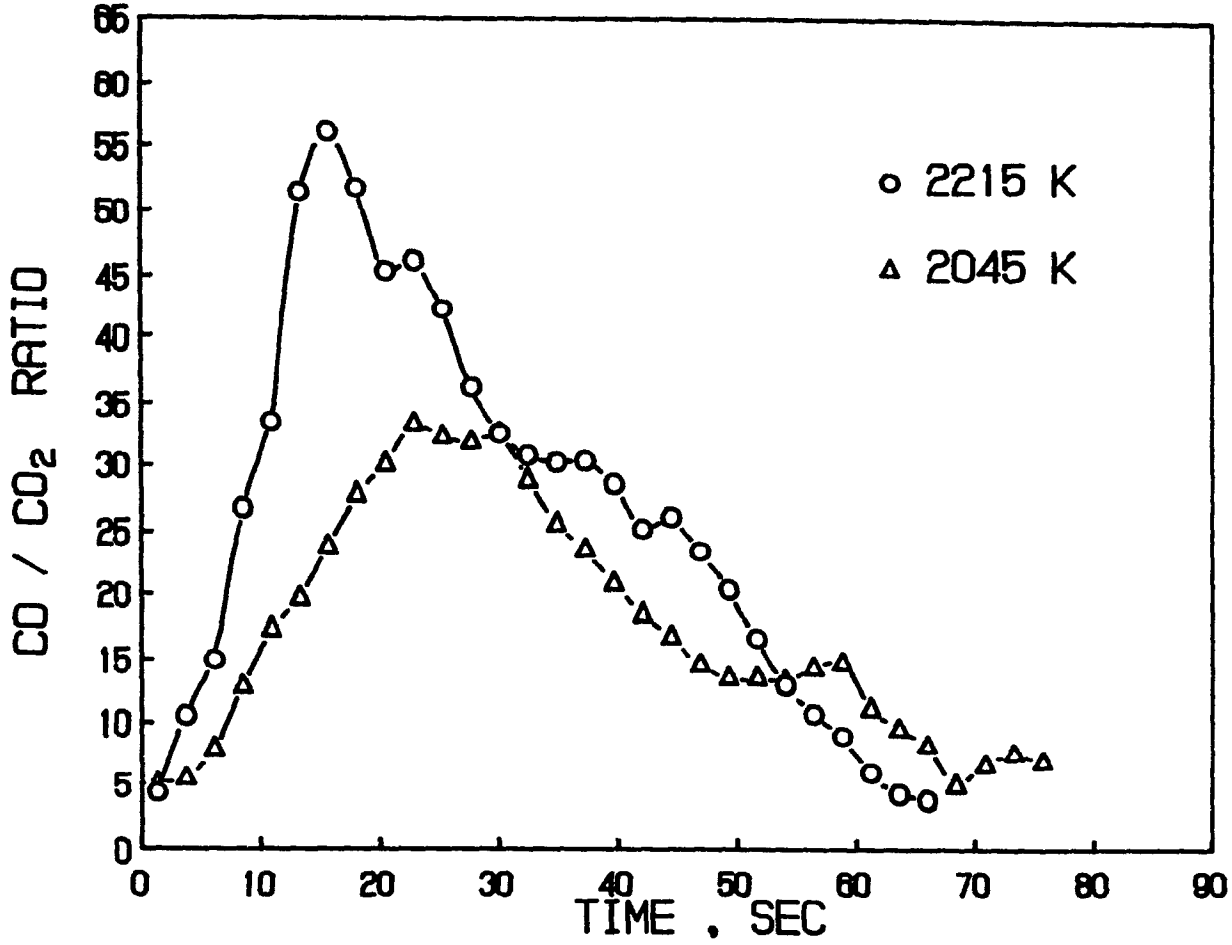

Figure 7.4 The Effect of Temperature on CO/CO_2 Ratio Versus Reaction Time for the Carbothermic Reduction of Nb_2O_5 ($dp\ Nb_2O_5$ = 10 μm) in the Presence of Iron : d_pC = <45 μm, d_p Fe = <45 μm, 17.6 wt. % C, 26.7 wt. % Fe, pellet dia. = 12.9 mm, pellet ht. = 16.7 mm

possibility that the reduction reaction might have occurred via the gaseous intermediates CO and CO_2, but is inconclusive.

7.6 Conversion-Time Relationship

The experimental rate data for two different graphite particle sizes were plotted according to several rate expressions which were previously discussed and presented in Chapter II. These equations were (a) diffusion controlling - Equations (2.13), (2.15), (2.19), and (2.20); (b) chemical reaction controlling - Equation (2.23), and (c) nucleation/logarithmic growth - Equations (2.29), and (2.31). Although the equations listed in (a) and (b) statistically fitted the conversion-time data as well as the equations of (c), they were rejected as appropriate models because their predicted dependencies of reaction rate on particle size were not observed. The choice of the current model as the most appropriate one will be justified in the following sections.

The examination of the reacted pellets led to the conclusion that the carbothermic reduction of niobium pentoxide particles takes place between the dissolved carbon in iron and/or randomly throughout the pellet at contact points between the carbon and the solid and/or liquid niobium pentoxide, at the interparticle level. The overall reduction of niobium pentoxide with time, under chemical-reaction control, has been represented by the logarithmic expression given by Equation (4.20) developed earlier.

The applicability of Equation (4.20) was further tested by

increasing the graphite particle diameter from 100 % less than 45 to 463 microns. The graphite and iron concentrations were kept constant at 17.6 (C/Nb_2O_5 (mole) = 7) and 26.7 wt. %, respectively, and the niobium pentoxide and iron particle diameters were also kept constant at 10 and <45 microns, respectively. The typical experimental conversion-time data at two different temperatures for pellets made with graphite and niobium pentoxide particle diameters of 100 % less than 45 and 10 microns, respectively, are given in Figure 7.5. The plots again show a relatively small induction period, which decreases with increasing temperature. The delay is between 5 to 10 seconds.

First order estimates for the time required for heating and melting of the oxide and iron at a reaction temperature of 2000 K, assuming a plasma energy efficiency of 30 %, was between 10 and 21 seconds for low (26.7 wt. %) and high (71.8 wt. %) initial iron concentrations, respectively. It is seen that, if the induction period is subtracted, the plot of $-\ln(1-x)$ versus time is linear as expected, but only to a certain conversion level beyond which the rate of conversion is less than the model predictions. The fractional conversion at which the deviation from the logarithmic model occurs, increases with increasing temperature. For the reaction conditions of Figure 7.5 and a temperature of 2125 K, the deviation starts at a conversion of 85 %. At a higher pellet temperature, 2215 K, it takes place at 88 % conversion. Similar results were obtained for pellets made with larger graphite particle diameter (463 microns).

The influence of higher initial iron concentration on the

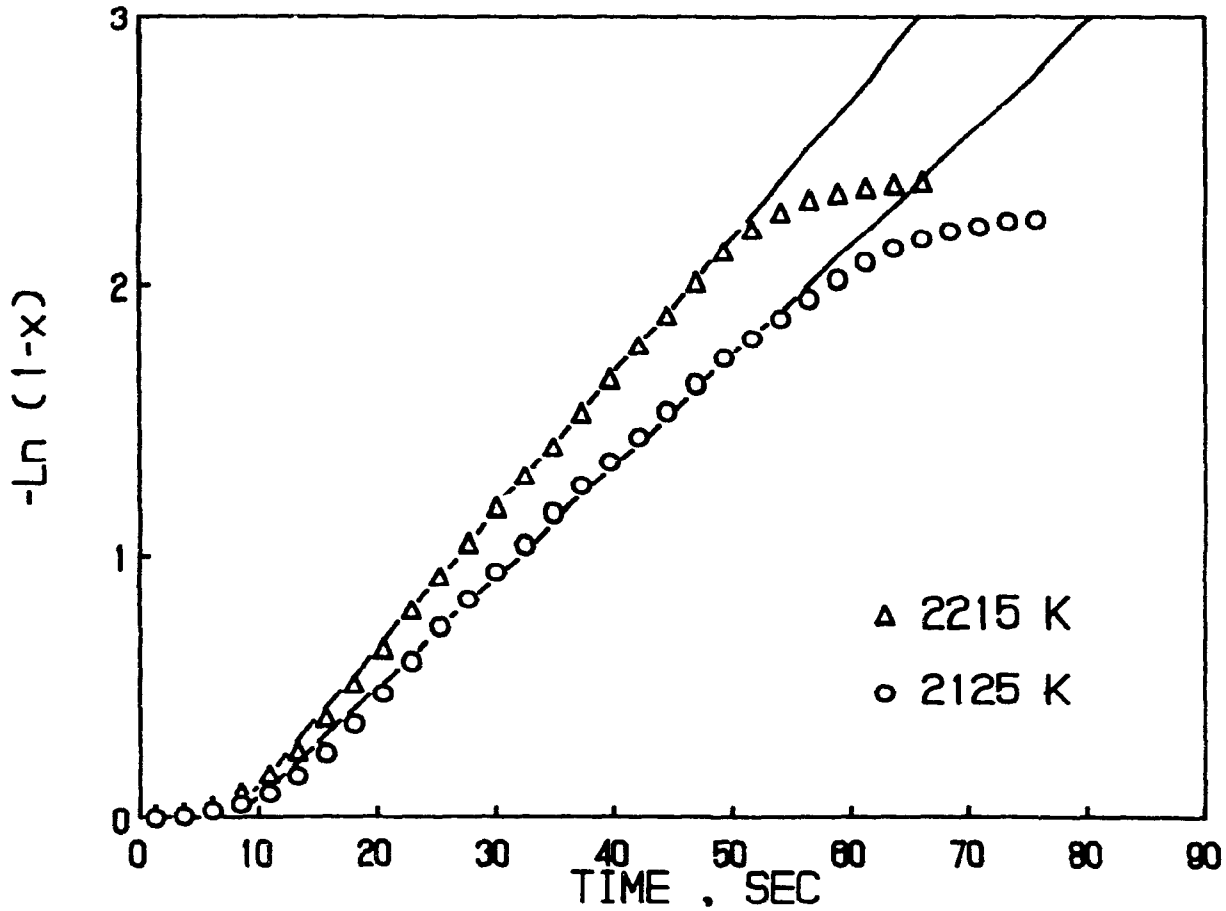

Figure 7.5 The Effect of Temperature on Conversion Using the Kinetic Model for the Carbothermic Reduction of Nb_2O_5 (d_p Nb_2O_5 = 10 μm) in the Presence of Iron : d_pC = <45 μm, d_p Fe = <45 μm, 17.6 wt. % C, 26.7 wt. % Fe, pellet dia. = 12.9 mm, pellet ht. = 16.7 mm

conversion-time relationship was also investigated. Figure 7.6 shows the typical conversion-time data for pellets with initial iron concentration of 71.8 wt. % at temperatures of 1680 and 1845 K, respectively. In another series of experiments, the C/Nb_2O_5 was increased from 7 to 10 and 14. The resulting initial iron concentration were 68.9 and 66.6 wt. %., respectively. Figure 7.7 shows typical conversion-time data for pellets containing initial iron concentration of 68.9 wt. % (C/Nb_2O_5 (mole) = 10) at temperatures of 1995 and 2125 K, respectively. Although the conditions are not exactly alike, the results are similar to those for lower initial iron concentration. They show that the fractional level of conversion at which deviation from the model occurs increases with temperature.

Again, the difference in the conversion levels at which deviation from the model occurs can be attributed to the effects of a heat transfer limitation which leads to a non-isothermal pellet rather than a change in rate controlling mechanism. Another contributing factor is the improved mobility of and the degree of contact between the reductants as the iron melts. This results in a higher conversion level before deviation from the model occurs.

If there was a change in the reaction mechanism, one would expect the deviation from kinetic to diffusion control to occur at lower conversion levels as the temperature increases. In the present case, the opposite effect is observed. These observations support using only the linear portion of the $-\ln(1-x)$ versus time data to calculate the overall reaction rate constant, since it is

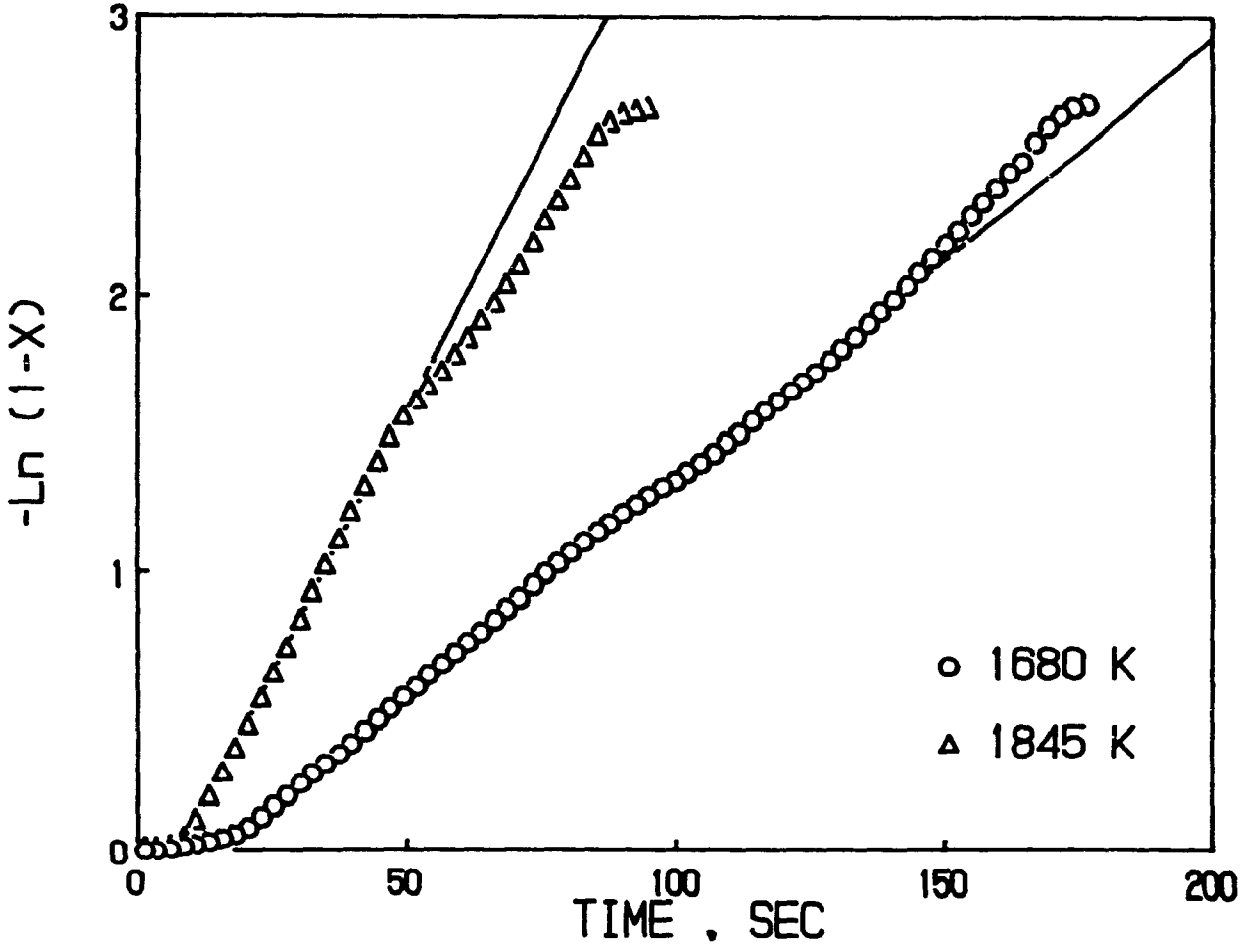

Figure 7.6 The Effect of Temperature on Conversion Using the Kinetic Model for the Carbothermic Reduction of Nb_2O_5 (d_p Nb_2O_5 = 10 μm) in the Presence of Iron : d_pC = <45 μm, d_p Fe = <45 μm, 6.7 wt. % C, 71.8 wt. % Fe, pellet dia. = 18.5 mm, pellet ht. = 14.3 mm

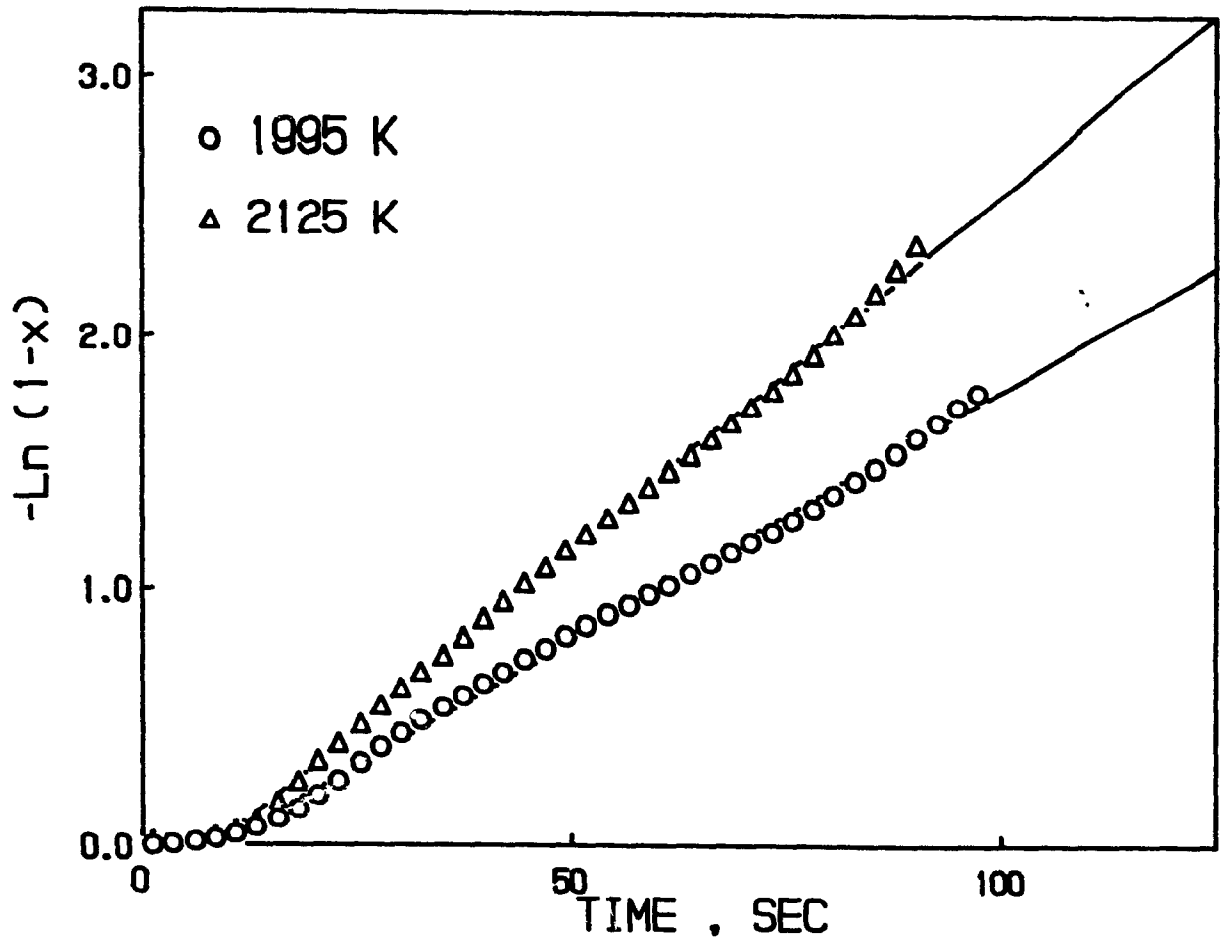

Figure 7.7 The Effect of Temperature on Conversion Using the Kinetic Model for the Carbothermic Reduction of Nb_2O_5 (d_p Nb_2O_5 = 10 μm) in the Presence of Iron : d_pC = <45 μm, d_p Fe = <45 μm, 9.5 wt. % C, 68.9 wt. % Fe, pellet dia. = 18.5 mm, pellet ht. = 14.0 mm

the temperature of the upper section of the pellet which was measured and reported.

7.7 Influence of Particle Diameter

Although there is some dissolution of the carbon in iron, the amount of iron added was never sufficient to completely dissolve all the carbon in the pellet for the respective series of experiments. The overall rate constant, K, as defined by Equation (4.17) was not expected to be influenced by the change in particle diameter. Accordingly, an Arrhenius plot of the rate constants of different particle diameters is expected to yield a single straight line, if ash diffusion is not contributing. Otherwise, the overall rate constant would decrease with increasing particle diameter due to a corresponding increase in the diffusion resistance.

The overall rate constants corresponding to the linear portion of -ln(1-X)-versus-time data were plotted according to an Arrhenius-type relationship in Figure 7.8 for pellets having different graphite particle diameters of 100 % less than 45 and 463 microns. The C/Nb_2O_5 mole ratio and the initial iron concentration in the pellet were 7 and 26.7 wt. %, respectively. The results of the treated experimental data for each of these cases are presented in Tables IV-A and IV-B of Appendix IV. The data of Figure 7.8 show that with pellets which were made with graphite particle diameters of 100 % less than 45 and 463 microns, there is a slight dependence of the overall rate constant on graphite particle size. The dependence is not large enough to justify the

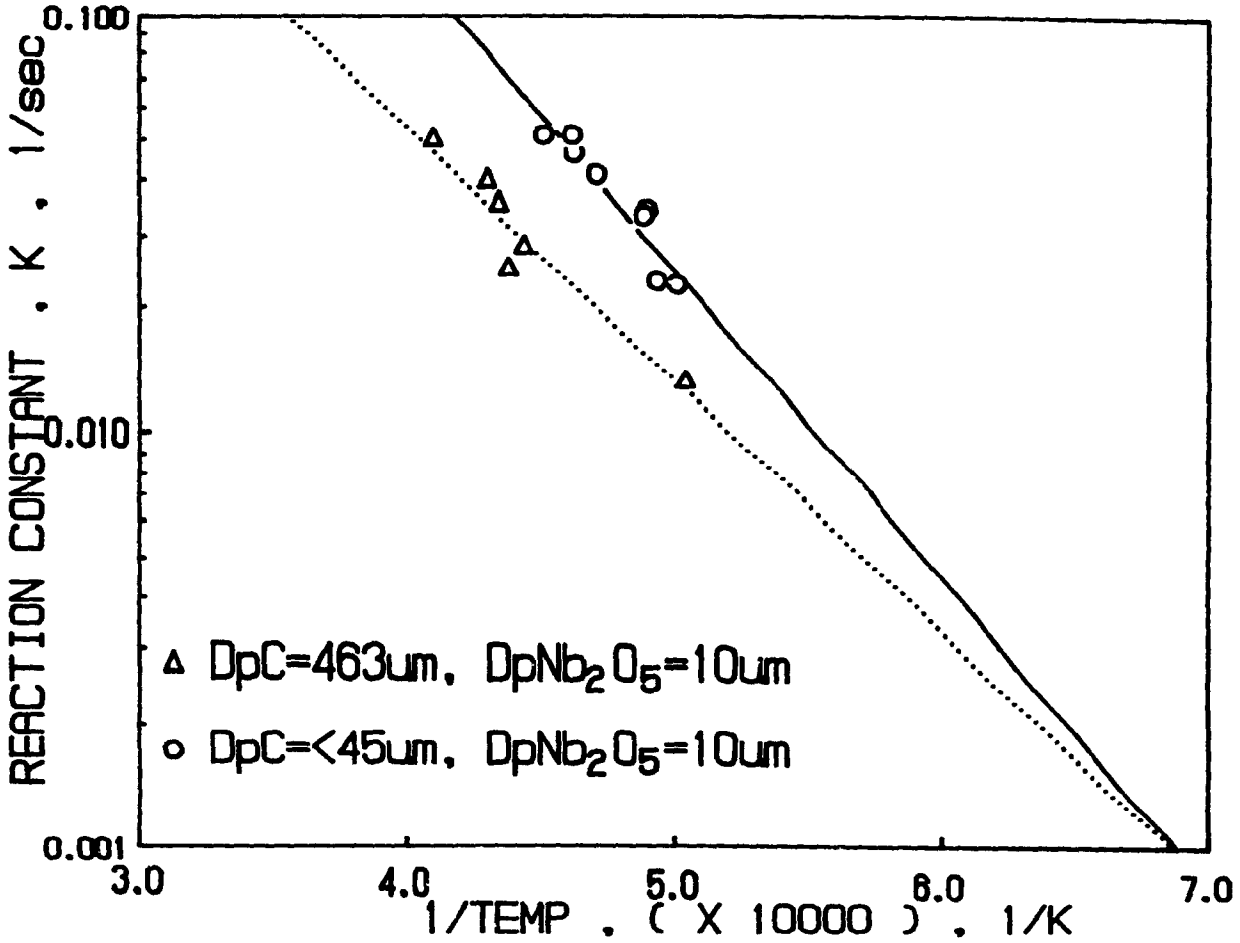

Figure 7.8 Arrhenius Plot for the Carbothermic Reduction of Nb_2O_5 for Different Graphite Particle Size in the Presence of Iron : d_p Nb_2O_5 = 10 μm, d_p C = <45, and 463 μm, d_p Fe = <45 μm, 17.6 wt. % C, 26.7 wt. % Fe, pellet dia. = 12.9 mm, pellet ht. = 16.7 mm

use of the other rate expressions. For instance, at a temperature of 2000 K, the ratio of the overall reaction rate constants corresponding to a graphite particle diameter ratio of 1:10.3 (<45 microns:463 microns) is only 1.7:1. If the reaction or diffusion controlled model was the appropriate one, the overall rate constants should be inversely proportional to the particle radius or the square of particle radius, respectively. That is, for a reaction or diffusion controlled model, the predicted ratios of the overall rate constants should be 10:1 or 100:1, respectively. The small dependence might have been due to the larger relative surface area which is available for better contact and reaction with the oxide for the graphite that was undissolved in the iron. Also it might be due to some diffusional effects, especially at the higher temperatures. It would appear that, as a first approximation, the overall rate constant is independent of graphite particle size and Equation (4.17) adequately represents the overall rate constant.

7.8 Influence of Temperature

The influence of temperature on the reaction rate for pellets made with different graphite particle diameters, and different initial graphite and iron concentrations was measured from 1575 to 2440 K. The choice of the temperature levels was dictated solely by the currents under which the arc was stable.

The Arrhenius plot of Figure 7.8 examines the effect of reaction temperature at a constant C/Nb_2O_5 mole ratio of 7 and an initial iron concentration of 26.7 wt. %. Two different graphite

particle diameters were used as shown. For graphite particle diameter of 100 % less than 45 microns and niobium pentoxide of 10 microns, the activation energy and 95 % confidence limit are 141.770 ± 51.313 kJ/mole with a correlation coefficient of 0.884. For graphite particle diameter of 463 microns and niobium pentoxide of 10 microns, the activation energy and 95 % confidence limit are 116.000 ± 46.336 kJ/mole with a correlation coefficient of 0.923. The solid and the dotted lines in Figure 7.8 are the resulting respective regression lines. If it is agreed that the reaction rate was independent of particle size, the average activation energy and the standard deviation for the carbothermic reduction of niobium pentoxide were 128.883 and 18.220 kJ/mole, respectively.

The Arrhenius plot in Figure 7.9 is for four sets of experiments. Three sets of data are for experiments for pellets which were made with C/Nb_2O_5 mole ratio of 7 and 10 and constant graphite and niobium pentoxide particle diameters of 100 % less than 45 and 10 microns, respectively. The data for the fourth set of experiment (represented by the open circle symbols) are for the reaction with pellets containing initial iron concentration of 26.7 wt. % iron and C/Nb_2O_5 mole ratio of 7 are reproduced for comparison. In the first set of experiment, the initial iron concentration was increased from 26.7 to 71.8 wt. %, and the C/Nb_2O_5 mole ratio was 7. The least squares fit of the data (represented by the star shaped symbols) gave an activation energy and 95 % confidence limit of 179.742 ± 55.453 kJ/mole, with a correlation coefficient of 0.856. The dashed straight line through this set

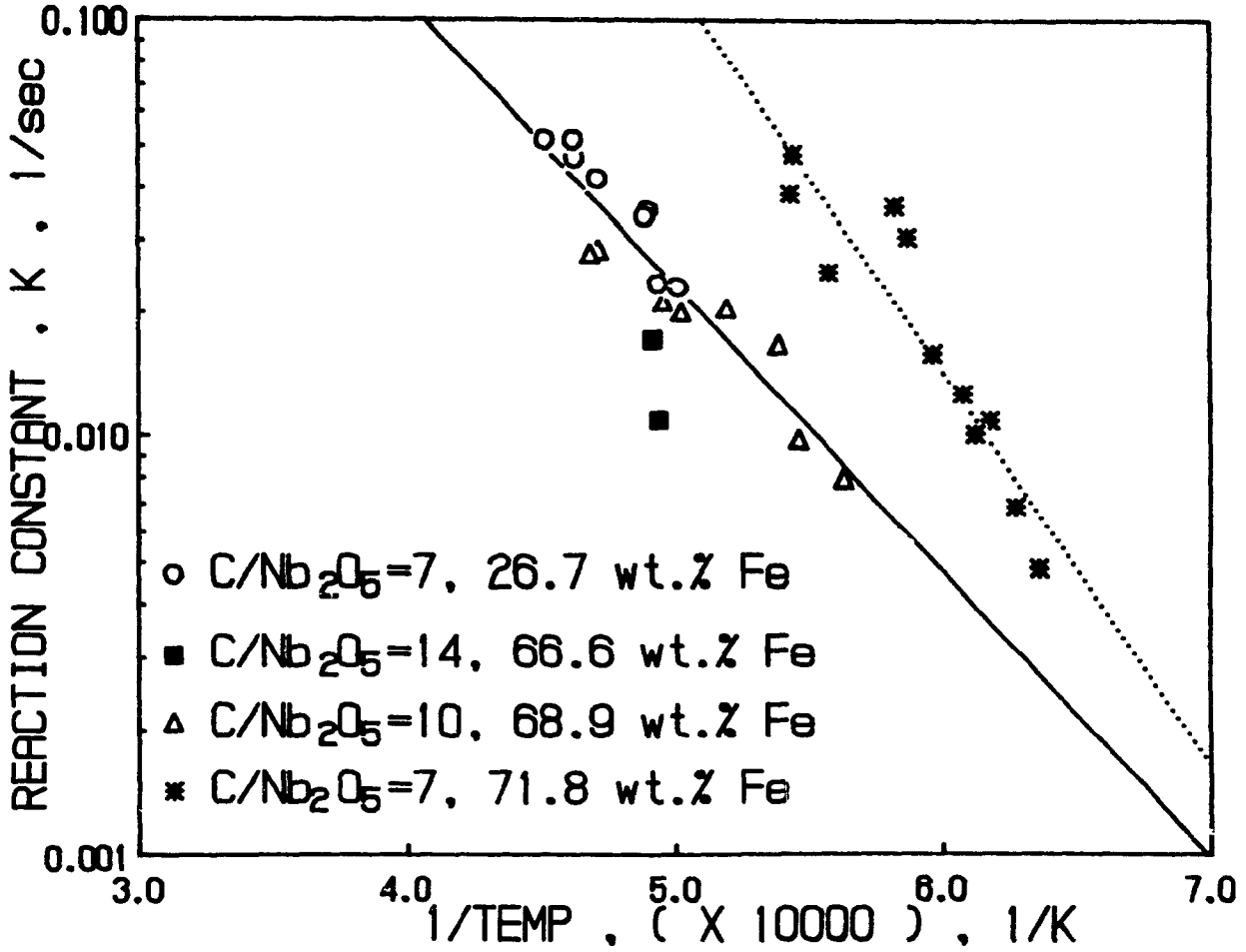

Figure 7.9 Arrhenius Plot for the Carbothermic Reduction of Nb_2O_5 for Different Initial Carbon and Iron Concentrations : d_p Nb_2O_5 = 10 μm, d_p C = <45 μm, d_p Fe = <45 μm, pellet dia. = 12.8 - 18.5 mm, pellet ht. = 14.3 - 20.6 mm

of data in Figure 7.9 is the resulting regression line. In the second set of experiments, the initial iron concentration was increased to 68.9 wt. % and the C/Nb_2O_5 mole ratio was 10. The least squares fit of the data (represented by the open triangles) gave an activation energy and 95 % confidence limit of 102.626 ± 38.642 kJ/mole, with a correlation coefficient of 0.875. The third set is for a couple of experiments which were performed with pellets containing C/Nb_2O_5 mole ratio of 14 and initial iron concentration of 66.6 wt. % and the data (represented by the filled squares) are also presented in Figure 7.9. The treated data are presented in Table IV-E of Appendix IV. From Figure 7.9, it can be seen that there is no difference in the reaction rates between pellets with C/Nb_2O_5 mole ratio of 7, 10 and 14 containing corresponding initial iron concentrations of 26.7, 68.9 and 66.6 wt. %. The reaction rate for pellets containing an initial iron concentration of 71.8 wt. % is the highest of the four sets of data presented in Figure 7.9 and will be discussed in the following section. The least squares fit for the data from the second and third sets of experiments gave an activation energy and 95 % confidence interval of 131.742 ± 12.738 kJ/mole, with a correlation coefficient of 0.884. The solid straight line through the data is the resulting regression line.

The average activation energy for all the data of Figures 7.8 and 7.9 was calculated to be 135.034 kJ/mole with a standard deviation of 33.945 kJ/mole.

7.9 Influence of Fe/C RATIO

The analysis of the kinetic data with respect to the initial iron/carbon (Fe/C) weight ratio was based on the graphite and iron content of the individual pellets. The experimental runs covered graphite and iron concentration ranges from 6.7 to 17.6 wt. % and 26.7 to 71.8 wt. %., respectively. The resulting Fe/C weight ratios were 1.5, 5.2, 7.3 and 10.7. The treated data are summarized in Tables IV-A to IV-E, inclusive, of Appendix IV. The initial graphite concentration was equal to or more than the amount required by the reaction stoichiometry to produce NbC. It was also always greater than the carbon solubility limit in iron at the respective reaction temperatures. As in the previous cases, only those data corresponding to the linear portion of the time-conversion expression (Equation 4.20) were considered.

The previously obtained overall activation energy value, the overall rate constants, and their corresponding temperatures were used to calculate respective values for the pre-exponential constant, A, as defined by the Arrhenius equation:

$$A = K/\exp(-E/RT) \qquad (7.1)$$

where K is the overall rate constant, E is the overall activation energy, and T is the pellet temperature. The calculated values for A were then plotted against the pellet Fe/C weight ratio and are shown in Figure 7.10. Using the one-tailed student t-test, it was shown that the average values of A were not statistically different for average Fe/C weight ratio of 1.5, 5.2 and 7.2

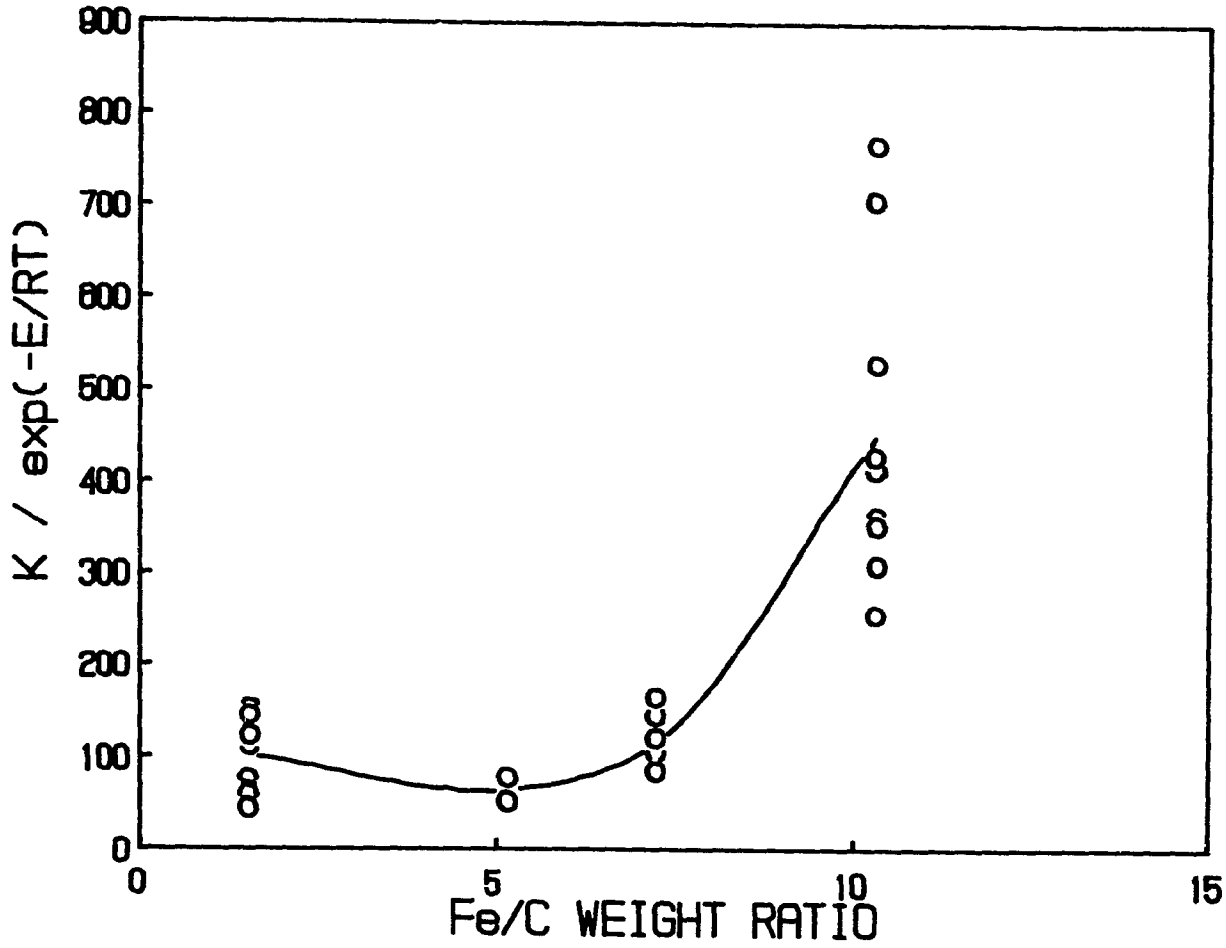

Figure 7.10 The Effect of Iron/Carbon Weight Ratio on Reaction Rate

respectively, at a 0.01 level of significance. For the higher average Fe/C weight ratios of 7.2 and 10.7, the values of A were statistically different.

Figure 7.10 shows that the rate of reduction is constant for Fe/C weight ratios between 1.5 to 7.2, but appears to increase for Fe/C weight ratio values above 7.2. This may be due to the improved contact between the graphite and niobium pentoxide attributed to the increasing amount of graphite available as dissolved carbon in iron. Caution should be exercised in increasing the Fe/C weight ratio, since too much iron would dilute the carbon in iron and result in a decrease in the reaction rate.

A comparison of the reaction constants for the carbothermic reduction of niobium pentoxide with increased initial carbon concentration and iron addition is shown in Table 7.3. The reaction constants were computed at 2000 K. The results show that large iron additions (> 26.7 wt. %) gave an increase in the reaction rate which was about three times greater than the effect of increased initial graphite concentration without iron additions. There was no difference in the reaction rates for reactions with and without iron additions less than 26.7 wt. %. The initial iron concentrations of 26.7 and 71.8 wt. % are equivalent to the Nb/Fe weight ratios for industrially produced ferroniobium and for a pourable Fe-NbC plasma produced ferroalloy, respectively.

7.10 CONCLUSION

1- The kinetics of the carbothermic reduction of niobium pentoxide in the presence of iron were studied in the

Table 7.3 Comparison of Reaction Constants for Carbothermic Reduction of Niobium Pentoxide With and Without Iron Addition at 2000 K

REACTION CONSTANT sec^{-1}	C/Nb_2O_5 (mole)	wt.% Fe	Fe/C (weight)
0.0187	7	0.0	0.0
0.0431	10	0.0	0.0
0.0204	7	26.7	1.5
0.1232	7	71.8	10.7

temperature range 1575 to 2440 K in an argon transferred-arc plasma. Influences of time, temperature, carbon and iron concentrations and graphite particle size in the pellet on the rate were determined experimentally, using single stationary pellets composed of niobium pentoxide, graphite and iron particles.

2- The microscopic examination of partially reacted pellets indicated that the reaction took place in a mollified or liquid state depending on the initial iron concentration and the reaction temperature of the pellet.

3- The overall reduction of niobium pentoxide in the presence of iron with time under chemical reaction control was represented by a logarithmic expression (Equation 4.20) based on the volumetric reaction model. Deviations from the model were observed to be less at high conversions and were attributed to unavoidable non-isothermal effects.

4- The Arrhenius plots of the experimental data indicated that the overall rate was essentially independent of graphite particle size, but was dependent on the Fe/C weight ratio. The reaction was chemical reaction controlled. The average activation energy was calculated to be 142.5 kJ/mole with a standard deviation of 33.2 kJ/mole.

5- Experimental data indicated a significant increase in the reaction rate with high initial iron concentrations. This is attributed to the reduction reaction taking place between the dissolved carbon in the iron and the niobium pentoxide.

CHAPTER VIII

CARBOTHERMIC REDUCTION OF PYROCHLORE IN THE PRESENCE OF IRON : EXPERIMENTAL RESULTS AND DISCUSSION

8.1 Introduction

Experiments were performed to study the time-conversion relationship, and the effect of pyrochlore and graphite particle sizes, iron and graphite concentrations and temperature on the rate for the carbothermic reduction of pyrochlore in the presence of iron. Specifically, it is the reduction of the niobium pentoxide contained in pyrochlore. In one series of experiments, the Nb/Fe weight ratio in the pellet was varied between 0.20 and 3.88 and the C/Nb_2O_5 mole ratio was kept constant at 7. The resulting initial iron and carbon concentrations in the pellet were between 64.0 and 8.4 wt. % and between 5.8 and 14.8 wt. %, respectively. In another set of experiments, the C/Nb_2O_5 mole ratio was increased to 14 and the Nb/Fe weight ratio was kept constant at 0.20. The resulting initial iron and carbon concentrations in the pellet were 58.9 and 11.4 wt. %, respectively. The pellet diameter was 12.9 mm and heights were between 16.9 and 19.8 mm, except in the case of high initial iron concentration, when it was 18.5 mm. (see Appendix I). A few runs were carried out with pellets of a smaller diameter (12.9 mm.) containing high initial iron concentration (58.9 wt. %) to determine any change in mechanism with pellet size. The graphite particle diameters used in the experiments were 100 % less than 45 (or <45) and 463 microns, the pyrochlore particle diameters were 60 and 230 microns and the

iron particle diameter was kept constant at 100 % less than 45 (or <45) microns. The C/Nb_2O_5 mole ratio for the reaction stoichiometry to produce NbC is 7 (Equation (4.8)), with the assumption that the remaining oxides in the pyrochlore are not reduced. The conversion equivalent to the complete reduction of the oxygen in the niobium pentoxide only in the pyrochlore to produce carbon monoxide (and carbon dioxide) is 0.67. The Nb/Fe weight ratio for commercial grade ferroniobium is about 1.5.

8.2 Microscopic Examinations

The reaction of the pellets containing initial iron concentration greater than 8.4 wt. % was observed to have taken place in a mollified state. Within a short period (about 5 seconds) after the plasma is started, the entire top of the pellet is melted. Although the average shape of the reacting pellet was still cylindrical, the top surface was in constant motion as bubbles of carbon monoxide (and carbon dioxide) rose to the surface and burst. Occasionally, some tiny droplets of liquid were ejected from the surface. These observations were more exaggerated at high pellet temperature. When the pellet had reacted for the desired length of time the plasma was extinguished; at this point the pellet collapsed into a distorted cylinder and froze, usually in less than one second after shutdown. The behaviour was similar to the reaction of niobium pentoxide and carbon in the presence of iron as discussed in the previous section.

The surface of an unreacted pellet was smooth and relatively non-porous. A partially reacted pellet exhibited a very porous

but hard surface as seen in Figure 8.1, where the initial iron concentrations were 19.8 and 64.0 wt. % and the C/Nb_2O_5 mole ratio was kept constant at 7, for Figure 8.1(a) and 8.1(b), respectively. The arc struck the top of the pellet and thus the temperature (and hence the rate of reaction) was the highest here. This also contributed to the melting and coalescing of the product. Examination of partially reacted pellets showed the presence of unreacted pyrochlore in larger concentration in the bottom half than in the top.

Because the reduction reaction left the pellet very hard, the specimens examined by scanning electron microscopy were obtained by fracturing the sample. A scanning electron micrograph of the typical reaction product with initial iron and carbon concentrations of 64.0 and 5.8 wt. %, respectively, is shown in Figure 8.2. EDX (energy dispersed x-ray spectrometer) analysis identified the white areas as iron-niobium rich, i.e. either a niobium oxide and/or NbC and iron matrix, which would be assumed to be the desired ferroniobium and/or ferro-niobium carbide product. The grey areas were rich in silicon, calcium and titanium and probably constitute the slag material. The complete separation of metal product from the slag was not possible with the present experimental set-up, since the proximity of the plasma flame to the reacting pellet promoted mixing. Also, the pellets were relatively small and complete melting was not desired or frequently achieved. The successful separation of metal and slag for the same reaction has been reported by Hilborn (1988) in the more appropriate Plasmacan reactor.

(a)

(b)

Figure 8.1 Photographs of Partially Reacted Pellets
(d_p Pyrochlore = 60 μm, d_pC = <45 μm, d_p Fe = <45 μm)
(a) 1765 K, x = 0.71, 13.0 wt. % C, 19.8 wt. % Fe,
pellet dia. = 12.9 mm, pellet ht. = 18.8 mm,
(b) 1495 K, x = 0.45, 5.8 wt. % C, 64.0 wt. % Fe,
pellet dia. = 18.5 mm, pellet ht. = 17.0 mm.

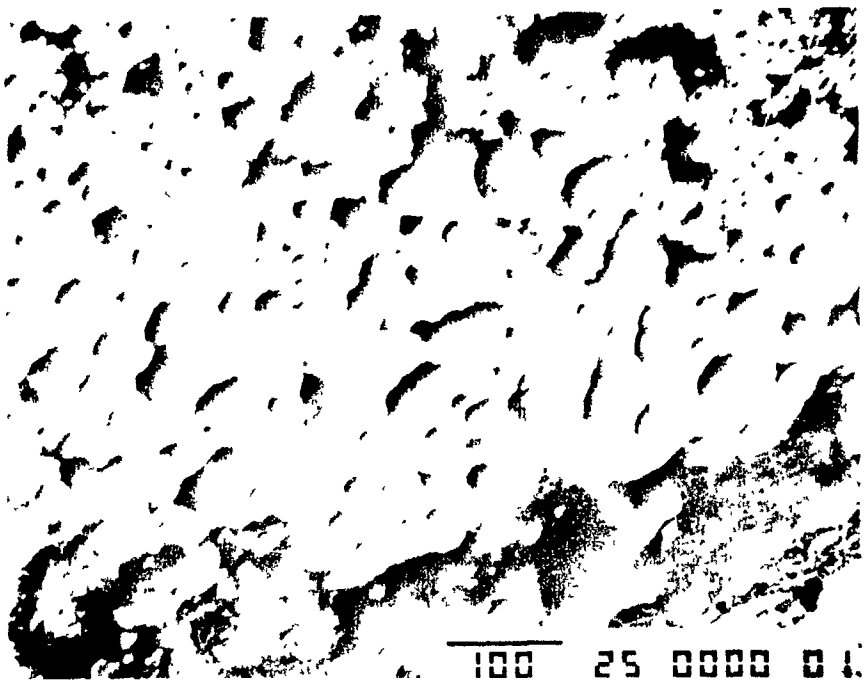

Figure 8.2 Scanning Electron Micrographs (With Back Scatter) of a Partially Reacted Pellet :
d_p Pyrochlore = 60 μm, d_p Fe = <45 μm, d_pC = <45,
X150, 1640 k, 5.8 wt. % C, 64.0 wt. % Fe,
pellet dia. = 18.5 mm, pellet ht. = 17.0 mm,

The melting points of Niobec's pyrochlore, iron and niobium carbide are about 1535, 1785 and 3875 K, respectively. The solubility of the NbC product in iron will be a function of the temperature and the iron concentration in the pellet. If there is insufficient iron for complete dissolution of the niobium carbide produced, the rest will precipitate from solution. The solid NbC would form either as an ash layer around the microscopic graphite and/or oxide particles or be dispersed randomly at the reaction (contact) points between the microscopic graphite and oxide particles. If the existence of gaseous intermediates (CO and CO_2) were major contributors to the progress of the reduction reaction, it would be expected that melting would hinder the reduction process because of the reduced porosity of the particle. Diffusion resistance through the product ash layer would also become apparent at relatively high temperatures. The role of iron in the reaction is most probably to improve contact between the carbon and the solid and/or liquid oxide particles. The reduction reaction takes place between the dissolved carbon in the iron and the oxide in the liquid state (Hilborn, 1988). Carbon dissolves readily in iron and it is probable that the iron will be saturated in carbon. Its concentration will be of the order of 4 to 6 wt. % for the temperature range 1430 to 2120 K (Chipman et. al., 1952). The amount of improvement in the reaction rate is dependent on the iron concentration. If there is insufficient dissolved carbon, further reduction will proceed by reaction with solid carbon and again the degree of contact between carbon and oxide becomes important. Diffusion limitations of the dissolved

carbon across the iron-oxide interface would also become apparent at relatively high temperatures. The foregoing discussion was supported by the experimental data for the influence of iron concentration and pyrochlore and graphite particle sizes on the reaction rate which are presented in later sections.

8.3 X-ray Analysis

As in the previous cases, a number of reacted pellets were selected for x-ray powder diffraction (XRD) analysis. The results of all these analyses are summarized in Table 8.1. The XRD analysis results showed that in the case where the initial carbon and iron concentrations were 14.8 and 8.4 wt. %, respectively with an average conversion of 0.72, the major and minor phases identified in the product were NbC and latrappite, respectively. Iron was not detected probably because its concentration was close to or less than the detection limit (about 5 wt. %) of the instrument. For the case when the initial iron concentration was increased to 19.7 wt. %, giving an initial carbon concentration of 13.0 wt. %, the major phase was identified as NbC. Latrappite, pyrochlore and iron were the minor phases. The average conversion for this sample was 0.75. The results indicate that there might have been some reduction of oxides other than niobium pentoxide, since reduction of the latter is equivalent to a conversion of 0.67 and traces of pyrochlore were still present in the product. When the initial iron concentration was increased further to 64.0 wt. %, giving an initial carbon concentration of 5.8 wt. %, the major phases were identified as NbC, pyrochlore and latrappite. The

Table 8.1 XRD Analysis of Products for the Carbothermic Reduction of Pyrochlore in the Presence of Iron

Wt.% IRON [1]	COMPOUNDS	
	Major Phases	Minor Phases
8.4	NbC	Latrappite
19.8	NbC	Latrapitte, Pyrochlore, Fe
64.0	NbC, Latrappite, Pyrochlore	Fe, C
58.9	NbC, Fe, Pyrochlore	Latrapitte, C
Sample from reactor walls[2]	Fe, compound of Nb	Latrapitte

1 - C/Nb_2O_5 mole ratio = 7.
2 - initial iron conc. of reacted pellet = 58.9 wt%.

minor phases were identified as iron and graphite. The average conversion for this sample was 0.65. The C/Nb_2O_5 ratio for all the cases presented above was 7. When the ratio was increased to 14, giving initial carbon and iron concentrations of 11.45 and 58.9 wt. %, respectively, the major phases identified were iron, NbC, and pyrochlore. Latrappite and graphite were identified as the minor phases. Analysis was also done on samples taken from the reactor walls. The major phases identified were iron and a niobium bearing compound. Latrappite was identified as the minor phase. These compounds probably reached the walls via vaporization of the reactants. These results were in agreement with those obtained by Hilborn (1988).

8.4 Mass Balance

Conversion was previously defined in Equation (3.4) the ratio of total oxygen in the carbon monoxide and carbon dioxide in the exhaust gas to the total initial oxygen in the oxide reactant(s). As for the previous cases, this method of measurement for conversion was checked for consistency by comparing the result to that calculated from the pellet's weight loss. The results, which are presented in Appendix V, indicate that there was fair agreement between the two methods. The fractional conversion by weight loss was consistently higher, but the difference was generally less than 0.20. The exceptions were for those cases when the pellet temperature was greater than 1955 K and the iron concentrations were highest (58.9 and 64.0 wt. %). These showed a difference of between 0.22 and 0.46, and were caused by

the evaporation and ejection of materials during the reaction. Very fine particles were subsequently entrained in the exhaust gas. Pellet size had no apparent effect on differences between the two methods of measuring conversion.

To identify what types of material were volatilized and ejected, approximate mass balances were done on the combined products from two sets of experiments under similar experimental conditions and conversions. The initial iron concentrations of the pellets were 19.8 and 64.0 wt. %, respectively and the C/Nb_2O_5 mole ratio was kept constant 7. The mass balances were based on the analyses for the thirteen most abundant elements present in the reactants. The elemental composition was measured by emission spectroscopy. The difference between the summation of the percentage elemental compositions and 100 % was all attributed to oxygen. The results are summarized in Tables 8.2 and 8.3. Since the elemental analysis did not include all the elements present in pyrochlore, the results by themselves are not considered very accurate. But if interpreted along with the XRD results previously presented for the sample taken from the reactor walls for experiments with initial iron concentration of 64.0 wt. % and C/Nb_2O_5 mole ratio of 7, they can give some useful information. They show that sodium, iron and probably some calcium are the main elements lost during the reaction. This further confirms the fact that iron losses also increase with increasing initial iron concentrations. It would be expected that fluorine would have also volatilized during the reaction. The calculated conversions based on the oxygen loss from the mass balance results were in

Table 8.2 Mass Balance for the Combined Products From Pellets With Initial Iron Concentration of 19.8 wt. %, (Experiment Numbers 167, 168 and 169)

Weight of pellets, before reaction - 20.50 grams
Weight of pellets, after reaction - 14.95 grams
Average conversion (based on exhaust gas analysis) - 0.75
Average conversion (based on O loss in mass balance) - 0.71
Average pellet temperature - 1940 K

	Before Reaction				After Reaction	
	pyrochlore		added	total		
Element	%	g	g	g	%	g
Fe	4.5	0.62	4.05	4.67	33.5	5.008
C	0.08	0.01	2.66	2.67	5.77	0.863
Al	0.005	0.001	-	0.001	0.005	0.001
Ca	8.06	1.111	-	1.111	5.26	0.786
K	0.36	0.049	-	0.049	0.08	0.012
Mg	0.44	0.061	-	0.061	0.33	0.049
Mn	0.30	0.041	-	0.041	0.06	0.009
Na	5.00	0.698	-	0.698	0.05	0.007
Nb	44.1	6.079	-	6.079	43.8	6.548
P	0.03	0.004	-	0.004	0.02	0.003
Sr	1.26	0.174	-	0.174	0.78	0.116
Ti	1.68	0.232	-	0.232	1.40	0.209
U	0.029	0.004	-	0.004	0.045	0.006
O + others (diff.)	33.89	4.709	-	4.709	9.00	1.345
TOTAL	100.0	13.785		20.49	100.0	14.962

Table 8.3 Mass Balance for the Combined Products From Pellets With Initial Iron Concentration of 64.0 wt. %, (Experiment Numbers 206 and 208)

Weight of pellets, before reaction - 29.68 grams
Weight of pellets, after reaction - 25.07 grams
Average conversion (based on exhaust gas analysis) - 0.66
Average conversion (based on O loss in mass balance) - 0.60
Average pellet temperature - 1755 K

	Before Reaction				After Reaction	
	pyrochlore		added	total		
Element	%	g	g	g	%	g
Fe	4.5	0.42	18.55	18.97	67.4	16.90
C	0.08	0.007	1.80	1.807	4.71	1.181
Al	0.005	0.00	-	0.00	0.005	0.001
Ca	8.06	0.752	-	0.752	3.78	0.948
K	0.36	0.033	-	0.033	0.11	0.027
Mg	0.44	0.041	-	0.041	0.14	0.035
Mn	0.30	0.028	-	0.028	0.30	0.075
Na	5.00	0.466	-	0.466	0.05	0.012
Nb	44.1	4.113	-	4.113	16.95	4.249
P	0.03	0.003	-	0.003	0.035	0.009
Sr	1.26	0.117	-	0.117	0.52	0.130
Ti	1.68	0.157	-	0.157	0.86	0.215
U	0.029	0.027	-	0.027	0.071	0.018
O + others (diff.)	33.89	3.161	-	3.161	5.07	1.271
TOTAL	100.0	9.326		29.68	100.0	25.068

good agreement with that calculated by the analysis for CO and CO_2 in the exhaust gas.

8.5 CO/CO_2 Ratio

Figure 8.3 shows the variation of CO and CO_2 concentrations with time that were typically obtained during the carbothermic reduction of pyrochlore in the presence of iron. Random samples were also taken from the exhaust gas and analyzed by gas chromatography; again carbon dioxide and carbon monoxide were the only gases detected.

A comparison of the CO/CO_2 ratio at two different temperatures, 1950 and 1795 K, using graphite and pyrochlore particle diameters of <45 and 60 microns, respectively, is shown in Figure 8.4. The average ratios for the rest of the experiments are summarized in Appendix V. Assuming complete gas equilibrium and that the reduction reaction had taken place via gaseous intermediates, the CO/CO_2 ratios at 1950 and 1795 K should be about 800 and 1000, respectively. Thus, the exhaust gas should essentially be all CO. From Figure 8.4., the highest values of CO/CO_2 were about 240 and 140, respectively, which are much less than expected. The scatter is due to taking the ratio of large and small numbers. As discussed in the previous sections, the presence of CO_2 in the exhaust gas does not necessarily confirm the reduction mechanism as occuring via the gaseous intermediates CO and CO_2. The CO_2 could be due to carbon deposition from the exhaust gas as it cools from the high temperatures in the plasma to slightly above room temperature (Turkdogan, 1980). This is

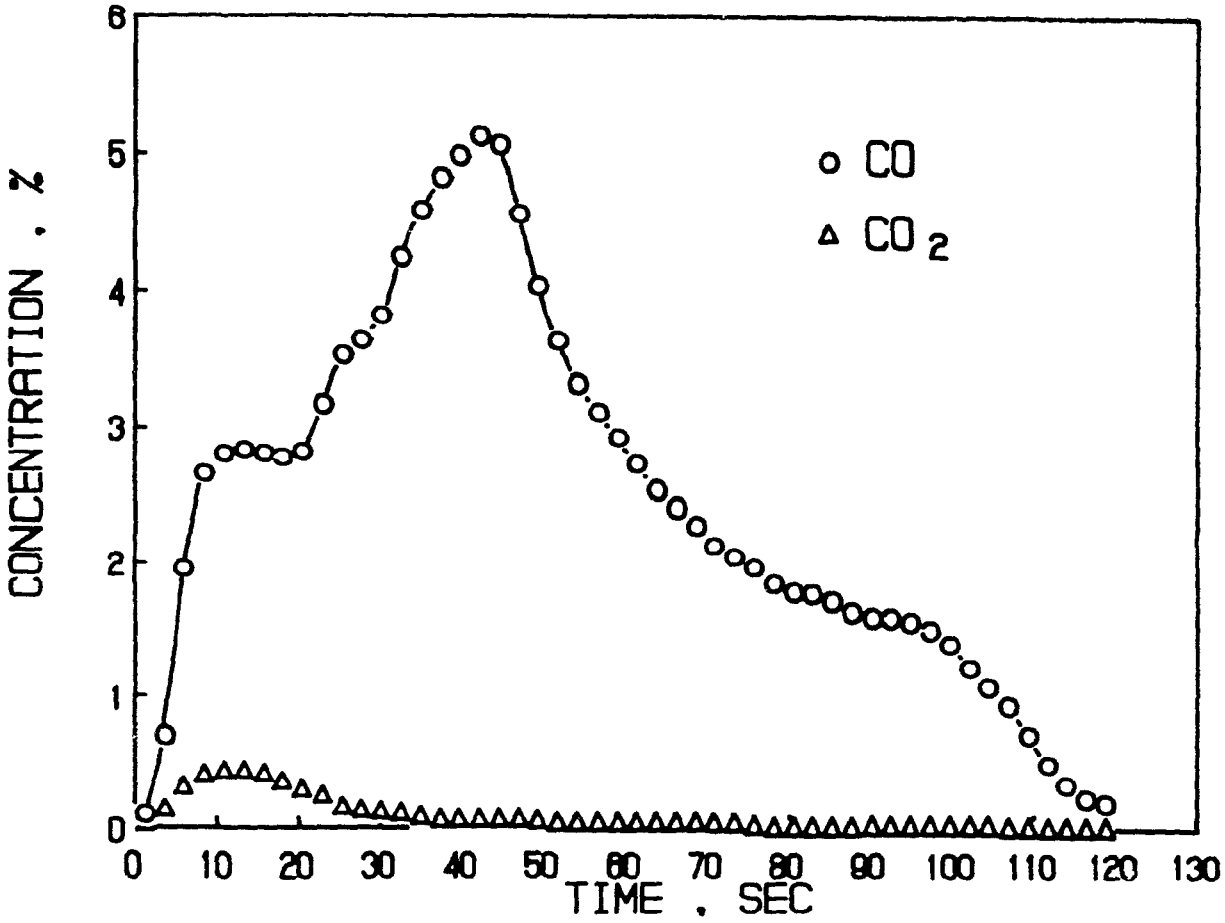

Figure 8.3 CO and CO_2 Concentration Versus Reaction Time for the Carbothermic Reduction of Pyrochlore (d_p Pyrochlore = 60 μm) in the Presence of Iron: d_pC = <45 μm, d_p Fe = <45 μm, 1795 K, 13.0 wt. % C, 19.8 wt. % Fe, pellet dia. = 12.8 mm, pellet ht. = 19.5 mm

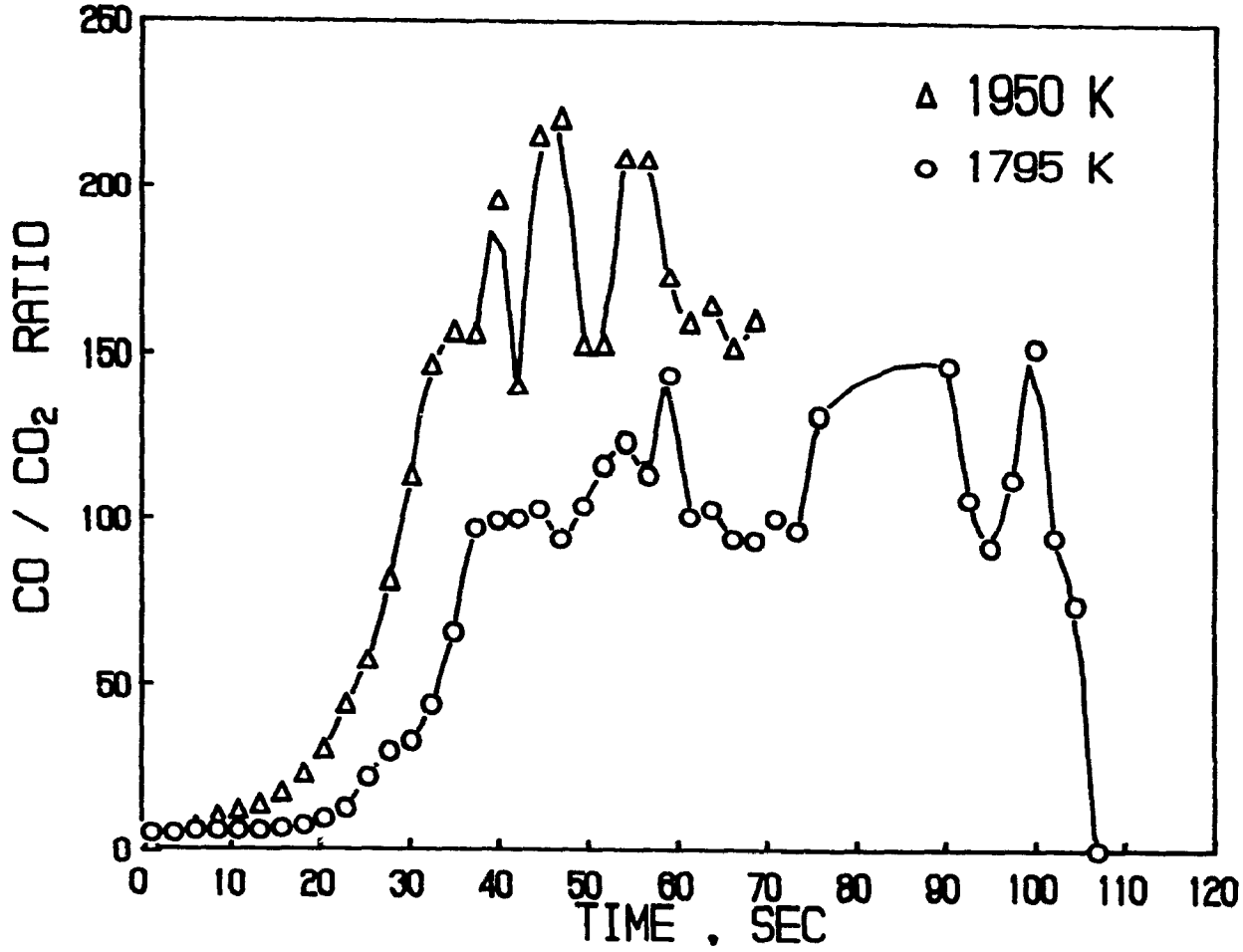

Figure 8.4 The Effect of Temperature on CO/CO_2 Ratio Versus Reaction Time for the Carbothermic Reduction of Pyrochlore (d_p Pyrochlore = 60 μm) in the Presence of Iron : $d_p C$ = <45 μm, d_p Fe = <45 μm, 13.0 wt. % C, 19.8 wt. % Fe, pellet dia. = 12.8 mm, pellet ht. = 19.6 mm

represented by the Equation (5.1). The temperature at which carbon deposition may start is below 1000 K, and this reaction is catalyzed by iron, cobalt and nickel (Turkdogan, 1980).

8.6 Conversion-Time Relationship

The examination of the reacted pellets led to the conclusion that the carbothermic reduction of pyrochlore particles takes place between the dissolved carbon in iron and/or randomly throughout the pellet at contact points between the carbon and the solid and/or liquid oxide, at the interparticle level. For reasons discussed before, the overall reduction of niobium pentoxide contained in pyrochlore with time, under chemical-reaction control, has been represented by the logarithmic expression given by Equation (4.20) developed earlier.

The applicability of Equation (4.20) was further tested by increasing the graphite and pyrochlore particle diameters from <45 to 463 microns and from 60 to 230 microns, respectively. The carbon and iron concentrations were kept constant at 13.0 (C/Nb_2O_5 (mole) = 7) and 19.8 wt. %, respectively and the iron particle diameter was also kept constant at <45 microns. The typical experimental conversion-time data at different temperatures for pellets made with graphite and pyrochlore particle diameters of 100 % less than 45 and 60 microns, respectively, are given in Figure 8.5. As before, the plots show that there is a relatively small induction period which decreases with increasing temperature. First order estimates for the time required for heating and melting of the oxide and iron at a reaction temperature of

1700 K, assuming a plasma energy efficiency of 30 %, was about 18 seconds. After the induction period, the plot of -ln(1-x) versus time is linear as expected, but only to a certain conversion level beyond which the rate of conversion is less than the model predictions. The fractional conversion at which the deviation from the logarithmic model occurs, increases with increasing temperature. At temperatures above 1800 K, practically all the niobium pentoxide contained in pyrochlore is reduced and deviation from the model does not occur before this. At this temperature the Fe-NbC forms a semi-solid product. For the reaction conditions of Figure 8.5 and a temperature of 1685 K, the deviation starts at a conversion of 55 %. At higher pellet temperatures (>1800 K), it takes place at 75 % conversion. This would suggest that there was reduction of some of the other oxides since the complete reduction of the contained niobium pentoxide in pyrochlore is 67 % conversion. Similar results were obtained for pellets made with combinations of larger graphite and pyrochlore particle diameters of 463 and 60 microns and 100 % less than 45 and 230 microns, respectively.

The influence of higher initial iron concentration on the conversion-time relationship was also investigated. Figure 8.6 shows the typical conversion-time data for pellets with initial iron concentration of 64.0 wt. % at temperatures of 1640 and 1780 K, respectively. In another series of experiments, the C/Nb_2O_5 was increased from 7 to 14. The resulting initial iron concentration was 58.9 wt. %. Figure 8.7 shows typical conversion-time data for pellets containing this initial iron concentration at

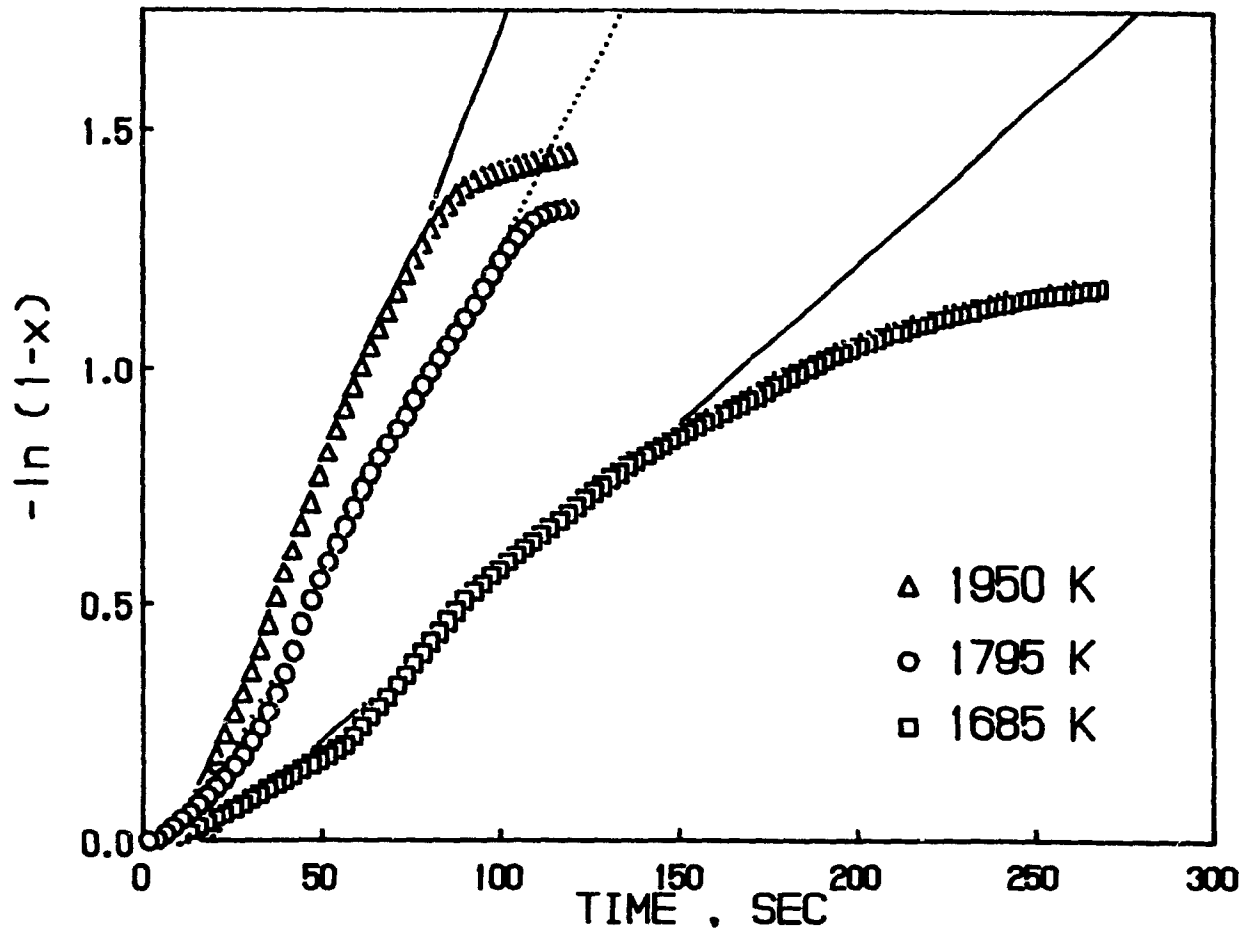

Figure 8.5 The Effect of Temperature on Conversion Using the Kinetic Model for the Carbothermic Reduction of Pyrochlore (d_p Pyrochlore = 60 μm) in the Presence of Iron : d_pC = <45 μm, d_p Fe = <45 μm, 13.0 wt. % C, 19.8 wt. % Fe, pellet dia. = 12.8 mm, pellet ht. = 19.6 mm

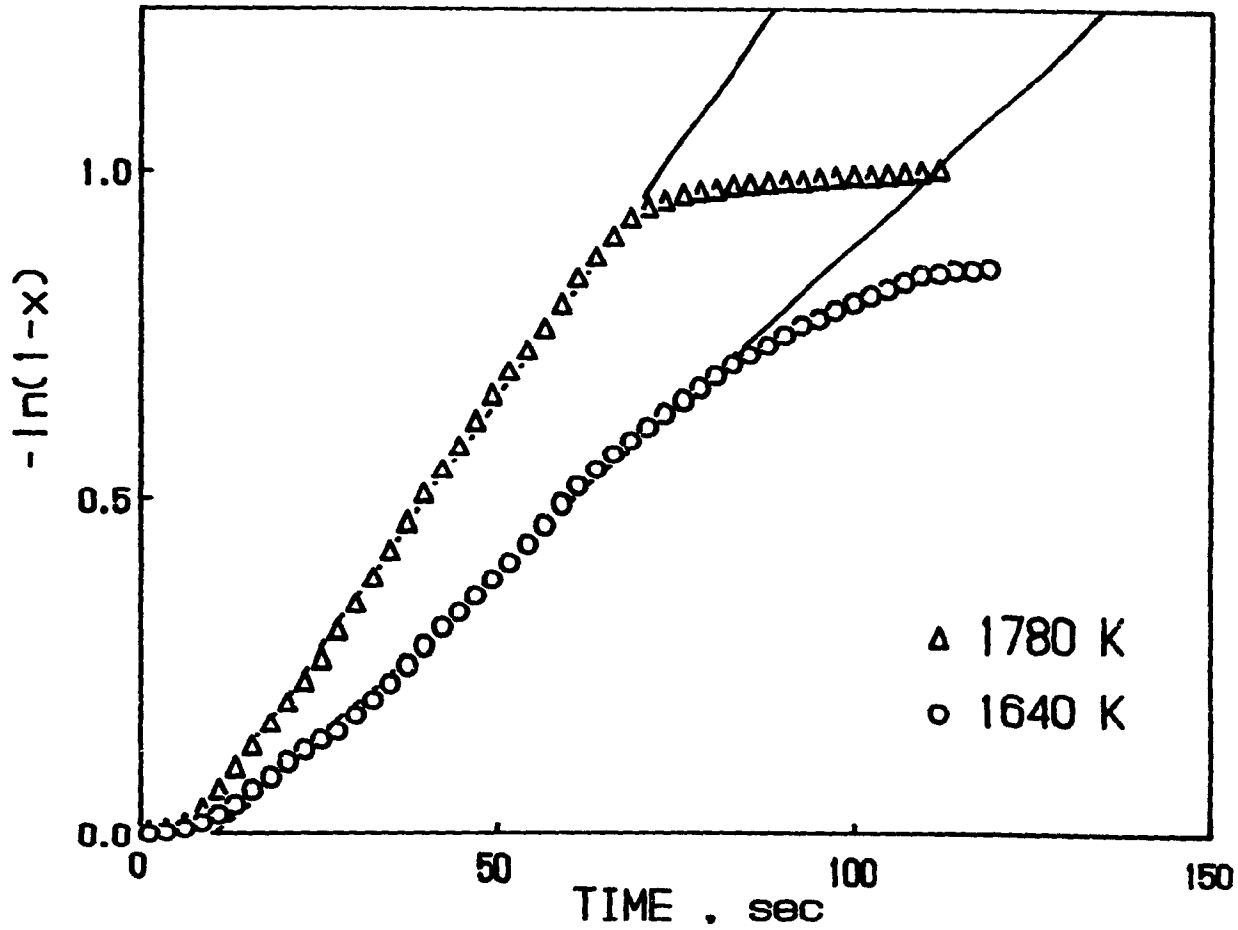

Figure 8.6 The Effect of Temperature on Conversion Using the Kinetic Model for the Carbothermic Reduction of Pyrochlore (d_p Pyrochlore = 60 μm) in the Presence of Iron : d_pC = <45 μm, d_p Fe = <45 μm, 5.8 wt. % C, 64.0 wt. % Fe, pellet dia. = 18.5 mm, pellet ht. = 17.0 mm

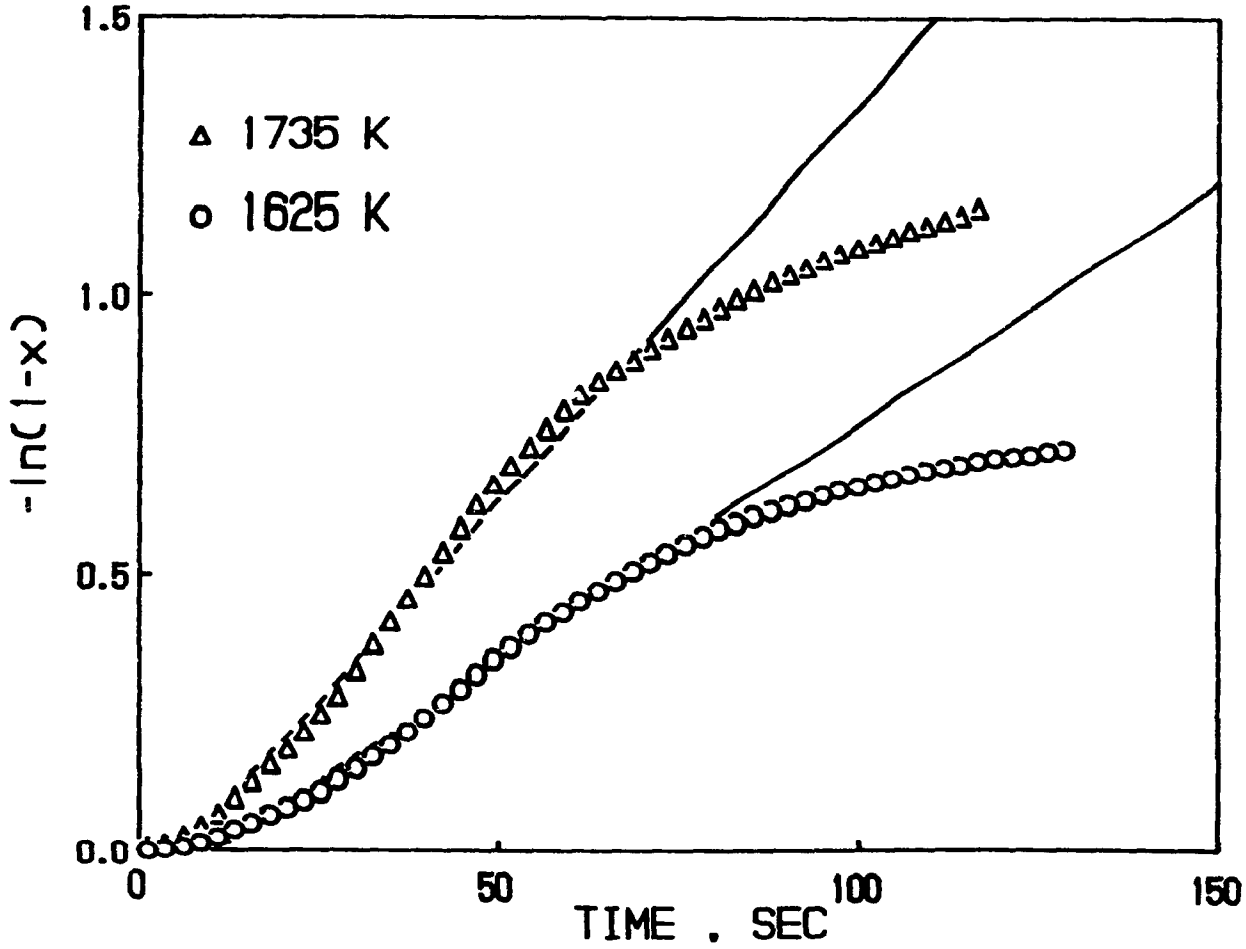

Figure 8.7 The Effect of Temperature on Conversion Using the Kinetic Model for the Carbothermic Reduction of Pyrochlore (d_p Pyrochlore = 60 μm) in the Presence of Iron : d_pC = <45 μm, d_p Fe = <45 μm, 11.4 wt. % C, 58.9 wt. % Fe, pellet dia. = 12.9 mm, pellet ht. = 16.5 mm

temperatures of 1625 and 1735 K, respectively. The results are similar to those for lower initial iron concentration. They show that the fractional level of conversion at which deviation from the model occurs increases with temperature.

The difference in the conversion levels at which deviation from the model occurs can be again attributed to the effects of a heat transfer limitation which leads to a non-isothermal pellet rather than a change in rate controlling mechanism. Another contributing factor is the improved mobility of and degree of contact between the reductants as the iron melts. This results in a higher conversion level before deviation from the model occurs.

If there was a change in the reaction mechanism, one would expect the deviation from kinetic to diffusion control to occur at lower conversion levels as the temperature increases. In the present case, the opposite effect is observed. These observations support using only the linear portion of the $-\ln(1-x)$ versus time data to calculate the overall reaction rate constant, since it is the temperature of the upper section of the pellet which was measured and reported.

8.7 Influence of Particle Diameter

Although there is some dissolution of the carbon in iron, the amount of iron added was never sufficient to completely dissolve all the carbon in the pellet. The overall rate constant, K, as defined by Equation (4.17), was not expected to be influenced by the change in particle diameter under chemical reaction control. Accordingly, an Arrhenius plot of the rate constants of

different particle diameters is expected to yield a single straight line, if ash diffusion is not limiting the reaction rate. Otherwise, the overall rate constant would decrease with increasing particle diameter due to a corresponding increase in the diffusion resistance.

The overall rate constants corresponding to the linear portion of -ln(1-x)-versus-time data were plotted according to an Arrhenius-type relationship in Figure 8.8 for pellets having different carbon and pyrochlore particle diameters of 100 % less than 45 and 463 microns and 60 and 230 microns, respectively. The C/Nb_2O_5 mole ratio and the initial iron concentration in the pellet were 7 and 19.8 wt. %, respectively. The results of the treated experimental data for each of these cases are presented in Tables V-A, V-B, and V-C of Appendix V. The data of Figure 8.8 show that, to a first approximation, the overall rate constants for pellets which were made with carbon particle diameters of 100 % less than 45 and 463 microns and constant pyrochlore particle diameter of 60 microns, all lie on the same line. In the case for pellets made with different pyrochlore particle diameters of 60 and 230 microns, respectively, and constant graphite particle diameter of 100 % less than 45 microns, there is a slight dependence of the overall rate constant on pyrochlore particle size. The dependence is not large enough to justify the use of the other rate expressions. For instance, at a temperature of 1835 K, the ratio of the overall reaction rate constants corresponding to a pyrochlore particle diameter ratio of 1:4 (60 microns:230 microns) and constant carbon particle diameter of <45 microns, is

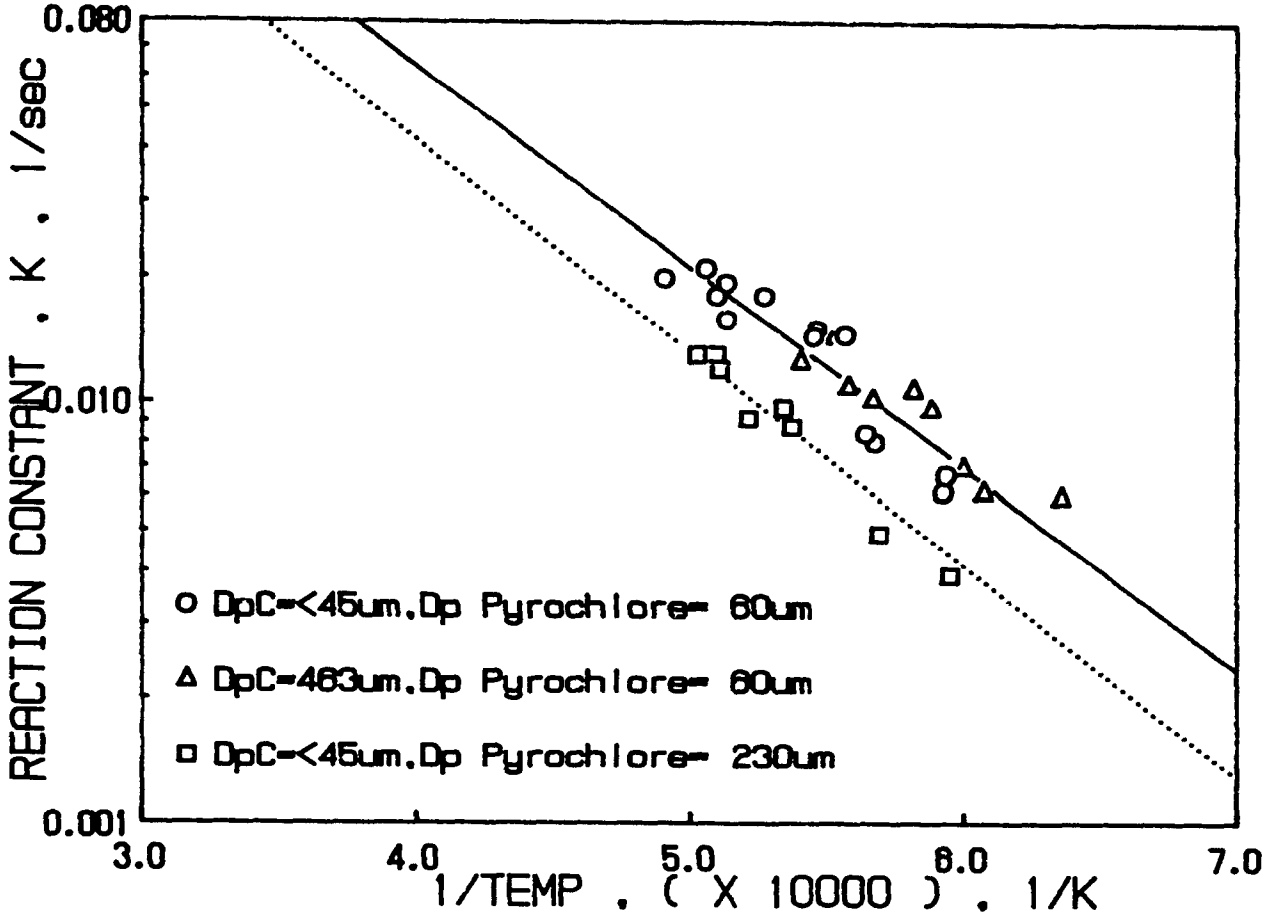

Figure 8.8 Arrhenius Plot for the Carbothermic Reduction of Pyrochlore for Different Graphite and Pyrochlore Particle Sizes in the Presence of Iron : d_p Pyrochlore = 60 and 230 μm, d_pC = <45, and 463 μm, d_p Fe = <45 μm, 17.6 wt. % C, 26.7 wt. % Fe, pellet dia. = 12.8 mm, pellet ht. = 19.5 mm

only 1.5:1. If the reaction or diffusion controlled model was the appropriate one, the overall rate constants should be inversely proportional to the particle radius or the square of particle radius, respectively. That is, for a reaction or diffusion controlled model, the predicted ratios of the overall rate constants should be 4:1 or 16:1, respectively. The small dependence might have been due to the larger relative surface area which become available for better contact and reaction with the carbon and/or the dissolved carbon in iron as discussed earlier. Thus, it would appear that the overall rate constant is independent of carbon and pyrochlore particle size and Equation (4.17) adequately represents the overall rate constant.

8.8 Influence of Temperature

The influence of temperature on the reaction rate for pellets made with different graphite and pyrochlore particle diameters and different initial carbon and iron concentrations was measured from 1430 to 2125 K. The choice of the temperature levels was dictated solely by the currents under which the arc was stable.

The Arrhenius plot of Figure 8.8 examines the effect of reaction temperature at a constant C/Nb_2O_5 mole ratio of 7 and an initial iron concentration of 19.8 wt. %. Different graphite and pyrochlore particle sizes were used as shown. For graphite particle diameter of 100 % less than 45 microns and pyrochlore of 60 microns, the activation energy and 95 % confidence interval are 100.828 ± 26.137 kJ/mole with a correlation coefficient of 0.867.

For graphite particle size of 463 microns and pyrochlore of 60 microns, the activation energy and 95 % confidence interval are 88.491 ± 43.032 kJ/mole with a correlation coefficient of 0.808. As discussed in the previous section, since the reaction rates for these two sets of experiments, all lie on the same line, the least squares fit for both sets of data gave an activation energy and 95 % confidence interval of 91.379 ± 17.808 kJ/mole. The solid straight line through the two sets of data (represented by the open circle and triangle symbols) is the resulting regression line. Finally, for the finer graphite particle size and a pyrochlore particle diameter of 230 microns (represented by the open square symbols), the activation energy and the 95 % confidence interval are 96.562 ± 29.272 kJ/mole with a correlation coefficient of 0.897. The dotted straight line is the resulting regression line. If it is agreed that the reaction rate was independent of particle size, the average activation energy was calculated to be 93.970 kJ/mole with a standard deviation of 3.665 kJ/mole.

The Arrhenius plot in Figure 8.9 is for three sets of experiments with pellets made with C/Nb_2O_5 mole ratio of 7 and 14 and constant graphite and pyrochlore particle diameters of 100% less than 45 and 60 microns, respectively. In the first set of experiments, the initial iron concentration was decreased from 19.8 to 8.4 wt. %, and the C/Nb_2O_5 mole ratio was 7. The least squares fit of the data (represented by the open triangle symbols) gave an activation energy and 95 % confidence limit of 114.169 ± 32.452 kJ/mole, with a correlation coefficient of 0.925. The dashed straight line through this set of data in Figure 8.9 is

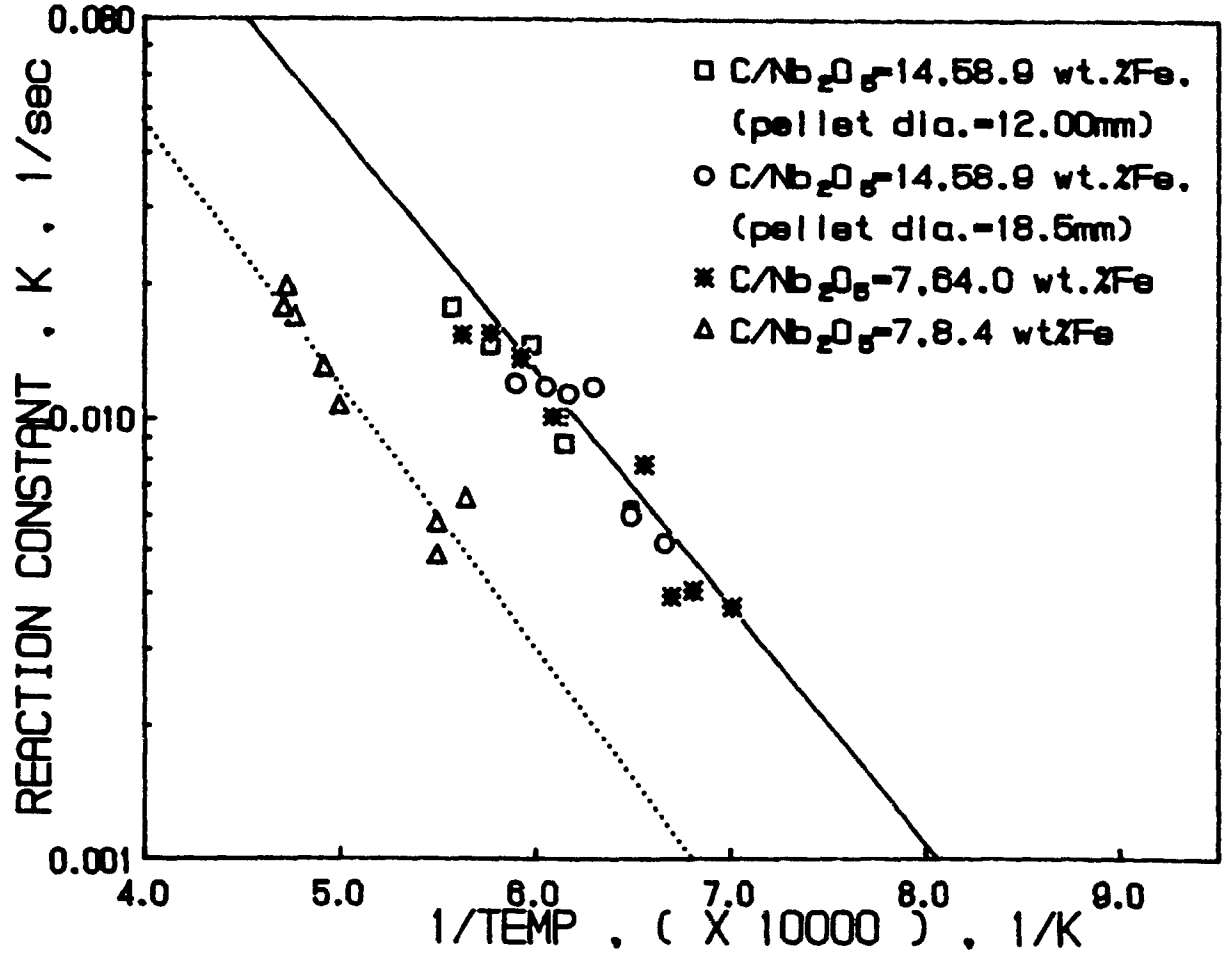

Figure 8.9 Arrhenius Plot for the Carbothermic Reduction of Pyrochlore for Different Initial Carbon and Iron Concentrations : d_p Pyrochlore = 60 μm, d_p C = <45 μm, d_p Fe = <45 μm, pellet dia. = 12.8 - 18.5 mm, pellet ht. = 16.1 - 20.6 mm

the resulting regression line. In the second set of experiments (represented by the star symbols) the initial iron concentration was increased to 64.0 wt. % and the C/Nb_2O_5 mole ratio was also 7. For the third set of experiments (represented by the open circle and square symbols), the C/Nb_2O_5 mole ratio was increased to 14, and the resulting initial iron concentration was 58.9 wt. %. Two pellet diameters were used in this third set. The treated data are presented in Table V-G of Appendix V. From the plotted data in Figure 8.9, it can be seen that there is no difference in the reaction rates between pellets with C/Nb_2O_5 mole ratio of 7 and 14 containing corresponding initial iron concentration of 64.0 and 58.9 wt. %. Also, the reaction rate is independent of pellet size. The least square fit for the data from the second and third sets experiments gave an activation energy and 95 % confidence interval of 97.500 ± 15.290 kJ/mole, with a correlation coefficient of 0.909. The solid straight line through the two data sets is the resulting regression line.

The average activation energy for all the data of Figure 8.8 and 8.9 was calculated to be 96.284 kJ/mole with a standard deviation of 14.532 kJ/mole.

8.9 Influence of Fe/C RATIO

The analysis of the kinetic data with respect to the iron/carbon (Fe/C) weight ratio was based on the carbon and iron content of the individual pellets. The experimental runs covered carbon and iron concentration ranges from 5.8 to 14.8 wt. % and 8.4 to 64.0 wt. %., respectively. The resulting Fe/C weight

ratios were 0.6, 1.5, 5.1 and 10.3. The treated data are summarized in Tables V-A to V-G of Appendix V. The initial carbon concentration was equal to or more than the amount required by the reaction stoichiometry to produce NbC. It was also always greater than the carbon solubility limit in iron at the maximum reaction temperatures. As in the previous cases, only those data corresponding to the linear portion of the time-conversion expression (Equation (4.20)) were considered.

The previously obtained overall activation energy values, the overall rate constants, and their corresponding temperatures were used to calculate respective values for the pre-exponential constant, A, as defined by the Arrhenius equation:

$$A = K/\exp(-E/RT) \qquad (8.1)$$

where K is the overall rate constant, E is the overall activation energy, and T is the pellet temperature. The calculated values for A were then plotted against the pellet Fe/C weight ratio and are shown in Figure 8.10. Using the one-tailed student t-test, it was shown that the average values of A were statistically different for average Fe/C weight ratio of 0.6, 1.5, and 5.1, respectively, at a 0.01 level of significance. For the higher average Fe/C weight ratios of 5.1 and 10.3, the values of A were not statistically different.

The rate of reduction is seen to increase with increasing Fe/C weight ratio, but changes very little after a threshold Fe/C weight ratio. This observation may be attributed to the existence

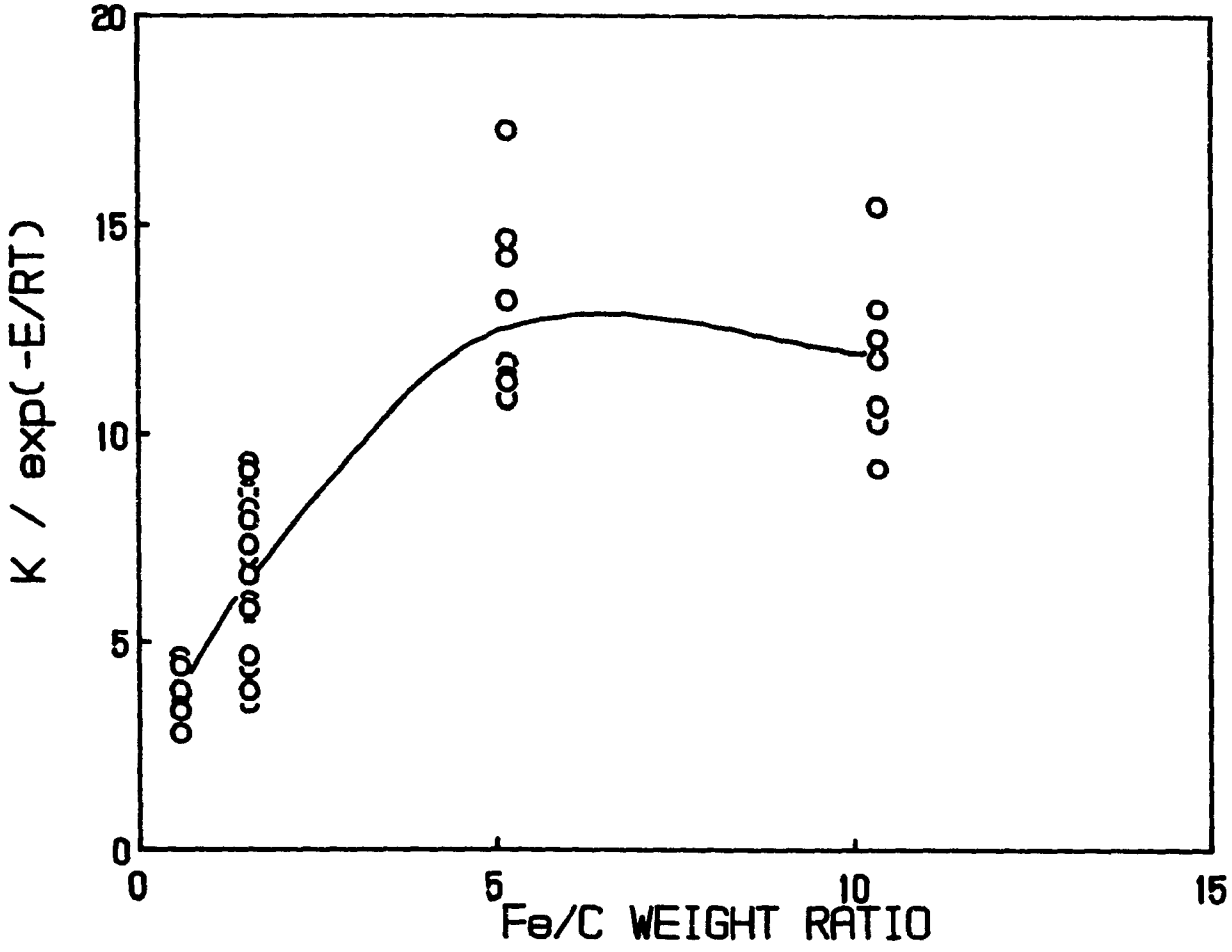

Figure 8.10 The Effect of Iron/Carbon Weight Ratio on Reaction Rate

of an optimum Fe/C weight ratio in the original mixture, yielding an optimum contact area, and consequently maximum reaction rate. The improved contact between the graphite and niobium pentoxide in pyrochlore could be due to the increasing amount of graphite available as dissolved carbon in iron. Further increasing the Fe/C weight ratio would only serve to dilute the dissolved carbon concentration in iron and result in a decrease in the reaction rate.

A comparison of the reaction constants for the carbothermic reduction of pyrochlore with increased initial carbon concentration and iron addition is shown in Table 8.4. The reaction constants were computed at 1823 K. The results show that there are comparable increases in the reaction rate with iron additions and with increased initial graphite concentrations without iron additions. The initial iron concentrations of 19.8 and 64.0 wt. % are equivalent to the Nb/Fe weight ratios for industrially produced ferroniobium and for a pourable Fe-NbC plasma produced ferroalloy, respectively.

As for the case of the carbothermic reduction of niobium pentoxide and pyrochlore without iron addition, a comparison of Figures 7.10 and 8.10 shows that for equivalent C/Nb_2O_5 mole ratios with iron addition, the reduction rates for niobium pentoxide is faster than that for pyrochlore. The difference in the reduction rate was also attributed to the diluting effect caused by the presence of the other oxides in the pyrochlore.

Table 8.4 Comparison of Reaction Constants for Carbothermic Reduction of Pyrochlore With and Without the Addition of Iron at 1823 K

REACTION CONSTANT sec^{-1}	C/Nb_2O_5 (mole)	Wt.% Fe	Fe/C (weight)
0.0100	7	0.0	0.0
0.0168	10	0.0	0.0
0.0107	7	19.8	1.52
0.0206	7	64.0	10.98

8.10 CONCLUSION

1- The kinetics of the carbothermic reduction of pyrochlore in the presence of iron were studied in the temperature range 1430 to 2125 K in an argon transferred-arc plasma. Influences of time, temperature, carbon and iron concentrations and graphite and pyrochlore particle sizes in the pellet on the rate were determined experimentally, using single stationary pellets composed of pyrochlore, graphite and iron particles.

2- The microscopic examination of partially reacted pellets indicated that the reaction took place in a mollified or liquid state depending on the initial iron concentration and the reaction temperature of the pellet.

3- The overall reduction of contained niobium pentoxide in pyrochlore in the presence of iron with time under chemical reaction control was represented by a logarithmic expression (Equation 4.20) based on the volumetric reaction model. Deviations from the model were observed to be less at high conversions and were attributed to unavoidable non-isothermal effects.

4- The Arrhenius plots of the experimental data indicated that the overall rate was essentially independent of carbon and pyrochlore particle sizes, but was dependent on the Fe/C weight ratio. The reaction was chemical reaction controlled. The average activation energy was calculated to be 96.3 kJ/mole with a standard deviation of 14.5 kJ/mole.

5- Experimental data indicated the existence of an optimum ratio of the Fe/C weight ratio in the original mix yielding an

optimum contact area, consequently, a maximum reduction rate.

CHAPTER IX

CARBOTHERMIC REDUCTION OF PYROCHLORE AND IRON OXIDE MIXTURE : EXPERIMENTAL RESULTS AND DISCUSSION

9.1 Introduction

The kinetics for the carbothermic reduction of pyrochlore with and without the presence of iron has been found to be adequately described by a logarithmic model. Analysis of the reaction products has also confirmed that a niobium carbide or a ferro-niobium carbide product is produced. This has also been demonstrated in an industrial type Plasmacan reactor (Hilborn, 1988). The use of iron powder was useful to examine the niobium reduction kinetics, but is not viable in a commercial process. It was therefore decided to conduct a preliminary investigation into the use of a clean iron oxide, ferric oxide, as the source of iron as might be envisaged in a commercial process.

Experiments were performed to study the time-conversion relationship, and the effect of iron (initially present as ferric oxide) concentration and temperature on the rate for the carbothermic reduction of pyrochlore. Specifically, it is the reduction of the niobium pentoxide contained in pyrochlore and ferric oxide. Experiments were performed with pellets in which the Nb/Fe weight ratio were 0.2 and 1.5 and the C/Nb_2O_5 mole ratio was kept constant at 7. The resulting initial ferric oxide and graphite concentrations in the pellet were 60.3 and 24.1 wt. % and 17.8 and 16.8 wt. %, respectively. The pellet diameter was 18.4 mm and heights were between 11.1 and 21.7 mm (see Appendix I). The graphite, ferric oxide and pyrochlore particle diameters used

in the experiments were 100 % less than 45 (or <45), 100 % less than 45, and 60 microns, respectively. The influence of particle size on reaction rate was not investigated in these cases. The C/Nb_2O_5 mole ratio for the reaction stoichiometry to produce NbC is 7 (Equation (4.8)), with the assumption that the remaining oxides in the pyrochlore are not reduced. In a mixture originally containing 24.1 wt. % ferric oxide, the niobium pentoxide contains 61 % of the oxygen while the ferric oxide contains 25 %. The total reduction of both oxides would thus give a fractional conversion of 0.86. With 60.3 wt. % initial ferric oxide, the niobium pentoxide contains 29 % of the oxygen, the ferric oxide contains 59 %, and total reduction of both oxides would result in a fractional conversion of 0.88. Since the overall rate measured cannot distinguish between the two sources of oxygen, low iron experiments would be biased towards the niobium pentoxide reduction rate, while high iron experiments would be biased towards the ferric oxide reduction rates. The Nb/Fe weight ratios for commercial grade ferroniobium and a pourable ferro-niobium carbide product are about 1.5 and 0.2, respectively.

9.2 Visual and Photographic Examinations

The reaction of the pellets containing initial ferric oxide concentration of 24.1 wt. % was observed to have taken place in a mollified state. Within a short period (about 5 seconds) after the plasma is started, the entire top of the pellet is melted. Although the average shape of the reacting pellet was still cylindrical, the top surface was in constant motion as bubbles of

carbon monoxide (and carbon dioxide) rose to the surface and burst. Occasionally, some tiny droplets of liquid were ejected from the surface. These observations were more exaggerated at high pellet temperature. When the pellet had reacted for the desired length of time the plasma was extinguished; at this point the pellet collapsed into a distorted cylinder and froze, usually in less than one second after shutdown. In the reactions with pellets containing higher initial ferric oxide concentration of 60.3 wt. %, there was more localized melting and coalescing of melted material rather than a global melting of the pellet as was observed in the previous case for lower initial ferric oxide concentration.

The surface of an unreacted pellet was smooth and relatively non-porous. A partially reacted pellet exhibited a very porous but hard surface as seen in Figure 9.1, where the initial ferric oxide concentrations were 24.1 and 60.3 wt. % and the C/Nb_2O_5 mole ratio was kept constant at 7, for Figure 9.1(a) and 9.1(b), respectively. The arc struck the top of the pellet and thus the temperature (and hence the rate of reaction) was the highest here. Close examination of the partially reacted pellets showed the presence of unreacted pyrochlore and ferric oxide in larger concentration in the bottom half than in the top.

The melting points of Niobec's pyrochlore, iron, ferric oxide and niobium carbide are about 1535, 1785, 1835 and 3875 K, respectively. The solubility of the NbC product in iron, formed by the carbothermic reduction of ferric oxide, will be a function of the temperature and the iron concentration in the pellet. If

(a)

(b)

Figure 5.1 Photographs of Partially Reacted Pellets
(d_p Pyrochlore = 60 μm, $d_p C$ = <45 μm, d_p Fe_2O_3 = <45 μm) :
a) 1670 K, x = 0.63, 16.8 wt. % C, 24.1 wt. % Fe_2O_3,
pellet dia. = 18.4 mm, pellet ht. = 11.1 mm,
b) 1460 K, x = 0.52, 17.6 wt. % C, 60.3 wt. % Fe_2O_3,
pellet dia. = 18.4 mm, pellet ht. = 20.9 mm.

there is insufficient iron produced for complete dissolution of the niobium carbide produced, the rest will precipitate from solution. The solid NbC would form either as an ash layer around the microscopic graphite and/or oxide particles or be dispersed randomly at the reaction (contact) points between the microscopic graphite and oxide particles. If gaseous intermediates (CO and CO_2) were major contributors to the progress of the reduction reaction, it would be expected that melting would hinder the reduction process because of the reduced porosity of the particle. Diffusion resistance through the product ash layer would also become apparent at relatively high temperatures. The role of the iron found in the reaction is most probably to improve contact between the carbon and the solid and/or liquid pyrochlore particles. This is achieved by the reduction reaction taking place between the dissolved carbon in the iron and the niobium pentoxide in the liquid state (Hilborn, 1988). The iron reduction is assumed to occur first since it is thermodynamically more favorable. Carbon dissolves readily in iron and it is probable that the iron will be saturated in carbon. Its concentration will be of the order of 4 to 5 wt. % for the temperature range 1410 to 1830 K (Chipman et. al.,1952). The amount of improvement in the reaction rate is dependent on the iron concentration. If there is insufficient dissolved carbon, further reduction will proceed by reaction with solid carbon and again the degree of contact between carbon and niobium pentoxide becomes important. Diffusion limitation of the dissolved carbon across the iron-oxide interface would also become apparent at relatively high temperatures.

The foregoing discussion was supported by the experimental data for the influence of iron concentration and pyrochlore and graphite particle sizes on the reaction rate which were presented in Chapter VIII.

9.3 X-ray Analysis

As in the previous cases, a number of reacted pellets were selected for x-ray powder diffraction (XRD) analysis. The results of all these analyses are summarized in Table 9.1. The XRD analysis results showed that in the case where the initial graphite and ferric oxide concentrations were 16.8 and 24.1 wt. %, respectively with an average conversion of 0.71, the major phase was identified as NbC. Latrappite, iron and carbon were identified as the minor phases and pyrochlore as a trace phase. For the case when the initial ferric oxide concentration was increased to 60.3 wt. %, giving an initial carbon concentration of 17.6 wt. %, iron and pyrochlore were identified as the major phases. Latrappite, carbon and NbC were the minor phases. The average conversion for this sample was 0.62; complete reduction of the ferric oxide alone would have required a fractional conversion of 0.59. The XRD results were similar to those obtained for the carbothermic reduction of pyrochlore with pure iron additions and which also had similar Nb/Fe weight ratios of 0.2 and 1.5. The C/Nb_2O_5 ratio for all the cases presented above was 7.

9.4 Mass Balance

Conversion was previously defined in Equation (3.4) as the

Table 9.1 XRD Analysis of Products for the Carbothermic Carbothermic Reduction of Pyrochlore and Ferric Oxide Mixture

Wt.% Fe_2O_3	COMPOUNDS	
	Major Phases	Minor Phases
24.1	NbC	Fe, C, Latrappite
60.3	Fe, pyrochlore	Latrappite, NbC, C

1 - C/Nb_2O_5 mole ratio = 7.

ratio of total oxygen in the carbon monoxide and carbon dioxide in the exhaust gas to the total initial oxygen in the oxide reactant(s). As for the previous cases, this method of measurement for conversion was checked for consistency by comparing the result to that calculated from the pellet's weight loss. Although the latter measurement was subject to higher experimental error, it was used primarily as an indicator for possible anomalies during an experimental run. The results, which are presented in Appendix VI, indicate that there was fair agreement between the two methods. The fractional conversion by weight loss was consistently higher, but the difference was generally less than 0.20. The exceptions were for those cases when the initial ferric oxide concentration was highest (60.3 wt. %). These showed differences between 0.21 and 0.24, which were caused by the evaporation and ejection of materials during the reaction. Very fine particles were subsequently entrained in the exhaust gas.

To identify what types of material were volatilized and ejected, approximate mass balances were done on the combined products from two sets of experiments under similar experimental conditions and conversions. The initial ferric oxide concentration of the pellets was 60.3 wt. % and the C/Nb_2O_5 mole ratio was 7. The mass balances were based on the analyses for the thirteen most abundant elements present in the reactants. The elemental composition was measured by emission spectroscopy. The difference between the summation of the percentage elemental compositions and 100 % was all attributed to oxygen. The results are summarized in Table 9.2. Since the elemental analysis did not include

Table 9.2 Mass Balance for the Product From Experiment Number 220

Weight of pellets, before reaction - 26.66 grams
Weight of pellets, after reaction - 16.18 grams
Average conversion (based on exhaust gas analysis) - 0.63
Average conversion (based on O loss in mass balance) - 0.88
Average pellet temperature - 1570 K

	Before Reaction				After Reaction	
	pyrochlore		added	total		
Element	%	g	g	g	%	g
Fe	4.5	0.262	11.247	11.509	57.70	9.330
C	0.08	0.004	4.756	4.760	9.81	1.587
Al	0.005	0.000	-	0.000	0.005	0.000
Ca	8.06	0.470	-	0.470	3.17	0.513
K	0.36	0.021	-	0.021	0.21	0.033
Mg	0.44	0.025	-	0.025	0.16	0.026
Mn	0.30	0.017	-	0.017	0.16	0.026
Na	5.00	0.291	-	0.291	1.06	0.171
Nb	44.10	2.571	-	2.571	21.10	3.414
P	0.03	0.002	-	0.002	0.03	0.005
Sr	1.26	0.073	-	0.073	0.44	0.071
Ti	1.68	0.098	-	0.098	0.96	0.155
U	0.029	0.017	-	0.017	0.063	0.010
O + otners (diff.)	33.89	1.976	4.833	6.809	5.132	0.830
TOTAL	100.0	5.827		26.663	100.0	16.171

all the elements present in pyrochlore, the results by themselves are not considered very accurate. But if interpreted along with the XRD results previously presented for a sample of the product from an experiment done with a pellet of the same composition, they show that iron (and/or ferric oxide) is the main element lost during the reaction. This is reflected in the fact that the calculated conversion based on the oxygen loss from the mass balance results was higher than that calculated by the analysis for CO and CO_2 in the exhaust gas.

9.5 CO/CO_2 Ratio

Measurements for CO and CO_2 were made in the exhaust gas to measure the progress of the reaction and to obtain some understanding of the reaction mechanism. Figure 9.2 shows the variation of CO and CO_2 concentrations with time that were typically obtained during the carbothermic reduction of pyrochlore and ferric oxide. Random samples were also taken from the exhaust gas and analyzed by gas chromatography to determine the types of gas present and their concentrations. Carbon dioxide and carbon monoxide were the only gases detected.

A comparison of the CO/CO_2 ratio at two different temperatures, 1635 and 1775 K, is shown in Figure 9.3. The average ratios for the rest of the experiments are summarized in Appendix VI. Assuming complete gas equilibrium and that the reduction reaction had taken place via gaseous intermediates, the CO/CO_2 ratios for the carbothermic reduction of ferric oxide and niobium pentoxide at 1635 and 1775 K should be about 1.2 and 1.5 and 1700

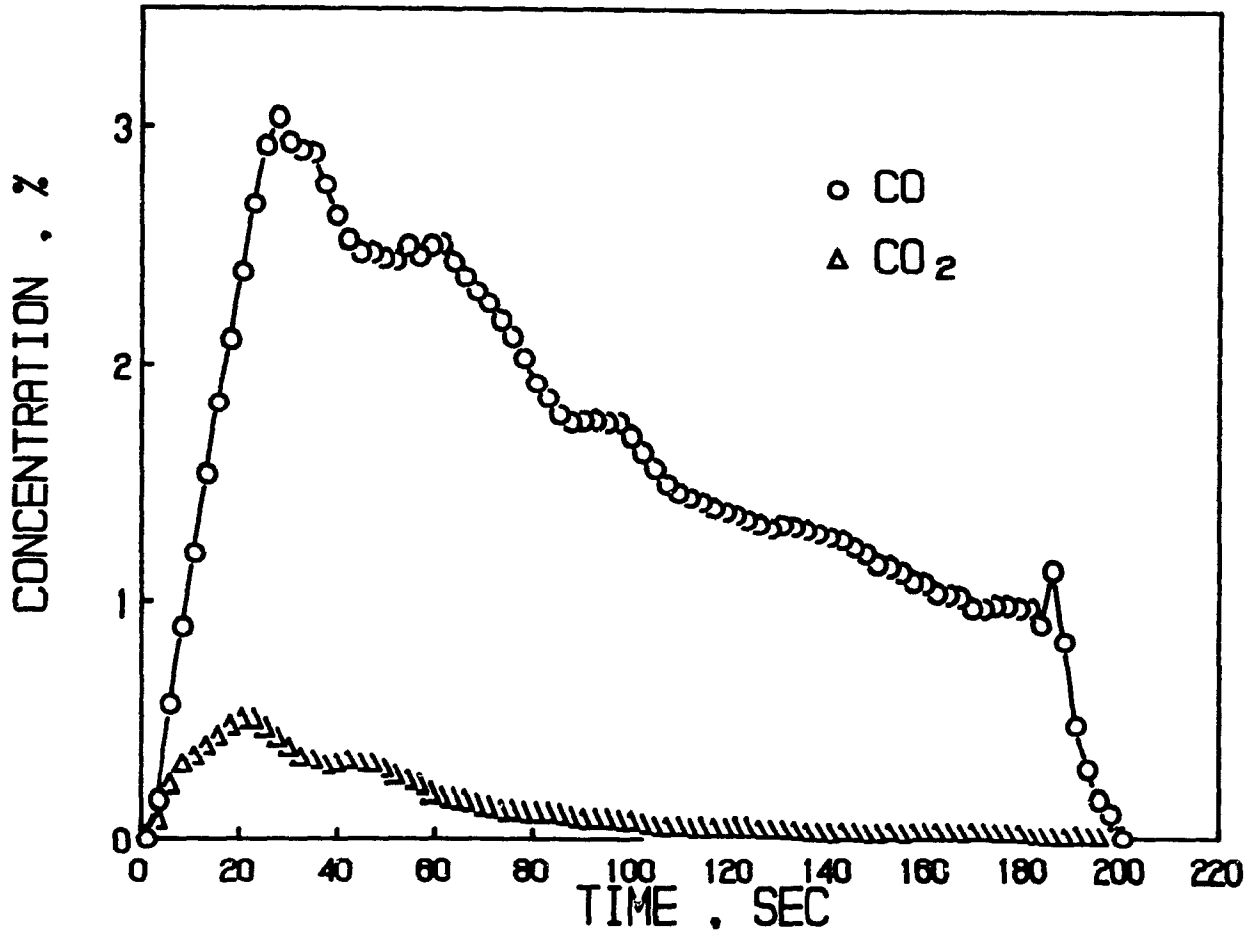

Figure 9.2 CO and CO_2 Concentration Versus Reaction Time for the Carbothermic Reduction of Pyrochlore and Fe_2O_3 Mixture : d_pC = <45 μm, d_p Pyrochlore = 60 μm, d_p Fe_2O_3 = <45 μm, 1635 K, 16.8 wt. % C, 24.1 wt. % Fe_2O_3, pellet dia. = 12.8 mm, pellet ht. = 19.5 mm

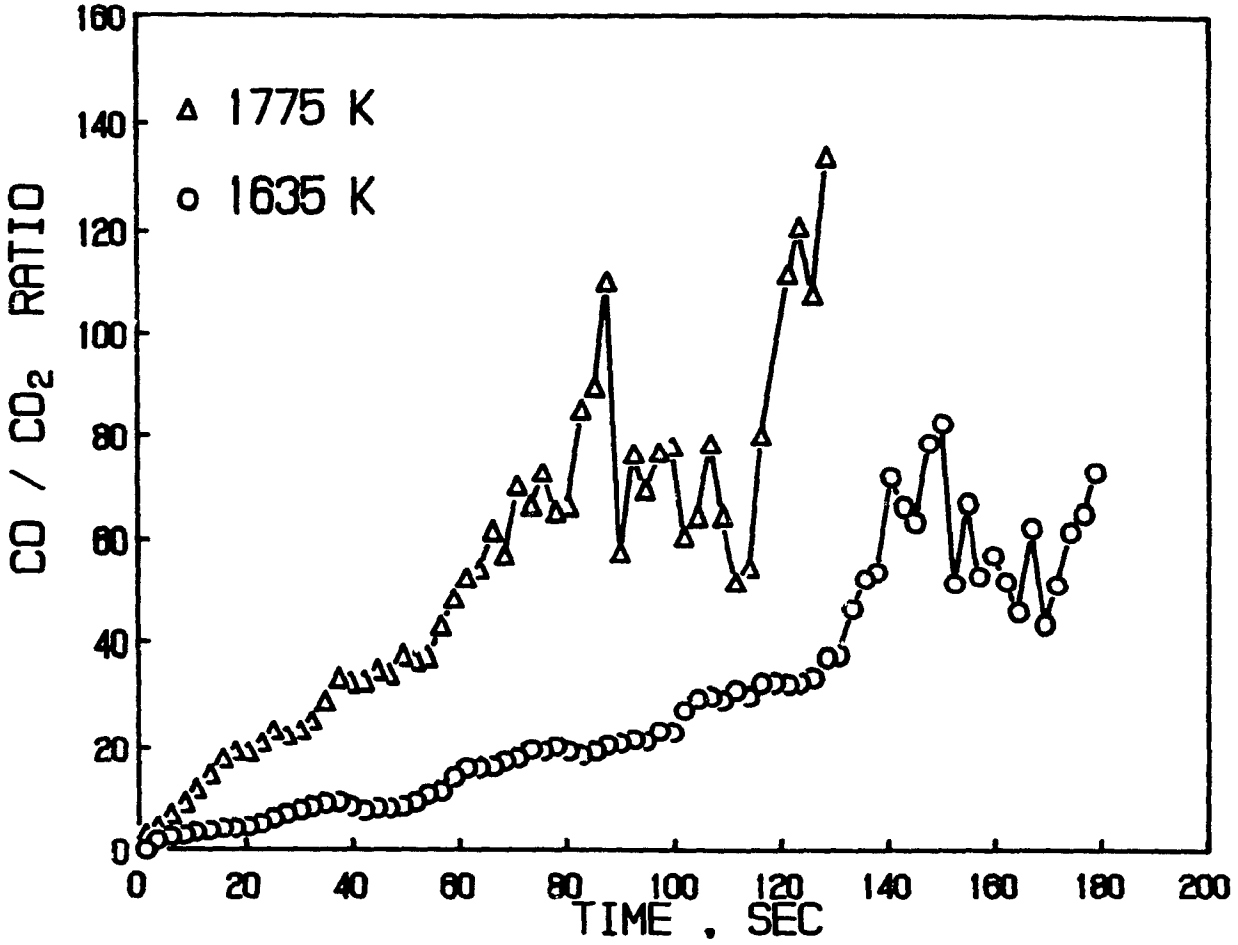

Figure 9.3 The Effect of Temperature on CO/CO_2 Ratio Versus Reaction Time for the Carbothermic Reduction of Pyrochlore and Fe_2O_3 Mixture : $d_p C$ = <45 μm, d_p pyrochlore = 60 μm, d_p Fe_2O_3 = <45 μm, 16.8 wt. % C, 24.1 wt. % Fe_2O_3, pellet dia. = 18.4 mm, pellet ht. = 11.4 mm

and 1100, respectively. Thus for the latter reduction reaction, the exhaust gas should essentially be all CO. From Figure 9.3, the highest values of CO/CO_2 were about 80 and 140, respectively, which are much less than expected for the carbothermic reduction of niobium pentoxide. The scatter is due to taking the ratio of large and small numbers. As discussed in the previous sections, the presence of CO_2 in the exhaust gas does not necessarily confirm the reduction mechanism as occurring via the gaseous intermediates CO and CO_2. The CO_2 could be due to carbon deposition from the exhaust gas as it cools from the high temperatures in the plasma to slightly above room temperature (Turkdogan, 1980). This is represented by Equation (5.1). The temperature at which carbon deposition may start is below 1000 K, and this reaction is catalyzed by iron, cobalt and nickel (Turkdogan, 1980).

As before, the presence of CO_2 in the exhaust suggests the possibility that the reduction reaction might have occurred via the gaseous intermediates CO and CO_2, but is inconclusive.

9.6 Conversion-Time Relationship

The experimental rate data were plotted according to Equation (4.20). The applicability of this model as the appropriate one was justified based on the results for the carbothermic reduction of niobium pentoxide, available as the pure oxide and as pyrochlore, with and without the presence of iron. The same expression was also used for the carbothermic reduction of ferric oxide (Rao, 1971), (Fruehan, 1977). Thus, it would be assumed that since the carbothermic reduction of ferric oxide is thermo-

dynamically more favorable, it would take place first at the contact points between the carbon and the solid and/or liquid ferric oxide, at the interparticle level. Then, the carbothermic reduction of pyrochlore particles would occur between the carbon which was dissolved in the previously formed iron and/or randomly throughout the pellet at contact points between the carbon and the solid and/or liquid niobium pentoxide, also at the interparticle level.

The typical experimental conversion-time data at different temperatures for pellets containing 24.1 wt. % ferric oxide are given in Figure 9.4. Again, a small induction period due to the initial heating of the pellet is observed. The delay is between 5 to 15 seconds and decreases with increasing temperature. The time required for heating and melting of the pyrochlore and ferric oxide at a reaction temperature of 1670 K, assuming a plasma energy efficiency of 30 %, was estimated to be about 25 seconds. After the induction period, the plot of $-\ln(1-x)$ versus time is linear as expected, but only to a certain conversion level beyond this the rate of conversion is less than the model predictions. The fractional conversion at which the deviation from the logarithmic model occurs, increases with increasing temperature. For the reaction conditions of Figure 9.4 and a temperature of 1670 K, the deviation starts at a conversion of 55 %. At higher pellet temperature of 1775 K, it takes place at 60 % conversion.

The influence of higher initial ferric oxide concentration on the conversion-time relationship was also investigated. Figure 9.5 shows the typical conversion-time data for pellets with

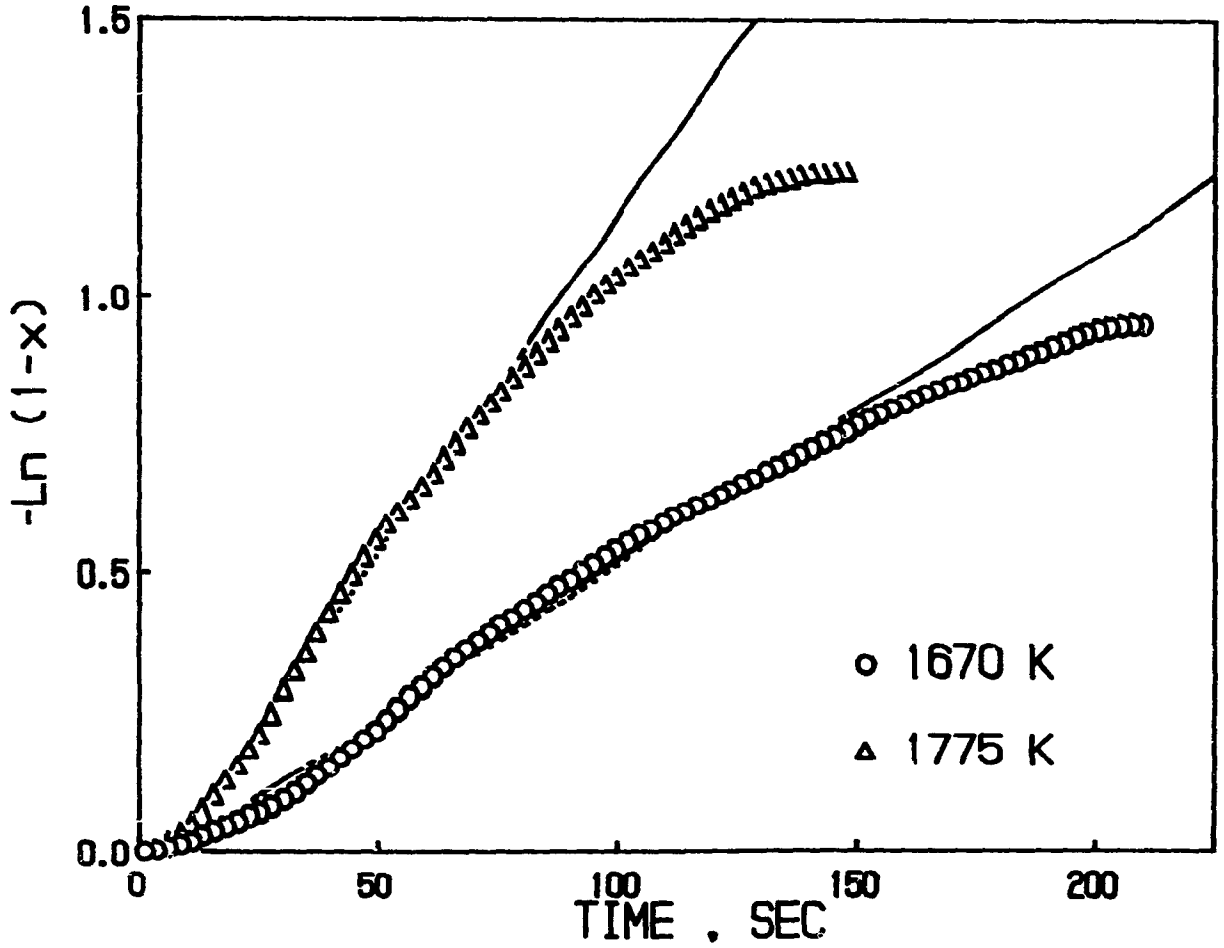

Figure 9.4 The Effect of Temperature on Conversion Using the Kinetic Model for the Carbothermic Reduction of Pyrochlore and Fe_2O_3 Mixture : $d_p C$ = <45 μm, d_p Pyrochlore = 60 μm, d_p Fe_2O_3 = <45 μm 16.8 wt. % C, 24.1 wt. % Fe_2O_3 , pellet dia. = 18.4 mm, pellet ht. = 11.4 mm

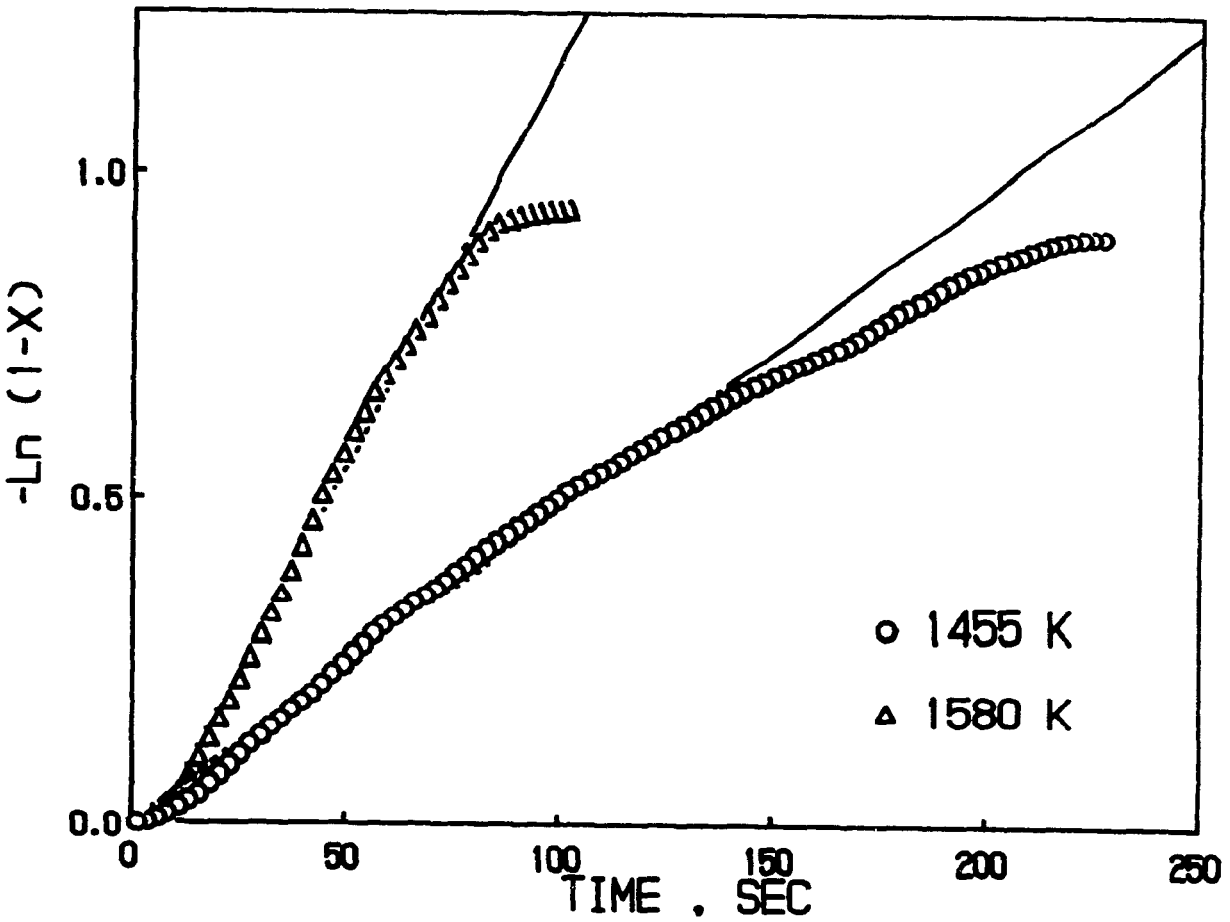

Figure 9.5 The Effect of Temperature on Conversion Using the Kinetic Model for the Carbothermic Reduction of Pyrochlore and Fe_2O_3 Mixture : $d_p C$ = <45 μm, d_p Pyrochlore = 60 μm, d_p Fe_2O_3 = <45 μm, 17.6 wt. % C, 60.3 wt. % Fe_2O_3, pellet dia. = 18.4 mm, pellet ht. = 21.1 mm

initial ferric oxide concentration of 60.3 wt. % at temperatures of 1455 and 1580 K, respectively. Although the temperatures are not exactly alike, the results are similar to those for lower initial ferric oxide concentration. They show that the fractional level of conversion at which deviation from the model occurs increases with temperature.

Both Figures 9.4 and 9.5 show no abrupt changes in the slope of the curves which indicates that the oxides are being reduced simultaneously and that the measured reaction rate constants are for the mixtures. Therefore at high initial ferric oxide concentrations, the measured reaction rates is biased towards that for carbothermic reduction of pure ferric oxide.

The difference in the conversion levels at which deviation from the model occurs can again be attributed to the effects of a heat transfer limitation which leads to a non-isothermal pellet rather than a change in rate controlling mechanism.

If there was a change in the reaction mechanism, one would expect the deviation from kinetic to diffusion control to occur at lower conversion levels as the temperature increases. In the present case, the opposite effect is observed. These observations support using only the linear portion of the $-\ln(1-x)$ versus time data to calculate the overall reaction rate constant, since it is the temperature of the upper section of the pellet which was measured and reported.

9.7 Influence of Temperature

The influence of temperature on the reaction rate for pel-

lets made with different initial ferric oxide concentrations and constant C/Nb_2O_5 mole ratio of 7 was measured from 1410 to 1830 K. The choice of the temperature levels was dictated solely by the currents under which the arc was stable.

The Arrhenius plot of Figure 9.6 examines the effect of reaction temperature at a constant C/Nb_2O_5 mole ratio of 7 and initial ferric oxide concentrations of 24.1 and 60.3 wt. %., respectively. The activation energy for the carbothermic reduction of the pyrochlore and ferric oxide mixture, with initial ferric oxide concentration of 24.1 wt. % is 150.468 ± 36.969 kJ/mole with a correlation coefficient of 0.904. For the case when the initial ferric oxide concentration was increased to 60.3 wt. %, the activation energy is 142.815 ± 49.807 kJ/mole, with a correlation coefficient of 0.845. The difference between the two activation energies is not statistically significant showing that the reaction mechanism does not change. The average activation energy was calculated to be 146.641 kJ/mole with a standard deviation of 5.411 kJ/mole. The solid and dashed straight lines in Figure 9.6 are the resulting regression lines.

9.8 Influence of Nb/Fe RATIO

The previously obtained activation energy values and the pre-exponential constants were used to calculate the overall reaction constants at a temperature of 1600 K for initial ferric oxide concentrations of 24.1 and 60.3 wt. % and constant C/Nb_2O_5 mole ratio of 7. The computed values for the overall rate constants and the corresponding equivalent Nb/Fe weight ratios are

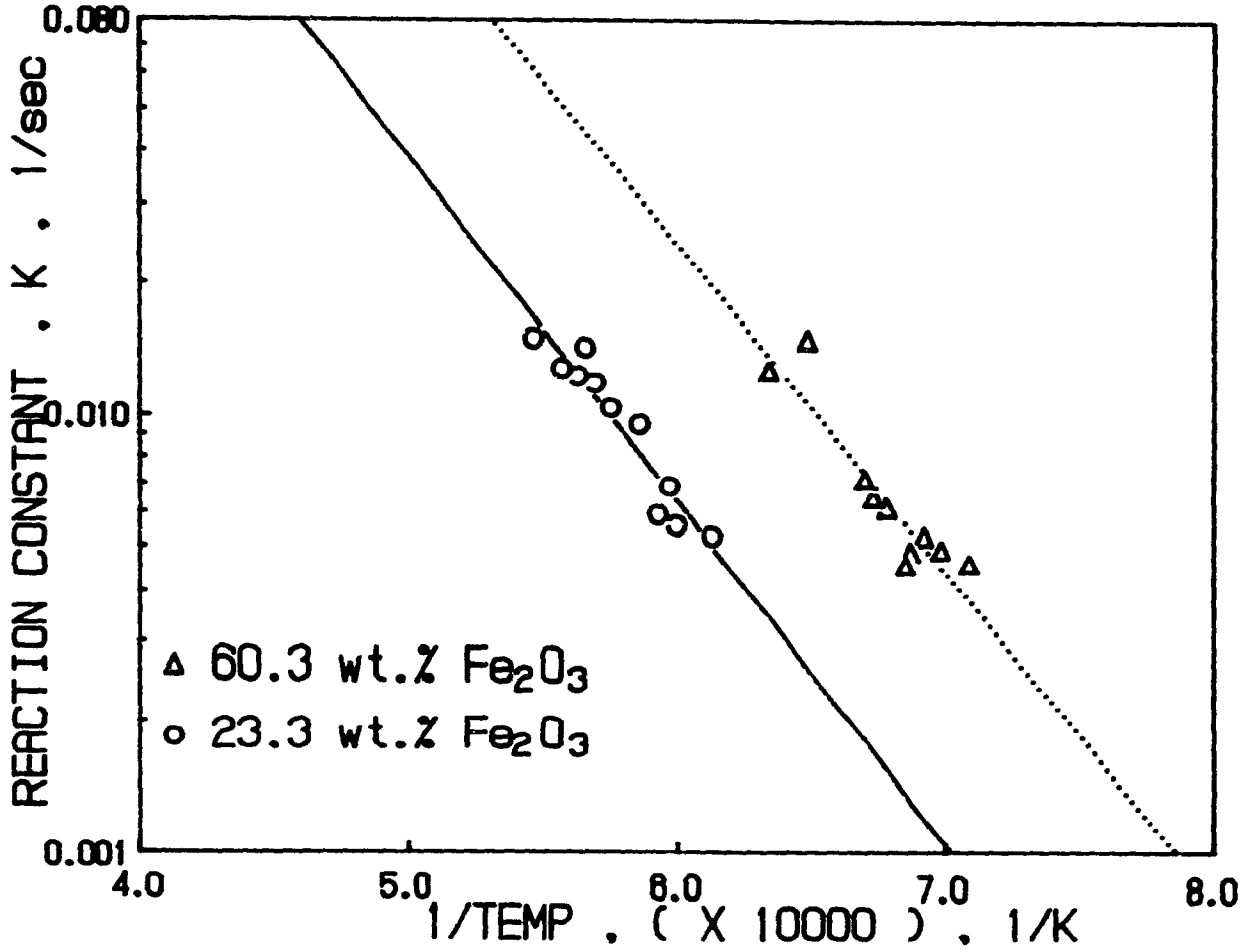

Figure 9.6 Arrhenius Plot for the Carbothermic Reduction of Pyrochlore and Fe_2O_3 for Different Initial Fe_2O_3 Concentrations : $d_p C$ = <45 μm, d_p Pyrochlore = 60 μm, d_p Fe_2O_3 = <45 μm, 24.1 and 60.3 wt. % Fe_2O_3, C/Nb_2O_5 (mole) = 7, pellet dia. = 18.4 mm, pellet ht. = 10.9 - 21.0 mm

summarized in Table 9.3. The rate of reduction is seen to increase with decreasing Nb/Fe weight ratio. This observation may be attributed to the improved contact between the graphite and the niobium pentoxide in pyrochlore due to the increasing amount of graphite available as dissolved carbon in iron. The iron is the product from the carbothermic reduction of ferric oxide. Also, another contributing factor is the increased amounts of iron particles that are formed, which have been reported to have a catalytic effect on the carbothermic reduction of ferric oxide (Ajersch, 1987).

The reaction rate constants for the reduction of pyrochlore in the presence of pure iron at 1600 K were also computed and are included in the Table 9.3 comparison. At a Nb/Fe ratio of 1.5, the rates for the two sources of iron are comparable, but at the lower ratio of 0.2 the rate with ferric oxide addition is twice as high. This could be attributed to the fact that with reacting mixtures containing high initial ferric oxide concentration, the carbothermic reduction of this oxide becomes the dominating reaction. The Nb/Fe wt. ratios of 1.5 and 0.2 are the weight ratios for industrially produced ferroniobium and for a pourable Fe-NbC plasma produced ferroalloy, respectively.

It should be noted that the activation energy for pyrochlore reduction in the presence of iron was 96.3 kJ/mole while that for pyrochlore reduction in the presence of ferric oxide was 146.5 kJ/mole suggesting a difference in reaction mechanism.

TABLE 9.3 Comparison of Reaction Constants for Carbothermic Reduction of Pyrochlore With Ferric Oxide and Iron Additions at 1600 K

REACTION CONSTANT sec^{-1}	Source of Iron	Nb/Fe^{1} (weight)
0.0159	Fe_2O_3	0.2
0.0040	Fe_2O_3	1.5
0.0084	Fe	0.2
0.0052	Fe	1.5

1. $C/Nb_2O_5 = 7$

9.9 CONCLUSION

1- The kinetics of the carbothermic reduction of mixtures of pyrochlore and ferric oxide were studied in the temperature range 1410 to 1830 K in an argon transferred-arc plasma. Influences of time, temperature and ferric oxide concentrations in the pellet on the rate were determined experimentally, using single stationary pellets composed of pyrochlore, graphite and ferric oxide particles.

2- The visual examination of partially reacted pellets indicated that the reaction took place in a mollified or liquid state depending on the initial iron concentration and the reaction temperature of the pellet.

3- The overall reduction of contained niobium pentoxide in pyrochlore and ferric oxide with time under chemical reaction control was represented by a logarithmic expression (Equation (4.20)) based on the volumetric reaction model. Deviations from the model were observed to be less at high conversions and were attributed to unavoidable non-isothermal effects.

4- The Arrhenius plots of the experimental data indicated that the overall rate was dependent on the Nb/Fe weight ratio. The reaction was chemical reaction controlled. The average activation energy was calculated to be 146.6 kJ/mole with a standard deviation of 5.4 kJ/mole. This value was larger than that for the carbothermic reduction of pyrochlore in pure iron, suggesting a difference in the reaction mechanism.

CHAPTER X

SUMMARY OF CONCLUSIONS, CONTRIBUTION TO KNOWLEDGE AND RECOMMENDATION FOR FUTURE WORK

10.1 SUMMARY OF CONCLUSIONS

1. The kinetics of the carbothermic reduction of pyrochlore and niobium pentoxide with and without the addition of iron in the temperature range 1410 - 2855 were studied in an argon transferred - arc plasma. Influences of time, temperature and particle size in the pellet were determined experimentally, using single stationary pellets.
2. A logarithmic expression (Equation 4.20) was proposed to describe the carbothermic reduction reaction systems under chemical reaction control. The experimental results confirmed the applicability of the model. The rates were lower than the model predictions above a certain conversion, the level of which increased with temperature, and carbon and iron concentrations.
3. The carbothermic reduction of pyrochlore and niobium pentoxide was independent of particle size but was influenced by the separation between the oxide and carbon particles. The experimental data indicated the existence of an optimum ratio of carbon and niobium pentoxide in the original mix yielding an optimum contact area, and consequently, a maximum reduction rate.
4. The activation energies for the carbothermic reduction of pyrochlore and niobium pentoxide were similar, 51.4 and 50.3

kJ/mole, respectively, but the reaction rate for the former was lower.

5. The carbothermic reduction of pyrochlore and niobium pentoxide in the presence of iron was independent of particle size but was enhanced by the presence of iron.
6. The activation energies for the carbothermic reduction of pyrochlore and niobium pentoxide in the presence of iron were 96.3 and 142.5 kJ/mole, respectively. The reduction rate of the former system was lower.
7. Preliminary investigation of the conversion rate for the carbothermic reduction of pyrochlore and ferric oxide mixture was done to simulate the type of materials that would be used in a commercial process. The rate data were also well represented by the logarithmic expression. Comparable reduction rates were observed with low iron and ferric oxide additions. At high iron and ferric oxide additions the reduction rate is higher for the latter case.
8. The activation energy for the carbothermic reduction of pyrochlore and ferric oxide mixture was calculated to be 146.6 kJ/mole.

10.2 CONTRIBUTION TO KNOWLEDGE

1. A transferred-arc plasma reactor system suitable for single particle kinetic studies of carbothermic reductions was designed and constructed. Experimental techniques were developed to measure carbothermic reaction kinetic data.
2. Comprehensive reaction kinetic data were measured for the car-

bothermic reduction of both pyrochlore and niobium pentoxide in the temperature ranges 1530-2440 and 1625-2855 K, respectively, in an argon plasma at atmospheric pressure.

3. Comprehensive reaction kinetic data were measured for the carbothermic reduction of both pyrochlore and niobium pentoxide in the presence of iron. The temperature ranges were 1430-2125 and 1575-2440 K, respectively.
4. Reaction kinetic data were measured for the simultaneous carbothermic reduction of pyrochlore and ferric oxide in the temperature range 1410-1830 K.
5. The same empirical rate expression was successfully fitted to all the kinetic data. As a first approximation the reaction rates were independent of the individual particle sizes.

10.3 RECOMMENDATIONS FOR FUTURE WORK

1. The continuous monitoring of carbon monoxide and carbon dioxide concentrations in the exhaust gas from the reactor allowed the overall rates of reaction to be measured but because the exhaust gas had an unknown time-temperature history, the reaction mechanism could not be unequivocally determined. It is thus recommended that a sampling probe system be developed to obtain and quench gas samples from the high temperature zone around the reacting pellets.
2. Because the original process envisaged by Liang and Munz (1981) made use of product carbon monoxide as the plasma gas, some tests should be performed in the presence of high concentrations of this gas. This would involve the use of a differ-

ent type of cathode system since tungsten is unstable in a plasma atmosphere of CO. Reaction rate measurements would also have to be based on analyses of the solid reaction products which is less accurate and more time-consuming than the techniques used in this work.

3. The present product, which contains excessive amounts of carbon must be tested as a direct alloying agent for steels. If it proves to be usable as is (because of the low concentrations usually required) the flow sheets of Liang and Munz (1981) should be modified to take advantage of this. If the material proves to be unsuitable some refining tests must be carried out.
4. Tests of the carbothermic reduction must also be carried out in a larger scale Plasmacan furnace to confirm the viability of the process on an industrial scale.

REFERENCES

Abraham, M.C., and Ghosh, A., "Kinetics of Reduction of Iron Oxide by Carbon," Iron and Steel Making, vol.6, No.1, pp.14-23, Jan. (1979)

Ajersch, F., "Chemical and Physical Characteristics Affecting the Reduction of Iron Oxide Pellets with Solid Carbon," Canadian Metallurgical Quarterly, vol.26, No.2, pp.1327-144, (1987)

Akashi, K., Ishizuka, R., and Mutobe, T., "Reduction of Metal oxides in a Direct Current Plasma Arc", 4th Inter. Conf. on Vacuum Metallurgy (1973).

Asada, C., and Adachi, T., "On Plasma Induction Melting", 3rd Int. Symp. on Electroslag and Other Special Melting Technologies, Ed. Bhat, G.K. and Simkovich, A., p.165 (June 1971).

Avrami, M., "Kinetics of Phase Change: I," J. Chem. Phys., vol.7,No.12, pp1103-1112, (1939)

Avrami, M., "Kinetics of Phase Change: II," J. Chem. Phys., vol 8,No.2,pp.212-224, (1940)

Avrami, M., "Kinetics of Phase Change: III," J. Chem. Phys., vol 9, No.2, pp.177-184, (1941)

Baddour, R.F., and Timmins, R.S., "The Application of Plasmas to Chemical Processing", The M.I.T. press (1967).

Bale, C.W., Pelton, A.D. and Thompson, W.T., Facility for the Analysis of Chemical Thermodynamics, Users Guide, 1st edition, McGill University/Ecole Polytechnique, June 1979.

Baldwin, B.G., "The Mechanism of The Reduction of Iron Oxides by Solid Coke," Journal of The Iron and Steel Institute, vol.179,pp.30-36, Jan.(1955)

Barcza, N.A., "Design and Applications of Large Scale Thermal Reactors in the Field of Pyrometallurgy," Mintek Report No. 0841/1a (August 1984)

Barcza, N.A.,"Application of Plasma Technology to Steel Processing", Plasma Technology in Metallurgical Processing, Fienman, J. (ed.), Chap. 11, p131-148, Iron and Steel Society (1987)

Barcza, N.A., Curr, T.R., and Maske, K.U., "Application of Thermal Plasma Technology to Large Scale Pyrometallurgical Processing," Paper presented at the Extraction Metallurgy'85 Symposium, organized by The Institute of Mining and Metallurgy, London, England, 9-12 September,1985.

Barcza, N.A., Curr, T.R., Winship, W.D., and Heanley, C.P., "The Production of Ferrochromium in a Transferred-Arc Plasma Furnace", 39th Electric Furnace Conference, p.243-260, (December 1981).

Barcza, N.A., and Stewart, A.B., "The Potential of Plasma Arc Technology for the Production of Ferroalloys," Preprint INFACON, Tokyo, Japan, (1983)

Barua, S.K., and Wynnyckyj, J.R., "Kinetics of the Silicothermic Reduction of Calcined Dolomite in Flowing Hydrogen," Canadian Metallurgical Quarterly, vol.20, No.3, pp.295-306, (1981)

Belitskus, D., "Aluminothermic Production of Metals and Alloys", Journal of Metals, Vol.24, p.30-34 (January 1972).

Bhat, G.K., "New Developments in Plasma Arc Melting", Journal of Vacuum Science Technology, 9, (November/December, 1972).

Bhat, G.K., "Plasma Technology and its Industrial Application", A survey report prepared for EPRI, Pittsburgh, Pa. (December 1981).

Biceroglu, O., "Chlorination Kinetics of ZrO2 in an RF Plasma Tailflame", Ph.D. Thesis, McGill University, (1978).

Bischoff, K.B. "Accuracy of the Pseudo Steady State Approximation for Moving Boundary Diffusion Problems", Chem. Eng. Sci., Vol.18, p.771-773 (1963).

Bodenstein, M., "The Mechanism of The Metallurgical Production of Zinc," Trans. American Electrochemical Society, Vol. 51,pp.365-376,(1927)

Borgianni, C., Capitelli, M., Cramarossa, F., Triolo, L., and Molinari, E., "The Behavior of Metal Oxides injected into an Argon Induction Plasma", Combut. Flame, vol.13, no.2, p.181-194, (1969).

Boulos, M.I., Gagne, R. and Barnes, R.N., "Effect of Swirl and Confinement on the flow and Temperature Field in an inductively Coupled R.F. Plasma", C. J. Ch. Eng., 58 (June 1980).

Bowen, J.H. and Cheng, C.K. "A Diffuse Interface Model for Fluid-Solid Reaction", Chem. Eng. Sci., 24, 1829 (1969).

Bramford, C.H., and Tipper, C.F.H., "Comprehensive Chemical Kinetics," vol. 22, "Reactions in the Solid State," Elsevier/North-Holland Inc., (1980).

Brent, A.D.," The Smelting of Ileminite in a dc Transferred-arc Plasma Furnace With a Molten Anode Configuration," Mintek Report No. M304, Council for Mineral Technology, 15 July, 1987.

Brent, A.D, MacRae, L.B., and Curr, T.R., " The Production of Manganese Ferroalloy in Transferred-arc Plasma Systems," Proceedings of The 69th Steelmaking Conference, Fifth International Iron and Steel Congress, Washington Meeting, April 6-9, 1986.

Brown, R.A.S., "Reaction of some Zirconium Compounds in a Plasma Jet", Presented at the CIMM Conference of Metallurgists, Kingston, Ontario, August 28-30 (1967).

Calvelo, A. and Cunningham, R.E. "Kinetics of Gas-Solid Reaction - Influence of Surface Area and Effective Diffusivity Profile", J. Catalysis, 17, 1 (1970).

Camacho, S.L., Technology Application Services Corporation (TASC), Raleigh, North Carolina, Private Communications (1977).

Carter, R.E., "Kinetic Model for Solid-Solid Reactions," J. Chem. Phys. vol.34, No.6, pp.2010-2015,(1961)

Chang, C.W., and Szekely, J., "Plasma Applications in Metal Processing", Journal of Metals, 34(2), (February 1982).

Chipman, J., Alfred, R.M., Gott, L.W., Small, R.B., Wilson, D.M., Thomson, C.N., Guernsey, D.L., and Fulton, J.C., "The Solubility Of Carbon In Molten Iron and Iron-Silicon And Iron-Manganese Alloys," ASM Trans., vol.44, pp.1215-1232, (1952)

Choi, H.K., "Energy Distribution in Transferred Arc Plasma Systems", Ph.D. Thesis, McGill University (1981).

Choi, H.K., and Gauvin, W.H., "Operating Characteristics and Energy Distribution in Transferred Plasma Arc Systems", Plasma Chemistry and Plasma Processing, vol. 2, no. 4, (December 1982).

Curr, T.R., Barcza, N.A., Maske, K.U., and Mooney, J.F., "The Design and Operation of Transferred-Arc Plasma Systems for Pyrometallurgical Applications", Proc. of the 6th Int. Symp. on Plasma Chemistry, Montreal, p.175-180 (July 1983).

Donyina, D.K.A., McLean, A., and Segsworth, R.S. "Treatment of Ferro- manganese Fines in an Extended Arc Flash Reactor", CIM Bulletin, Vol.75, no.847, (November 1982).

Doraiswamy, L.K., and Sharma, M.M, "Heterogeneous Reactions: Analysis, examples, and Reactor Design," vol. 1, "Gas-Solid and Solid-Solid Reactions," Chap. 21.,John Wiley and Sons. Inc. (1984)

Drouet, M.G. (ed.), "Plasma Technology: Review of The State Of the Art and Its Potential in Canada," Canadian Electrical Association Research Report, No. 126,322,(1984)

Dunwald, H., and Wagner, C., "Measurement of Diffusion Rate in the Process of Dissolving Gases in Solid Phases," Z. Physik. Chem.(Leipzig), vol.b24, No.1, pp.53-58, (1934)

Eckert, H.W., "The Induction Arc: A State of the Art Review", High T. Scie., 6, 99-134, (1974).

El-Guindy, M.I., and Davenport, W.G., "Kinetics and Mechanism of Ilmenite Reduction With Graphite," Metall. Trans., vol.1, pp.1729-1734, June(1970)

Elliott, R.P, "Constitution of Binary Alloys, First Supplement," McGraw-Hill Co., New York, (1965)

Engineering and Mining Journal, vol 187, no.4, p45 (April,1986)

Engineering and Mining Journal, vol 189, no.7, p19 (July,1988)

Eriksson, S., Johansson, B., and Santen, S. "The Plasmadust Process for Recovery of Metals from Waste Oxides", TMS paper selection, Paper No.A83-39, The Metallurgical Society of the AIME. (1983).

Everest, D.A., Sayce, I.G., and Selton, B., "Preparation of Ultrafine Silica Powders By Evaporation Using a THermal Plasma," Symposium on Electrochemical Engineering, Institution of Chemical Engineers, London, (1971).

Fauchais, P., " Chemie et Utilization des Plasmas," Journal Francais de L'Electrothermie, (8), p36-47,(1985).

Fauchais, P., Bourdin, E., and Coudert, J.F., "Generalities on the Physical ad Chemical processes in a thermal Plasma", Int. Chem. Eng. 23(2) (April 1983).

Fey, M.G. "Electric Arc Heaters for the Process Industries", Industrial Electric Heating Conference, Cincinnatti, Ohio, (Feb. 1976).

Fey, M.G., and McDonald, J., "Electrode Erosion in Electric Arc Heaters", AIChE Symp. Series (1979).

Feinman, J.(ed.), " Plasma Technology in Metallurgical Processes," Iron and Steel Society Inc. (1987)

Filho, O. de S.P., and de Fuccio, R. "Mining, Ore Preparation and Ferroniobium Production at CBMM", Niobium '81, Proceedings of the International Symposium, San Francisco, Calif. (November 8-11, 1981).

Flemings, M.C. (chairman), The Committee on Plasma Process For Extractive Metallurgy, "Plasma Processing of Materials," U.S National Materials Advisory Board, Publication NMAB-415, National Academy Press (1985).

Fruehan, R.J., The Rate of Reduction of Iron Oxides," Metall. Trans. B, vol.8b, pp.279-286, June(1977)

Fruehan, R.J., and Martonik, L.J., "The Rate of Reduction of MgO by Carbon," Metall. Trans. B, vol. 7B, pp.537-542, Dec.(1976)

Gans, I., and Gauvin, W.H., " The Plasma Production of Ultrafine Silica," Canadian Journal of Chemical Engineering, vol.66,No.3, (June,1988)

Gaskell, D.R. "Introduction to Metallurgical Thermodynamics", McGraw-Hill Book Company (1973)

Gauvin, W.H., and Choi, H.K., "Plasmas in Extractive Metallurgy", Proc. of Symp. on Plasma Processing and Synthesis of Materials, Sponsored by the Materials Research Society, Boston, (November 1983).

Gauvin, W.H., Drouet, M.G., and Munz, R.J., "Development in Plasma Processes for Extractive Metallurgy," Journal of Metals, 39 (12), (December, 1987)

Gauvin, W.H. and Kubanek, G.R., "A Novel Transferred-Arc Plasma Reactor for Chemical and Metallurgical Applications", Patent pending (1981).

Gauvin, W.H., Kubanek, G.R., and Irons, G.A., "The Plasma Production of Ferromolybdenum Process Development and Economics", J. of Metals (1981).

Gilles, H.L. and Clump, C.W., "Reduction of Iron ore with Hydrogen in a Direct Current Plasma Jet", Ind. Eng. Chem. Process Des. and Dev., 9(2) 194, (1970).

Ginstling, A.M., and Brounstein, B.I., "Concerning the Diffusion Kinetics of Reactions in Spherical Particles," J. Appl. Chem. USSR (English Transl.), vol.23, No.12, pp.1327-38,(1950)

Gold, R.G., Sandall, W.R., Cheplick, P.G. and MacRae, D.R., "Plasma Reduction of Iron Oxide with Hydrogen and Natural Gas at 100 kW and 1 MW", Ironmaking and Steelmaking, (1), 10, (1977).

Goldsmith, J.R., Sheer, C., and Korman, S. "Refractory Metals Production By The High Intensity Plasma Process", 3rd Intl. Symp. on Electroslag and Other Special Melting Techniques Pt.III, Bhat, G.K. and Simkovich, A. (eds.) (June 8-10, 1971).

Greenwald, H., and Groteke, D.E., "Use of the Inert-Arc Furnace for the Catalyzed Reduction of Iron and Other Oxide Ores", Third International Symposium of Electroslag Technology, Pittsburg (1971).

Guha, J.P., and Kolar, D. "Systems of Niobium Monocarbide with Transitional Metals", J. Less-Common Metals, vol. 29, pp33-40, (1972).

Guile, A.E., "Factors in Erosion of Non-Refractory Cathodes of Electric Arc Heaters", Proceedings of the Fifth Int. Symp. on Plasma Chemistry, Edinburgh (July 1981).

Guile, A.E.,, "Electric Arcs: Their Electrode Processes and Engineering Applications", IEE Proceedings, vol.131, Pt.A, No.7 (September 1984).

Habashi, F. "Principles of Extractive Metallurgy," Gordon and Breach, N.Y., vol.1, (1969)

Hamblyn, S.M.L., "Plasma Technology and its Application to Extractive Metallurgy", Minerals Sci. Engng., 9, No.3, 151 (July 1977).

Hiam, J.R. and Brazier, W. "Niobium-Bearing HSLA Steel Sheet and Strip Products", Niobium '81, Proceedings of the International Symposium, San Francisco, Calif. (November 8-11, 1981).

Hilborn, M.M., "Production Of Ferro-Niobium In The Plasmacan Furnace", M.Eng. Thesis , McGill University, (January, 1988).

Holm, R., "The Vaporization of the Cathode in the Electric Arc", J. Applied Phys., 20 (July 1949).

Howell, W.J., Eckert, C.A., and Anderson, R.N., "Carbothermic Reduction Using Liquid Metal Solvents," J. of Metals, vol. 40, No. 7, pp.21-23, July (1988)

Hulbert, S.F., "Models for Solid-state Reactions in Powdered Compacts: A Review," J. Br. Ceram. Soc., vol.6, pp.11-20, (1969)

Hulbert, S.F., and Klawitter, J.J., "Kinetics and Mechanism of the Reaction Between Zinc Oxide and Barium Carbonate," J. Am. Ceram. Soc., vol.50, No.9, pp.484-488, Sept.(1967)

Hunter, W.L., and Fursman, O.C., "Electric-arc Furnace Reduction of Tin Slag For Production of Columbium-Tantalum Bearing Alloy," U.S. Bureau of Mines, Report of Investigation No. 6734, (1966)

Hussein M.K., Kolta, G.A., Saba, A.E., and El Roundi, A.M., "Kinetics of Calcium Phosphate Reduction by Carbon," Thermochima Acta, vol.10, pp.177-186. (1974)

Jach, J.,"The Thermal Decomposition of $NaBrO_3$ Part I-Unirradiated Material," J. Phys. Chem. Solids, vol.24, pp.63-73, (1963)

Jander, W., "Reactions in Solid State at High Temperatures: I," Z. Anorg. Allgem. Chem., vol.163[1-2], pp.1-30, (1927)

Kayima, K., Kitahara, N., Morinaka, I., Sakura, K., Ozawa, M. and Tanaka, M., "Reduction of Molten Iron Oxide and FeO Bearing Slags by H2-Ar Plasma", Transactions ISIJ, vol.24 (1984).

Keown, S.R., and Pickering, F.B. "Niobium in Stainless Steels", Niobium '81, Proceedings of the International Symposium, San Francisco, Calif. (November 8-11, 1981).

Kieffer, R. and Braun, H. "Vanadium, Niobium, Tantalum", Springer-Verlag, Heidelberg (1963).

Klinger, E., Strauss, E.L., and Komarek, K.L., "Reactions Between Silica and Graphite," J. Am. Ceram. Soc., vol.49, No.7, pp.369-375, July(1966)

Kolchin, O.P. "Chemism of Reducing Niobium from its Pentoxide with Carbon", Soviet Journal of Non-Ferrous Metals, vol.11, no.7, p.49 (July 1970).

Kor, G.J.W., "The Thermal Decomposition of Mn_2O_3 and the Reduction of Mn_2O_3 by C and CO," Metall. Trans. B., vol.9B, pp.307-311, June(1978)

Kriebaum, J., "Plasma Spouted Bed Calcination of Lac Dore Vanadium Ore Concentrate," M.Eng Thesis, McGill University, December 1986.

Kroger, C., and Ziegler, G., "Reaction Rate of Glass Batch Melting: II," Glastech. Ber., vol.27, No.6, pp.199-212 (1954)

Kubanek, G.R., Gauvin, W.H., Irons, G.A., Choi, H.K., "The Industrial Applications of Plasmas to Metallurgical Process", Conference Proceedings, 4th Int. Symp. on Plasma Chemistry, Zurich, Switzerland (August 1979).

Kubaschewski, O., and Alcock, C.B., "Metallurgical Thermochemistry," Pergamon Press, New York, NY, (1977)

Levenspiel, O. "Chemical Reaction Engineering", 2nd edition, John Wiley and Sons, Inc. (1972).

Liang, A. "Ferroniobium Production of Plasma Technology - A Techno Economic Assessment", M.Eng. Thesis, McGill University (1982).

Liang, A. and Munz, R.J., "Ferroniobium Production by Plasma Technology - A Techno-Economic Assessment", Proceedings from 2nd World Congress of Chem. Engng., Montreal, Canada (October 1981).

Lin, L.J., and Rao, Y.K., "Reduction of Lead Oxide by Carbon," Inst. Min. Metall., Trans., Sect.C, vol.84, pp.C76-C86, (1975)

MacRae, D.R., "Plasma Processing in Extractive Metallurgy: The Falling Film Plasma Reactor", Plasma Chemical Processing, A.I.Ch.E. Symp. Series 186(75) (1979).

MacRae, D.R., Gold, R.G., Thompson, C.D., and Sandall, W.R., "Ferrovanadium Production by Plasma Carbothermic Reduction of Vanadium Oxide", 34th Electric Furnace Conference, St.Louis, Mo. (Dec. 1976).

Manker, E., Vice President, Marketing, Niobec Inc., Montreal, Quebec, private communication (1981).

Maru, y., Kuramasu, Y., Awakura, Y., and Kondo, Y., "Kinetic Studies of the Reaction Between $Cr_{23}C_6$ and Cr_2O_3 Particles," Metall.Trans. vol.4, pp.2591-2598, Nov.(1973)

Maske, K.U., "The reduction of Chromite in a Transferred-arc Plasma Furnace," Mintek Report No. M178, Council for Mineral Technology, 25 January, 1985.

Maske, K.U. and Moore, J.J., "The Application of plasmas to High Temperature reduction Metallurgy", High Temp. Tech., 1(1), 51-63, (August 1982).

Matsui, I, Kunii, D., and Furusawa, T., "Study of Char Gasification by Carbon Dioxide. 1. Kinetic Study by Thermogravimetric Analysis," Ind. Eng. Chem. Res., vol.26, pp.91-95, (1987)

Matsumoto, O., and Kanzaki, Y., "Plasma Nitriding Reaction of Metals", 6th International Symposium on Plasma Chemistry, Montreal, Quebec. Boulos, M.J., and Munz, R.J. (Eds.) (July 24-28, 1983).

Matsumoto, O., Naka, H., Shimoda, N., and Kanzaki, Y., "Carbothermic Reduction of Al_2O_3 in a Plasma Arc", 6th International Symposium on Plasma Chemistry, ISPC-6, Symposium Proceedings, vol.1, Montreal, Canada, (July 24-28, 1983)

Matsumoto, O. and Saito, M. "Formation of Niobium Carbide by the Carbonization of Nb205 in an Argon Plasma Arc", High Temperature Science, 6 (1974).

Mehmetoglu,, M.T., and Gauvin, W.H. "Characteristics of a Transferred-Arc Plasma", A.I.Ch.E. Journal, vol.29, no.2, p.207 (March 1983).

Mehmetoglu, M.T., Munz,R.J., and Gauvin, W.H., "The Production of Ferrochromium In An rf Plasma Tailflame," 7th International Symposium on Plasma Chemistry, Timmermans, C.J. (ed.), Eidenhoven,The Netherlands, vol.4, p1180-1185, July 1-5,1985.

Metal Bulletin, "Platinum," pp45-45, April (1985)

Miller, G.L. "Tantalum and Niobium", Butterworth Publication Ltd., London (1959).

Mimura, K., Ito, Y., and Nanjo, M., "The Production of Pure Niobium by Combination of Carbon Reduction Smelting and Electron Beam Melting," Bull. Res. Inst. Miner. Dressing Metall., vol.41, No.2, pp.141-154, Dec.(1985)

Moiseyev, G.K., Popov,S.K., Kadyshevskiy, V.S., Drayenkov, A.N., and Samyltyrov,T.Kh., "Thermodynamic Calculations Simulating the Reaction Between Niobium Pentoxide and Carbon", Russian Metallurgy, (4), p.46-49 (1981).

Munz, R.J., "The Decomposition of Molybdenum Disulphide in an Induction Plasma Tailflame", Ph.D. Thesis, McGill University, (1974).

Munz, R.J. and Gauvin, W.H., "The Decomposition Kinetics of Molybdenite in an Argon Plasma", A.I.Ch.E. J., 21, 6, 1132 (1975).

Nagamori, M., "Thermodynamics of the Carbothermic Reactions for Ferroniobium," Centre Recherches Minerales, Government of Quebec, May (1984)

Nagamori, M. and Plumpton, A.J. "High Temperature Benefication of a Tantalum-Niobium Concentrate By Selective Ferroalloying". C.I.M. Bullitin, vol. 78, No.874, pp.92-98, Feb (1985)

National Academy of Sciences, U.S., "Electroslag Remelting and Plasma Arc Melting," NMAB 324, Washington, D.C., (1976)

Nauman, E.B., and Buffham, B.A., "Mixing in Continous Flow Systems," John Wiley and Sons, Inc, (1983)

Neuschutz, D., et al., "Development of 3-Phase Plasma Furnaces at Krupp," Iron and Steel Engineering (May 1985)

Noesen, S.J., Trans. Vac. Met. Conf. American Vacuum Society, p.503, (1967)

Ono, K. and Moriyama, J. "Fundamental Study on Carbothermic Reduction of Niobium Oxide in High-Temperature Vacuum Furnace", 4th Inter. Conf. on Vacuum Metallurgy (1973).

Ono, K., Ueda, Y., and Moriyama, J., "Fundamental Study on the Production of Niobium by the Carbothermic Reduction-Electron Beam Melting Combination Method," Trans. JIM, vol.21, pp.319-324, (1980)

Padilla, R., and Sohn, H.Y., "The Reduction of Stannic Oxide with Carbon," Metall. Trans. B,vol. 10B, pp.109-115, Mar.(1979)

Padilla, R., and Sohn, H.Y., "Sintering Kinetics and Alumina Yield in Lime-Soda Sinter Process for Alumina from Coal Wastes," Metall. Trans. B, Vol. 16B, pp.385-395, June(1985)

Parisi, P.J. "A Novel Transferred-Arc Reactor", M.Eng. Thesis, McGill University (August 1984).

Parisi, P.J. "Heat Transfer and Particulate Feeding to a Cylindrical Enclosure in the Presence of a Plasma Transferred-Arc." Ph.D. Thesis, McGill University, February 1988.

Patai, S., and Hoffman, E., "The Oxidation of Carbon Black by Solid Potassium Perchlorate," J. Am. Chem. Soc., vol.72, pp.5098-5101, Nov.(1950)

Pfender, E., "Plasma Generation," Materials Research Society Symposia Proceedings, vol.30, Szkely,J., and Apelian, D.,(eds.), p13-35,(North-Holland Publishers, 1984)

Pfender, E., Boulous, M., and Fauchais, P., "Methods and Principles of Plasma Generation," Plasma Technology in Metallurgical Processing, Feinman, J., (ed.), Chap. 4, p27-47, Iron and Steel Society Inc. (1987)

Pickles, C.A., et al. "An Investigation of a New Technique for the Production of Ferro-chromium Alloys". Paper no.14, 15th Annual Conference of Metallurgists, Toronto (Canada) (August 1976).

Pickles, C.A. and Alcock, C.B. "Production of Ferronickel and Ferrovanadium from Fly Ash in an Extended Arc Flash Reactor", J. of Metals, vol.35, no.12, (December 1983).

Pickles, C.A., Mclean, A., Alcock, C.B. and Segsworth, R.S., "Investigation of a New Technique for the Treatment of Steel Plant Waste Oxides in an Extended Arc Flash Reactor", Advances in Extractive Metallurgy, IMM, London (1977).

Pinkuss, M.L. and Guimaraes, H. "Mining, Ore Preparation and Ferro-Niobium Production at Mineracao Catalao", Niobium '81, Proceedings of the International Symposium, San Francisco, Calif. (November 8-11, 1981).

Rains, R.K. and Kadlec, R.H., "The Reduction of AlO to Aluminium in a Plasma", Metall. Trans., Vol.1, 1501-1506, (1970).

Rao, Y.K., "The Kinetics of Reduction Of Hematite by Carbon," Metall. Trans., vol.2, pp.1439-1447, May(1971)

Rao, Y.K., "A Physico-Chemical Model for Reactions Between Particulate Solids Occurring Through Gaseous Intermediates-1. Reduction of Hematite by Carbon," Chem. Eng. Sci., vol.29, pp.1435-1445, (1974)

Rao, Y.K., and Chang, Y.K., "A Physico-Chemical Model for Reactions Between Particulate Solids Occurring Through Gaseous Intermediates-II. General Solutions.," Chem. Eng. Sci., vol.29, pp.1933-1938, (1974)

Rao, Y.K., and Jalan, B.P., "A Study of the Rates of Carbon-Carbon Dioxide Reaction in the Temperature Range 839° to 1050° C," Metall. Trans., vol.3, pp.2465-2477, Sept.(1972)

Reed, T.B., "Induction Coupled Plasma Torch", J. Appl. Physics, 32, 821, (1961).

Reid, K.J., "Direct steelmaking Based on Solid-Plasma Interactions", Proc. 53rd Annual Meeting, Minn. Section, AIME and 41st Annual Mining Symp., p.6-1 to 6-25 (1980).

Reid, K.J., Murawa, M., and Girgis,N.M., "Plasma Smelting of Copper-Nickel Concentrate for Minimal Environmental Impact," Proceedings 6th International Symposium on Plasma Chemistry, ISPC-6, Boulos,M., and Munz, R.J.,(eds.), Montreal, Quebec,(1983)

Rokenbauer, W. "Production of Niobium Metal and Compounds from Tantalite-Columbite Natural Ores and Synthetic Tantalum-Niobium Concentrates", Niobium '81, Proceedings of the International Symposium, San Francisco, Calif. (November 8-11, 1981).

Rosenquist, T. "Principles of Extractive Metallurgy", 2nd edition, McGraw-Hill Book Co. (1983).

Sayeh, N.N., "Variable Property Flow and Heat Transfer to Single Spheres", Ph.D. Thesis, McGill University, (1977).

Sayce, I.G., "Some Applications of Thermal Plasmas to Material Processing", Paper presented at World Electrotech. Congress, Moscow, USSR, Sec. 4A, No.107 (July 1977).

Schnell, C.R., Hamblyn, S.M.L., Hengartner, K. and Wissler, M. "The Industrial Application of Plasma Technology for the Production of Fumed Silica", Powder Technology, 20, 15-20, (1978).

Schoukens, A.F.S., and Curr, T.R., "The Production of Manganese Ferroalloys in Transferred-Arc Plasma Systems," Proceedings of The ISS/AIME 42nd Electric Furnace Conference, Toronto, 1984.

Segsworth, R.S., and Alcock, C.B. "Extended Arc Furnace and Process for Melting Particulate Charge therein", U.S. Patent 4006284, to Tibur Metals Ltd., (Feb. 1977).

Serin B., and Ellickson, R.T., "Determination of Diffusion Coefficients," J. Chem. Phys., vol.9, pp.742-746, Oct.(1941)

Seryakov, G.V, Baks, S.A., Strashun, E.P., and Tulyakov, N.V., "Nature of Limiting Step in the Chlorination of Titanium Dioxide Briquetted with Carbon," J. Appl. Chem. USSR, vol.43, No.8, pp.1653-1658, Aug.(1970)

Sharp, J.H., Brindley, G.W., and Narahari Achar,B.N, "Numerical Data for Some Commonly Used Solid State Reactions," J. Am. Ceram. Soc., vol.49, No.7, pp.379-382, (1966)

Sheer, C., Korman, S. and Gibson, J.O., U.S. Patent 3101308 (1963).

Shimada, S., Koyama, T., Kodaira, K., and Mastushita T., "Formation of NbC and TaC Solid-State Reaction," J. Material Science, vol.18, pp.1291-1296, (1983)

SKF Steel Engineering A.B., Information Brochure Hofors, Sweden (1983).

Smith, J.M. "Chemical Engineering Kinetics", 3rd edition, McGraw-Hill Book Co. (1981).

Sohn, H.Y., and Szekely, J., "A Structural Model for Gas-Solid Reactions with a Moving Boundary - III. A Generalized Dimensionless Representation of the Irreversible Reaction Between a Porous Solid and a Reaction Gas," Chem. Eng. Sci., vol.27, p.763, (1972)

Sohn, H.Y., and Szekely, J., "Reactions Between Solids Through Gaseous Intermediates-I Reactions Controlled by Chemical Reactions," Chem. Eng. Sci., vol.28, pp.1789-1801, (1973)

Sommerville, I.D., Mclean, A., and Alcock, C.B., "The Plasma Treatment of Waste Dusts, Fines and Slags," 115th TMS/AIME Annual Meeting, New Orleans, March 2-6, (1986)

Stokes, C.S., "Chemistry in High Temperature Plasma Jet", Adv. Chem. Ser. 80, Section 33, American Chemical Society, "Washington (1969).

Stuart, H. "Niobium in Perspective", Niobium '81, Proceedings of the International Symposium, San Francisco, Calif. (November 8-11, 1981).

Suri, A.K. and Gupta, C.K. "On the Carbothermic Reduction of Niobium and Vanadium Oxides", Trans. of the Indian Institute of Metals, vol.31, no.2 (April 1978).

Szekely, J. and Evans, J.W. "A Structural Model for Gas-Solid Reactions with a Moving Boundary", Chem. Eng. Sci., 25, 1091 (1970).

Szekely, J. and Evans, J.W. "Studies in Gas-Solid Reactions: Part I. A Structural Model for the Reaction of Porous Oxides with a Reducing Gas", Metall. Trans., 2, 1691 (1971a).

Szekely, J. and Evans, J.W. "Studies in Gas-Solid Reactions: Part II. An Experimental Study of Nickel Oxide Reduction with Hydrogen", Metall. Trans., 2, 1699 (1971b).

Szekely, J., Evans, J.W. and Sohn, H..Y. "Gas-Solid Reactions", Academic Press, New York (1976).

Tamhankar, S.S, and Doraiswamy, L.K., "Analysis of Solid-Solid Reactions: A Review," AIChE Journal, vol.25, No.4, pp.561-582, July(1979)

Taniuchi, K., and Mimura, K. "Arc-Plasma Reduction of Vanadium Oxide with Carbon", Sci. Rep. RITV, A-Vol.27, No.1 (1978).

Taplin, J.H., "Steady-State Kinetic Model for Solid-Fluid Reactions," J. Chem. Phys., vol.59, No.1, pp.194-199, July(1973)

Taplin, J.H., "Index of Reaction - A Unifying Concept for the Reaction Kinetics of Powders," J. Am. Ceram. Soc., vol.57, No.3, pp.140-143, Mar.(1974)

Tezuka, By.H., Sugiura, S., and Sugiyama, T. "Refining of Nickel-Base Alloys in a Plasma Induction Furnace", Proc. of 4th Int. Conf. on Vacuum Metall. (1974).

Tomas, J., Pereira, E., and Ronco, J., "Kinetic Study of The Solid-State Reaction Between Phthalic Anhydride and Sulfathiazole," I and EC Process Design and Development, vol.8, No.1, pp.120-124, Jan.(1969)

Tsantrizos, P. "The Characteristics Of Titanium Tetrachloride Plasmas in a Transferred-Arc Systems," Ph.D. Thesis, McGill University, March 1988.

Tsantrizos, P., ad Gauvin, W.H., "Operating Characteristics and Energy Distribution in a Nitrogen Transferred Arc Plasma", Canadian Journal of Chem. Engng. vol.60, no.6, (1982).

Turkdogan, E.T., "Physical Chemistry of High Temperature Technology," Academic Press, (1980)

Turkdogan, E.T., and Vinters, J.V., "Kinetics of Oxidation of Graphite and Charcoal in Carbon Dioxide," Carbon, vol.7, pp.101-117, (1969)

Turkdogan, E.T., and Vinters, J.V., "Gaseous Reduction of Iron Oxides: Part III. Reduction-Oxidation of Porous and Dense Iron Oxides and Iron," Metall. Trans., vol.3, pp.1561-1574, June(1972)

Tylko, J.K., to Plasma Holdings NV, UK Patent Application No. 7913337 (1979).

Tylko, J.K., Moore, J.J., and Reid, K.J., "Extraction of Metals in the new Sustained Shockwave Plasma (SSP) Reactor", Extraction Metallurgy '81, Inst. of Mining and Metall. Papers presented at a Symposium organized by IMM in London. (21-23 September 1981).

Udupa, A.R., Moore, J.J., and Smith, K.A., "Initial Studies of Chalcopyrite-Lime-Carbon Reactions Within a Plasma Environment", Paper presented at 113th AIME Annual Meeting, Los Angeles, California, TMS paper Selection No. A84-41 (Feb. 26-March 2, 1984).

Udupa, A.R., Moore, J.J., and Smith, K.A.,"Carbothermic Reduction of Chalcopyrite in the Presence of a Desulfurizer in a Plasma Medium," Metallurgical Transaction B, vol. 18B, p519-527, (September,1987)

Upadhya, K., Moore J.J., and Reid, K.J., "Application of Plasma Technology in Iron and Steelmaking", Journal of Metals, 36(2) (February 1984).

Upadhya, K., Moore, J.J, and Reid, K.J., "Application of Thermodynamic and Kinetic Principles in the Reduction of Metal Oxides in a Plasma Enviroment," Metallurgical Transaction B, Vol. 17B, pp197-207, March (1986)

Valensi, G., Kinetics of the Oxidation of Metallic Spherules and powders," Compt Rend., vol.22, No.4, pp.309-312, (1936)

Volkert, G. and Frank, K.D. "Metallurgy of Ferroalloys", Chapter 10, 2nd edition, Springer-Verlag, Berline Heidelberg, New York (1972).

Weast, R.C. and Astley, M.J., "CRC Handbook of Physics and Chemistry," 61st Edition, CRC Press, Inc., Boca Raton, Fla., (1979)

Welty, J.R., "Engineering Heat Transfer," John Wiley and Sons, Inc., (1974)

Wickens, A.J. "Formation of Boron Carbide in an High Intensity Arc Plasma", Chemistry and Industry, no.8, p.316-317 (3rd April 1976).

Winkler, O. and Bakish, R. "Vacuum Metallurgy", Elsevier Publishing Company, Amsterdam (1971).

Wynnyckyj, J.R., and Rankin, W.J., "An Intrinsic-Transport Model for Solid-Solid Reactions Involving a Gaseous Intermediate," Metall. Trans. B, Vol.19b, pp.73-81, Feb.(1988)

Yun, T.S., "Direct Reduction of Ferric Oxide by Solid Carbon in Vacuum," Trans. ASM, vol.54, pp.129-142,(1961)

Zhuravlev, I., Lessokhin, I.G., and Tempel'man, R.G., "Kinetics of the Reaction for the Formation of Aluminates and the Role of Mineralizers in This Process," J. Appl. Chem. USSR (English Transl.) vol.21, No.9, pp.887-902, (1948)

Zimmerley, S.R., and Back, A.E., "Smelting Process for Recovering Columbium and/or Tantalum from Low-Grade Ore Materials Containing Same," U.S. Patent No. 2972530, Feb. 21, (1961)

Appendix I

Composition and Dimension of Pellets

APPENDIX I

Composition and Dimensions of Pellets

Nb2O5	Pyrochlore	Graphite	Molasses	Iron	Iron Oxide	C/Nb2O5 Mole Ratio	Graphite Particle Size	Nb2O5 or Pyrochlore Particle Size	Diameter	Diameter Standard Deviation	Height	Height Standard Deviation	Porosity
wt. %	wt. %	wt. %	wt. %	wt. %	wt. %		microns	microns	mm	mm	mm	mm	-
70.2	n/a	22.2	7.6	0.0	0.0	7	<45	10	12.89	0.03	15.1	0.5	0.44
70.2	n/a	22.1	7.6	0.0	0.0	7	165	10	12.97	0.02	16.7	0.3	0.47
70.2	n/a	22.1	7.6	0.0	0.0	7	165	10	12.94	0.01	14.0	0.4	0.40
70.2	n/a	22.1	7.6	0.0	0.0	7	463	10	12.87	-	14.8	0.1	0.41
78.2	n/a	14.8	7.0	0.0	0.0	5	<45	10	12.89	0.01	15.5	0.1	0.43
64.8	n/a	29.2	6.0	0.0	0.0	10	<45	10	12.91	0.00	17.8	0.3	0.44
58.1	n/a	36.7	5.1	0.0	0.0	14	<45	10	12.92	0.01	20.6	0.3	0.44
53	n/a	16.8	4.7	25.5	0.0	7	<45	10	12.90	0.02	16.7	0.6	0.44
53	n/a	16.8	4.7	25.5	0.0	7	463	10	12.85	0.01	16.9	0.4	0.42
20.9	n/a	6.6	2.4	70.1	0.0	7	<45	10	18.47	0.01	14.3	0.2	0.40
20.9	n/a	9.4	1.2	68.1	0.0	10	<45	10	18.49	0.01	15.9	0.2	0.42
20.1	n/a	12.7	1.8	65.4	0.0	14	<45	10	18.47	-	17.1	0.1	0.41
n/a	79.7	15.4	4.8	0.0	0.0	7	<45	60	12.86	0.02	16.1	0.5	0.28
n/a	79.7	15.4	4.8	0.0	0.0	7	<45	60	18.47	0.01	11.3	0.0	0.30
n/a	79.7	15.4	4.8	0.0	0.0	7	165	60	13.07	0.01	17.2	0.1	0.36
n/a	79.7	15.4	4.8	0.0	0.0	7	463	60	12.84	0.01	16.6	0.9	0.31
n/a	79.7	15.4	4.8	0.0	0.0	7	<45	31	12.85	0.13	16.7	0.2	0.32
n/a	79.7	15.4	4.8	0.0	0.0	7	<45	90	12.88	0.01	15.4	0.2	0.26
n/a	79.7	15.4	4.8	0.0	0.0	7	<45	230	12.85	0.01	15.0	0.2	0.24
n/a	85.4	9.8	4.7	0.0	0.0	5	<45	60	12.85	-	17.6	0.3	0.27
n/a	75.3	20.7	4.0	0.0	0.0	10	<45	60	12.91	-	19.4	0.1	0.32
n/a	69.1	26.6	4.3	0.0	0.0	14	<45	60	12.92	0.00	21.9	0.1	0.32
n/a	73.6	14.2	4.1	8.1	0.0	7	<45	60	12.83	0.00	18.0	0.1	0.30
n/a	65.0	12.5	3.4	19.1	0.0	7	<45	60	12.82	0.06	19.6	0.0	0.31
n/a	65.0	12.5	3.4	19.1	0.0	7	463	60	12.84	0.01	20.5	0.1	0.35
n/a	65.0	12.5	3.4	19.1	0.0	7	<45	230	12.82	0.01	18.4	0.1	0.27
n/a	29.5	5.7	2.4	62.5	0.0	7	<45	60	18.47	0.00	16.9	0.1	0.40
n/a	29.1	11.2	1.7	57.9	0.0	7	<45	60	18.47	0.02	19.5	0.1	0.40
n/a	29.1	11.2	1.7	57.9	0.0	7	<45	60	12.94	0.02	16.4	0.3	0.40
n/a	57.2	16.3	3.1	0.0	23.3	7	<45	60	18.38	0.02	11.4	0.2	0.30
n/a	21.6	17.6	1.7	0.0	59.6	7	<45	60	18.45	0.04	21.1	0.3	0.41

n/a - not applicable

Appendix II

Experimental Data for Chapter V

TABLE II-A

Argon Gas Flowrate - 4.5 E-4 Ncu.m/s
Carbon Concentration - 24.0 wt.%
C/Nb2O5 Mole Ratio - 7
Nb2O5 Particle Diameter - 10 microns
Graphite Particle Diameter - <45 microns
Average Pellet Diameter - 12.9 mm

Expt. No.	Pellet Height	Pellet Temperature	95% confidence intreval, +/-	Conversion CO/CO2	Conversion Wt. loss	Reaction Constant	95% confidence interval, +/-	Reaction Time
	mm	K	K			1/s	1/s	s
1	15.4	1765	6	0.98	1.00	0.027	0.001	184
2	14.8	1805	12	0.92	0.92	0.026	0.001	184
3	14.5	1810	18	0.58	0.59	0.021	0.000	71
4	15.0	1830	19	0.64	0.66	0.027	0.001	66
5	15.7	2285	35	1.00	1.01	0.040	0.001	95
6	15.9	2555	45	0.91	1.08	0.050	0.001	71
7	15.5	2270	37	0.90	1.02	0.038	0.001	83
8	15.6	2300	36	0.89	1.02	0.035	0.001	85
9	14.4	2545	46	0.95	1.04	0.063	0.004	71
10	14.7	2505	44	0.94	1.03	0.058	0.004	71
11	14.6	2485	48	0.99	1.01	0.053	0.003	83
12	14.6	2240	22	0.94	1.00	0.041	0.002	83
13	15.0	2480	26	0.94	1.00	0.061	0.004	71
14	15.0	2335	9	0.93	0.90	0.037	0.001	102
15	14.6	1675	50	0.77	0.85	0.015	0.001	119

TABLE II- B

Argon Gas Flowrate - 4.5 E-4 Ncu.m/s
Carbon Concentration - 24.0 wt.%
C/Nb2O5 Mole Ratio - 7
Nb2O5 Particle Diameter - 10 microns
Graphite Particle Diameter - 165 microns
Average Pellet Diameter - 12.9 mm

Expt. No.	Pellet Height	Pellet Temperature	95% confidence intreval, +/-	Conversion CO/CO2	Conversion Wt. loss	Reaction Constant	95% confidence interval, +/-	Average Reaction CO/CO2 Ratio	Reaction Time
	mm	K	K			1/s	1/s		s
16	16.6	2105	4	0.45	0.64	0.0100	0.0003	19	95
17	17.3	1645	7	0.29	0.42	0.0073	0.0003	14	78
18	16.7	2020	9	0.32	0.44	0.0085	0.0004	18	83
19	16.4	2195	30	0.48	0.63	0.0149	0.0012	16	71
20	16.8	2190	34	0.47	0.63	0.0157	0.0004	20	71
21	17.2	2070	33	0.48	0.62	0.0139	0.0004	18	85
22	16.6	2255	6	0.57	0.73	0.0234	0.0012	15	92
23	14.1	2290	37	0.81	0.86	0.0231	0.0005	15	88
24	14.3	2495	17	0.79	0.91	0.0332	0.0009	16	71
25	14.2	2350	36	0.87	0.98	0.0296	0.0005	18	92
26	14.3	2435	26	0.85	0.95	0.0325	0.0012	15	90
27	13.9	2450	33	0.84	0.91	0.0303	0.0007	14	88
28	16.4	1905	22	0.46	0.59	0.0106	0.0003	14	114
29	13.3	2095	21	0.60	0.65	0.0122	0.0004	14	138
30	16.4	1695	12	0.28	0.48	0.0074	0.0004	10	66
31	16.8	1625	9	0.26	0.38	0.0071	0.0003	10	66
32	16.7	1755	18	0.38	0.70	0.0084	0.0003	12	90

TABLE II- C

Argon Gas Flowrate - 4.5 E-4 Ncu.m/s
Carbon Concentration - 24.0 wt.%
C/Nb2O5 Mole Ratio - 7
Nb2O5 Particle Diameter - 10 microns
Graphite Particle Diameter - 465 microns
Average Pellet Diameter - 12.9 mm

Expt. No.	Pellet Height	Pellet Temperature	95% confidence intreval, +/-	Conversion CO/CO2	Wt. loss	Reaction Constant	95% confidence interval, +/-	Average CO/CO2 Ratio	Reaction Time
	mm	K	K			1/s	1/s		s
33	14.6	1710	15	0.49	0.57	0.0099	0.0004	26	128
34	14.6	1770	22	0.60	0.70	0.0130	0.0004	25	116
35	14.7	2465	51	0.92	1.00	0.0221	0.0019	30	126
36	14.8	2515	26	0.88	0.93	0.0228	0.0009	50	138
37	14.9	2625	40	0.82	0.88	0.0228	0.0007	30	119
38	14.9	2695	27	1.00	1.02	0.0410	0.0014	24	100
39	14.8	2855	31	0.94	1.05	0.0368	0.0019	35	100
40	14.8	2780	36	0.92	1.01	0.0355	0.0005	24	95
41	14.8	2590	28	0.90	0.98	0.0292	0.0010	22	119
42	14.7	1960	15	0.50	0.61	0.0158	0.0009	24	110

TABLE II- D

Argon Gas Flowrate - 4.5 E-4 Ncu.m/s
Carbon Concentration - 24.0 wt.%
C/Nb2O5 Mole Ratio - 5
Nb2O5 Particle Diameter - 10 microns
Graphite Particle Diameter - <45 microns
Average Pellet Diameter - 12.9 mm

Expt. No.	Pellet Height	Pellet Temperature	95% confidence intreval, +/-	Conversion CO/CO2	Wt. loss	Reaction Constant	95% confidence interval, +/-	Average CO/CO2 Ratio	Reaction Time
	mm	K	K			1/s	1/s		s
43	15.7	2150	20	0.74	0.87	0.0094	0.0001	16	190
44	15.5	2145	17	0.80	0.90	0.0086	0.0002	11	220
45	15.6	1975	8	0.65	0.82	0.0061	0.0002	18	205
46	15.4	2070	12	0.78	0.91	0.0134	0.0003	19	195
47	15.4	2050	12	0.69	0.78	0.0128	0.0007	15	186

TABLE II- E

Argon Gas Flowrate - 4.5 E-4 Ncu.m/s
Carbon Concentration - 24.0 wt.%
C/Nb2O5 Mole Ratio - 10
Nb2O5 Particle Diameter - 10 microns
Graphite Particle Diameter - <45 microns
Average Pellet Diameter - 12.9 mm

Expt. No.	Pellet Height	Pellet Temperature	95% confidence intreval, +/-	Conversion CO/CO2	Wt. loss	Reaction Constant	95% confidence interval, +/-	Average CO/CO2 Ratio	Reaction Time
	mm	K	K			1/s	1/s		s
48	17.6	1945	10	1.00	1.07	0.0358	0.0010	25	160
49	18.1	1830	5	0.99	1.05	0.0477	0.0012	25	145
50	18.0	1925	12	1.00	1.08	0.0410	0.0024	30	140
51	17.6	2080	16	1.00	1.05	0.0432	0.0011	22	140
52	17.4	2000	19	0.98	1.06	0.0334	0.0013	14	138

TABLE II- F

Argon Gas Flowrate - 4.5 E-4 Ncu.m/s
Carbon Concentration - 24.0 wt.%
C/Nb2O5 Mole Ratio - 14
Nb2O5 Particle Diameter - 10 microns
Graphite Particle Diameter - <45 microns
Average Pellet Diameter - 12.9 mm

Expt. No.	Pellet Height mm	Pellet Temperature K	95% confidence intreval, +/- K	Conversion CO/CO2	Wt. loss	Reaction Constant 1/s	95% confidence interval, +/- 1/s	Average Reaction CO/CO2 Ratio	Time s
53	21.1	1990	17	1.0	1.09	0.0535	0.0009	28	88
54	20.6	1910	17	1.0	1.08	0.0596	0.0089	30	66
55	20.8	1855	10	1.0	1.11	0.0443	0.0009	30	135
56	20.3	1955	15	1.0	1.10	0.0362	0.0005	33	157
57	20.4	1950	10	0.98	1.08	0.0344	0.0004	35	210
58	20.3	1855	5	0.99	1.09	0.0434	0.0018	40	166

TABLE II- G

Argon Gas Flowrate - 4.5 E-4 Ncu.m/s
Carbon Concentration - 24.0 wt.%
C/Nb2O5 Mole Ratio - 14
Nb2O5 Particle Diameter - 10 microns
Graphite Particle Diameter - <45 microns
Average Pellet Diameter - 12.9 mm
BINDER - WATER ONLY

Expt. No.	Pellet Height mm	Pellet Temperature K	95% confidence intreval, +/- K	Conversion CO/CO2	Wt. loss	Reaction Constant 1/s	95% confidence interval, +/- 1/s	Average Reaction CO/CO2 Ratio	Time s
59	8.5	1895	6	0.61	0.98	0.0173	0.0007	20	90

Appendix III

Experimental Data for Chapter VI

TABLE III - A

Argon Gas Flowrate - 4.5 E-4 Ncu.m/s
Carbon Concentration - 16.25 wt.%
C/Nb2O5 Mole Ratio - 7
Pyrochlore Particle Diameter - 60 microns
Graphite Particle Diameter - <45 microns
Average Pellet Diameter - 12.9 mm

Expt. No.	Pellet Height	Pellet Temperature	95% confidence intreval, +/-	Conversion CO/CO2	Wt. loss	Reaction Constant	95% confidence interval, +/-	Reaction Time
	mm	K	K			1/s	1/s	s
60	16.9	2160	29	0.93	1.07	0.0171	0.0003	170
61	16.6	2130	47	0.96	1.07	0.0183	0.0002	170
62	16.6	2140	30	0.69	0.87	0.0150	0.0003	97
63	15.8	1950	27	0.78	0.86	0.0118	0.0005	172
64	15.7	2330	40	0.83	0.95	0.0234	0.0005	120
65	15.9	1825	12	0.77	0.87	0.0102	0.0002	170
66	15.9	1785	25	0.80	0.84	0.0103	0.0004	196
67	15.6	2115	16	0.83	0.86	0.0154	0.0003	160
68	15.7	2330	40	0.84	0.91	0.0223	0.0005	121
69	15.9	2130	31	0.78	0.92	0.0172	0.0011	112

TABLE III - B

Argon Gas Flowrate - 4.5 E-4 Ncu.m/s
Carbon Concentration - 16.25 wt.%
C/Nb2O5 Mole Ratio - 7
Pyrochlore Particle Diameter - 60 microns
Graphite Particle Diameter - 165 microns
Average Pellet Diameter - 13.1 mm

Expt. No.	Pellet Height	Pellet Temperature	95% confidence intreval, +/-	Conversion CO/CO2	Wt. loss	Reaction Constant	95% confidence interval, +/-	Reaction Time
	mm	K	K			1/s	1/s	s
70	17.2	1810	26	0.77	0.93	0.0100	0.0002	168
71	17.3	1695	17	0.65	0.88	0.0076	0.0002	158
72	17.2	1825	17	0.79	0.88	0.0090	0.0001	176
73	17.1	1980	27	0.77	0.89	0.0130	0.0005	120
74	17.2	2090	38	0.85	1.00	0.0141	0.0002	143
75	17.3	2075	22	0.82	0.84	0.0139	0.0004	142
76	17.2	2085	28	0.78	0.93	0.0137	0.0005	128
77	17.3	2360	53	0.82	0.97	0.0253	0.0003	83
78	17.2	2440	30	0.92	0.92	0.0313	0.0004	114
79	17.2	2345	38	0.79	0.87	0.0261	0.0006	103
80	17.1	1745	28	0.73	0.83	0.0065	0.0000	209
81	17.6	1865	24	0.75	0.85	0.0119	0.0005	115

TABLE III - C

Argon Gas Flowrate - 4.5 E-4 Ncu.m/s
Carbon Concentration - 16.25 wt.%
C/Nb2O5 Mole Ratio - 7
Pyrochlore Particle Diameter - 60 microns
Graphite Particle Diameter - 463 microns
Average Pellet Diameter - 12.8 mm

Expt. No.	Pellet Height	Pellet Temperature	95% confidence intreval, +/-	Conversion CO/CO2	Wt. loss	Reaction Constant	95% confidence interval, +/-	Reaction Time
	mm	K	K			1/s	1/s	s
82	17.5	1775	33	0.79	0.86	0.0094	0.0001	162
83	17.2	2165	32	0.84	1.01	0.0178	0.0002	112
84	17.4	1800	29	0.63	0.77	0.0084	0.0000	108
85	15.5	2135	33	0.73	0.87	0.0165	0.0006	107
86	15.9	2405	43	0.81	0.92	0.0212	0.0007	90
87	16.0	2345	29	0.84	0.93	0.0209	0.0008	97

TABLE III - D

Argon Gas Flowrate - 4.4 E-4 Ncu.m/s
Carbon Concentration - 16.25 wt.%
C/Nb2O5 Mole Ratio - 7
Pyrochlore Particle Diameter - 230 microns
Graphite Particle Diameter - <45 microns
Average Pellet Diameter - 12.8 mm

Expt. No.	Pellet Height	Pellet Temperature	95% confidence intreval, +/-	Conversion CO/CO2	Wt. loss	Reaction Constant	95% confidence interval, +/-	Reaction Time
	mm	K	K			1/s	1/s	s
88	15.5	1810	28	0.80	0.96	0.0096	0.0002	192
89	14.9	1530	8	0.75	0.92	0.0052	0.0001	262
90	14.8	1905	10	0.75	0.91	0.0092	0.0002	188
91	14.9	2235	28	0.81	1.00	0.0135	0.0004	151
92	14.9	2355	27	0.86	1.00	0.0184	0.0004	130
93	15.0	2355	28	0.85	1.00	0.0182	0.0006	138
94	14.9	1845	25	0.80	0.92	0.0087	0.0001	209
95	14.8	2130	46	0.79	0.91	0.0120	0.0006	140

TABLE III - E

Argon Gas Flowrate - 4.5 E-4 Ncu.m/s
Carbon Concentration - 16.25 wt.%
C/Nb2O5 Mole Ratio - 7
Nb2O5 Particle Diameter - 98 microns
Graphite Particle Diameter - <45 microns
Average Pellet Diameter - 12.9 mm

Expt. No.	Pellet Height	Pellet Temperature	95% confidence intreval, +/-	Conversion CO/CO2	Wt. loss	Reaction Constant	95% confidence interval, +/-	Reaction Time
	mm	K	K			1/s	1/s	s
96	15.2	1715	17	0.78	0.87	0.0095	0.0003	172
97	15.6	1885	28	0.79	0.87	0.0112	0.0004	168
98	15.4	1745	4	0.77	0.88	0.0093	0.0002	194
99	15.2	2165	22	0.82	0.91	0.0140	0.0008	151
100	15.5	2120	6	0.79	0.91	0.0139	0.0007	151
101	15.7	2335	22	0.82	1.00	0.0202	0.0009	137
102	15.5	2305	21	0.82	0.93	0.0182	0.0008	132

TABLE III - F

Argon Gas Flowrate - 4.5 E-4 Ncu.m/s
Carbon Concentration - 16.25 wt.%
C/Nb2O5 Mole Ratio - 7
Pyrochlore Particle Diameter - 31 microns
Graphite Particle Diameter - <45 microns
Average Pellet Diameter - 12.9 mm

Expt. No.	Pellet Height	Pellet Temperature	95% confidence intreval, +/-	Conversion CO/CO2	Wt. loss	Reaction Constant	95% confidence interval, +/-	Reaction Time
	mm	K	K			1/s	1/s	s
103	17.0	1725	15	0.82	0.91	0.0103	0 31	197
104	16.5	1810	5	0.80	0.96	0.0126	0.0002	161
105	16.8	1875	11	0.77	0.86	0.0121	0.0004	132
106	16.5	2120	21	0.84	0.93	0.0170	0.0007	127
107	16.5	2150	18	0.84	0.93	0.0172	0.0009	144
108	17.0	2305	17	0.85	0.95	0.0247	0.0010	132
109	16.5	2280	18	0.92	0.98	0.0258	0.0010	132

TABLE III - G

Argon Gas Flowrate - 4.5 E-4 Ncu.m/s
Carbon Concentration - 10.35 wt.%
C/Nb2O5 Mole Ratio - 5
Pyrochlore Particle Diameter - 60 microns
Graphite Particle Diameter - <45 microns
Average Pellet Diameter - 12.9 mm

Expt. No.	Pellet Height	Pellet Temperature	95% confidence intreval, +/-	Conversion CO/CO2	Wt. loss	Reaction Constant	95% confidence interval, +/-	Average CO/CO2 Ratio	Reaction Time
	mm	K	K			1/s	1/s		s
110	17.8	1820	17	0.48	0.69	0.0043	0.0001	15	253
111	17.8	1805	4	0.50	0.68	0.0038	0.0000	10	240
112	17.7	1785	3	0.50	0.63	0.0040	0.0001	15	176
113	17.8	1830	18	0.52	0.70	0.0032	0.0001	12	318
114	17.8	1835	15	0.50	0.64	0.0038	0.0000	9	220

TABLE III - H

Argon Gas Flowrate - 4.5 E-4 Ncu.m/s
Carbon Concentration - 21.6 wt.%
C/Nb2O5 Mole Ratio - 10
Pyrochlore Particle Diameter - 60 microns
Graphite Particle Diameter - <45 microns
Average Pellet Diameter - 12.9 mm

Expt. No.	Pellet Height	Pellet Temperature	95% confidence intreval, +/-	Conversion CO/CO2	Wt. loss	Reaction Constant	95% confidence interval, +/-	Average CO/CO2 Ratio	Reaction Time
	mm	K	K			1/s	1/s		s
115	19.3	1870	34	0.89	1.13	0.0187	0.0005	250	260
116	19.4	1935	29	0.79	1.12	0.0186	0.0009	-	224
117	19.3	1775	21	0.95	1.10	0.0193	0.0004	-	254
118	19.3	1915	32	0.93	1.10	0.0170	0.0005	-	286

TABLE III - I

Argon Gas Flowrate - 4.5 E-4 Ncu.m/s
Carbon Concentration - 27.83 wt.%
C/Nb2O5 Mole Ratio - 14
Pyrochlore Particle Diameter - 60 microns
Graphite Particle Diameter - <45 microns
Average Pellet Diameter - 12.9 mm

Expt. No.	Pellet Height	Pellet Temperature	95% confidence intreval, +/-	Conversion CO/CO2	Wt. loss	Reaction Constant	95% confidence interval, +/-	Average CO/CO2 Ratio	Reaction Time
	mm	K	K			1/s	1/s		s
119	22.0	1665	4	0.89	1.03	0.0169	0.0006	-	248
120	21.8	1605	9	0.99	1.10	0.0148	0.0010	-	340
121	22.0	1695	16	0.93	1.18	0.0133	0.0004	-	340
122	21.8	1660	12	0.97	1.14	0.0141	0.0004	-	330

TABLE III - J

Argon Gas Flowrate - 4.5 E-4 Ncu.m/s
Carbon Concentration - 16.25 wt.%
C/Nb2O5 Mole Ratio - 7
Pyrochlore Particle Diameter - 60 microns
Graphite Particle Diameter - <45 microns
Average Pellet Diameter - 18.5 mm

Expt. No.	Pellet Height	Pellet Temperature	95% confidence intreval, +/-	Conversion CO/CO2	Conversion Wt. loss	Reaction Constant	95% confidence interval, +/-	Average Reaction CO/CO2 Ratio	Reaction Time
	mm	K	K			1/s	1/s		s
123	16.5	1765	10	0.66	0.82	0.0054	0.0000	120	244
124	16.6	1615	16	0.66	0.78	0.0048	0.0000	150	270

TABLE III - K

Argon Gas Flowrate - 4.5 E-4 Ncu.m/s
Carbon Concentration - 16.25 wt.%
C/Nb2O5 Mole Ratio - 7
Pyrochlore Particle Diameter - 60 microns
Graphite Particle Diameter - <45 microns
Average Pellet Diameter - 18.5 mm
BINDER - WATER ONLY

Expt. No.	Pellet Height	Pellet Temperature	95% confidence intreval, +/-	Conversion CO/CO2	Conversion Wt. loss	Reaction Constant	95% confidence interval, +/-	Average Reaction CO/CO2 Ratio	Reaction Time
	mm	K	K			1/s	1/s		s
125	12.9	1780	10	0.33	0.60	0.0097	0.0004	30	95

Appendix IV

Experimental Data for Chapter VII

TABLE IV - A

Argon Gas Flowrate - 4.5 E-4 Ncu.m/s
Carbon Concentration - 17.6 wt.%
Iron Concentration - 26.7 wt.%
C/Nb2O5 Mole Ratio - 7
Nb2O5 Particle Diameter - 10 microns
Graphite Particle Diameter - <45 microns
Iron Particle Diameter - <45 microns
Average Pellet Diameter - 12.9 mm

Expt. No.	Pellet Height	Pellet Temperature	95% confidence intreval, +/-	Conversion CO/CO2	Conversion Wt. loss	Reaction Constant	95% confidence interval, +/-	Average Reaction CO/CO2 Ratio	Reaction Time
	mm	K	K			1/s	1/s		s
126	16.9	2000	9	0.83	1.10	0.0229	0.0001	20	95
127	17.8	2050	10	0.79	1.12	0.0336	0.0012	20	64
128	16.3	2025	10	0.78	1.05	0.0233	0.0011	18	80
129	16.6	2165	15	0.89	1.31	0.0465	0.0012	30	80
130	16.2	2125	13	0.90	1.22	0.0152	0.0011	29	71
131	17.1	2215	12	0.91	1.26	0.0515	0.0009	30	61
132	16.7	2165	8	0.92	1.26	0.0514	0.0008	30	61
133	16.1	2045	13	0.84	0.82	0.0347	0.0015	15	71

TABLE IV - B

Argon Gas Flowrate - 4.5 E-4 Ncu.m/s
Carbon Concentration - 17.6 wt.%
Iron Concentration - 26.7 wt.%
C/Nb2O5 Mole Ratio - 7
Nb2O5 Particle Diameter - 10 microns
Graphite Particle Diameter - 463 microns
Iron Particle Diameter - <45 microns
Average Pellet Diameter - 12.9 mm

Expt. No.	Pellet Height	Pellet Temperature	95% confidence intreval, +/-	Conversion CO/CO2	Conversion Wt. loss	Reaction Constant	95% confidence interval, +/-	Average Reaction CO/CO2 Ratio	Reaction Time
	mm	K	K			1/s	1/s		s
134	17.1	2285	12	0.78	0.99	0.0249	0.0003	25	83
135	17.2	2255	8	0.84	1.02	0.0285	0.0004	30	85
136	17.0	2305	8	0.89	1.12	0.0358	0.0005	40	85
137	17.2	2330	5	0.92	1.16	0.0399	0.0006	40	83
138	17.1	2440	11	0.93	1.18	0.0499	0.0008	28	73
139	16.1	1985	12	0.79	0.94	0.0133	0.0002	40	140

TABLE IV - C

Argon Gas Flowrate - 4.5 E-4 Ncu.m/s
Carbon Concentration - 6.7 wt.%
Iron Concentration - 71.8 wt.%
C/Nb2O5 Mole Ratio - 7
Nb2O5 Particle Diameter - 10 microns
Graphite Particle Diameter - <45 microns
Iron Particle Diameter - <45 microns
Average Pellet Diameter - 18.5 mm

Expt. No.	Pellet Height	Pellet Temperature	95% confidence intreval, +/-	Conversion CO/CO2	Wt. loss	Reaction Constant	95% confidence interval, +/-	Average CO/CO2 Ratio	Reaction Time
	mm	K	K			1/s	1/s		s
140	14.4	1575	6	0.51	1.17	0.0048	0.0048	12	160
141	14.3	1620	8	0.92	1.57	0.0108	0.0003	15	181
142	14.3	1680	7	0.93	1.83	0.0157	0.0002	17	174
143	14.4	1650	5	0.96	1.82	0.0127	0.0003	16	200
144	14.6	1705	5	1.00	2.08	0.0302	0.0004	20	120
145	14.5	1795	11	0.56	1.12	0.0249	0.0006	17	47
146	14.4	1840	6	0.97	1.61	0.0474	0.0006	24	90
147	14.3	1720	17	0.98	1.69	0.0358	0.0009	21	104
148	14.4	1845	15	0.93	1.70	0.0381	0.0006	23	95
149	13.9	1635	9	0.72	1.53	0.0101	0.0001	28	179
150	14.4	1600	8	0.65	1.12	0.0068	0.0001	20	172

TABLE IV - D

Argon Gas Flowrate - 4.5 E-4 Ncu.m/s
Carbon Concentration - 9.5 wt.%
Iron Concentration - 68.9 wt.%
C/Nb2O5 Mole Ratio - 10
Nb2O5 Particle Diameter - 10 microns
Graphite Particle Diameter - <45 microns
Iron Particle Diameter - <45 microns
Average Pellet Diameter - 18.5 mm

Expt. No.	Pellet Height	Pellet Temperature	95% confidence intreval, +/-	Conversion CO/CO2	Wt. loss	Reaction Constant	95% confidence interval, +/-	Average CO/CO2 Ratio	Reaction Time
	mm	K	K			1/s	1/s		s
151	16.0	1780	8	0.34	0.75	0.0079	0.0004	12	100
152	16.1	1860	9	0.79	1.38	0.0163	0.0009	20	105
153	16.1	1930	9	0.91	1.60	0.0199	0.0002	21	130
154	16.0	2135	2	0.98	1.70	0.0275	0.0007	26	124
155	15.7	1995	15	1.00	1.60	0.0195	0.0004	26	150
156	16.1	2125	7	1.00	1.64	0.0280	0.0004	30	124
157	16.0	2020	11	0.91	2.28	0.0208	0.0006	22	118
158	15.5	1830	7	0.65	1.13	0.0096	0.0005	17	165

TABLE IV - E

Argon Gas Flowrate - 4.5 E-4 Ncu.m/s
Carbon Concentration - 12.9 wt.%
Iron Concentration - 66.6 wt.%
C/Nb2O5 Mole Ratio - 14
Nb2O5 Particle Diameter - 10 microns
Graphite Particle Diameter - <45 microns
Iron Particle Diameter - <45 microns
Average Pellet Diameter - 18.5 mm

Expt. No.	Pellet Height	Pellet Temperature	95% confidence intreval, +/-	Conversion CO/CO2	Wt. loss	Reaction Constant	95% confidence interval, +/-	Average CO/CO2 Ratio	Reaction Time
	mm	K	K			1/s	1/s		s
159	17.3	2025	12	0.71	1.56	0.0108	0.0004	16	140
160	17.4	2035	7	0.85	1.76	0.0169	0.0005	30	116

Appendix V

Experimental Data for Chapter VIII

TABLE V - A

Argon Gas Flowrate - 4.5 E-4 Ncu.m/s
Carbon Concentration - 12.98 wt.%
Iron Concentration - 19.6 wt.%
C/Nb2O5 Mole Ratio - 7
Pyrochlore Particle Diameter - 60 microns
Graphite Particle Diameter - <45 microns
Iron Particle Diameter - <45 microns
Average Pellet Diameter - 12.9 mm

Expt. No.	Pellet Height	Pellet Temperature	95% confidence intreval, +/-	Conversion CO/CO2	Conversion Wt. loss	Reaction Constant	95% confidence interval, +/-	Average CO/CO2 Ratio	Reaction Time
	mm	K	K			1/s	1/s		s
161	19.5	1690	5	0.69	0.81	0.0061	0.0001	69	234
162	18.8	1765	9	0.71	0.82	0.0080	0.0002	83	234
163	19.6	1775	10	0.72	0.82	0.0084	0.0003	83	265
164	19.8	1835	7	0.74	0.83	0.0143	0.0013	80	130
165	19.5	1795	3	0.75	0.90	0.0144	0.0004	100	114
166	19.6	1835	5	0.74	0.86	0.0148	0.0007	65	133
167	19.6	1950	5	0.73	0.89	0.0156	0.0007	62	124
168	19.7	1900	4	0.76	0.95	0.0178	0.0002	70	133
169	19.7	1980	8	0.76	0.91	0.0210	0.0008	95	121
170	19.6	1960	12	0.77	0.91	0.0179	0.0006	95	119
171	19.7	1950	3	0.77	0.88	0.0192	0.0004	175	119
172	19.8	2035	7	0.76	1.12	0.0198	0.0006	75	104
173	19.5	1685	10	0.70	0.83	0.0067	0.0002	100	260

TABLE V - B

Argon Gas Flowrate - 4.5 E-4 Ncu.m/s
Carbon Concentration - 12.98 wt.%
Iron Concentration - 19.6 wt.%
C/Nb2O5 Mole Ratio - 7
Pyrochlore Particle Diameter - 60 microns
Graphite Particle Diameter - 463 microns
Iron Particle Diameter - <45 microns
Average Pellet Diameter - 12.9 mm

Expt. No.	Pellet Height	Pellet Temperature	95% confidence intreval, +/-	Conversion CO/CO2	Conversion Wt. loss	Reaction Constant	95% confidence interval, +/-	Average CO/CO2 Ratio	Reaction Time
	mm	K	K			1/s	1/s		s
174	20.4	1645	8	0.69	0.81	0.0062	0.0002	40	255
175	20.6	1575	5	0.62	0.74	0.0059	0.0006	57	265
176	20.5	1720	11	0.67	0.81	0.0106	0.0002	54	150
177	20.4	1850	12	0.69	0.82	0.0124	0.0003	58	135
178	20.6	1810	5	0.68	0.81	0.0143	0.0004	83	100
179	20.5	1700	6	0.70	0.83	0.0096	0.0003	56	190
180	20.6	1670	17	0.64	0.78	0.0069	0.0001	40	193
181	20.6	1755	9	0.69	0.81	0.0101	0.0003	60	160
182	20.5	1795	10	0.68	0.81	0.0108	0.0002	76	155

TABLE V - C

Argon Gas Flowrate - 4.5 E-4 Ncu.m/s
Carbon Concentration - 12.98 wt.%
Iron Concentration - 19.6 wt.%
C/Nb2O5 Mole Ratio - 7
Pyrochlore Particle Diameter - 230 microns
Graphite Particle Diameter - <45 microns
Iron Particle Diameter - <45 microns
Average Pellet Diameter - 12.9 mm

Expt. No.	Pellet Height	Pellet Temperature	95% confidence intreval, +/-	Conversion CO/CO2	Conversion Wt. loss	Reaction Constant	95% confidence interval, +/-	Average CO/CO2 Ratio	Reaction Time
	mm	K	K			1/s	1/s		s
183	18.3	1695	6	0.58	0.77	0.0060	0.0002	60	196
184	18.4	1680	6	0.64	0.64	0.0039	0.0001	38	205
185	18.4	1875	8	0.86	0.86	0.0096	0.0004	80	148
186	18.4	1920	9	0.84	0.84	0.0090	0.0003	50	150
187	18.4	1990	9	0.91	0.91	0.0129	0.0003	75	120
188	18.6	1965	8	0.89	0.89	0.0129	0.0005	100	120
189	18.3	1955	7	0.92	0.92	0.0118	0.0005	100	107
190	18.4	1860	3	0.86	0.86	0.0087	0.0003	120	157
191	18.6	1760	11	0.72	0.72	0.0049	0.0002	45	210

TABLE V - D

Argon Gas Flowrate - 4.5 E-4 Ncu.m/s
Carbon Concentration - 14.80 wt.%
Iron Concentration - 8.44 wt.%
C/Nb2O5 Mole Ratio - 7
Pyrochlore Particle Diameter - 60 microns
Graphite Particle Diameter - <45 microns
Iron Particle Diameter - <45 microns
Average Pellet Diameter - 12.9 mm

Expt. No.	Pellet Height	Pellet Temperature	95% confidence intreval, +/-	Conversion CO/CO2	Conversion Wt. loss	Reaction Constant	95% confidence interval, +/-	Average CO/CO2 Ratio	Reaction Time
	mm	K	K			1/s	1/s		s
192	18.0	1820	10	0.61	0.79	0.0057	0.0001	60	220
193	18.0	1820	10	0.64	0.81	0.0048	0.0001	45	234
194	17.9	1775	5	0.62	0.79	0.0065	0.0002	110	190
195	18.1	2000	11	0.66	0.93	0.0106	0.0007	55	155
196	18.1	2035	14	0.69	0.96	0.0129	0.0005	60	143
197	18.0	2120	13	0.73	1.00	0.0196	0.0011	70	126
198	18.0	2125	21	0.73	0.91	0.0176	0.0009	170	119
199	17.9	2095	15	0.72	0.95	0.0166	0.0006	100	143

TABLE V - E

Argon Gas Flowrate - 4.5 E-4 Ncu.m/s
Carbon Concentration - 5.83 wt.%
Iron Concentration - 64.0 wt.%
C/Nb2O5 Mole Ratio - 7
Pyrochlore Particle Diameter - 60 microns
Graphite Particle Diameter - <45 microns
Iron Particle Diameter - <45 microns
Average Pellet Diameter - 18.5 mm

Expt. No.	Pellet Height	Pellet Temperature	95% confidence intreval, +/-	Conversion CO/CO2	Conversion Wt. loss	Reaction Constant	95% confidence interval, +/-	Average Reaction CO/CO2 Ratio	Reaction Time
	mm	K	K			1/s	1/s		s
200	17.0	1495	3	0.45	0.67	0.0039	0.0001	7	210
201	17.0	1430	11	0.42	0.74	0.0037	0.0001	9	184
202	16.9	1470	4	0.44	0.67	0.0040	0.0001	8	157
203	16.9	1525	4	0.51	0.84	0.0077	0.0002	15	119
204	16.9	1640	7	0.60	0.97	0.0100	0.0002	15	119
205	17.0	1635	9	0.60	0.96	0.0100	0.0003	15	130
206	17.0	1735	7	0.66	1.10	0.0154	0.0003	17	95
207	16.7	1690	10	0.61	1.08	0.0137	0.0005	18	124
208	17.1	1780	15	0.65	1.11	0.0153	0.0002	20	112

TABLE V - F

Argon Gas Flowrate - 4.5 E-4 Ncu.m/s
Carbon Concentration - 11.45 wt.%
Iron Concentration - 58.9 wt.%
C/Nb2O5 Mole Ratio - 14
Pyrochlore Particle Diameter - 60 microns
Graphite Particle Diameter - <45 microns
Iron Particle Diameter - <45 microns
Average Pellet Diameter - 18.5 mm

Expt. No.	Pellet Height	Pellet Temperature	95% confidence intreval, +/-	Conversion CO/CO2	Conversion Wt. loss	Reaction Constant	95% confidence interval, +/-	Average Reaction CO/CO2 Ratio	Reaction Time
	mm	K	K			1/s	1/s		s
209	19.6	1590	7	0.62	1.08	0.0118	0.0003	23	133
210	19.5	1625	4	0.61	0.95	0.0114	0.0008	20	143
211	19.4	1650	3	0.63	1.07	0.0117	0.0005	22	152
212	19.4	1695	8	0.68	1.12	0.0120	0.0005	50	167
213	19.4	1545	7	0.45	0.84	0.0060	0.0004	13	167
214	19.4	1450	6	0.27	0.65	0.0061	0.0003	60	133
215	19.4	1500	4	0.45	0.83	0.0052	0.0003	12	172

TABLE V - G

Argon Gas Flowrate - 4.5 E-4 Ncu.m/s
Carbon Concentration - 11.45 wt.%
Iron Concentration - 58.9 wt.%
C/Nb2O5 Mole Ratio - 14
Pyrochlore Particle Diameter - 60 microns
Graphite Particle Diameter - <45 microns
Iron Particle Diameter - <45 microns
Average Pellet Diameter - 12.9 mm

Expt. No.	Pellet Height	Pellet Temperature	95% confidence intreval, +/-	Conversion CO/CO2	Conversion Wt. loss	Reaction Constant	95% confidence interval, +/-	Average Reaction CO/CO2 Ratio	Reaction Time
	mm	K	K			1/s	1/s		s
216	16.1	1625	9	0.55	1.25	0.0087	0.0003	18	128
217	16.6	1735	11	0.71	1.17	0.0145	0.0005	35	116
218	16.3	1675	6	0.72	1.13	0.0145	0.0007	20	143
219	16.7	1795	10	0.76	1.23	0.0177	0.0006	60	133

Appendix VI

Experumental Data for Chapter IX

TABLE VI - A

Argon Gas Flowrate - 4.5 E-4 Ncu.m/s
Carbon Concentration - 16.8 wt.%
Ferric Oxide Concentration - 24.07 wt.%
C/Nb2O5 Mole Ratio - 7
Pyrochlore Particle Diameter - 60 microns
Graphite Particle Diameter - <45 microns
Ferric Oxide Particle Diameter - <45 microns
Average Pellet Diameter - 18.4 mm

Expt. No.	Pellet Height	Pellet Temperature	95% confidence intreval, +/-	Conversion CO/CO2	Conversion Wt. loss	Reaction Constant	95% confidence interval, +/-	Average CO/CO2 Ratio	Reaction Time
	mm	K	K			1/s	1/s		s
220	11.1	1670	5	0.63	0.70	0.0056	0.0002	20	200
221	11.7	1675	7	0.62	0.73	0.0069	0.0002	15	220
222	11.4	1795	4	0.72	0.89	0.0128	0.0002	50	130
223	11.5	1830	8	0.70	0.90	0.0149	0.0006	50	115
224	11.5	1775	6	0.71	0.87	0.0123	0.0003	60	138
225	11.6	1685	7	0.54	0.62	0.0059	0.0002	25	175
226	11.6	1740	10	0.64	0.81	0.0104	0.0004	30	140
227	11.4	1710	11	0.62	0.77	0.0095	0.0002	40	140
228	11.2	1755	12	0.67	0.83	0.0119	0.0004	60	128
229	10.9	1770	5	0.70	0.85	0.0143	0.0005	80	135
230	11.6	1635	11	0.60	0.72	0.0053	0.0001	35	200

TABLE VI - B

Argon Gas Flowrate - 4.5 E-4 Ncu.m/s
Carbon Concentration - 17.62 wt.%
Ferric Oxide Concentration - 60.32 wt.%
C/Nb2O5 Mole Ratio - 7
Pyrochlore Particle Diameter - 60 microns
Graphite Particle Diameter - <45 microns
Ferric Oxide Particle Diameter - <45 microns
Average Pellet Diameter - 18.4 mm

Expt. No.	Pellet Height	Pellet Temperature	95% confidence intreval, +/-	Conversion CO/CO2	Conversion Wt. loss	Reaction Constant	95% confidence interval, +/-	Average CO/CO2 Ratio	Reaction Time
	mm	K	K			1/s	1/s		s
231	21.4	1455	5	0.60	0.76	0.0049	0.0001	6	220
232	21.7	1580	4	0.61	0.82	0.0126	0.0003	6	100
233	21.6	1540	9	0.63	0.85	0.0148	0.0006	15	120
234	21.0	1410	9	0.61	0.71	0.0046	0.0001	5	210
235	21.0	1445	6	0.58	0.69	0.0053	0.0002	6	205
236	20.9	1435	5	0.59	0.65	0.0049	0.0002	5	210
237	20.9	1460	7	0.52	0.56	0.0045	0.0001	4	205
238	21.0	1485	7	0.68	0.85	0.0064	0.0001	7	205
239	20.9	1495	8	0.69	0.93	0.0071	0.0001	10	190
240	20.8	1475	3	0.69	0.80	0.0061	0.0000	8	215